Classical Integrable Field Theories with Defects and near-Integrable Boundaries

Robert Charles Parini

PhD

University of York
Mathematics

March 2018

Abstract

In the first part of this thesis algebro-geometric solutions for the sine-Gordon and KdV equations in the presence of a type I integrable defect are found, generalising the previously known soliton solutions. Elliptic (genus one) solutions where the defect induces only a phase shift are obtained via ansätze for the fields on each side of the defect. Algebro-geometric solutions for arbitrary genus and involving soliton emission by the defect are constructed using a Darboux transformation, exploiting the fact that the defect equations have the form of a Bäcklund transformation at a point. All the soliton and phase-shifted elliptic solutions to the defect equations are recovered as limits of the algebro-geometric solutions constructed in this way.

Certain energy and momentum conserving defects for the Kadomtsev-Petviashvili equation are then presented as a first step towards the construction of integrable defects in higher dimensions.

Algebro-geometric solutions to the sine-Gordon equation on the half-line with an integrable two parameter boundary condition are obtained by imposing a corresponding restriction on the Lax pair eigenfunction or, alternatively, as a Darboux transformation of the known algebro-geometric solution for the Dirichlet boundary.

Finally, the collision of sine-Gordon solitons with a Robin type boundary is examined. This boundary is typically non-integrable but becomes an integrable Neumann or Dirichlet boundary for certain values of a boundary parameter. Depending on the boundary parameter and initial velocity an antikink may be reflected into various combinations of kinks, antikinks and breathers. The soliton content of the field after the collision is numerically determined by computing the discrete scattering data associated with the inverse scattering method. A highlight of this investigation is the discovery of an intricate structure of resonance windows caused by the production of a breather which can collide multiple times with the boundary before escaping as a lighter breather or antikink.

Contents

List of Figures

Introduction

For a dynamical system integrability is, loosely, the property that the system can be solved exactly: that given suitable initial conditions the state of the system at any future time can be expressed in terms of known functions. Integrability is then a very satisfying and attractive concept since complex dynamical systems typically require careful approximations to produce meaningful results.

More concretely, a system with n degrees of freedom described by the Hamiltonian, H, is integrable in the Liouville sense if there exists n constants of motion F_i which are functions of the canonical coordinates $\{q_i, p_i\}_{i=1}^n$ that are independent (in the sense that their gradients are linearly independent) and in involution with one another,

$$\frac{dF_i}{dt} = \{F_i, H\} = 0\,, \qquad \{F_i, F_j\} = \sum_{k=1}^{n} \frac{\partial F_i}{\partial q_k}\frac{\partial F_j}{\partial p_k} - \frac{\partial F_i}{\partial p_k}\frac{\partial F_j}{\partial q_k} = 0\,, \qquad i, j = 1, \ldots, n\,,$$

(see, for example, [1]). Then the Liouville-Arnold theorem states that integrability guarantees the existence of a change of coordinates from the original canonical coordinates to the 'action-angle' coordinates $\{I_i, \phi_i\}_{i=1}^n$ where the equations of motion become

$$\frac{dI_i}{dt} = 0\,, \qquad \frac{d\phi_i}{dt} = \omega_i(I)\,,$$

for some functions ω_i of I_i [2]. The new equations of motion can then be solved in a straightforward manner.

Classical integrable field theories are even more special. Since fields have an infinite number of degrees of freedom an integrable field theory is constrained by an infinite number of independent conservation laws. This allows for solutions like solitons which have particle-like scattering properties despite the nonlinearity of the field theory.

The prototypical classical integrable field theory is the Korteweg-de Vries (KdV) equation,

$$u_t - 6uu_x + u_{xxx} = 0\,,$$

originally derived by Diederik Korteweg and Gustav de Vries as a model for shallow water waves in 1895 [3]. The solitary wave solutions to this equation vindicated John Scott Russell's much earlier observation in 1834 of 'a large solitary elevation' travelling along the Union Canal on the outskirts of Edinburgh and his subsequent experiments [4]. Following the numerical simulations of Zabusky and Kruskal in 1965 [5] this 'singular and beautiful phenomenon', as Russell called it, became known as a soliton: a stable solitary wave which maintains its shape and velocity, experiencing only a phase shift, after colliding with another soliton. A single soliton solution to the KdV equation is shown in Fig. (1a).

The integrability of the KdV equation became apparent in 1967 when Gardner, Greene, Kruskal and Miura developed the 'inverse scattering method' [6] which, given an initial field $u(x,0)$ that decays sufficiently rapidly as $|x| \to \infty$, can be used to solve the KdV equation for $u(x,t)$ at a future time t. This method relies upon writing the KdV equation as the compatibility condition of the two linear equations

$$\psi_{xx} = (u - \lambda)\psi \,, \tag{1a}$$

$$\psi_t = 3(u + \lambda)\psi_x - \psi_{xxx} \,, \tag{1b}$$

involving the eigenfunction ψ and spectral parameter λ. It will be immediately recognised that (1a) is, surprisingly, just the time-independent Schrödinger equation for a potential u. Treating (1a) as a scattering problem, the initial data $u(x,0)$ is encoded in terms of the 'scattering data': the reflection coefficient $R(\lambda)$, bound state eigenvalues λ_n and corresponding normalisation coefficients c_n. In particular, the bound state eigenvalues correspond to the presence of solitons. The time evolution of the scattering data is very simple and can be obtained using (1b). Then the field $u(x,t)$ at a later time can be constructed from the corresponding scattering data by solving the Gel'fand-Levitan-Marchenko equation.

If u does not decay as $|x| \to \infty$ but is instead periodic in x then the spectrum of (1a) generally consists of a sequence of continuous segments $[E_{2k-1}, E_{2k}]$, $k = 1, 2, \ldots$ on the real line separated by gaps $(-\infty, E_1), (E_2, E_3), \ldots, (E_{2k-1}, E_{2k}), \ldots$ where the length of the k^{th} gap tends to zero as $k \to \infty$ [7]. In 1974-75, the inverse scattering method was adapted to treat initial data corresponding to a finite number of gaps [8, 9, 10, 11, 12, 13]. A historical account of this rapid period of development involving many researchers is given in [14] and §1.6 of [15], along with many more references. A key observation was that the basis of eigenfunctions for (1a), $\psi_1(\lambda)$ and $\psi_2(\lambda)$, can be described as a single function $\Psi(P)$ on the genus g hyperelliptic Riemann surface

$$\left\{ P = (\lambda, \mu) \in \mathbb{C}^2 \,|\, \mu^2 = \prod_{k=1}^{2g+1} (\lambda - E_k) \right\} .$$

$\Psi(P)$ is a type of function known as a Baker-Akhiezer function [16, 17]. The corresponding solutions to the KdV equation $u(x,t)$ are known as 'finite-gap' or 'algebro-geometric' solutions and can be written in terms of Riemann theta functions [18, 10, 11, 19]. These solutions have the appearance of periodic or quasi-periodic trains of solitons and some examples of them are shown in Fig. (1b) and Fig. (1c). The multi-soliton solutions can be recovered from the algebro-geometric solutions by contracting the g pairs of finite-length segments to points $E_{2k-1}, E_{2k} \to \lambda_k$ which sends the periods to infinity [20, 21, 22, 19].

It is a general feature of classical integrable field theories that they admit a Lax pair formulation [23], which is to say that they can be written as the compatibility condition of two linear eigenvalue problems such as (1) for KdV. With this framework the inverse scattering method and the construction of algebro-geometric solutions has been generalised to many other integrable models including the sine-Gordon equation [24, 25, 26] ,

$$u_{tt} - u_{xx} + \sin u = 0 \,,$$

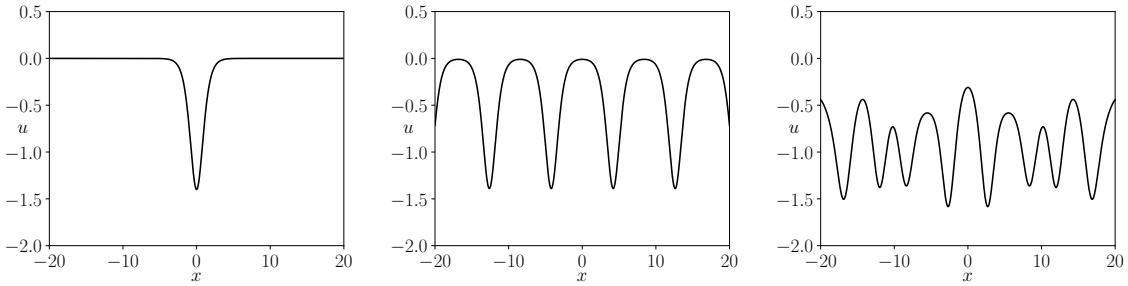

(a) A single soliton solution. (b) A genus $g = 1$ solution. (c) A genus $g = 3$ solution.

Figure 1: Some solutions to the KdV equation.

which will be a particular focus of this thesis. The sine-Gordon equation has an infinite number of degenerate energy vacua at $u = 2\pi n$, $n \in \mathbb{Z}$ and soliton solutions which interpolate between them [27]. Kinks interpolate up from $u = 2\pi n$ to $u = 2\pi(n+1)$ and are therefore said to have topological charge 1 while antikinks interpolate down from $u = 2\pi n$ to $u = 2\pi(n-1)$ and have topological charge -1. Clearly, the total topological charge can be fixed by a suitable choice of boundary conditions for u as $|x| \to \infty$. Kinks and antikinks may also form a bound state, known as a breather, which has an internal oscillatory mode.

Another field theory which will be highlighted in this thesis is a 2+1 dimensional generalisation of the KdV equation known as the Kadomtsev-Petviashvili (KP) equation [28]

$$3\varepsilon^2 u_{yy} = \partial_x \left[4u_t - 6uu_x - u_{xxx}\right] , \quad \varepsilon^2 = \pm 1 ,$$

which describes long-wavelength water waves that vary slowly in the y direction compared to the x. The KP equation is also integrable by an extension of the inverse scattering method [29, 30, 31]. When $\varepsilon^2 = 1$ the KP equation (called KP2) has line soliton solutions which are constant in the direction orthogonal to the direction of propagation [32, 33, 34] and whose interactions have been observed experimentally [35]. When $\varepsilon^2 = -1$ the KP equation (called KP1) has unstable line soliton solutions [28, 31] but stable lump soliton solutions which decay in all directions [36, 37, 38, 39, 40]. Both KP equations have algebro-geometric solutions [41, 42, 19] and the genus $g = 2$ solutions for KP2 have been shown experimentally to model two-dimensional periodic waves in a hexagonal pattern [43, 44].

Given the delicate nature of nonlinear integrable field theories it is perhaps surprising that they often appear as models of real world systems, albeit under certain approximations. As mentioned before, the KdV equation was derived in the context of shallow water waves [3, 45]. It also has several other applications [46, 47] as a model of, for example, arterial blood pulses [48, 49, 50], small amplitude waves in plasma [51, 52, 53] and internal waves at the interface of two fluids of different densities [52] which have been observed in the ocean [54].

The sine-Gordon equation can be derived as the continuum limit of a chain of pendulums coupled to their nearest neighbours by torsional springs where the field $u(x,t)$ is the angle between a pendulum at each point and its equilibrium position [55, 47]. The sine-Gordon equation also appears in many other contexts [56, 47] including several biological models [57]. For example, the coupled pendulum model which has sine-Gordon as its continuum limit appears as a mechanical analogue for the dynamics of base pairs in DNA

[58, 59, 60, 61]. Another application is to long Josephson junctions, two superconductors separated by a thin insulating layer, where $u(x,t)$ describes the phase difference between the wave functions of the two superconductors in time and along the junction [62].

The physically imposed constraints of finite space and impurities naturally suggest modifications to integrable field theories in the form of external and internal boundary conditions. Olsen and Samuelsen studied numerically the sine-Gordon equation on the interval $[0,l]$ with boundary conditions $u_x(0) = u_x(l) = \beta$ to model the effect of an external magnetic field applied to a Josephson junction line of length l containing a soliton [63]. They found that a kink colliding with a boundary may collapse into radiation or produce one or more kinks, antikinks or breathers depending on the initial velocity of the soliton and the parameter β related to the external magnetic field. Similar results for the sine-Gordon equation on the half-line with the Robin boundary condition $u_x + 2ku = 0$, $k \in \mathbb{R}$ will be presented later in this thesis although using a more sophisticated method where the soliton content of the field after collision is numerically recorded by computing the corresponding bound state eigenvalues associated with the Lax pair formulation for sine-Gordon.

The magnetic and Robin boundary conditions allow the total energy of the system, modified by suitable boundary terms, to be conserved but break the integrability of the sine-Gordon equation that is present on the full line. However, there are boundaries which are compatible with integrability. The simplest examples are the Dirichlet $u = u_0$ and Neumann $u_x = 0$ boundaries. Sklyanin found that for the sine-Gordon equation the boundary $u_x = M\sin(u/2)$ is integrable [64] while $u_x = M\cos(u/2)$ was later obtained by Tarasov [65]. Ghoshal and Zamolodchikov (GZ) then constructed the boundary

$$u_x = M\sin\left(\frac{u-\phi}{2}\right), \quad M,\phi \in \mathbb{R}, \tag{2}$$

by requiring the conservation of low-lying energy-like charges [66]. It was subsequently established in [67] that the sine-Gordon equation on the half-line with the boundary (2) is integrable and that for this system there exists an infinite number of conservation laws in involution.

Solitons encountering the GZ boundary (2) may flip topological charge but are otherwise perfectly reflected [68, 69]. Algebro-geometric solutions to the sine-Gordon equation on the half-line have also been found for the integrable boundaries $u = u_0 \pmod{2\pi}$ [70] and $u_x = M\sin(u/2)$ [71]. Part of this thesis will discuss the construction of algebro-geometric solutions to the more general boundary (2).

As with boundaries, introducing a defect or impurity into an integrable field theory typically breaks the integrability of the system but there are defects for which this is not the case. Bowcock, Corrigan and Zambon constructed defects which preserve, with the addition of suitable defect terms, an infinity of conserved quantities for the total system [72], including momentum [73, 74, 75]. The conservation of momentum seems quite surprising since the presence of a defect at a particular point $x = x_D$ naturally breaks translation invariance. However, the defect is also 'topological' in the sense that the sewing conditions at $x = x_D$ which define the defect by relating the fields on each side do not explicitly depend on the defect position and so the defect could be placed anywhere without affecting its properties.

Integrable defects are categorised into two types: type I defects are parameterised by a constant while the type II defect equations contain a dynamical parameter in addition to the fields [76]. Type I defects, which will be a focus here, have been found for several integrable 1+1 dimensional field theories including the sine-Gordon [73] and other affine Toda field theories corresponding to the root data of $a_n^{(1)}$ [74] (sine-Gordon corresponding to $a_1^{(1)}$) as well as the nonlinear Schrödinger, Korteweg-de Vries (KdV), modified KdV (mKdV) [75] and complex sine-Gordon equations [77].

This thesis will be particularly concerned with the KdV and sine-Gordon equations with a type I integrable defect. In both cases soliton solutions have been found where a single soliton experiences a phase shift upon passing through the defect but the soliton velocity is unchanged [78, 75]. For sine-Gordon the defect may also cause the topological charge of the soliton to change sign and for KdV the soliton may become a travelling singularity after passing through the defect. The precise outcome depends on the choice of defect parameter and velocity of the initial soliton. Beyond these phase-shifted solutions, 'one-to-two' soliton solutions have also been found for sine-Gordon [78] and KdV [75], where a defect storing sufficient energy and momentum is able to emit a soliton. However, the precise time of this emission would need to be fixed by further initial conditions than the incoming soliton and defect parameter. All these solutions were originally found analytically by direct substitution of an ansatz for the fields on the half-line each side of the defect which satisfies the field theories away from the defect and can be arranged to solve the sewing conditions at the defect.

In this thesis algebro-geometric solutions to the type I defect equations will be presented for the sine-Gordon and KdV equations which generalise all the known soliton solutions. Their construction will employ Bäcklund transformations which in the context of integrable systems are traditionally used to generate solutions to integrable field theories on the full line (for example, [79, 80, 81, 82, 83, 84]). If $u(x,t)$ satisfies an integrable field theory and together $u(x,t)$ and $v(x,t)$ satisfy the relevant Bäcklund transformation equations then v also satisfies the integrable field theory. The Bäcklund transformation was introduced by Bäcklund in 1883 [85] for what is today called the sine-Gordon equation while the Bäcklund transformation for the KdV equation is due to Wahlquist and Estabrook [80]. In both of these cases the application of a Bäcklund transformation typically adds (and in a special case removes) a soliton depending on the choice of parameter appearing in the Bäcklund transformation.

As observed in [73], the type I integrable defect equations for sine-Gordon and KdV have the form of a Bäcklund transformation but applied to a particular point in space rather than over the full line. In this sense the x derivatives present in the defect sewing conditions are considered 'frozen'. However, if a u and v are found which satisfy the appropriate Bäcklund transformation equations everywhere then they will in particular satisfy the defect sewing conditions at the defect point $x = x_D$. So the field

$$w(x,t) = \begin{cases} u(x,t) & \text{if } x \leq x_D \\ v(x,t) & \text{if } x \geq x_D \end{cases} \tag{3}$$

where u and v together satisfy the appropriate Bäcklund transformation equations will

satisfy the integrable field theory on $x < 0$ and $x > 0$ and the defect equations at $x = x_D$.

This was essentially the approach used in [86] to re-derive the delayed phase-shifted soliton solution of [73] for the sine-Gordon equation as well as solutions involving soliton creation by the defect. However, contrary to [86], taking (3) as the definition of a defect (i.e. the restriction of an 'unfrozen' Bäcklund transformation) does not allow for new solutions compared to the 'frozen' integrable defects discussed here. The possibility of soliton creation by the 'frozen' defect was already discussed in [78] and the annihilation of a soliton by the defect is a special case of the phase-shifted solution in [73] which occurs when the defect parameter equals $\exp(-\theta)$ where θ is the rapidity of the incoming soliton. It will be emphasised here that the field (3) is simply a certain type of solution to the integrable defects which have the form of 'frozen' Bäcklund transformations. It might be that there are solutions to these integrable defects which are not of the form (3) and satisfy the defect equations *only* at x_D but such solutions do not appear to have been found. A more algebraic description of the relationship between defects in space, or time, and Bäcklund transformations has been given in [87].

It will prove convenient to implement the Bäcklund transformation on the level of the Lax pair as a Darboux transformation that relates the Lax eigenfunctions for u to the corresponding eigenfunctions for v such that u and v satisfy the appropriate Bäcklund transformation equations. For example, if u_0 and ψ_0 satisfy the KdV equation and the Lax equation (1) then so does

$$u_1 = u_0 - 2\partial_x^2 \ln(f_1)\,, \qquad \psi_1 = \partial_x \psi_0 - \psi_0\, \partial_x \ln(f_1)$$

where $f_1(x,t) = \psi_0(x,t,\lambda = \sigma_1)$ for some choice of σ_1 [88]. The transformation $(u_0, \psi_0) \to (u_1, \psi_1)$ is a Darboux transformation for the KdV equation and u_0 and u_1 satisfy a Bäcklund transformation.

The modification of integrable field theories by boundaries and defects and in particular the behaviour of the soliton and algebro-geometric solutions for the KdV and sine-Gordon equations in the presence of these modifications is the central topic of this thesis which is outlined below.

Thesis Outline

Chapter 1 recalls the type I integrable defects for the sine-Gordon and KdV equations and their previously known phase-shifted soliton solutions, where the soliton is delayed by the defect for sine-Gordon and advanced for KdV, as well as the 'one-to-two' soliton solutions where a soliton is emitted by the defect. For both sine-Gordon and KdV new phase-shifted soliton solutions are found where the soliton is advanced by an excited sine-Gordon defect and delayed for KdV. It is noted that for sine-Gordon and KdV both phase-shifted solutions can be obtained as limits of the 'one-to-two' solution solution in which the initial position of the emitted soliton is taken to $\pm\infty$. It is also recalled that the 'one-to-two' soliton solution itself satisfies the Bäcklund transformation equations everywhere as well as the defect equations at a point and the relevance of Bäcklund transformations to the construction of solutions to the type I defect equations, as mentioned above, is further elucidated.

Chapter 2 recalls the algebro-geometric solutions for the sine-Gordon and KdV equations, together with the necessary background from the theory of Riemann surfaces, algebraic curves and theta functions.

Chapter 3 constructs phase-shifted elliptic (genus one) solutions to the sine-Gordon type I defect equations via an ansatz method similar in spirit to the construction of phase-shifted soliton solutions in [78] but significantly more involved. Two phase-shifted elliptic solutions are found and it is checked that in the limit in which their period tends to infinity that the delayed and advanced single soliton solutions to the defect equations are recovered. The reality conditions for the phase-shifted elliptic solutions are examined and it is found that for a certain choice of elliptic field to the left of the defect that there is a range of values for the defect parameter such that the phase-shifted field to the right of the defect becomes complex valued. This phenomenon has no analogue in the soliton case where the reality conditions can always be satisfied for any choice of initial soliton velocity and defect parameter.

In **Chapter 4** new algebro-geometric solutions of the form (3) are found for the sine-Gordon and KdV models with a type I integrable defect. The Bäcklund transformation is implemented as a Darboux transformation which is used to algebraically compute v from u and the Lax eigenfunctions corresponding to u. Reality and regularity conditions for the algebro-geometric solutions are given and, depending upon the precise choice of branch points for the algebraic curve corresponding to u, this restricts the possible values of the defect parameter in order for v to be real and non-singular. It is noted that the field v to the right of the defect typically has an additional soliton compared to the field u and that, just as in the purely solitonic case, phase-shifted solutions are found in the limit where the initial position of this additional soliton is sent to $\pm\infty$. It is verified that in suitable limits the purely solitonic solutions to the defect equations and the phase-shifted elliptic solutions found in chapter 3 are recovered from the more general algebro-geometric solutions found in this chapter.

Chapter 5 constructs certain energy and momentum conserving defects for the KP equation. It is shown that for a defect placed along the line $y = 0$ or $x = 0$ that if the defect equations are assumed to have the same form as a Bäcklund transformation but applied along the defect line then the energy and both components of the linear momentum are conserved. A Lagrangian description is found for the defect along $y = 0$ while the difficulties involved in doing the same for the $x = 0$ defect are discussed.

Chapter 6 reviews the algebro-geometric solution to the Dirichlet boundary problem $u = u_0 \pmod{2\pi}$ found in [70] before constructing an algebro-geometric solution to the GZ integrable boundary (2) using a Bäcklund transformation of the Dirichlet solution. It is shown that an equivalent result can also be achieved by directly imposing a restriction on the Lax pair eigenfunctions equivalent to the GZ boundary condition. However, there remains in either case an unresolved sign ambiguity related to the necessity to solve the Dirichlet boundary mod 4π, rather than mod 2π.

Chapter 7 examines the sine-Gordon equation on the half-line with the typically non-integrable Robin boundary $u_x + 2ku = 0$ parameterised by $k \in \mathbb{R}$ at $x = 0$. It is explained that this boundary is 'near-integrable' in the sense that it is the linearisation in u of the integrable Sklyanin boundary and when $k = 0$ or $k \to \infty$ it becomes the

integrable Neumann $u_x = 0$ and Dirichlet $u = 0$ boundaries respectively. It is shown that the energy for this system is conserved but, outside of the integrable limits, the next highest energy-like conserved quantity for sine-Gordon is not. To understand how the Robin boundary interpolates between the two integrable limits an antikink is sent towards the boundary for a range of initial antikink velocities, v_0, and k. In each case the soliton content of the field is determined by first waiting until any produced solitons are sufficiently far away from the boundary so that the portion of the field which contains them can be approximated as being on the integrable full line. Then the bound state eigenvalues for the Lax pair scattering problem across this interval of the reflected field are computed numerically, revealing the velocity and frequency (if a breather) of each soliton present. It is found that generally the antikink is reflected into various combinations of a kink, an antikink and one or more breathers depending on v_0 and k. A map of these outcomes is produced for $v_0 \in [0.01, 0.99]$, $k \in [0, 0.5]$ showing how the result of the antikink/boundary collision interpolates between the integrable Neumann and Dirichlet limits. In particular, a region of the initial parameter space is observed with an intricate structure of resonance windows arising from the creation of an intermediate breather which after colliding with the boundary may collide again or escape the boundary as an antikink or lighter breather, the outcome being strongly dependent on the breather phase.

Chapter 8 summarises the results presented in this thesis and discusses some possible lines of enquiry for the future.

Appendices A and B explicitly repeat, for convenience, the well known multi-soliton limit and partial soliton limit (where a genus $g + 1$ solution becomes a genus g solution plus a soliton) respectively for the algebro-geometric solutions to the sine-Gordon and KdV equations on the full line.

Finally, **Appendix C** describes the `cxroots` Python module [89] written by the present author to find the roots of a complex analytic function within a given contour. A summary is given of the mathematical method, based on [90], which uses contour integration to construct a polynomial whose roots approximate the desired roots. This type of rootfinding problem appears when numerically computing the bound state eigenvalues for the Lax scattering problem in chapter 7.

Acknowledgements

I must first thank my supervisor, Ed Corrigan, for his time, advice and uncanny ability to pose interesting questions. The answers to some of them are contained here. I also thank Atsushi Higuchi and Evgeny Sklyanin for their comments and suggestions as part of my thesis advisory panel. I am thankful too for the camaraderie of the PhD students of the mathematics department that I have been fortunate enough to know during my time at the University of York.

I also wish to thank Patrick Dorey for introducing me to the elegant world of solitons and integrable systems as a lecturer at Durham University and for his subsequent encouragement, patience and hard work as a collaborator.

My heartfelt thanks go to my parents, Claire and Clive, for their unwavering love and support throughout my entire life and to my recently departed grandad, George, for his kindness and good-natured spirit. To my wife, Ellie, thank you for sharing these years with me and making them all the sweeter.

Finally, I gratefully acknowledge the support of the EPSRC for my studentship.

Declaration

> I declare that this thesis is a presentation of original work and I am the sole author. This work has not previously been presented for an award at this, or any other, university. All sources are acknowledged as references.

Most of chapter 1 is review but, in particular, certain phase-shifted soliton solutions for the defect equations: (1.10) and (1.24) with $p_0 - q_0 = -|\chi|$, and the appearance of all the phase-shifted soliton solutions in the limit of the 'one-to-two' soliton solution in §1.1.3 and §1.2.2 is the original work of the author and contained in

- E. Corrigan and R. Parini. "Type I integrable defects and finite-gap solutions for KdV and sine-Gordon models". *Journal of Physics A: Mathematical and Theoretical* **50**.28 (2017). arXiv: `1612.06904`

Chapters 3 and 4 are based on the key results of the above paper. The detail of the calculation and examination in the above paper is the work of the present author while the coauthor, Ed Corrigan, provided the direction and context for this investigation.

No claim to originality is made for the contents of chapter 2 or appendices A and B.

Chapters 5 and 6, on momentum and energy conserving defects for the KP equation and algebro-geometric solutions to the GZ integrable boundary condition for sine-Gordon respectively, contain the unpublished original work of the present author.

Chapter 7, with the exception of §7.1 and §7.2, is based on

- R. Arthur, P. Dorey, and R. Parini. "Breaking integrability at the boundary: The sine-Gordon model with Robin boundary conditions". *Journal of Physics A: Mathematical and Theoretical* **49**.16 (2016). arXiv: `1509.08448`

The contribution of the present author to this paper was to implement the numerical method in §7.4 and, with Patrick Dorey, produce and analyse the results shown here in sections 7.5-7.9. In addition, Patrick Dorey provided the initial idea for the method in §7.4 and was largely responsible for the analysis of the Robin boundary vacuua in §7.3. Robert Arthur previously discussed antikink collisions with the Robin boundary as part of his unpublished Master's thesis [93], also cited below, which provided some initial observations that were built upon in the above paper. A summary of the above paper's conclusions is also contained in

- P. E. Dorey and R. Parini. "Integrability breaking on the boundary" (2018)

which is currently awaiting review.

The complex rootfinding software `cxroots` [89], demonstrated in appendix C, was written by the present author although the mathematical theory on which it is based, summarised in §C.1, is not original.

1 | Integrable defects

One approach to modifying 1+1 dimensional integrable field theories is to introduce an internal boundary or 'defect' at a point, as in Fig. (1.1). This defect is defined by a set of sewing conditions which relates the fields and their derivatives on each side of the defect to one another.

Arbitrarily chosen defect conditions will not generally preserve the integrability of the system but integrable defects have been found for certain models including the sine-Gordon, Liouville and free field theories [73] as well as the KdV, mKdV and nonlinear Schrödinger equations [75]. This chapter reviews the type I integrable defects, which are only parameterised by a constant, for the sine-Gordon and KdV equations and reconsiders their effect on solitons, leading to some new results.

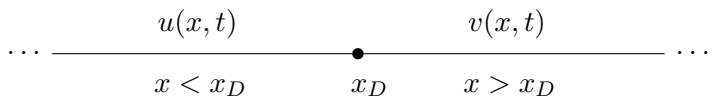

Figure 1.1: Placement of a defect for a 1+1 dimensional field theory.

1.1 Sine-Gordon equation

The derivation of the integrable defect for the sine-Gordon equation in [73] is similar to the approach to integrable external boundaries taken in [66] which will later be touched upon in §7.2. This method starts from a Lagrangian description of the model,

$$\mathcal{L} = \Theta(x_D - x)\mathcal{L}_{SG}[u] + \delta(x - x_D)\mathcal{D}[u, v] + \Theta(x - x_D)\mathcal{L}_{SG}[v]\,, \tag{1.1}$$

where $\mathcal{L}_{SG}$ is the Lagrangian for the sine-Gordon equation

$$\mathcal{L}_{SG}[u] = \frac{1}{2}u_t^2 - \frac{1}{2}u_x^2 - 1 + \cos u\,.$$

Assuming for the moment that $\mathcal{D}$ depends only on u, u_x, u_t, v, v_x, v_t then the variation of the action

$$\delta S = \int dt \left[\delta u \left(-u_x + \frac{\delta \mathcal{D}}{\delta u} - \partial_t \frac{\delta \mathcal{D}}{\delta u_t}\right) + \delta u_x \frac{\delta \mathcal{D}}{\delta u_x} + \delta u \left(v_x + \frac{\delta \mathcal{D}}{\delta v} - \partial_t \frac{\delta \mathcal{D}}{\delta v_t}\right) + \delta v_x \frac{\delta \mathcal{D}}{\delta v_x}\right]\Bigg|_{x=x_D}$$

implies that $\mathcal{D}$ does not depend on u_x or v_x (and would not depend on any other x derivatives) and determines the defect conditions at $x = x_D$ to be

$$u_x = \frac{\delta \mathcal{D}}{\delta u} - \partial_t \frac{\delta \mathcal{D}}{\delta u_t}\,, \tag{1.2a}$$

$$v_x = -\frac{\delta \mathcal{D}}{\delta v} + \partial_t \frac{\delta \mathcal{D}}{\delta v_t}\,. \tag{1.2b}$$

Integrable partial differential equations, such as sine-Gordon, possess an infinite number of independent conserved quantities in involution. Requiring that the first few of these be conserved in the presence of a defect places very strong constraints on the defect conditions. In particular, it turns out [73] to be sufficient to require that the total energy,

$$E = \int_{-\infty}^{x_D} \left[\frac{1}{2}u_t^2 + \frac{1}{2}u_x^2 + 1 - \cos u\right] dx + \int_{x_D}^{\infty} \left[\frac{1}{2}v_t^2 + \frac{1}{2}v_x^2 + 1 - \cos v\right] dx + E_D\,, \tag{1.3}$$

and next non-trivial energy-like conserved charge,

$$E_3 = \int_{-\infty}^{x_D} \mathcal{E}_3[u]dx + \int_{x_D}^{-\infty} \mathcal{E}_3[v]dx + E_{D3}\,, \tag{1.4}$$

where, as will be recalled in §7.2,

$$\mathcal{E}_3[u] = \frac{1}{8}\left(u_t^4 + 6u_t^2u_x^2 + u_x^4 + 4(u_{tt} + u_{xx})\sin u + 4u_t\partial_t(u_{tt} + 3u_{xx}) + 4u_x\partial_x(3u_{tt} + u_{xx})\right)\,,$$

are both conserved with the addition of suitable defect contributions, E_D and E_{D3}.

Conservation of energy is not seriously constraining since, using (1.2), it only requires

$$\partial_t \left[E_{\mathcal{D}} + \mathcal{D} - u_t\frac{\delta \mathcal{D}}{\delta u_t} - v_t\frac{\delta \mathcal{D}}{\delta v_t}\right]\Bigg|_{x=x_D} = 0 \tag{1.5}$$

which is satisfied by taking, as [73] does,

$$\mathcal{D} = \frac{uv_t - vu_t}{2} - E_D\,,$$

where E_D is a functional of the fields u and v only and not their derivatives. However, the conservation of E_3 is more stringent and constrains E_D to be [73]

$$E_D = -2\left(\sigma\cos\frac{u+v}{2} + \frac{1}{\sigma}\cos\frac{u-v}{2}\right) + 2\left(\sigma + \frac{1}{\sigma}\right)\,, \qquad \sigma \in \mathbb{R}\,, \tag{1.6}$$

where the arbitrary real constant σ is known as the defect parameter. The constant term is of course arbitrary but has been added so that if $u(x_D) = v(x_D) = 2\pi n$, $n \in \mathbb{Z}$ then the defect contribution to the energy is, intuitively, $E_D = 0$. The defect equations (1.2) at $x = x_D$ then become

$$u_x = v_t - \sigma\sin\left(\frac{u+v}{2}\right) - \frac{1}{\sigma}\sin\left(\frac{u-v}{2}\right)\,, \tag{1.7a}$$

$$v_x = u_t + \sigma\sin\left(\frac{u+v}{2}\right) - \frac{1}{\sigma}\sin\left(\frac{u-v}{2}\right)\,. \tag{1.7b}$$

For simplicity it will be assumed that $\sigma \geq 0$. However, if a (u, v) pair satisfying the defect equations for a positive σ is known then it is always possible to obtain a solution corresponding to defect parameter $-\sigma$ using the symmetry $(\sigma, u, v) \to (-\sigma, u, v + 2\pi)$ of (1.7).

1.1.1 Phase-shifted soliton solutions

Before remarking further on the form of these sewing conditions it is worth briefly considering some simple solutions to these equations. Suppose the field to the left of the defect, $u(x, t)$, is a single kink soliton as shown in Fig. (1.2a) and described by

$$e^{iu/2} = \frac{1 + iE_\theta}{1 - iE_\theta}, \qquad E_\theta = \exp\left[\cosh(\theta)x - \sinh(\theta)t - x_\theta\right], \tag{1.8}$$

where θ is the rapidity of the soliton and $\theta > 0$ corresponds to a soliton moving in the positive direction along the x axis. The single antikink solution to sine-Gordon may be obtained by sending the constant $x_\theta \to x_\theta + i\pi$ so that $E_\theta \to -E_\theta$.

It was found in [73] that one possible solution for the field to the right of the defect, $v(x, t)$, is a phase-shifted version of the original soliton,

$$e^{iv/2} = \frac{1 + i\delta E_\theta}{1 - i\delta E_\theta}, \qquad \delta = \coth\left(\frac{\eta - \theta}{2}\right), \tag{1.9}$$

where the defect parameter $\sigma = e^{-\eta}$. In this case the defect delays the soliton and if $\eta < \theta$ then δ is negative so the topological charge of the soliton is reversed, flipping the incoming kink to an antikink, as shown in Fig. (1.2c). If $\eta > \theta$ the soliton retains its character but is still delayed, as in Fig. (1.2b). If $\eta = \theta$ then the soliton is infinitely delayed and therefore captured by the defect leaving behind a 2π discontinuity at $x = x_D$, as shown in Fig. (1.2d).

For the phase-shifted solution (1.8), (1.9) the field at sufficiently early times (say at $t \to -\infty$) is continuous across the defect so the initial energy stored in the defect, given by (1.6), is zero. But suppose that initially the field has a 2π discontinuity across the defect which is to say that the defect starts in an excited state with energy equal to that of a soliton of rapidity η, as shown in Fig. (1.3a). This situation corresponds to a new purely phase-shifted soliton solution,

$$e^{iv/2} = -\frac{1 + i\delta^{-1}E_\theta}{1 - i\delta^{-1}E_\theta}, \tag{1.10}$$

where the phase shift is now the inverse of the previous case and therefore a soliton is advanced by the defect instead of delayed. But as before the kink remains a kink if $\eta > \theta$, as in Fig. (1.3b), and is flipped to an antikink if $\eta < \theta$, as in Fig. (1.3c). If $\theta = \eta$ then $\exp(iv/2) = -1$ and the final field configuration is the same as before: a 2π discontinuity at the defect, as shown in Fig. (1.3d). However, the interpretation of what happens to the soliton as $\theta \to \eta$ is different. For (1.9) the soliton is infinitely phase-shifted backwards so it never emerges from the defect while for (1.10) the soliton is infinitely phase-shifted forwards and hence should be considered to have already emerged an infinitely long time ago and at finite times lies at $x \to \infty$.

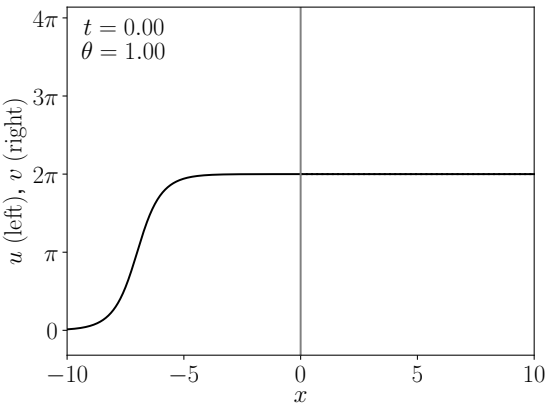

(a) An initial kink soliton with rapidity θ, as described by (1.8), incident on an integrable defect at $x = 0$ with the field initially continuous across the defect.

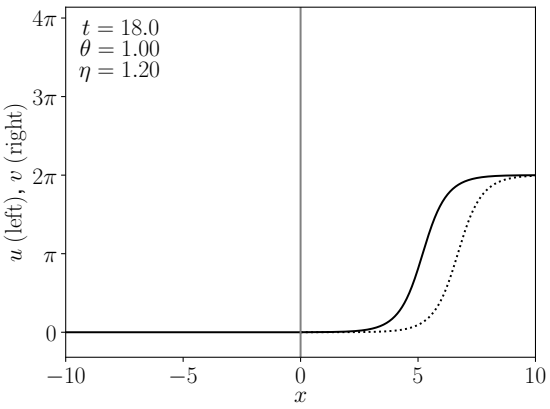

(b) When $\eta > \theta$ the soliton is transmitted but phase-shifted backwards.

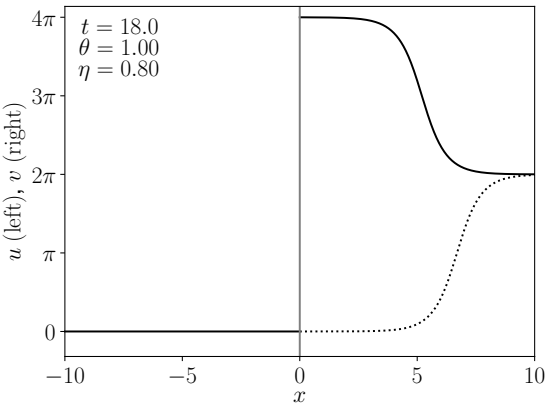

(c) When $\eta < \theta$ the soliton is transmitted but phase-shifted backwards and its topological charge is flipped, in this case from a kink to an antikink.

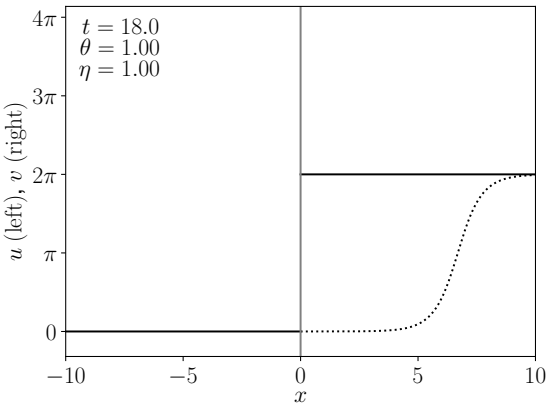

(d) When $\eta = \theta$ the soliton is captured by the defect.

Figure 1.2: Examples of an initial soliton (a) incident on an initially continuous type I integrable defect being transmitted (b), transmitted and flipped (c) and captured (d) for different values of the defect parameter $\sigma = \exp(-\eta)$ according to (1.9). The dotted lines show the single soliton solution (1.8) in the absence of the defect for comparison.

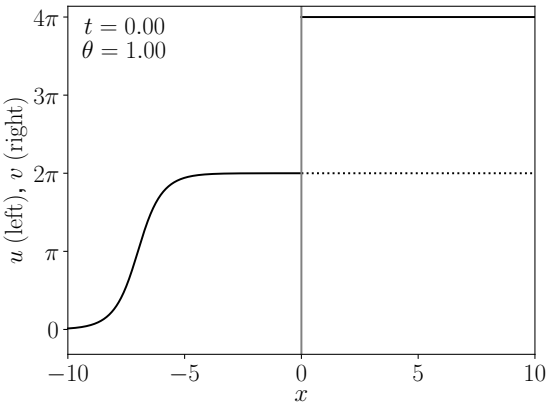

(a) An initial kink soliton where the field to the left of the defect at $x = 0$ is the soliton with rapidity θ described by (1.8) but the field has a discontinuity of magnitude 2π across the defect.

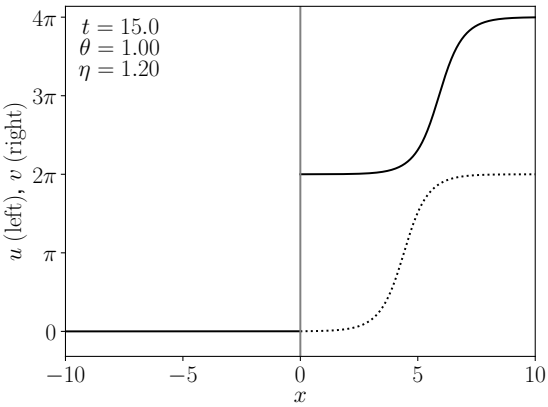

(b) When $\eta > \theta$ the soliton is transmitted but phase-shifted forwards.

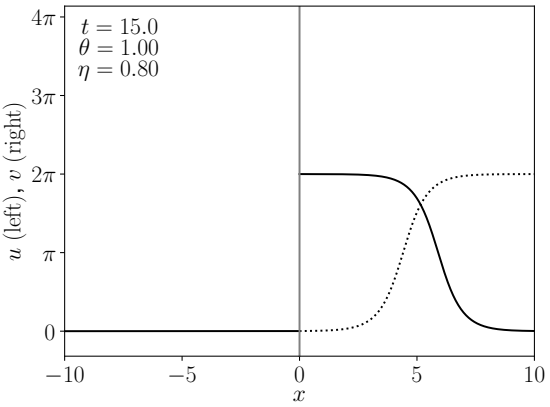

(c) When $\eta < \theta$ the soliton is transmitted but phase-shifted forwards and its topological charge is flipped, in this case from a kink to an antikink.

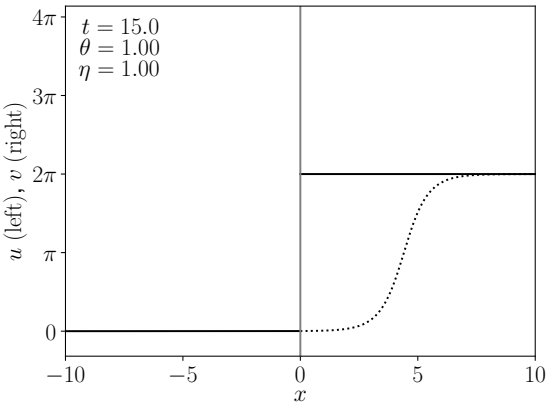

(d) When $\eta = \theta$ the soliton is captured by the defect.

Figure 1.3: Examples of an initial soliton (a) incident on an initially excited type I integrable defect being transmitted (b), flipped (c) and captured (d) for different values of the defect parameter $\sigma = \exp(-\eta)$ according to (1.10). The dotted lines show the single soliton solution (1.8) in the absence of the defect for comparison.

Of course for a given (u, v) one can always find another solution to sine-Gordon with the defect (1.7) by simply adding a multiple of 4π to v but since this does not meaningfully alter the dynamics it will not be considered distinct from the solutions discussed here.

1.1.2 Soliton emission

As well as being able to capture solitons a defect can also emit a soliton if it has sufficient energy. The existence of an emitting soliton solution can be seen as a consequence of the symmetry of the defect equations (1.7) under $(u, v) \to (v - 2\pi, u)$. Under this symmetry the soliton capture solution where u is (1.8) and $v = 2\pi$ is transformed to a soliton creation solution,

$$e^{iu/2} = 1\,, \qquad e^{iv/2} = \frac{1 + iE_\eta}{1 - iE_\eta}\,, \quad E_\eta = \exp\left[\cosh(\eta)x - \sinh(\eta)t - x_\eta\right]\,. \tag{1.11}$$

Before the new kink (or antikink if $E_\eta \to -E_\eta$) emerges there is a $2\pi \pmod{4\pi}$ discontinuity at the defect and after it emerges the field is continuous $(\mathrm{mod}\ 4\pi)$ across the defect. Energetically, this must be the case since, as noted in [78], the defect with a 2π discontinuity has energy $E_D = 8\cosh\eta$ which is precisely the energy of a soliton of rapidity η and after the emission $E_D = 0$ and all the energy is transferred to the new soliton.

So if the defect starts in an excited state with a 2π discontinuity then it is possible for a soliton to emerge but the position of this soliton x_η or indeed whether it is a kink or antikink is not fixed by the given u or defect parameter $\sigma = e^{-\eta}$. In a physical situation some additional information about v would be necessary in order to fix x_η. For example, if it is known that the field is initially continuous $(\mathrm{mod}\ 4\pi)$ then by the energetic argument above no soliton can be emitted, therefore fixing $x_\eta \to \infty$.

In the context of quantum field theory the free choice of x_η seems to correspond to the fact that the transmission matrix associated with a soliton passing through the defect has a pole at a certain complex rapidity that can be interpreted as an unstable soliton-defect bound state with a finite decay width [78].

1.1.3 One-to-two soliton solution

In order to generalise the two phase-shifted soliton solutions consider the soliton creation case above but on a background with an additional soliton of rapidity θ. This one-to-two soliton solution to the defection equations consists of the field u given by (1.8) to the left of the defect and the field v given by

$$e^{iv/2} = \frac{1 + i\delta E_\theta \pm iE_\eta \mp \delta^{-1}E_\theta E_\eta}{1 - i\delta E_\theta \mp iE_\eta \mp \delta^{-1}E_\theta E_\eta}\,, \tag{1.12}$$

to the right of the defect. Again, the initial position for the created soliton, x_η, and the choice of $\pm$ (which corresponds to the created soliton being a kink or antikink), is not fixed by the given u or defect parameter $\sigma = e^{-\eta}$.

It has been noted [78] that the phase shift δ experienced by a single soliton passing through the defect is the square root of the total phase shift experienced by the same soliton being overtaken by a soliton of rapidity η. However, it can now be seen that the phase-shifted solutions (1.9) and (1.10) can be alternatively and directly obtained from (1.12) by taking the limits $x_\eta \to \infty$ or $x_\eta \to -\infty$, respectively. In this way (1.12) represents a more general solution to the defect equations for the case where the incoming u is a single soliton.

1.1.4 Defects, momentum and Bäcklund transformations

A very important property of the defect equations (1.7) for what follows is that, as observed in [73], they have the form of Bäcklund transformation equations for sine-Gordon [85, 84] but applied only at the point $x = x_D$ rather than for all x. As mentioned in the introduction, this Bäcklund transformation is commonly used, together with Bianchi's permutability theorem [95], to take a solution to the sine-Gordon equation on the full line $u(x,t)$ and generate another solution $v(x,t)$ which contains an additional soliton compared to u with rapidity equal to η where the Bäcklund parameter $\sigma = \exp(-\eta)$ (as in, for

example, [79, 81, 83]). If u already has a soliton with rapidity η then the application of a Bäcklund transformation destroys it.

This use is equivalent to the ability of integrable defects to capture or emit a soliton and, in fact, the u (1.8) and v (1.12) that constitute the one-to-two soliton solution for the defect equations are also related to each other by a Bäcklund transformation. That is to say that (1.8) and (1.12) actually solve the defect equations (1.7) for *all* x as well as at the point $x = x_D$ where the defect is located. This might have been anticipated since the fields (1.8) and (1.12) are completely independent of the defect's position so they would have to solve the defect equations for any choice of position x_D.

This independence of the defect position on its effects seems related to the fact that despite breaking translation invariance the integrable defect can be shown [73] to conserve the total momentum of the system,

$$P = -\int_{-\infty}^{x_D} u_t u_x - \int_{x_D}^{\infty} v_t v_x + P_D \,, \tag{1.13}$$

with the defect contribution to the momentum being,

$$P_D = -2\left(\sigma - \frac{1}{\sigma}\right) + 2\left(\sigma \cos\frac{u+v}{2} - \frac{1}{\sigma}\cos\frac{u-v}{2}\right)\Big|_{x=x_D} . \tag{1.14}$$

In fact, the conservation of momentum provides an equivalent constraint to the conservation of E_3 and can be used, together with conservation of energy, to derive the defect equations (1.7) in the first place [73].

The integrable defect is also reflectionless in the sense that if one considers a linearised model (i.e. the Klein-Gordon equation instead of sine-Gordon) then a plane wave

$$u = \left(e^{ikx} + Re^{-ikx}\right)e^{-i\omega t} \,, \qquad v = Te^{i(kx-\omega t)} \,, \qquad \omega^2 = 1 + k^2 \,, \tag{1.15}$$

incident on the linearised integrable defect at x_D is purely transmitted so the reflection coefficient $R = 0$ [73]. In fact, it was noted in [78] that the integrable defects considered here appear to provide a classical, Lagrangian description of the purely transmitting defects for the quantum sine-Gordon model that were examined much earlier in [96], although from a very different perspective. Along with being reflectionless, the position independence of the defect is also apparent in this linearised model since the transmission coefficient

$$T = \frac{\sinh\eta + i\cosh\theta}{\cosh\eta - i\sinh\theta} \,, \tag{1.16}$$

depends on $k = \sinh\theta$, $\omega = \cosh\theta$ and $\sigma = \exp(-\eta)$ but not the position of the defect. There would therefore be no way for someone positioned to the left or right of the defect to determine its position by observing the plane wave at their position. The same is true in the full nonlinear picture if an observer to the left of the defect sent a soliton moving right then an observer to the right of the defect could determine the defect parameter based on the delay of the soliton but would be blind to the position of the defect.

An interesting example of position independence and reflectionlessness being linked

appears when one considers the linearisation of the defect

$$u_x = v_t - \sigma \sin\left(\frac{u+v}{2}\right) - \chi \sin\left(\frac{u-v}{2}\right) ,$$
$$v_x = u_t + \sigma \sin\left(\frac{u+v}{2}\right) - \chi \sin\left(\frac{u-v}{2}\right) ,$$

which is integrable for sine-Gordon only when $\chi = 1/\sigma$. For the plane wave (1.15) one finds that

$$R = \frac{e^{2ikx_D}(\sigma\chi - 1)}{1 + k^2 + (k + i\sigma)(k + i\chi)} , \qquad T = \frac{k(i\chi - i\sigma - 2\omega)}{1 + k^2 + (k + i\sigma)(k + i\chi)} . \tag{1.17}$$

Now generally the reflection coefficient $R \neq 0$ and it depends on the position of the defect x_D. An observer to the left of the defect would therefore be able to detect the position of the defect based on the change of phase of the reflected wave. An observer to the right would still be unable to detect the position of the defect since they only perceive the transmitted wave. This is a case where requiring the position independence or the reflectionlessness of the defect are equivalent conditions and both lead to the integrability condition $\chi = 1/\sigma$. Although it will not be attempted here, it would be interesting to see if some more precise statement could be made about position independence and purely transmitting defects or impurities in general.

In summary, the role of the defect, at least for the solutions considered here, appears to be to connect a given field in $x < x_D$ to its Bäcklund transformed field in $x > x_D$ with Bäcklund parameter equal to the defect parameter. This suggests a systematic method of constructing solutions to the defect equations by taking a solution to sine-Gordon on the full line, $u(x,t)$ and performing a Bäcklund transformation to find $v(x,t)$. A field satisfying the defect sewing equations at the point $x = x_D$ and the sine-Gordon equation everywhere else is then simply u for $x < x_D$ and v for $x > x_D$. The application of this idea to algebro-geometric type solutions in the presence a defect will be implemented for sine-Gordon in §4.2 using the method of Darboux transformations.

1.2 Korteweg-de Vries equation

Another example of an integrable model which permits integrable defects is the Korteweg-de Vries (KdV) equation,

$$u_t - 6uu_x + u_{xxx} = 0 . \tag{1.18}$$

The equations describing an integrable defect are written in terms of the potentials p and q where $p_x = u$ and $q_x = v$ are the fields satisfying the KdV equation in the regions $x < x_D$ and $x > x_D$ respectively. Requiring conservation of energy and momentum leads to the defect conditions at $x = x_D$ [75],

$$p_x + q_x = 2\sigma + \frac{1}{2}(p - q)^2 \tag{1.19a}$$
$$p_t + q_t = 2(p_x^2 + p_x q_x + q_x^2) - (p - q)(p_{xx} - q_{xx}) \tag{1.19b}$$
$$p_{xx} + q_{xx} = (p - q)(p_x - q_x) , \tag{1.19c}$$

where $\sigma \in \mathbb{R}$ is again the defect parameter. It is necessary to specify that (1.19c) holds, even though it is the x derivative of (1.19a), since the defect conditions are restricted to the point $x = x_D$ and therefore the x derivatives are frozen.

1.2.1 Phase-shifted soliton solutions

The one soliton solution for KdV is

$$p = p_0 - \frac{2aE_a}{1+E_a} + c_0 x + 3c_0^2 t\,, \qquad E_a = \exp\left[a\left(x - \left(a^2 - 6c_0\right)t - x_a\right)\right]\,, \tag{1.20}$$

which in terms of the original field is

$$u = p_x = -\frac{2a^2 E_a}{(1+E_a)^2} + c_0 = -\frac{a^2}{2}\mathrm{sech}^2\left[\frac{a}{2}\left(x - \left(a^2 - 6c_0\right)t - x_a\right)\right] + c_0\,, \tag{1.21}$$

where p_0, c_0, x_a, a are real constants. The c_0 can be removed since $u \to u - c_0$ together with $(x,t) \to (x - 6c_0 t, t)$ is a symmetry of the KdV equation (2.59) but it will be kept for now.

If the field to the left of the defect is the one soliton solution (1.20) then a possibility for the field to the right of the defect is the phase-shifted one soliton solution [75],

$$q = q_0 - \frac{2a\Delta E_a}{1+\Delta E_a} + c_0 x + 3c_0^2 t\,, \tag{1.22}$$

$$v = q_x = -\frac{2a^2 \Delta E_a}{(1+\Delta E_a)^2} + c_0\,. \tag{1.23}$$

Introducing a new parameter χ such that $\sigma = -\chi^2/4 + c_0$, the defect equations (1.19) imply that,

$$\chi^2 = (p_0 - q_0)^2\,, \qquad \Delta = \frac{p_0 - q_0 - a}{p_0 - q_0 + a} = \frac{|\chi| \mp a}{|\chi| \pm a}\,. \tag{1.24}$$

In [75] the phase shift was just given as $(|\chi| - a)/(|\chi| + a)$ since the positive square root for $p_0 - q_0$ was chosen but either choice is valid from the point of view of the defect equations since only $(p_0 - q_0)^2$ is fixed. It is therefore emphasised here that there are two distinct phase-shifted solutions corresponding to whether $p_0 - q_0 = \pm\,|\chi|$.

Note that the sign of a is unimportant since both the original field (1.21) and the phase shifted field (1.23) are invariant under the transformation $a \to -a$.

If $p_0 - q_0 = |\chi|$ then the soliton is advanced by the defect [1] while if $p_0 - q_0 = -\,|\chi|$ then it is delayed. As noted in [75], if $|\chi| > |a|$ then the soliton remains a soliton but if instead $|\chi| < |a|$ then Δ is negative and the denominator of (1.22) will be zero for some value of x, t so in this case the soliton is transformed by the defect into a travelling singularity. If $|a| = |\chi|$ then, depending on the sign of $p_0 - q_0$, $\Delta = 0$ or $\Delta \to \infty$ but in either case $v = q_x = c_0$ so the soliton is captured by the defect. All these possibilities are demonstrated in Fig. (1.4).

[1] In [75] it was stated that the case $p_0 - q_0 = |\chi|$ corresponds to the incoming soliton being delayed by the defect but it seems this was only meant in the general sense that it experiences a negative delay, i.e. a positive shift forwards compared to the original soliton. To be clear, a 'delayed' soliton in this thesis refers to a negative shift in position from the position the soliton would be in if there were no defect and an 'advanced' soliton refers to a positive shift.

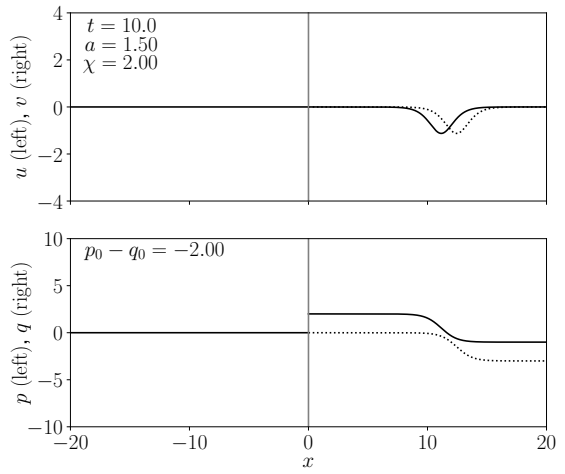

(a) When $|\chi| > |a|$ and $p_0 - q_0 = -|\chi|$ the soliton is delayed.

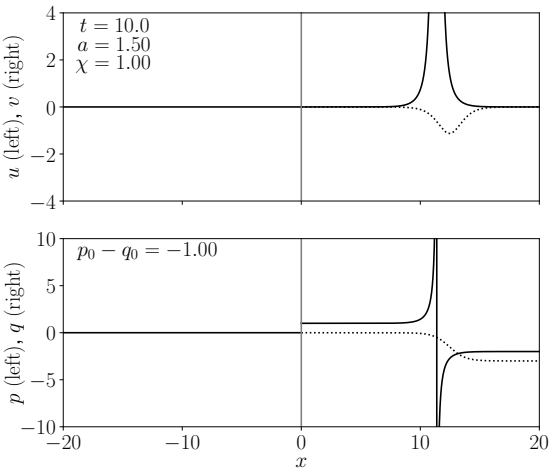

(b) When $|\chi| < |a|$ and $p_0 - q_0 = -|\chi|$ the soliton becomes singular and is delayed.

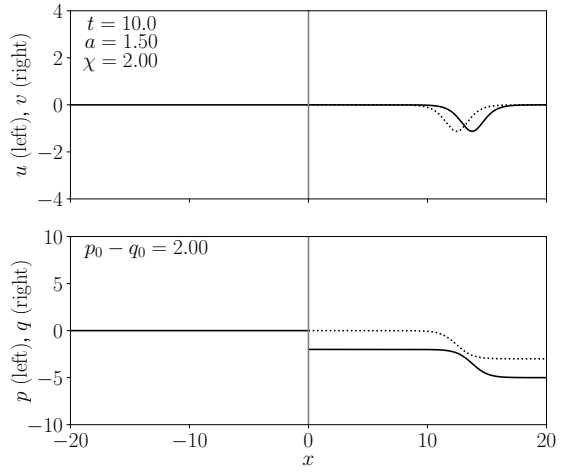

(c) When $|\chi| > |a|$ and $p_0 - q_0 = |\chi|$ the soliton is advanced.

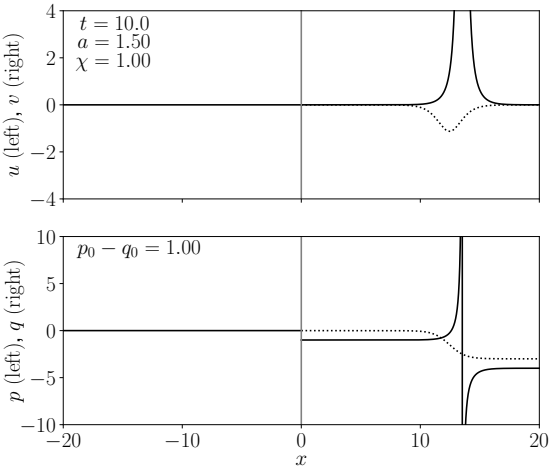

(d) When $|\chi| < |a|$ and $p_0 - q_0 = |\chi|$ the soliton becomes singular and is advanced.

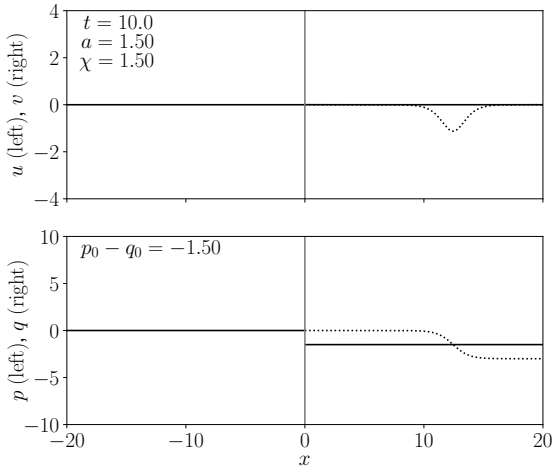

(e) When $|\chi| = |a|$ the soliton is captured.

Figure 1.4: Examples of outcomes for a single KdV soliton (1.21) passing through the type I integrable defect (1.19) placed at $x = 0$ where the field to the right of the defect is the phase-shifted one soliton solution (1.23). In each of these examples the solid line in the lower diagram plots the potentials p, q where $p_0 = 0$ and $c_0 = 0$ have been chosen and the solid line in the upper diagram shows the corresponding fields $u = p_x$ and $v = q_x$. In each case the dotted line in the region $x > 0$ plots the original one soliton potential (1.20) and field (1.21) in the absence of the defect for comparison.

1.2.2 One-to-two soliton solution

In addition to the purely phase-shifted solutions the ability of a defect to capture a soliton coupled with the fact that the defect equations (1.19) are invariant under the exchange of p and q implies that solutions involving soliton creation exist. In particular the one-to-two soliton solution with p given by (1.20) and q by

$$\begin{aligned} q = p_0 - a + \frac{(a^2-\chi^2)(1+E_a-E_\chi-E_aE_\chi)}{(a-\chi)(1+E_aE_\chi)-(a+\chi)(E_a+E_\chi)} + c_0 x + 3c_0^2 t\,, \\ E_\chi = \exp\left[\chi\left(x-(\chi^2-6c_0)t-x_\chi\right)\right]\,, \end{aligned} \tag{1.25}$$

satisfies the defect equations (1.19). This one-to-two soliton solution to the defect equations was considered before in [75] as part of a discussion of the singular solutions to the integrable defect equations. However, it is recognised here that in the limits $x_\chi \to \pm\infty$ the two phase-shifted potentials with $p_0 - q_0 = \mp|\chi|$ are recovered.

The integrable defect (1.19) is constructed to preserve the total energy [75, 91] [2]

$$E = \int_{-\infty}^{x_D}\left[-u^3-\frac{1}{2}u_x^2\right]dx + \int_{x_D}^{\infty}\left[-v^3-\frac{1}{2}v_x^2\right]dx + E_D\,, \tag{1.26a}$$

$$E_D = (p-q)\left[p_x^2+p_xq_x+q_x^2-\sigma(p-q)^2-\frac{3}{20}(p-q)^4\right]\Big|_{x=x_D}\,, \tag{1.26b}$$

and total momentum of the system [75],

$$P = \int_{-\infty}^{x_D}\left[\frac{1}{2}u^2\right]dx + \int_{x_D}^{\infty}\left[\frac{1}{2}v^2\right]dx + P_D\,, \tag{1.27a}$$

$$P_D = \left[-\sigma(p-q)-\frac{1}{12}(p-q)^3\right]\Big|_{x=x_D}\,. \tag{1.27b}$$

One might wonder how these conservation laws allow for a soliton to be emitted by the defect. To avoid issues with infinite energy assume for the moment that $c_0 = 0$. At an initial time ($t \to -\infty$) before the soliton meets the defect one finds that at the defect $p - q = |\chi|$. The energy in the system is then the energy of the soliton $|a|^5/5$ plus the energy in the defect which is $|\chi|^5/10$ (using $\sigma = -\chi^2/4$). In the final configuration ($t \to \infty$) $p - q = -|\chi|$ at the defect and the energy in the system is the energy of the original and emitted solitons $|a|^5/5 + |\chi|^5/5$ plus the energy in the defect which is now $-|\chi|^5/10$. So the energy of the additional soliton is precisely compensated for by the change in the defect energy. Similarly, the momentum stored in the defect is initially $|\chi|^3/6$ and then finally $-|\chi|^3/6$, compensating for the momentum of the emitted soliton, $|\chi|^3/3$.

As was the case for sine-Gordon, the one-to-two soliton solution (1.25) is really a family of solutions parameterised by the initial position of the created soliton x_χ, however, it is possible to pick out particular solutions with additional constraints. This is made easier by noticing that at asymptotic times, when the fields at the defect vanish, (1.19a) implies that $p - q = \pm|\chi|$. Therefore if it is imposed that initially $p - q = -|\chi|$ then the defect energy is already at its asymptotic minimum and cannot compensate for the energy of an additional soliton. This constraint eliminates the possibility of soliton emission and instead picks out the delayed purely phase-shifted solution (1.22) with $p_0 - q_0 = -|\chi|$.

[2] (1.26) has the opposite sign compared to [75, 91]. (6.27) of [91] corrects a sign error in (9.25) of [75].

2 | Algebro-geometric solutions of integrable systems

So far only soliton solutions to the KdV and sine-Gordon equations have been examined but both of these models (and many other integrable systems) allow for more general solutions of algebro-geometric type which will be recalled in this chapter. Some necessary background on the theory of algebraic curves and Riemann surfaces will also be presented in order to state the formulation of these solutions.

2.1 Lax pairs and algebraic curves

This section recalls how algebraic curves appear as the spectral curves of certain integrable systems following [26, 19, 15]. Many integrable systems possess the Lax pair formulation

$$\Psi_x = U\Psi\,, \qquad \Psi_t = V\Psi\,. \tag{2.1}$$

where $\Psi(\lambda, x, t)$ is a matrix valued function and $\lambda \in \mathbb{C}$ the spectral parameter. The evolution equation for the corresponding integrable system is then the compatibility condition

$$U_t - V_x + [U, V] = 0\,.$$

Suppose that there exists a matrix valued function $W(\lambda, x, t)$ which is a rational function of λ such that

$$W_x = [U, W]\,, \qquad W_t = [V, W]\,, \tag{2.2}$$

and consider the eigenvalue problem for W

$$(W(\lambda, x, t) - \mu)h(\mu, \lambda, x, t) = 0\,, \tag{2.3}$$

with eigenvalue μ and eigenfunction h. Abbreviating $(\lambda, \mu) = P$, the function

$$\psi(P, x, t) = \Psi(\lambda, x, t)h(P, 0, 0)\,, \tag{2.4}$$

is simultaneously a solution of the Lax pair and an eigenfunction of W,

$$\psi_x(P, x, t) = U(\lambda, x, t)\psi(P, x, t)\,, \tag{2.5a}$$

$$\psi_t(P, x, t) = V(\lambda, x, t)\psi(P, x, t)\,, \tag{2.5b}$$

$$W(\lambda, x, t)\psi(P, x, t) = \mu\psi(P, x, t)\,. \tag{2.5c}$$

The fact that ψ solves the Lax pair is a direct consequence of (2.1) and the definition of ψ, (2.4). To obtain (2.5c) first note that $W\Psi$ satisfies the Lax pair (2.1),

$$(W\Psi)_x = UW\Psi, \qquad (W\Psi)_t = VW\Psi\,. \tag{2.6}$$

but solutions to the Lax pair are unique up to a choice of normalisation. Indeed, ΨA would also satisfy the Lax pair for any matrix $A(\lambda)$ constant in x and t. Therefore, with the normalisation $\Psi(\lambda, 0, 0) = I$, where I is the identity matrix one finds

$$W(\lambda, x, t)\Psi(\lambda, x, t) = \Psi(\lambda, x, t)W(\lambda, 0, 0)\,. \tag{2.7}$$

This relation together with (2.4) and (2.3) verifies (2.5c) since

$$W(\lambda, x, t)\Psi(\lambda, x, t)h(P, 0, 0) = \Psi(\lambda, x, t)W(\lambda, 0, 0)h(P, 0, 0) = \mu\Psi(\lambda, x, t)h(P, 0, 0)\,.$$

The eigenvalues μ are determined by the characteristic equation of W

$$\mathrm{Det}[W(\lambda, x, t) - I\mu] = 0\,. \tag{2.8}$$

The coefficients of μ in the characteristic equation can always be expressed in terms of $\mathrm{Tr}\,[W^p]^q$ for integer p, q [97, 98] and therefore since

$$\frac{d}{dt}\mathrm{Tr}\left[W^k\right] = \mathrm{Tr}\left[kW_tW^{k-1}\right] = k\mathrm{Tr}\left[VW^k - WVW^{k-1}\right] = 0\,, \quad \frac{d}{dx}\mathrm{Tr}\left[W^k\right] = 0\,,$$

(due to the invariance of the trace under cyclic permutation) the coefficients of the characteristic equation, as well as μ itself, are independent of x, t. The characteristic equation therefore defines an algebraic curve, known as the spectral curve, in $\mathbb{C}^2$,

$$\left\{(\lambda, \mu) \in \mathbb{C}^2 \mid \mathrm{Det}[W(\lambda) - I\mu] = 0\right\}\,. \tag{2.9}$$

If W is an $n \times n$ matrix then this algebraic curve corresponds to an n sheeted Riemann surface. This surface will be the topic of discussion in the next section.

2.2 Algebraic curves and Riemann surfaces

At this point it is convenient to recall some definitions and classical results in the fields of Riemann surfaces and algebraic geometry which will be relevant to the integrable systems considered here.

A *Riemann surface*, R, is a connected one-dimensional complex analytic manifold [99]. This statement deserves some unpacking. Firstly, R is a Hausdorff topological space so for any two distinct points $x, y \in R$ there are two non-intersecting open sets U and V which are neighbourhoods of x and y respectively. The surface R consists of a collection of open sets $\{U_\alpha\}$ which cover the surface so that $R = \cup_\alpha U_\alpha$ where α indexes the set. For each U_α there is a *local parameter* or chart z_α which is a homeomorphism from U_α to an open subset of $\mathbb{C}$. In addition, these local parameters should be compatible which means that

for any two local parameters z_1, z_2 either $U_1 \cap U_2 = \emptyset$ or their transition function,

$$z_2 \circ z_1^{-1} : z_1(U_1 \cap U_2) \to z_2(U_1 \cap U_2)\,, \tag{2.10}$$

is holomorphic [99].

A simple but useful example of a Riemann surface is the graph,

$$G = \{(\lambda, g(\lambda)) \in \mathbb{C}^2 \mid \lambda \in U\}\,, \tag{2.11}$$

of a holomorphic function g defined on an open subset U of the complex plane. This surface consists of a single open set, the whole of G, with the local parameter $\pi_\lambda : G \to U$ which is the projection from $(\lambda, g(\lambda))$ to λ. π_λ is homeomorphic since the inverse $\pi_\lambda^{-1} : U \to G$ is just the map from λ to the ordered set of points $(\lambda, g(\lambda))$.

The Riemann surfaces of particular interest here are defined by algebraic curves. An *algebraic curve* C is a subset of $\mathbb{C}^2$

$$C = \left\{(\lambda, \mu) \in \mathbb{C}^2 \mid \mathcal{P}(\lambda, \mu) = 0\right\}\,, \tag{2.12}$$

where $\mathcal{P}$ is a polynomial in λ and μ with complex coefficients. The polynomial $\mathcal{P}(\lambda, \mu)$ and its locus of roots C is called *irreducible* if $\mathcal{P}$ cannot be written as the product of two non-constant polynomials. An algebraic curve C is called *non-singular* or smooth if the gradient of $\mathcal{P}$ on the curve is non-zero, i.e.

$$\nabla\mathcal{P}|_{\mathcal{P}=0} = \left(\frac{\partial\mathcal{P}}{\partial\mu}, \frac{\partial\mathcal{P}}{\partial\lambda}\right)\Bigg|_{\mathcal{P}(\lambda,\mu)=0} \neq 0\,. \tag{2.13}$$

Non-singular, irreducible algebraic curves are Riemann surfaces [100, 19, 99]. Essentially, this is because non-singular algebraic curves are locally graphs and the irreducibility ensures all these graphs are connected.

To show this more concretely, as in [100] for example, let $p = (\lambda_0, \mu_0)$ be a point on C where $\partial_\mu\mathcal{P} \neq 0$. Then the implicit function theorem for holomorphic functions [100] states that in the neighbourhood of p, U_p, there exists a holomorphic function $g_p(\lambda)$ such that $U_p \cap C$ is the graph $(\lambda, g_p(\lambda))$. If $\partial_\mu\mathcal{P} = 0$ then, since C is non-singular, $\partial_\lambda\mathcal{P} \neq 0$ and the same argument can be applied but with the surface being equivalent locally to the graph $(h_p(\mu), \mu)$. So in either case the surface C is covered by a collection of open sets U_p with the local parameter for each set being the homeomorphic projection π_λ from $(\lambda, g_p(\lambda))$ to λ if $\partial_\mu\mathcal{P}(\lambda_0, \mu_0) \neq 0$ or the projection π_μ from $(h_p(\mu), \mu)$ to μ if otherwise.

It remains to check that any two of these local parameters are compatible. If two of the local parameters are projections to λ then the transition function $\pi_\lambda \circ \pi_\lambda^{-1}$ is the identity which is holomorphic. The same is true if both local parameters are projections to μ. If one local parameter is π_λ and the other π_μ then the transition function $(\pi_\mu \circ \pi_\lambda^{-1})(\lambda)$, defined on the intersection of their domains V, is simply the holomorphic function $g_p(\lambda)$ for some point $p \in V$. Similarly, $(\pi_\lambda \circ \pi_\mu^{-1})(\mu)$ is the holomorphic function $h_p(\mu)$ defined on V.

The final requirement is that C is connected. This could fail to hold if $\mathcal{P}$ was factorizable into two polynomials whose locus of roots is unconnected. For example, if

$\mathcal{P}(\lambda,\mu) = (\mu-\lambda)(\mu-\lambda-1)$ then the resulting surface would be the union of two graphs: $\{(\lambda,\mu)\in\mathbb{C}^2 \mid \mu=\lambda\}$ and $\{(\lambda,\mu)\in\mathbb{C}^2 \mid \mu=\lambda+1\}$. However, these graphs do not intersect so while they are each individually Riemann surfaces their union is not. Requiring $\mathcal{P}$ to be irreducible means that it cannot be factorised as $\mathcal{P}(\lambda,\mu) = \mathcal{Q}(\lambda,\mu)\mathcal{R}(\lambda,\mu)$ where $\mathcal{Q}$ and $\mathcal{R}$ are non-constant polynomials. It can be proved (for example in the book [101]) that requiring $\mathcal{P}$ to be irreducible is sufficient to ensure that C is connected.

2.2.1 Hyperelliptic curves

An important class of algebraic curves (which includes the spectral curves for the sine-Gordon and KdV equations) are of the form

$$C = \left\{ (\lambda,\mu)\in\mathbb{C}^2 \mid \mathcal{P}(\lambda,\mu) = \mu^2 - \prod_{i=1}^{N}(\lambda-\lambda_i) = 0 \right\}, \qquad N\geq 1\,, \tag{2.14}$$

which is known as a rational curve for $N=1$ or 2, an elliptic curve for $N=3$ or 4 and a hyperelliptic curve for $N>4$. This curve is non-singular if all λ_i are distinct. The points where $\partial_\mu\mathcal{P}=0$ are known as *branch points* and in particular $(\lambda_i,0)$ for $i=1,\ldots,N$ are all branch points.

The local parameters for this surface can be constructed in accordance with the general case above. For points in the neighbourhood of (λ_0,μ_0) where $\lambda_0\neq\lambda_i$ then $\partial_\mu\mathcal{P}\neq 0$ so the local parameter is the projection

$$\pi_\lambda :\ (\lambda,\mu)\to\lambda\,, \tag{2.15}$$

with the natural inverse

$$\lambda\to\left(\lambda,\ \sqrt{\prod_{i=1}^{N}(\lambda-\lambda_i)}\right), \tag{2.16}$$

where the branch of the square root is chosen using straight line analytic continuation from (λ_0,μ_0) [15].

At the branch points $(\lambda_i,0)$, $\partial_\mu\mathcal{P}=0$ so in these neighbourhoods the local parameter is the other projection $\pi_\mu:(\lambda,\mu)\to\mu$. It will, however, prove more convenient to have a local parameter expressed in terms of λ, specifically [15]

$$(\lambda,\mu)\to\tau_i=\sqrt{\lambda-\lambda_i}\,, \tag{2.17}$$

where the inverse is given by

$$\tau_i\to\left(\lambda_i+\tau_i^2,\ \tau\sqrt{\prod_{\substack{j=1\\ j\neq i}}^{N}\left(\tau_i^2+\lambda_i-\lambda_j\right)}\right). \tag{2.18}$$

For sufficiently small τ the above square root is a single valued holomorphic function since

expanding around $\tau = 0$ gives

$$\mu = \tau \left(\sqrt{\prod_{\substack{j=1 \\ j\neq i}}^{N} (\lambda_i - \lambda_j)} + O(\tau^2) \right) .$$

Mirroring the construction of the Riemann sphere $\mathbb{C} \cup \infty$ from the complex plane, a Riemann surface can be made into a compact Riemann surface by including points at infinity where $(\lambda \to \infty, \mu \to \infty)$ and introducing compatible local parameters. The situation at infinity for the hyperelliptic curve (2.14) depends on whether N is even, $N = 2g + 2$, or odd, $N = 2g + 1$ where $g \in \mathbb{N}$. Consider the transformation $(\lambda, \mu) \to (l, m)$ where [1]

$$l = \frac{1}{\lambda} , \qquad m = \frac{\mu}{\lambda^{g+1}} , \tag{2.19}$$

from a neighbourhood of infinity on the surface C,

$$U_\infty = \{(\lambda, \mu) \in C \mid \ |\lambda| > c\} ,$$

for some $c > |\lambda_i| , \ i = 1, \ldots, N$ to the corresponding neighbourhood on the transformed surface $\tilde{C}$,

$$V_0 = \{(l, m) \in \tilde{C} \mid 0 < |l| < c^{-1}\} .$$

For $N = 2g + 1$ the curve $\mathcal{P} = 0$ becomes

$$m^2 = l \prod_{i=1}^{2g+1} (1 - l\lambda_i) , \tag{2.20}$$

so that V_0 is the neighbourhood of the point $(l, m) = (0, 0)$. This point is a branch point of the curve (2.20) and therefore the local parameter in this neighbourhood is, according to (2.17), $\sqrt{l}$. For $N = 2g + 2$ the curve $\mathcal{P} = 0$ becomes

$$m^2 = \prod_{i=1}^{2g+2} (1 - l\lambda_i) , \tag{2.21}$$

so V_0 describes the neighbourhoods of two distinct points $(l, m) = (0, \pm 1)$ where in both cases the local parameter is l.

Returning to the original coordinates (λ, μ) the conclusion is, as in [102, 1], that for odd $N = 2g + 1$

$$(\lambda, \mu) \to \infty \iff \lambda \to \infty ,$$

so the hyperelliptic curve C can be compactified to $\hat{C}$ by introducing a single point at ∞

$$\hat{C} = C \cup \{\infty\} , \tag{2.22}$$

and ∞ is a branch point with local parameter

$$(\lambda, \mu) \to \frac{1}{\sqrt{\lambda}} . \tag{2.23}$$

While for even $N = 2g + 2$ there was a point at infinity on each of the two sheets $\infty^{\pm}$

$$(\lambda, \mu) \to \infty^{\pm} \iff \lambda \to \infty\,, \quad \frac{\mu}{\lambda^{g+1}} \to \pm 1\,,$$

so the surface C is compactified to $\hat{C}$ by

$$\hat{C} = C \cup \{\infty^{+}, \infty^{-}\}\,, \tag{2.24}$$

and in the neighbourhood of both infinities, which are not branch points, a local parameter is

$$(\lambda, \mu) \to \frac{1}{\lambda}\,. \tag{2.25}$$

In what follows the Riemann surface of the curve (2.14) will always be considered to be the compactified Riemann surface $\hat{C}$.

Topologically, $\hat{C}$ can be constructed by glueing two copies of the Riemann sphere (the upper and lower sheets) together along the branch cuts which can be chosen as the segments joining the pairs (λ_1, λ_2), …, $(\lambda_{2g+1}, \lambda_{2g+2})$ if $N = 2g + 2$ and (λ_1, λ_2), …, (λ_{2g+1}, ∞) if $N = 2g + 1$. This construction, demonstrated in Fig. (2.1), shows that the compact hyperelliptic Riemann surface is topologically a g-holed torus where the integer $g \geq 0$ is known as the *genus*. More generally, it can be proved that every compact Riemann surface is diffeomorphic to a g-holed torus for a unique value of g [100].

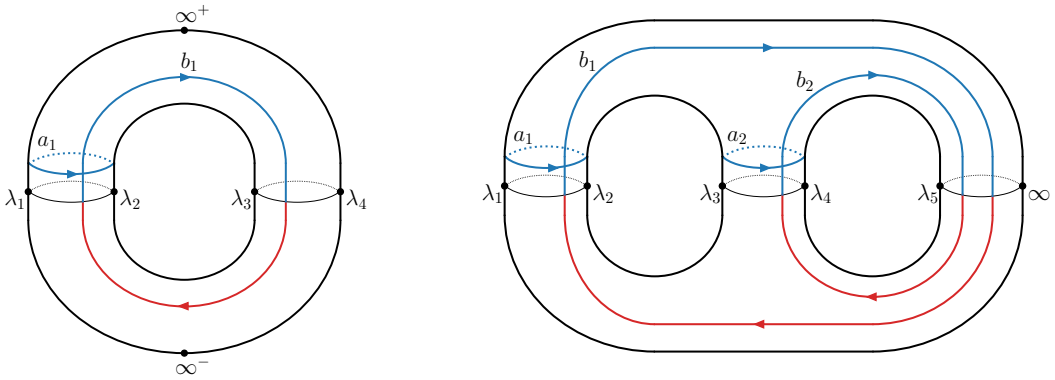

(a) Genus $g = 1$ surface with $N = 2g + 2$.

(b) Genus $g = 2$ surface with $N = 2g + 1$.

Figure 2.1: Examples of hyperelliptic Riemann surfaces whose branch points are $\{\lambda_i\}_{i=1}^{N}$ (and ∞ for (b)) together with a basis of cycles a_i, b_i. The portions of the cycles in blue are on the 'upper' sheet and the portions in red are on the 'lower' sheet.

2.2.2 Basis of cycles

The algebro-geometric solutions of interest in this thesis involve quantities defined in terms of integrals along cycles on the Riemann surface. Following [103], a *cycle* is a closed oriented curve which is either smooth or piecewise-smooth with a finite number of kinks.

The *intersection index*, $\gamma_1 \circ \gamma_2$ of two cycles γ_1 and γ_2 is calculated by assigning to each point where the cycles intersect, P, a number $(\gamma_1 \circ \gamma_2)_P = \pm 1$ depending on whether the frame formed by the tangents $\dot{\gamma}_1$ and $\dot{\gamma}_2$ at the point P is right handed $(+1)$ or left handed

(a) Right-handed intersection: $(\gamma_1 \circ \gamma_2)_P = 1$. (b) Left-handed intersection: $(\gamma_1 \circ \gamma_2)_P = -1$.

Figure 2.2: Intersection numbers at a point of intersection, P.

(-1), as shown in Fig. (2.2). The intersection index is then the sum,

$$\gamma_1 \circ \gamma_2 = \sum_{\substack{P \in \text{points of} \\ \text{intersection}}} (\gamma_1 \circ \gamma_2)_P \, . \tag{2.26}$$

Two oriented curves γ_1, γ_2 are considered *homologous*, $\gamma_1 \sim \gamma_2$, if their difference is the boundary of some oriented two-dimensional domain. As discussed in [103], a consequence of this definition is that if two oriented curves are homotopic (they can be continuously deformed into one another) then they are homologous but the converse is not necessarily true, as demonstrated in Fig. (2.3). This definition also permits an arithmetic of cycles in the sense that a cycle γ may be separated into closed portions γ_1, γ_2 whose sum is homologous to the original cycle $\gamma \sim \gamma_1 + \gamma_2$, as shown in Fig. (2.4). If the sum of cycles is homologous to zero (i.e. their sum is a boundary) $\gamma_1 + \gamma_2 \sim 0$ then it can be said that $\gamma_1 \sim -\gamma_2$. This is consistent with the common notation that if the orientation of a curve γ is reversed then it can be denoted $-\gamma$.

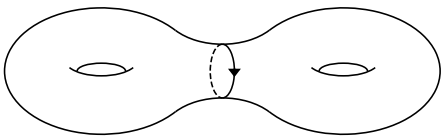

Figure 2.3: This cycle bounds a region of the double torus (half of it in this case) so it is homologous to zero even though it is not homotopic to a point.

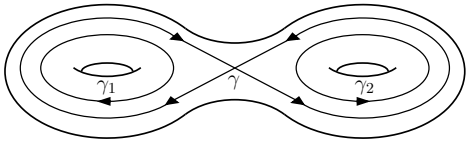

Figure 2.4: Cycles can be divided into closed portions whose sum is homologous to the original cycle: $\gamma \sim \gamma_1 + \gamma_2$.

The classes of homologous cycles on the Riemann surface R form a group of one-dimensional homologies denoted $H_1(R)$. A set of independent cycles $a_1, \ldots, a_g, b_1, \ldots, b_g$ such that

$$a_i \circ a_j = b_i \circ b_j = 0 \, , \qquad a_i \circ b_j = \delta_{ij} \, , \tag{2.27}$$

is a *canonical basis of cycles* for the homology group $H_1(R)$ on a Riemann surface of genus g. That is to say that for any cycle γ on R,

$$\gamma \sim \sum_{i=1}^{g} n_i a_i + \sum_{i=1}^{g} m_i b_i \, , \quad n_i, m_i \in \mathbb{Z} \, ,$$

for some integer n_i, m_i. A canonical basis of cycles for some examples of hyperelliptic

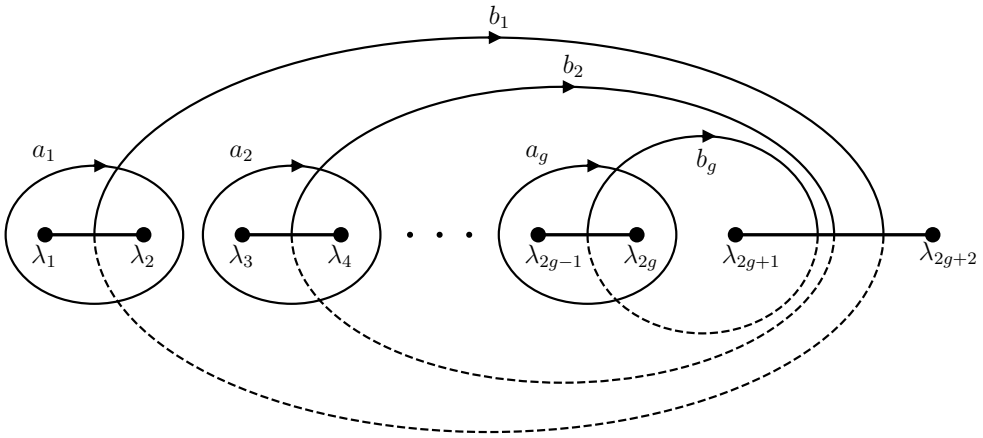

Figure 2.5: A canonical basis of cycles a_i, b_i for a hyperelliptic Riemann surface plotted in the complex plane of λ. The parts of the cycles which are dashed are on the 'lower' sheet of μ and while the solid parts are on the 'upper' sheet.

Riemann surfaces are shown on tori in Fig. (2.1) and plotted in the complex plane of λ in Fig. (2.5).

It is worth noting that the choice of canonical basis is not unique. If the $2g$ dimensional vector of cycles (a, b) is a canonical basis then any other canonical basis, $(\tilde{a}, \tilde{b})$, is given by [99]

$$\begin{pmatrix} \tilde{a} \\ \tilde{b} \end{pmatrix} = M \begin{pmatrix} a \\ b \end{pmatrix}, \quad M \in Sp(g, \mathbb{Z}), \tag{2.28}$$

where M is a $2g \times 2g$ symplectic matrix of integers,

$$Sp(g, \mathbb{Z}) = \left\{ M \in GL(2g, \mathbb{Z}) \mid J = M^T J M \right\}, \qquad J = \begin{pmatrix} 0 & I_g \\ -I_g & 0 \end{pmatrix},$$

and I_g is the $g \times g$ identity matrix.

2.3 Abelian differentials and integrals

Following [99], the differentials and integrals needed to define the algebro-geometric solutions for the KdV and sine-Gordon equations can now be introduced.

The function (0-form) $f(z, \bar{z})$, differential (1-form) $w = p(z, \bar{z})dz + q(z, \bar{z})d\bar{z}$ and 2-form $S = s(z, \bar{z})dz \wedge d\bar{z}$ are defined on the Riemann surface if they are invariant under the coordinate changes given by the transition function (2.10) for each pair of local parameters. The functions $f(z, \bar{z}), p(z, \bar{z}), q(z, \bar{z}), s(z, \bar{z})$ are taken to be smooth and complex valued. The differential operator d transforms k forms to $k + 1$ forms by

$$df = \partial_z f dz + \partial_{\bar{z}} f d\bar{z}, \tag{2.29a}$$

$$dw = (\partial_z q - \partial_{\bar{z}} p) dz \wedge d\bar{z}, \tag{2.29b}$$

$$dS = 0. \tag{2.29c}$$

The exterior product $\wedge$ of two differentials w_1 and w_2 is

$$w_1 \wedge w_2 = (p_1 q_2 - q_1 p_2) dz \wedge d\bar{z} \,. \tag{2.30}$$

The differentials of interest here are *Abelian differentials* which are meromorphic differentials defined on a Riemann surface. The differential w is meromorphic if it can be written in the neighbourhood of any local parameter z as

$$w = f(z) dz \,, \tag{2.31}$$

where $f(z)$ is a meromorphic function. In the neighbourhood of a point P with local parameter z such that $z(P) = 0$ an Abelian differential can be written as the series

$$w = \sum_{k=N(P)}^{\infty} c_k z^k dz \,, \tag{2.32}$$

where $N(P) \in \mathbb{Z}$. Just as in the complex plane, the residue of w at P is

$$\mathrm{res}_P(w) \equiv c_{-1} = \frac{1}{2\pi i} \oint_\gamma w \,, \tag{2.33}$$

where γ is a small positively oriented simple cycle around P. Based on their residues Abelian differentials are categorised into three different 'kinds' [104, 99, 19]:

- *Abelian differentials of the first kind* are holomorphic, i.e. they can be written as $f(z)dz$ for a holomorphic function $f(z)$ and local parameter z.
- *Abelian differentials of the second kind* are meromorphic differentials whose residue at every singular point is equal to zero.
- *Abelian differentials of the third kind* are general meromorphic differentials.

2.3.1 Abelian integrals

Differentials for which $dw = 0$ are called *closed* and holomorphic differentials are closed on the Riemann surface since $\partial_{\bar{z}} f(z) = 0$. The integrals of any closed differential over two homologous paths are equal [99],

$$\int_\gamma w = \int_{\tilde{\gamma}} w \,, \qquad \text{if } \gamma \sim \tilde{\gamma} \text{ and } dw = 0 \,. \tag{2.34}$$

This follows from the definition of homology, that $\gamma - \tilde{\gamma} = \partial D$ where ∂D is the oriented boundary of some oriented two-dimensional domain D, and Stokes' theorem,

$$\iint_D dw = \oint_{\partial D} w \,,$$

which applies for any differential w.

A consequence of this is that, for a Riemann surface R, an *Abelian integral of the first kind*

$$\Omega(P) = \int_{P_0}^{P} w \tag{2.35}$$

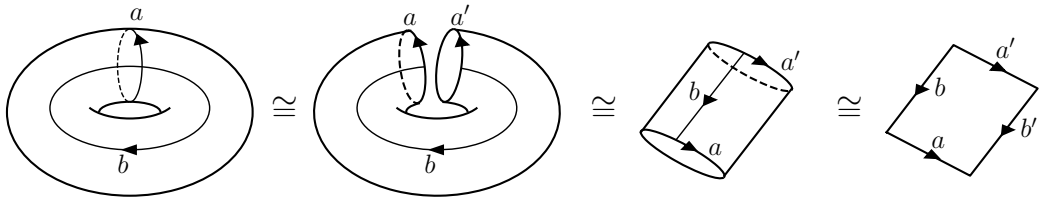

Figure 2.6: Gluing a torus.

for some basis point $P_0 \in R$ is a multivalued function on R but any two of those values for a given P are related by the integral of some closed cycle γ which can written in the basis $\gamma = m_i a_i + n_i b_i$ for some $m, n \in \mathbb{Z}^g$. This is to say that $\Omega(P)$ is only defined on R modulo a linear combination of the *periods* of w,

$$\mathcal{A}_i = \oint_{a_i} w\,, \qquad \mathcal{B}_i = \oint_{b_i} w\,. \tag{2.36}$$

Abelian integrals of the second kind are also valued modulo the $\mathcal{A}$ and $\mathcal{B}$ periods of the corresponding differential since the residues of any singular points are all zero.

For an Abelian differential of the third kind with poles at the points $\{P_j\}$ the corresponding *Abelian integral of the third kind* is valued modulo the $\mathcal{A}$ and $\mathcal{B}$ periods as well as the periods around each of their poles, $2\pi i \operatorname{res}_{P_j}(w)$.

2.3.2 Riemann's bilinear identity

The period integrals $\mathcal{A}_i$, $\mathcal{B}_i$ and $\tilde{\mathcal{A}}_i$, $\tilde{\mathcal{B}}_i$ of a closed differential w and a closed or Abelian differential $\widetilde{w}$ (without poles on any of the a_i or b_i cycles) are related by the very useful *Riemann Bilinear identity* [100],

$$\int_{\partial \mathring{R}} \widetilde{w}(P) \int_{P_0}^{P} w = \sum_{j=1}^{g} \left(\mathcal{A}_j \widetilde{\mathcal{B}}_j - \widetilde{\mathcal{A}}_j \mathcal{B}_j \right) \tag{2.37}$$

where $\mathring{R}$ is the simply connected surface obtained by removing all the a_i and b_i cycles from the Riemann surface R. The positively oriented boundary of this region is

$$\partial \mathring{R} = \sum_{i=1}^{g} a_i + b_i - a_i' - b_i' \tag{2.38}$$

where a_i' and b_i' are identified on R with a_i and b_i respectively, as illustrated in Fig. (2.6).

This can be proved [100] by first considering two points P_j, P_j' which lie on a_j and a_j' respectively but coincide on R. This means that, since $\tilde{w}$ is defined on R,

$$\tilde{w}(P_j) = \tilde{w}(P_j')\,.$$

On R the path from P_j to P_j' is closed and homotopic to the cycle b_i, as illustrated in

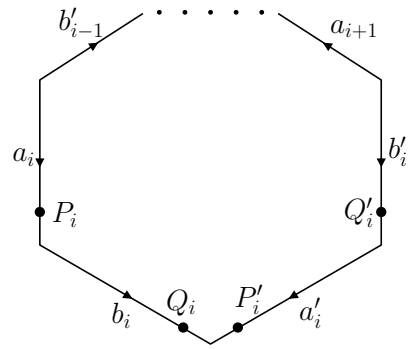

Figure 2.7: Illustration for the proof of the Riemann bilinear identity.

Fig. (2.7), and since w is closed the integral,

$$W(P) = \int_{P_0}^{P} w\,,$$

obeys the relation,

$$W(P'_j) - W(P_j) = \int_{P_j}^{P'_j} w = \mathcal{B}_j\,.$$

The same consideration for two points Q_j, Q'_j lying on b_j and b'_j which coincide on R gives

$$\tilde{w}(Q_j) = \tilde{w}(Q'_j)\,, \qquad W(Q'_j) - W(Q_j) = -\mathcal{A}_j\,.$$

So now evaluating the left hand side of (2.37) gives

$$\begin{aligned}\int_{\partial \mathring{R}} \tilde{w}W &= \sum_{i=1}^{g}\left(\int_{q\in b_i}\tilde{w}(q)W(q) - \int_{q'\in b'_i}\tilde{w}(q')W(q') + \int_{p\in a_i}\tilde{w}(p)W(p) - \int_{p'\in a'_i}\tilde{w}(p')W(p')\right)\\ &= \sum_{i=1}^{g}\left(\int_{q\in b_i}\tilde{w}(q)\mathcal{A}_i - \int_{p\in a_i}\tilde{w}(p)\mathcal{B}_i\right)\\ &= \sum_{i=1}^{g}\left(\widetilde{\mathcal{B}}_i\mathcal{A}_i - \widetilde{\mathcal{A}}_i\mathcal{B}_i\right)\,.\end{aligned}$$

2.3.3 Basis of Abelian differentials

The description for the basis of Abelian differentials on a compact Riemann surface R is based on the *residue theorem*,

$$\sum_{P\in\text{poles of } w} \text{res}_P(w) = 0\,, \tag{2.39}$$

for any Abelian differential w. This can be proved [100] using the expression (2.33) for the residue at the pole P_i as an integral around γ_i which is the positively oriented boundary of the neighbourhood U_i. Let $D = R\backslash\{U_i\}$ then $\partial D = -\sum_i \gamma_i$ and

$$\sum_i \text{res}_{P_i}(w) = \frac{1}{2\pi i}\sum_i \oint_{\gamma_i} w = -\frac{1}{2\pi i}\int_{\partial D} w = 0\,,$$

since w is holomorphic in D. The residue theorem implies that any meromorphic differential can be represented as a linear combination of [99]:

- Differentials of the first kind (holomorphic).
- Differentials of the second kind with one singularity at the point p of order $N+1$ denoted by $\omega_p^{(N)}$. In the neighbourhood of p

$$\omega_p^{(N)} = \left(\frac{1}{z_p^{N+1}} + O(1) \right) dz_p \,, \quad N \geq 1 \,, \tag{2.40}$$

  with local parameter $z_p(P)$ chosen so that $z_p(p) = 0$.
- Differentials of the third kind, denoted ω_{p-q}, with simple poles at p and q with residues $+1$ and -1 respectively. In the neighbourhoods of p, q

$$\omega_{p-q} = \left(\frac{1}{z_p} + O(1) \right) dz_p \qquad \text{near p} \tag{2.41a}$$

$$\omega_{p-q} = \left(-\frac{1}{z_q} + O(1) \right) dz_q \qquad \text{near q} \tag{2.41b}$$

2.3.4 Normalised basis of holomorphic differentials

For a compact Riemann surface the dimension of the space of holomorphic differentials (Abelian differentials of the first kind) is equal to its genus [105]. In particular, for a hyperelliptic Riemann surface the basis of holomorphic differentials is [104]

$$\eta_j = \frac{\lambda^{j-1}}{\mu} d\lambda \,, \quad j = 1, \ldots, g \,. \tag{2.42}$$

The *normalised basis of holomorphic differentials* is $\omega_j = C_{jk}\eta_k$ where the coefficients C_{jk} are defined by the normalisation condition

$$\oint_{a_i} \omega_j = 2\pi i \delta_{ij} \,. \tag{2.43}$$

The *Riemann matrix*,

$$B_{ij} = \oint_{b_i} \omega_j \,, \tag{2.44}$$

is a symmetric $g \times g$ matrix whose real part is strictly negative.

The symmetry of B follows from the Riemann bilinear identity (2.37) when $w = \omega_i$ and $\tilde{w} = \omega_j$ [100]. In this case the left hand side of (2.37) vanishes as the contour integral of a holomorphic differential leaving,

$$0 = \sum_{k=1}^{g} 2\pi i \left(\delta_{ki} B_{kj} - \delta_{kj} B_{ki} \right) = 2\pi i \left(B_{ij} - B_{ji} \right) \,.$$

The restriction $\mathrm{Re}[B] < 0$ can also be obtained from (2.37) but with $w = \omega$ and $\widetilde{w} = \overline{\omega} = \overline{f(z)} d\bar{z}$ [100]. To see this it is convenient to rewrite the left hand side of (2.37) as

$$\int_{\partial \mathring{R}} \overline{\omega} \Omega = \iint_{\mathring{R}} d\left(\overline{\omega} \Omega \right) = \iint_{\mathring{R}} d\Omega \wedge \overline{\omega} + \Omega d\overline{\omega} = \iint_{\mathring{R}} \omega \wedge \overline{\omega} \,, \qquad \Omega(P) = \int_{P_0}^{P} \omega \,,$$

where the first equality uses Stokes' theorem, the second follows from the definitions of the differential operator (2.29) and exterior product (2.30) and the last equality holds since $\overline{\omega}$ is closed. So the Riemann bilinear identity in this case reads

$$\iint_R iw \wedge \overline{w} = -2\pi \sum_{j=1}^{g} \left(\delta_{ji}\overline{B}_{jk} + \delta_{ji}B_{jk}\right) = -4\pi \mathrm{Re}\, B$$

while calculating the exterior product explicitly gives

$$\iint_R i\omega \wedge \overline{\omega} = \iint_R i|f|^2 dz \wedge d\bar{z} = \iint_R 2|f|^2 dx \wedge dy \geq 0$$

where $dz = dx + idy$ and $d\bar{z} = dx - idy$, and where equality is achieved if and only if $w \equiv 0$. Therefore, assuming $w \not\equiv 0$, $\mathrm{Re}[B] < 0$.

2.3.5 Normalised differentials of the second and third kind

Abelian differentials of the second, $\omega_p^{(N)}$, or third kind, ω_{p-q}, are normalised by requiring that their $a-$periods are zero,

$$\oint_{a_i} \omega_p^{(N)} = 0\,, \qquad \oint_{a_i} \omega_{p-q} = 0\,, \qquad \forall\, a_i\,. \tag{2.45}$$

An unnormalised Abelian differential of the second or third kind can be normalised by adding a suitable linear combination of holomorphic differentials.

The b period of a normalised Abelian differential of the second kind can be related to the normalised holomorphic differentials, ω, using the Riemann bilinear identity (2.37) with $w = \omega$ and $\widetilde{w} = \omega_p^{(N)}$ [19]. Let $\Omega(P)$ be the normalised integral of the first kind. Then, since $\omega_p^{(N)}$ is holomorphic on R except at p,

$$\int_{\partial \mathring{R}} \omega_p^{(N)}\Omega = \oint_{\gamma_p} \Omega \frac{dz_p}{z_p^{N+1}} = \frac{2\pi i}{N!}\,\frac{d^N}{dz_p^N}\Omega(z_p)\bigg|_{z_p=0} = \frac{2\pi i}{N!}\,\frac{d^{N-1}}{dz_p^{N-1}}\omega(z_p)\bigg|_{z_p=0}\,,$$

where γ_p is a small positively oriented cycle bounding the neighbourhood of p. So, by the Riemann bilinear identity,

$$\oint_{b_i} \omega_p^{(N)} = \frac{1}{N!}\,\frac{d^{N-1}}{dz_p^{N-1}}\omega(z_p)\bigg|_{z_p=0}\,. \tag{2.46}$$

For defining differentials of the second and third kinds it is helpful to note that, given a finite set of points P_i on the Riemann surface R, there exists an Abelian differential which is holomorphic on $R\backslash P_i$ with poles at P_i whose principle parts can be arbitrarily chosen except for the necessity to satisfy the residue theorem (2.39) [19]. A normalised Abelian differential is uniquely determined by its poles and principal parts [105].

2.4 Theta functions

The algebro-geometric solutions and the corresponding Lax pair eigenfunctions for integrable systems are written in terms of *Riemann theta functions*,

$$\theta(z,B)=\sum_{n\in\mathbb{Z}^g} e^{\frac{1}{2}n\cdot Bn+n\cdot z}\,,\quad z\in\mathbb{C}^g\,, \tag{2.47}$$

where B is the Riemann matrix (2.44) associated with the Riemann surface R and $g\geq 1$ is the genus of R. Theta functions are quasi-periodic in the sense that

$$\theta(z+2\pi ip+Bq,B)=e^{-\frac{1}{2}q\cdot Bq-q\cdot z}\theta(z,B)\,,\qquad p,q\in\mathbb{Z}^g. \tag{2.48}$$

In this thesis the theta function will often be abbreviated to $\theta(z)\equiv\theta(z,B)$.

2.4.1 Abel map, divisors, and the Jacobi inversion problem

Let Λ be the lattice generated by the periods of the normalised holomorphic differential,

$$\Lambda=\{2\pi ip+Bq,\ p,q\in\mathbb{Z}^g\}\,, \tag{2.49}$$

then the Jacobian of the Riemann surface R of genus g is $\mathrm{Jac}(R)=\mathbb{C}^g/\Lambda$. The normalised Abelian integral of the first kind modulo Λ is called the *Abel map*,

$$A\,:\,R\to\mathrm{Jac}(R)\,,\qquad A(P)=\int_{P_0}^{P}\omega\ \in\mathrm{Jac}(R)\,. \tag{2.50}$$

The domain of the Abel map can be naturally extended to act on a formal sum of points known as a *divisor*, $\mathcal{D}$, by

$$A(\mathcal{D})=\sum_{j=1}^{N}n_jA(P_j)\,,\qquad \mathcal{D}=\sum_{j=1}^{N}n_jP_j\,,\qquad n_j\in\mathbb{Z}\,,\quad P_j\in R\,, \tag{2.51}$$

For a function f with $P_1,\ldots,P_n$ zeros with multiplicities $p_1,\ldots,p_n$ and $Q_1,\ldots,Q_m$ poles of order $q_1,\ldots,q_m$ its divisor, $\mathrm{div}(f)$, is defined as

$$\mathrm{div}(f)=\sum_{i=1}^{n}p_iP_i-\sum_{i=1}^{m}q_iQ_i\,. \tag{2.52}$$

A divisor is called positive, $\mathcal{D}\geq 0$, if all the multiplicities $n_j\geq 0$. For a hyperelliptic Riemann surface a positive divisor is called *special* if it contains two or more points on different sheets but with the same projection into the complex λ plane [106].

The *Jacobi inversion problem* is the problem of inverting the Abel map, i.e. for a given $\xi\in\mathrm{Jac}(R)$ find the points $P_1,\ldots,P_g\in R$ such that

$$\sum_{k=1}^{g}\int_{P_0}^{P_k}\omega_j=\xi_j\,,\quad j=1,\ldots,g\,. \tag{2.53}$$

The solution to this problem involves the vector of Riemann constants, $K \in \mathbb{C}^g$, where [19]

$$K_j = \frac{2\pi i + B_{jj}}{2} - \frac{1}{2\pi i} \sum_{k \neq j} \oint_{a_k} \left(\omega_k(P) \int_{P_0}^{P} \omega_l \right) , \tag{2.54}$$

as well as the function

$$F(P) = \theta \left(\int_{P_0}^{P} \omega - \xi - K \right) . \tag{2.55}$$

Provided that ξ is such that $F(P) \not\equiv 0$ then $F(P)$ has precisely g zeros, $P_1, \ldots, P_g$, which provide the unique solution to the Jacobi inversion problem (2.53) [105]. However, $F(P) \equiv 0$ if and only if the divisor $\mathcal{D} = P_1 + \cdots + P_g$ is special [107, 105]. An important corollary is therefore that if the divisor $\mathcal{D} = P_1 + \cdots + P_g$ is non-special then the function

$$F(P) = \theta \left(\int_{P_0}^{P} \omega - A(\mathcal{D}) - K \right) , \tag{2.56}$$

has precisely g zeros, $P_1, \ldots, P_g$, on the Riemann surface R [105, 19].

2.5 Baker-Akhiezer functions

The Lax pair eigenfunctions corresponding to algebro-geometric solutions for integrable systems can now be defined as Baker-Akhiezer functions [16, 17]. Following the exposition of [105, 19], first choose:

- A compact Riemann surface R of genus g.
- A finite set of points $Q_1, \ldots, Q_n$ on R.
- A local parameter z_j for each Q_j where the inverse $k_j = 1/z_j$ is such that $k_j(Q_j) = \infty$.
- A polynomial, $q_j(k_j)$, in k_j for each Q_j.
- A positive, non-special divisor $\mathcal{D} = P_1 + \cdots + P_g > 0$ on $R \backslash \{Q_j\}$.

Then a Baker-Akhiezer function, $\psi(P)$, satisfies the following properties:

(i) $\psi(P)$ is a meromorphic function on $R \backslash \{Q_j\}$ with poles only at the points $P_1, \ldots, P_g$ of the divisor $\mathcal{D}$, specifically $\mathrm{div}(\psi|_{R\backslash\{Q_j\}}) + \mathcal{D} \geq 0$.

(ii) At Q_j the function $\psi(P)$ is singular but $\psi(P) \exp(-q_j(k_j(P)))$ is analytic in the neighbourhood of Q_j.

The above conditions uniquely define the Baker-Akhiezer function up to a multiplicative constant [105].

To construct the Baker-Akhiezer function explicitly, introduce the normalised Abelian integral of the second kind $\Omega(P)$ obeying

$$\Omega(P) \to q_j(k_j(P)) \quad \text{as} \quad P \to Q_j \, , \tag{2.57}$$

together with the corresponding b-period, $V_i = \oint_{b_i} d\Omega$, $i = 1, \ldots, g$. Then with an arbitrary choice of basis point $P_0 \neq Q_i$ the Baker-Akhiezer function up to a multiplicative constant

is [19, 105]

$$\psi(P) = e^{\Omega(P)} \frac{\theta\left(\int_{P_0}^{P} \omega - D + V\right)}{\theta\left(\int_{P_0}^{P} \omega - D\right)}\,, \tag{2.58}$$

where $D = K + A(\mathcal{D})$, K is the vector of Riemann constants (2.54) and $A(P)$ the Abel map (2.51) with basis point P_0. In practice, D can be chosen directly as an arbitrary complex vector since for any $D \in \mathbb{C}^g$ a divisor $\mathcal{D}$ can be found to satisfy $D = K + A(\mathcal{D})$ [42].

It is worth briefly motivating the form of (2.58). The exponential term in (2.58) ensures the correct asymptotic form near the singularities Q_i while, from §2.4.1, the zeros of $\theta(\int_{P_0}^{P} \omega - D)$ (and hence the poles of $\psi(P)$ on $R\backslash\{Q_j\}$) are precisely $P_1, \ldots, P_g$. The theta function in the numerator ensures that $\psi(P)$ is single valued on R since if M_γ is the monodromy operator which adds a cycle $\gamma = \sum_i n_i a_i + m_i b_i$ to the integration path $\int_{P_0}^{P}$ then,

$$\begin{aligned} M_\gamma \psi(P) &= e^{\Omega(P)+Vm} \frac{\theta\left(\int_{P_0}^{P} \omega + 2\pi i n + Bm - D + V\right)}{\theta\left(\int_{P_0}^{P} \omega + 2\pi i n + Bm - D\right)} \\ &= e^{\Omega(P)+Vm} \frac{\theta\left(\int_{P_0}^{P} \omega - D + V\right) e^{-\frac{1}{2} m\cdot Bm - m\cdot(\int_{P_0}^{P} \omega - D + V)}}{\theta\left(\int_{P_0}^{P} \omega - D\right) e^{-\frac{1}{2} m\cdot Bm - m\cdot(\int_{P_0}^{P} \omega - D)}} = \psi(P)\,. \end{aligned}$$

2.6 Algebro-geometric solutions for KdV

The Korteweg-de Vries (KdV) equation,

$$u_t - 6uu_x + u_{xxx} = 0\,, \tag{2.59}$$

is the compatibility condition of the Lax pair,

$$\psi_{xx} = (u - \lambda)\psi\,, \tag{2.60a}$$

$$\psi_t = (2u + 4\lambda)\psi_x - u_x\psi\,, \tag{2.60b}$$

with eigenfunction $\psi(x, t, \lambda)$ and spectral parameter $\lambda \in \mathbb{C}$.

To indicate how the algebraic curve corresponding to the algebro-geometric solutions of the KdV equation appears it is convenient to instead rewrite the Lax pair equations as

$$\phi_x = U\phi\,, \qquad \phi_t = V\phi\,, \tag{2.61}$$

where

$$\phi = \begin{pmatrix} \psi \\ \psi_x \end{pmatrix},\ U = \begin{pmatrix} 0 & 1 \\ u - \lambda & 0 \end{pmatrix},\ V = \begin{pmatrix} -u_x & 4\lambda + 2u \\ (4\lambda + 2u)(u - \lambda) - u_{xx} & u_x \end{pmatrix} \tag{2.62}$$

so that the compatibility condition,

$$U_t - V_x + [U, V] = 0\,, \tag{2.63}$$

is the KdV equation.

Following the discussion in §2.1 the algebraic curve will be the characteristic equation of the matrix W satisfying

$$W_x = [U, W]\,, \qquad W_t = [V, W]\,. \tag{2.64}$$

It turns out that W can be constructed from the Lax matrices corresponding to the stationary equations of the KdV hierarchy [8, 103, 15]. As in, for example, [15] the n^{th} equation in the KdV hierarchy can be written as

$$\text{KdV}_n: \quad \partial_{t_n} u = 2\partial_x f_{n+1} \tag{2.65}$$

where t_n is the n^{th} 'higher time' coordinate and the functions f_n of the field u and its x derivatives satisfy the recursion relations

$$f_0 = 1\,, \qquad \partial_x f_{n+1} = -\frac{1}{4}\partial_x^3 f_n + u\partial_x f_n + \frac{1}{2}\partial_x u f_n\,. \tag{2.66}$$

The first few equations in the the KdV hierarchy are then

$$\begin{aligned}
&\text{KdV}_0: \quad u_{t_0} = u_x \\
&\text{KdV}_1: \quad u_{t_1} = -\frac{1}{4}u_{xxx} + \frac{3}{2}uu_x + c_1 u_x \\
&\text{KdV}_2: \quad u_{t_2} = \frac{1}{16}u_{xxxxx} - \frac{5}{8}uu_{xx} - \frac{5}{4}u_x u_{xx} + \frac{15}{8}u^2 u_x + c_1\left(-\frac{1}{4}u_{xxx} + \frac{3}{2}uu_x\right) + c_2 u_x
\end{aligned}$$

where c_i are integration constants. These equations can also be represented as

$$\text{KdV}_n: \quad \partial_{t_n} U - \partial_x V^{[n]} + [U, V^{[n]}] = 0 \tag{2.67}$$

where

$$V^{[n]} = \begin{pmatrix} -\frac{1}{2}\partial_x F_n & F_n \\ (u-\lambda)F_n - \frac{1}{2}\partial_x^2 F_n & \frac{1}{2}\partial_x F_n \end{pmatrix}, \qquad F_n = \sum_{k=0}^{n} f_{n-k}\lambda^k\,. \tag{2.68}$$

The KdV equation (2.59) is KdV_1 where $c_1 = 0$ and $t_1 \equiv 4t$ so that $u_t \equiv 4u_{t_1}$. The corresponding U and V from (2.62) are $V^{[0]}$ and $4V^{[1]}\big|_{c_1=0}$ respectively.

It was shown in [8, 9] (see also the account of [14] and the references therein) that the finite-gap solutions to the KdV equation (or any other equation in the KdV hierarchy) are solutions of the stationary KdV hierarchy. Therefore, the sought algebro-geometric solutions to the KdV equation satisfy

$$U_t - V_x + [U, V] = 0 \tag{2.69}$$

$$-V_x^{[n]} + \left[U, V^{[n]}\right] = 0 \tag{2.70}$$

for some choice of n and constants $\{c_i\}_{i=1}^n$. From here it can also be shown that [15]

$$-V_t^{[n]} + \left[V, V^{[n]}\right] = 0 \tag{2.71}$$

and so $V^{[n]}$ is the required matrix W which satisfies (2.64). The characteristic equation of

$V^{[n]}$ is therefore independent of (x,t) and has the form (since $V^{[n]}$ is traceless)

$$0 = \mathrm{Det}[V^{[n]}(\lambda) - Ii\mu] = -\mu^2 + \mathrm{Det}[V^{[n]}(\lambda)] \tag{2.72}$$

where $i\mu$ are the eigenvalues of $V^{[n]}$ and $\mathrm{Det}[V^{[n]}(\lambda)]$ is a monic polynomial of order $2n+1$.

For example, in the $n=1$ case one finds

$$\mu^2 = \lambda^3 + 2c_1\lambda^2 + \lambda\left(c_1^2 - c_1 u - \frac{3}{4}u^2 + \frac{1}{4}u_{xx}\right) + \frac{1}{16}\left((4c_1+2u)(u_{xx} - 4c_1u - 2u^2) - u_x^2\right).$$

The stationary KdV_1 equation $0 = -u_{xxx} + 6uu_x + 4c_1u_x$ which u satisfies can be integrated once to give $A = -u_{xx} + 3u^2 + 4c_1u$ and again to give $Au + B = -\frac{1}{2}u_x^2 + u^3 + 2c_1u^2$ for some constants A, B. The characteristic equation is therefore

$$\mu^2 = \lambda^3 + 2c_1\lambda^2 + \left(c_1^2 - \frac{A}{4}\right)\lambda + \frac{1}{8}\left(B - 2Ac_1\right) \tag{2.73}$$

which defines a genus 1 curve where the constants $A, B, c_1 \in \mathbb{R}$ if $u \in \mathbb{R}$.

For general n the corresponding spectral curve is a hyperelliptic curve of the form

$$\mu^2 = \prod_{i=1}^{2g+1}(\lambda - \lambda_i) \tag{2.74}$$

where n is identified as the genus g of the corresponding compactified Riemann surface and the branch points λ_i are real constants which for convenience will be ordered

$$\lambda_1 < \lambda_2 < \cdots < \lambda_{2g+1}\,.$$

Returning to the scalar Lax pair (2.60), the corresponding eigenfunction can now be constructed as a Baker-Akhiezer function defined on the compact Riemann surface corresponding to the curve (2.74). It will be assumed and later checked that the Baker-Akhiezer function satisfying (2.60) has an essential singularity only at the point ∞, which is a branch point of (2.74), and the asymptotic expansion around this point is [41, 108, 105, 19]

$$\psi(x,t,P) = \left(1 + \sum_{n=1}^{\infty}\xi_n(x,t)k^{-n}\right)e^{ikx+4ik^3t}\,, \tag{2.75}$$

where $k^{-1} = 1/\sqrt{\lambda}$ is the local parameter in the neighbourhood of infinity. Then, as in §2.5, introduce the normalised Abelian differentials of the second kind Ω_1 and Ω_3 defined by their asymptotic properties in the neighbourhood of ∞,

$$\Omega_1 \to k - \frac{c_1}{k} + O(k^{-2})\,, \qquad \Omega_3 \to k^3 - \frac{c_3}{k} + O(k^{-2})\,, \tag{2.76}$$

where c_1 and c_3 are determined by the choice of Riemann surface and local parameter k^{-1}. The corresponding $b-$periods are $U_i = \oint_{b_i} d\Omega_1$ and $W_i = \oint_{b_i} d\Omega_3$. For a particular choice of $D \in \mathbb{C}^g$, the Baker-Akhiezer function is then uniquely (since (2.75) provides a

normalisation) constructed as

$$\psi(P) = \frac{\theta\left(\int_\infty^P \omega + iUx + 4iWt - D\right)\theta(D)}{\theta\left(\int_\infty^P \omega - D\right)\theta(iUx + 4iWt - D)} e^{i\Omega_1(P)x + 4i\Omega_3(P)t}\,. \tag{2.77}$$

where the basis point P_0 of the integral of the first kind is chosen to be at ∞.

As in [41, 108, 105, 19], the uniqueness theorem for Baker-Akhiezer functions stated in §2.5 can be used to check that ψ satisfies the Lax pair and to derive the field u which solves the KdV equation. The function $(\partial_{xx} + \lambda)\psi(P)$ is a Baker-Akhiezer function satisfying the same analytic properties (i) and (ii), given in §2.5, as ψ except that the form of its singularity at ∞,

$$(\partial_{xx} + \lambda)\psi(P) = \left(2i\partial_x\xi_1 + O\left(k^{-1}\right)\right) e^{ikx + 4ik^3t}\,, \tag{2.78}$$

has a different normalisation than (2.75). So by the uniqueness of Baker-Akhiezer functions,

$$(\partial_{xx} + \lambda)\psi = 2i(\partial_x\xi_1)\psi \equiv u\psi\,, \tag{2.79}$$

which is the first Lax equation (2.60a). The second Lax equation (2.60b) can also be checked similarly. Using $u = 2i\partial_x\xi$, in the neighbourhood of ∞

$$\left(\partial_t - (2u + 4\lambda)\partial_x\right)\psi(P) = \left(4\xi_1\partial_x\xi_1 - 4\partial_x\xi_2 + O\left(k^{-1}\right)\right) e^{ikx + 4ik^3t} \tag{2.80}$$

but the $O(k^{-1})$ term in the expansion of $(\partial_{xx} + \lambda - u)\psi(P)$ at ∞ gives

$$4\xi_1\partial_x\xi_1 - 4\partial_x\xi_2 = -2i\partial_{xx}\xi_1 \tag{2.81}$$

and therefore

$$\left(\partial_t - (2u + 4\lambda)\partial_x\right)\psi = -2i(\partial_{xx}\xi_1)\psi \equiv -u_x\psi\,, \tag{2.82}$$

as required.

It will also be useful to obtain the solution to the potential KdV equation

$$p_t - 3p_x^2 + p_{xxx} = 0 \tag{2.83}$$

which becomes the KdV equation after differentiating and setting $p_x = u$. Comparing the asymptotic expansions at ∞ of $(\partial_{xx} + \lambda)\psi$ and $u\psi$ at orders $O(k^{-1})$ and $O(k^{-2})$ one finds

$$\partial_x\xi_2 = \frac{1}{2}\partial_x\left(\xi_1^2 + i\partial_x\xi_1\right)\,, \tag{2.84}$$

$$\partial_x\xi_3 = \xi_2\partial_x\xi_1 + \frac{i}{2}\partial_{xx}\xi_2\,, \tag{2.85}$$

and then the $O(k^{-1})$ term in the expansion of $\psi_t - (2u + 4\lambda)\psi_x + u_x\psi$ at ∞ implies that

$$\partial_t\xi_1 - 6i(\partial_x\xi_1)^2 + \partial_{xxx}\xi_1 = 0\,, \tag{2.86}$$

which is precisely the potential KdV equation (2.83) with $p = 2i\xi_1$.

All that remains is to explicitly compute ξ_1. Comparing the expansion of $\log(\psi)$ in k^{-1}

at ∞ for the explicit expression (2.77) with the asymptotic form (2.75) gives

$$\begin{aligned}\log(\psi) = k^{-1}\frac{\partial}{\partial k^{-1}}\left[\log\left(\frac{\theta\left(\int_\infty^P\omega + iUx + 4iWt - D\right)\theta(D)}{\theta\left(\int_\infty^P\omega - D\right)\theta(iUx + 4iWt - D)}\right)\right]\Bigg|_{k^{-1}=0}\\ + i\left(k - \frac{c_1}{k}\right)x + 4i\left(k^3 - \frac{c_3}{k}\right)t + O(k^{-2})\\ = \frac{\xi_1}{k} + ikx + 4ik^3t + O(k^{-2})\end{aligned}$$

and therefore

$$\xi_1 = \frac{\partial}{\partial k^{-1}}\left[\log\theta\left(\int_\infty^P\omega + iUx + 4iWt - D\right) - \log\theta\left(\int_\infty^P\omega - D\right)\right]\Bigg|_{k^{-1}=0} - ic_1x - 4ic_3t\,.$$

A constant in x, t can be subtracted from p while maintaining the potential KdV equation (2.83) so p can be taken to be

$$p = 2i\,\frac{\partial}{\partial k^{-1}}\left[\log\theta\left(\int_\infty^P\omega + iUx + 4iWt - D\right)\right]\Bigg|_{k^{-1}=0} + 2c_1x + 8c_3t\,. \tag{2.87}$$

The $\partial_{k^{-1}}$ can now be rewritten by noting that the integral of the first kind $\int_\infty^P\omega$ in the neighbourhood of ∞ with local parameter $z_\infty = k^{-1}$ can be expanded as [19]

$$\int_\infty^P\omega = -Uz_\infty + O(z_\infty^2)$$

since, from the Riemann bilinear relation (2.46),

$$U = \oint_{b_i} d\Omega_1 = -\oint_{b_i}\omega_\infty^{(1)} = -\omega(z_\infty = 0)\,.$$

Therefore, the differentiation with respect to k^{-1} in (2.87) can be replaced with $i\partial_x$ so that

$$p = -2\partial_x\log\theta(iUx + 4iWt - D) + 2c_1x + 8c_3t\,. \tag{2.88}$$

Then the field $u(x,t) = p_x$ which solves the KdV equation is

$$u(x,t) = -2\partial_{xx}\log\theta(iUx + 4iWt - D) + 2c_1\,, \tag{2.89}$$

which is sometimes referred to as the 'Its-Matveev' formula obtained in [10, 18]. In order for the solution (2.89) to be real and non-singular the branch points λ_i and the constant vector D must both be real [42, 19]. This is discussed further in §2.6.2.

2.6.1 Explicit formulas for integrals of the second kind

For computational purposes it is worth considering the integrals of the second kind defined by the asymptotic expansions (2.76) more explicitly. In the notation of (2.40),

$$\Omega_1(P) = -\int_{\lambda_{2g+1}}^P\omega_\infty^{(1)}\,,\qquad \Omega_3(P) = -3\int_{\lambda_{2g+1}}^P\omega_\infty^{(3)}\,. \tag{2.90}$$

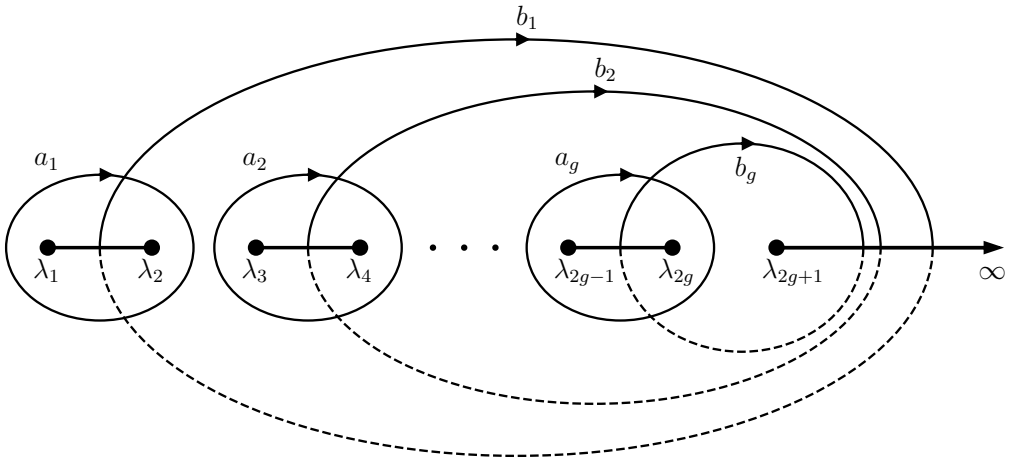

Figure 2.8: Basis of cycles, as in Fig. (2.5), but pictured for KdV specifically. For each pair of branch points, λ_{2i-1} and λ_{2i}, there is an a_i cycle enclosing the cut joining λ_{2i-1} to λ_{2i} and a b_i cycle which starts on the upper sheet of the $[\lambda_{2i-1}, \lambda_{2i}]$ cut and crosses over to the lower sheet through the $[\lambda_{2g+1}, \infty]$ cut before returning to the $[\lambda_{2i-1}, \lambda_{2i}]$ cut.

With the local parameter in the neighbourhood of infinity being $k^{-1} = z_\infty = 1/\sqrt{\lambda}$ the corresponding differentials are

$$d\Omega_1 = \frac{\lambda^g}{2\mu} d\lambda + \sum_{i=1}^{g} \alpha_i \omega_i \,, \tag{2.91a}$$

$$d\Omega_3 = \frac{3}{4}\left(\frac{2\lambda^{g+1} - \widehat{E}\lambda^g}{\mu}\right) d\lambda + \sum_{i=1}^{g} \beta_i \omega_i \,, \qquad \widehat{E} = \sum_{i=1}^{2g+1} \lambda_i \,, \tag{2.91b}$$

where the constants α_i, β_i are fixed by the normalisation that $\oint_{a_i} d\Omega_1 = \oint_{a_i} d\Omega_3 = 0$. A direct computation of the $O(k^{-1})$ term in the expansion of Ω_1 and Ω_3 at ∞ reveals that

$$c_1 = 2\sum_{k=1}^{g} \alpha_k C_{kg} + \frac{1}{2}\sum_{i=1}^{2g+1} \lambda_i \,, \tag{2.92a}$$

$$c_3 = 2\sum_{k=1}^{g} \beta_k C_{kg} + \frac{3}{4}\sum_{i=1}^{2g+1} \lambda_i^2 - \frac{3}{8}\left(\sum_{i=1}^{2g+1} \lambda_i\right)^2 . \tag{2.92b}$$

The b-periods U and W can be conveniently written in terms of the holomorphic differential normalization constants C_{ij} using the Riemann bilinear relation (2.46),

$$U_i := \oint_{b_i} d\Omega_1 = -\oint_{b_i} \omega_\infty^{(1)} = -\omega(z_\infty = 0) = 2C_{ig} \,, \tag{2.93a}$$

$$W_i := \oint_{b_i} d\Omega_3 = -3\oint_{b_i} \omega_\infty^{(3)} = -\frac{1}{2}\left.\frac{d^2}{dz_\infty^2}\omega\right|_{z_\infty=0} = 2C_{i(g-1)} + C_{ig}\sum_{k=1}^{2g+1} \lambda_k \,. \tag{2.93b}$$

2.6.2 Reality and regularity conditions

For a generic choice of branch points and constant vector D the algebro-geometric solution to the KdV equation (2.89) may be complex and/or have singular points. However, as mentioned in the introduction, the KdV equation is often thought of as modelling certain

waves in fluid dynamics so it is common to require that solutions to the KdV equation be real and non-singular and the same shall be done here. For this it is first required that the branch points λ_i be real [42, 19], as expected from the $g = 1$ example for the spectral curve (2.73). The reality condition on D can be derived, as in [19] for example, by considering the transformation $\tau : (\lambda, \mu) \to (\overline{\lambda}, -\overline{\mu})$ which transforms the basis of cycles pictured in Fig. (2.8) as

$$\tau a_i = -a_i \,, \qquad \tau b_i = b_i \,. \tag{2.94}$$

The action of τ on a differential $f(\lambda)d\lambda$ is denoted $\tau^*[f(\lambda)d\lambda] = f(\tau(\lambda))d\tau(\lambda)$ and for the unnormalised basis of differentials of the first kind (2.42),

$$\tau^*\eta_j = \frac{\overline{\lambda}^{j-1}}{-\overline{\mu}} d\overline{\lambda} = -\overline{\eta}_j \,. \tag{2.95}$$

The a-period of η is therefore real since

$$\overline{A}_{kj} = \oint_{a_j} \overline{\eta}_k = -\oint_{a_j} \tau^*\eta_k = -\oint_{\tau a_j} \eta_k = \oint_{a_j} \eta_k = A_{kj} \,.$$

This means that the normalisation coefficients $C_{ij} = 2\pi i A^{-1}_{ij}$ are purely imaginary which implies, using (2.93), that

$$\overline{U} = -U \,, \qquad \overline{W} = -W \,. \tag{2.96}$$

and that the action of τ on the normalised holomorphic differentials is

$$\tau^*\omega = C\tau^*\eta = -C\overline{\eta} = \overline{\omega} \,. \tag{2.97}$$

The Riemann matrix is therefore real,

$$\overline{B}_{ij} = \oint_{b_j} \overline{\omega}_i = \oint_{b_j} \tau^*\omega_i = \oint_{\tau b_j} \omega_i = \oint_{b_j} \omega_i = B_{ij} \,, \tag{2.98}$$

so the Riemann theta function obeys the simple relation

$$\overline{\theta(z, B)} = \theta(\overline{z}, B) \,. \tag{2.99}$$

The normalisation coefficients for Ω_1, α_i, are purely imaginary since

$$\alpha_i = \frac{i}{2\pi} \oint_{a_i} \frac{\lambda^g}{2\mu} d\lambda = -\frac{i}{2\pi} \oint_{\tau a_i} \frac{\lambda^g}{2\mu} d\lambda = -\frac{i}{2\pi} \oint_{a_i} \tau^* \left[\frac{\lambda^g}{2\mu} d\lambda \right] = \frac{i}{2\pi} \oint_{a_i} \frac{\overline{\lambda}^g}{2\overline{\mu}} d\overline{\lambda} = -\overline{\alpha}_i$$

and therefore the constant c_1, given by (2.92a), is real. Combining all these relations it is clear that if $D \in \mathbb{R}^g$ that the field u

$$u(x,t) = -2\partial_{xx} \log \theta \left(iUx + 4iWt - D \right) + 2c_1 \,, \tag{2.100}$$

is real since the argument of the theta function and c_1 are real.

The singularities of u appear at the places where [19]

$$\theta \left(iUx + 4iWt - D \right) = 0 \,,$$

but if $D \in \mathbb{R}^g$ then $\theta\left(iUx + 4iWt - D\right)$, from the definition (2.47), is a convergent sum of exponentials with real exponents and is therefore strictly positive. The requirements that $D \in \mathbb{R}^g$ and $\lambda_i \in \mathbb{R}$ therefore ensure that u is real and non-singular.

2.7 Algebro-geometric solutions for sine-Gordon

In light cone coordinates

$$\xi = \frac{t-x}{4}\,, \qquad \rho = \frac{t+x}{4}\,, \tag{2.101}$$

the Lax pair for the sine-Gordon equation will be chosen to be

$$\psi_\rho = U(u)\psi = \begin{pmatrix} 0 & i\lambda e^{-iu} \\ ie^{iu} & 0 \end{pmatrix}\psi\,, \qquad \psi_\xi = V(u)\psi = \begin{pmatrix} -\frac{iu_\xi}{2} & i \\ i\lambda^{-1} & \frac{iu_\xi}{2} \end{pmatrix}\psi\,, \tag{2.102}$$

which is similar to the one given in [26]. In these variables the sine-Gordon equation is

$$u_{\xi\rho} = -4\sin u\,. \tag{2.103}$$

The spectral curve corresponding to the algebro-geometric solutions for the sine-Gordon equation is hyperelliptic and has the form

$$\mu^2 = \lambda\prod_{i=1}^{2N}(\lambda - \lambda_i)\,, \tag{2.104}$$

where the branch points λ_i lie either on the negative real axis or in complex conjugate pairs [25]. Analogously to the KdV equation, this can be derived by realising the finite-gap solutions to the sine-Gordon equation as the stationary solutions (here in the higher analogues of the ρ coordinate) of the sine-Gordon/modified KdV (SG-mKdV) hierarchy [15]. The form of the spectral curve is also deduced in [19] without reference to the SG-mKdV hierarchy by direct substitution of W in the form of a power series in λ into

$$W_x = [U, W]\,, \qquad W_t = [V, W]\,.$$

The Lax pair eigenfunctions for sine-Gordon are again Baker-Akhiezer functions but they have two singularities, one at 0 and one at ∞ [26]. Following [26], one looks for four Baker-Akhiezer functions, ψ_i^+ and ψ_i^-, $i = 1, 2$, which in the neighbourhood of 0 have asymptotic forms,

$$\begin{aligned} \psi_1^\pm(\xi,\rho,P) &= e^{\pm ik_0\xi}\left(1 + \sum_{s=1}^{\infty} f_{s1}(\xi,\rho)\,k_0^{-s}\right) \\ \psi_2^\pm(\xi,\rho,P) &= \pm e^{\pm ik_0\xi}\,\frac{1}{\sqrt{\lambda}}\left(1 + \sum_{s=1}^{\infty} f_{s2}(\xi,\rho)\,k_0^{-s}\right) \end{aligned} \qquad \text{near } 0, \quad k_0 = \frac{1}{\sqrt{\lambda}} \tag{2.105}$$

with local parameter $z_0 = k_0^{-1} = \sqrt{\lambda}$. While in the neighbourhood of ∞

$$\begin{aligned}\psi_1^{\pm}(\xi,\rho,P) &= e^{\pm ik_\infty\rho}\, c_1(\xi,\rho)\left(1+\sum_{s=1}^{\infty} g_{s1}(\xi,\rho)\, k_\infty^{-s}\right)\\ \psi_2^{\pm}(\xi,\rho,P) &= \pm e^{\pm ik_\infty\rho}\,\frac{c_2(\xi,\rho)}{\sqrt{\lambda}}\left(1+\sum_{s=1}^{\infty} g_{s2}(\xi,\rho)\, k_\infty^{-s}\right)\end{aligned} \qquad \text{near } \infty, \quad k_\infty = \sqrt{\lambda} \tag{2.106}$$

with local parameter $z_\infty = k_\infty^{-1} = 1/\sqrt{\lambda}$.

The Baker-Akhiezer functions matching these asymptotic forms for a particular choice of constant D are

$$\psi_1^{\pm}(\xi,\rho,P) = \frac{\theta(D)\,\theta\left(iB_\infty\rho + iB_0\xi + D \pm \int_0^P \omega\right)}{\theta\left(D \pm \int_0^P \omega\right)\,\theta(iB_\infty\rho + iB_0\xi + D)}\, e^{\pm i\Omega_\infty(P)\rho \pm i\Omega_0(P)\xi}\,, \tag{2.107a}$$

$$\psi_2^{\pm}(\xi,\rho,P) = \pm\frac{\theta(D)\,\theta\left(iB_\infty\rho + iB_0\xi + B_L + D \pm \int_0^P \omega\right)}{\theta\left(D \pm \int_0^P \omega\right)\,\theta(iB_\infty\rho + iB_0\xi + B_L + D)}\, e^{\pm i\Omega_\infty(P)\rho \pm i\Omega_0(P)\xi + \Omega_L(\lambda)}\,, \tag{2.107b}$$

where B_∞ and B_0 are the b-periods of the normalised Abelian integrals of the second kind $\Omega_\infty(P)$ and $\Omega_0(P)$ defined by the asymptotic forms

$$\Omega_\infty(P) \to k_\infty + O(k_\infty^{-1})\,, \qquad \lambda \to \infty\,, \tag{2.108a}$$

$$\Omega_0(P) \to k_0 + O(k_0^{-1})\,, \qquad \lambda \to 0\,, \tag{2.108b}$$

and $\Omega_L(\lambda)$ is simply

$$\Omega_L(\lambda) = -\frac{1}{2}\int_1^\lambda \frac{dt}{t} = -\frac{1}{2}\log(\lambda)\,, \qquad (B_L)_i = -\frac{1}{2}\oint_{b_i}\frac{d\lambda}{\lambda} = i\pi\,, \tag{2.109}$$

where the logarithm is taken to be principal valued so that $\Omega_L(1) = 0$. It is conceptually neater to think of the two sets of $\pm$ solutions as corresponding to the two different points on the Riemann surface that have the same λ. Since, denoting $P^\pm = (\pm\mu, \lambda)$,

$$\int_0^{P^+}\omega = -\int_0^{P^-}\omega\,, \quad \Omega_\infty(P^+) = -\Omega_\infty(P^-)\,, \quad \Omega_0(P^+) = -\Omega_0(P^-)\,.$$

Therefore, (2.107) may be rewritten as

$$\psi_1(\xi,\rho,P^\pm) = \frac{\theta(D)\,\theta\left(iB_\infty\rho + iB_0\xi + D + \int_0^{P^\pm}\omega\right)}{\theta\left(D + \int_0^{P^\pm}\omega\right)\,\theta(iB_\infty\rho + iB_0\xi + D)}\, e^{i\Omega_\infty(P^\pm)\rho + i\Omega_0(P^\pm)\xi}\,, \tag{2.110a}$$

$$\psi_2(\xi,\rho,P^\pm) = \pm\frac{\theta(D)\,\theta\left(iB_\infty\rho + iB_0\xi + i\pi\mathbb{1} + D + \int_0^{P^\pm}\omega\right)}{\theta\left(D + \int_0^{P^\pm}\omega\right)\,\theta(iB_\infty\rho + iB_0\xi + i\pi\mathbb{1} + D)}\, e^{i\Omega_\infty(P^\pm)\rho + i\Omega_0(P^\pm)\xi + \Omega_L(\lambda)}\,, \tag{2.110b}$$

where $\mathbb{1}_i = 1$ for $i = 1, \ldots, g$.

Again, the uniqueness of the Baker-Akhiezer functions is key to confirming their role as

the Lax pair eigenfunctions and deriving the field u which solves the sine-Gordon equation. As described in [26], $\psi_{1\rho}$ and $\lambda\psi_2$ both satisfy the same properties (i) and (ii), given in §2.5, since they have the same asymptotic form at 0 and ∞. They are therefore related by a function of ξ, ρ and by comparing the coefficients of $\sqrt{\lambda}$ at ∞ it can be shown that $\psi_{1\rho} = i(c_1/c_2)\lambda\psi_2$. Making similar comparisons one can verify that

$$\psi_\rho = \begin{pmatrix} 0 & i\lambda\frac{c_1}{c_2} \\ i\frac{c_2}{c_1} & 0 \end{pmatrix}\psi\,, \qquad \psi_\xi = \begin{pmatrix} \frac{\partial_\xi c_1}{c_1} & i \\ i\lambda^{-1} & \frac{\partial_\xi c_2}{c_2} \end{pmatrix}\psi\,, \tag{2.111}$$

and to match with (2.102) let

$$c_1 = e^{-\frac{iu}{2}}\,, \qquad c_2 = e^{\frac{iu}{2}}\,.$$

Then evaluating (2.110) at $P = \infty$ and noting that $\int_0^\infty \omega = -i\pi\mathbb{1}$ provides an explicit formula for u

$$\frac{c_2}{c_1} = e^{iu} = \left(\frac{\theta(iB_\infty\rho + iB_0\xi + D)}{\theta(iB_\infty\rho + iB_0\xi + D + i\pi\mathbb{1})}\right)^2. \tag{2.112}$$

Making a change of variables back to x, t and defining

$$V = \frac{B_\infty - B_0}{4}\,, \qquad W = \frac{B_\infty + B_0}{4}\,. \tag{2.113}$$

gives

$$e^{iu(x,t)/2} = \frac{\theta(iVx + iWt + D)}{\theta(iVx + iWt + D + i\pi\mathbb{1})}\,, \tag{2.114}$$

which was originally constructed by Kozel and Kotlyarov in [25].

2.7.1 Explicit formulas for integrals of the second kind

The integrals of the second kind defined by (2.108) are, in the notation of (2.40),

$$\Omega_\infty(P) = -\int_0^P \omega_\infty^{(1)}\,, \qquad \Omega_0(P) = -\int_\infty^P \omega_0^{(1)}\,, \tag{2.115}$$

Explicitly, the corresponding differentials are

$$d\Omega_\infty = \frac{\lambda^g}{2\mu}d\lambda + \sum_{i=1}^g \alpha_i\omega_i\,, \tag{2.116a}$$

$$d\Omega_0 = -\frac{\sqrt{\Lambda}}{2\lambda\mu}d\lambda + \sum_{i=1}^g \beta_i\omega_i, \qquad \Lambda = \prod_{i=1}^{2g}\lambda_i\,, \tag{2.116b}$$

where the constants α_i, β_i are fixed by the normalization conditions $\oint_{a_i} d\Omega_\infty = \oint_{a_i} d\Omega_0 = 0$. Using the Riemann bilinear relation (2.46) the b periods can be conveniently expressed as

$$(B_\infty)_i = 2C_{ig}\,, \qquad (B_0)_i = -\frac{2C_{i1}}{\sqrt{\Lambda}}\,. \tag{2.117}$$

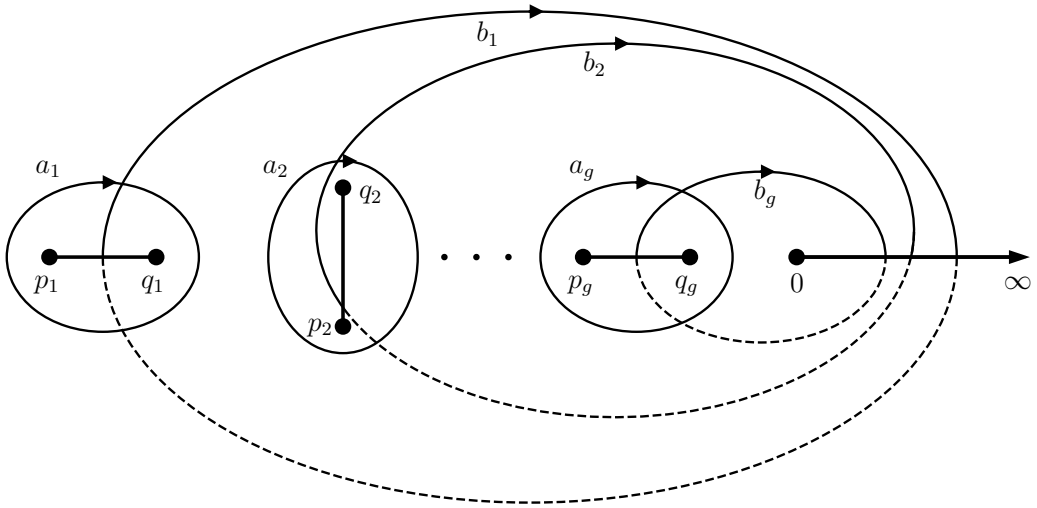

Figure 2.9: A basis of cycles, as in Fig. (2.5), but pictured for sine-Gordon specifically. For each pair of branch points, p_i and q_i, there is an a_i cycle enclosing the cut joining p_i to q_i and a b_i cycle which starts on the upper sheet of the $[p_i, q_i]$ cut and crosses over to the lower sheet through the $[0, \infty]$ cut before returning to the $[p_i, q_i]$ cut.

2.7.2 Reality conditions

As mentioned in the introduction the field satisfying the sine-Gordon equation is often physically interpreted as an angle or real phase so it is common to require the field to be real. It is perhaps worth remarking that there is a generalisation of the sine-Gordon equation known as the 'complex sine-Gordon' model [109, 110] for which integrable defects [77] and boundaries [111, 112] have been constructed. Nevertheless, the attention of this thesis will remain restricted to the sine-Gordon equation and its real solutions.

To isolate the real solutions it will be convenient to rewrite the hyperelliptic curve (2.104) as

$$\mu^2 = \lambda \prod_{i=1}^{g} (\lambda - p_i)(\lambda - q_i)\,, \tag{2.118}$$

where, for the reality of the field u, the branch points satisfy [25],

$$p_i < q_i < 0 \quad \text{or} \quad p_i = \overline{q_i} \quad \text{for } i = 1, \ldots, g\,. \tag{2.119}$$

As in [19] and the previous KdV case the reality properties of the theta function and certain period integrals can be derived by considering the transformation $\tau : (\lambda, \mu) \to (\overline{\lambda}, -\overline{\mu})$. The set of branch points is invariant under this transformation and the chosen basis of cycles, pictured in (2.9), transforms as

$$\tau(a_i) = -a_i \tag{2.120a}$$

$$\tau(b_i) = b_i \qquad \text{if } p_i, q_i \in \mathbb{R} \tag{2.120b}$$

$$\tau(b_i) = b_i - a_i \qquad \text{if } p_i = \overline{q}_i\,. \tag{2.120c}$$

A graphical proof of the last relation can be found in Fig. 4.4 of [19]. The action of τ on

the a-periods is the same as in the KdV case discussed in §2.6.2 and therefore

$$C_{ij} = -\overline{C_{ij}}\,, \qquad \tau^*\omega = \overline{\omega}\,. \tag{2.121}$$

The normalisation coefficients C_{ij} being purely imaginary implies, from the Riemann bilinear relations (2.117), that the b-periods of the differentials of the second kind, B_0 and B_∞, are both purely imaginary. The reality or lack thereof of the Riemann matrix can be deduced as

$$\overline{B}_{ij} = \oint_{b_j} \overline{\omega}_i = \oint_{b_j} \tau^*\omega_i = \oint_{\tau b_j} \omega_i = \begin{cases} \oint_{b_j} \omega_i = B_{ij} & \text{if } p_i, q_i \in \mathbb{R} \\ \oint_{b_j} \omega_i - \oint_{a_j} \omega_i = B_{ij} - 2\pi i \delta_{ij} & \text{if } p_i = \overline{q}_i \end{cases} \tag{2.122}$$

and therefore the Riemann theta function defined by (2.47) obeys the relation

$$\overline{\theta(z,B)} = \theta\left(\bar{z} + i\pi(\kappa - \mathbb{1}), B\right)\,, \qquad \kappa_i = \begin{cases} 1, & \text{if } p_i, q_i \in \mathbb{R} \\ 0, & \text{if } p_i = \overline{q}_i \end{cases} \quad i = 1 \dots g. \tag{2.123}$$

The reality of (2.114) is then equivalent to the statement

$$e^{\frac{iu}{2}} e^{-\frac{i\overline{u}}{2}} = \frac{\theta(iVx + iWt + D)\theta(iVx + iWt + \overline{D} + i\pi\kappa - i\pi\mathbb{1})}{\theta(iVx + iWt + D + i\pi\mathbb{1})\theta(iVx + iWt + \overline{D} + i\pi\kappa)} = 1\,,$$

which holds if

$$\overline{D} + i\pi\kappa = D - 2i\pi\varepsilon\,, \quad \varepsilon \in \mathbb{Z}^g\,, \tag{2.124}$$

or equivalently,

$$\mathrm{Im}[D] = \frac{\pi}{2}\kappa + \pi\varepsilon\,. \tag{2.125}$$

However, this expression has some inconsequential degrees of freedom since the field u, given by (2.114), is invariant under shifts of

$$D \to D + 2\pi i N + BM\,, \quad N, M \in \mathbb{Z}^g\,, \quad \sum_{i=1}^{g} M_i = 2n\,,\ n \in \mathbb{Z}\,. \tag{2.126}$$

So only the values of ε modulo 2 actually affect u. The reality conditions on D are therefore summarised by

$$\begin{gathered} D = x_0 + \frac{i\pi}{2}\kappa + i\pi\varepsilon\,, \qquad x_0 \in \mathbb{R}^g\,, \quad \kappa\,,\ \varepsilon \in \mathbb{Z}^g\,, \\ \varepsilon_i = 0 \text{ or } 1\,, \quad \kappa_i = \begin{cases} 1, & \text{if } p_i, q_i \in \mathbb{R} \\ 0, & \text{if } p_i = \bar{q}_i \end{cases} \qquad i = 1 \dots g\,. \end{gathered} \tag{2.127}$$

with x_0 and $\epsilon_i = 0, 1$ being free choices.

2.8 Numerical evaluation

This thesis contains several figures involving algebro-geometric solutions to the KdV and sine-Gordon equations, namely figures 1b, 1c, 3.2, 4.1, 4.2, 6.1 and 6.2. In order to produce

these plots the Riemann matrix B, normalisation constants C and, where necessary, the Abel map were numerically computed for a given hyperelliptic algebraic curve using the algorithm of [113]. The implementation of this algorithm used here was written by the present author in Python using the `NumPy` [114] and `SciPy` [115] packages and based on a Matlab implementation by the authors of [113] [1]. The Riemann theta functions and their derivatives were numerically computed using part of the `Abelfunctions` library [116, 117]. All the figures in this thesis were displayed using the `Matplotlib` library for Python [118].

[1] The author would like to thank Christian Klein and Jörg Frauendiener for providing a copy of their Matlab code for computing algebro-geometric solutions to the sine-Gordon equation using their algorithm [113].

3 | Phase-shifted elliptic solutions for sine-Gordon with a defect

Before tackling the question of how the general algebro-geometric solutions for sine-Gordon (2.114) and KdV (2.89) behave in the presence of an integrable defect it is worthwhile to see how far the direct phase-shifted ansatz approach used in [73] and §1.1.1 can be taken. Here, this method is applied to the simplest algebro-geometric solutions for sine-Gordon which are known as elliptic solutions since they correspond to the case when the genus $g = 1$ and the underlying algebraic curve (2.118) is elliptic.

For $g = 1$ it is convenient to use the notation of Jacobi theta functions [1]

$$\vartheta_1(z,B) = -\vartheta_2(z+i\pi,B) \qquad \vartheta_2(z,B) = \sum_{n=-\infty}^{\infty} \exp\left(\frac{B}{2}\left(n+\frac{1}{2}\right)^2 + z\left(n+\frac{1}{2}\right)\right)$$
$$\vartheta_3(z,B) = \theta(z,B) \qquad \vartheta_4(z,B) = \theta(z+i\pi,B)$$

and throughout this section the abbreviations $\vartheta_k(z) = \vartheta_k(z,B)$ and $\vartheta_k = \vartheta_k(0,B)$ will will be used. In this notation the fields u in the region $x \leq x_D$ and v in $x \geq x_D$ are given by

$$e^{iu/2} = \frac{\vartheta_3(z)}{\vartheta_4(z)}\,, \quad e^{iv/2} = \frac{\vartheta_3(z+\Delta)}{\vartheta_4(z+\Delta)}\,, \quad z = iVx + iWt + D\,, \tag{3.1}$$

where V, W and D are as in §2.7 and Δ is the phase shift which must be solved for using the defect equations (1.7). It will be helpful to note that the branch points p_1, q_1 are related to the theta constants ϑ_i by [120, §13.20(7)]

$$p_1 = C^2\vartheta_3^4\,, \qquad q_1 = C^2\vartheta_4^4\,, \tag{3.2}$$

and therefore the b-periods of the differentials of the second kind are, according to (2.117),

$$B_\infty = 2C\,, \qquad B_0 = -\frac{2C}{\sqrt{p_1 q_1}} = \frac{2}{C\vartheta_3^2\vartheta_4^2}\,, \tag{3.3}$$

where the square root was simplified using $C^2 < 0$ and $\vartheta_3^2\vartheta_4^2 > 0$.

Inserting the ansatz (3.1) into the defect equations (1.7) and using [119, §21.6]

$$2i\frac{d}{dz}\left[\frac{\vartheta_3(z)}{\vartheta_4(z)}\right] = -\vartheta_2^2\,\frac{\vartheta_1(z)\vartheta_2(z)}{\vartheta_4(z)^2}\,, \tag{3.4}$$

[1] The more common definition of Jacobi theta functions, $\vartheta_k(u,q)$, used in [119] and implemented in Mathematica, is related to the notation used here by $\vartheta_k(u = z/(2i), q = \exp(B/2))$.

to evaluate the derivatives yields the pair of equations

$$\begin{aligned}\frac{\vartheta_3(z)^2-\vartheta_4(z)^2\sigma^2+Y^2(\vartheta_3(z)^2\sigma^2-\vartheta_4(z)^2)-2YV\vartheta_1(z)\vartheta_2(z)\vartheta_2^2\sigma-4iY_zW\vartheta_3(z)\vartheta_4(z)\sigma}{2Y\vartheta_3(z)\vartheta_4(z)\sigma}=0\\ \frac{\vartheta_3(z)^2+\vartheta_4(z)^2\sigma^2-Y^2(\vartheta_3(z)^2\sigma^2+\vartheta_4(z)^2)+2YW\vartheta_1(z)\vartheta_2(z)\vartheta_2^2\sigma+4iY_zV\vartheta_3(z)\vartheta_4(z)\sigma}{2Y\vartheta_3(z)\vartheta_4(z)\sigma}=0\end{aligned} \tag{3.5}$$

where

$$Y=e^{iv/2}=\frac{\vartheta_3(z+\Delta)}{\vartheta_4(z+\Delta)}\,,\qquad Y_z=\frac{i\vartheta_2^2}{2}\frac{\vartheta_1(z+\Delta)\vartheta_2(z+\Delta)}{\vartheta_4(z+\Delta)^2}\,.$$

Solving for Y (Y_z will be checked later) and using (3.3) together with the well-known relations between the squares of Jacobi theta functions [119, §21.2]

$$\begin{aligned}\vartheta_1^2(z)\vartheta_2^2&=\vartheta_4^2(z)\vartheta_3^2-\vartheta_3^2(z)\vartheta_4^2\,,&\qquad\vartheta_3^2(z)\vartheta_2^2&=\vartheta_2^2(z)\vartheta_3^2+\vartheta_1^2(z)\vartheta_4^2\,,\\ \vartheta_2^2(z)\vartheta_2^2&=\vartheta_3^2(z)\vartheta_3^2-\vartheta_4^2(z)\vartheta_4^2\,,&\qquad\vartheta_4^2(z)\vartheta_2^2&=\vartheta_1^2(z)\vartheta_3^2+\vartheta_2^2(z)\vartheta_4^2\,,\end{aligned} \tag{3.6}$$

yields

$$Y=\frac{\vartheta_1(z)\vartheta_2(z)\vartheta_2^2C\sigma\pm\vartheta_3(z)\vartheta_4(z)\sqrt{(C^2\vartheta_3^4+\sigma^2)(C^2\vartheta_4^4+\sigma^2)}}{C^2\vartheta_3^2\vartheta_4^2\vartheta_4^2(z)+\vartheta_3^2(z)\sigma^2}\,. \tag{3.7}$$

In order to isolate the shift Δ compare (3.7) with the addition formula [119] [2]:

$$\frac{\vartheta_3(z+\Delta)}{\vartheta_4(z+\Delta)}=\frac{\vartheta_4}{\vartheta_3}\,\frac{\vartheta_1(z)\vartheta_2(z)\vartheta_1(\Delta)\vartheta_2(\Delta)-\vartheta_3(z)\vartheta_4(z)\vartheta_3(\Delta)\vartheta_4(\Delta)}{\vartheta_1^2(z)\vartheta_1^2(\Delta)-\vartheta_4^2(z)\vartheta_4^2(\Delta)}\,. \tag{3.8}$$

The task is then to find a relationship between Δ and the parameters C and σ to ensure the equality of (3.7) and (3.8) for all z. Because any theta function can be written in terms of any other pair using (3.6), it is helpful to eliminate $\vartheta_1(z)$ and $\vartheta_2(z)$ before equating the coefficients of $\vartheta_3(z)$ and $\vartheta_4(z)$. This can be done by equating (3.7) with (3.8) and rearranging to find

$$\begin{aligned}\vartheta_1(z)\vartheta_2(z)\left(\vartheta_2^2C\sigma F(z)-\vartheta_1(\Delta)\vartheta_2(\Delta)G(z)\right)=\\ -\vartheta_3(z)\vartheta_4(z)\left(\vartheta_3(\Delta)\vartheta_4(\Delta)G(z)\pm F(z)\sqrt{(C^2\vartheta_3^4+\sigma^2)(C^2\vartheta_4^4+\sigma^2)}\right)\,,\end{aligned} \tag{3.9}$$

where

$$F(z)=\frac{\vartheta_3}{\vartheta_4}\left(\vartheta_1^2(\Delta)\vartheta_1^2(z)-\vartheta_4^2(\Delta)\vartheta_4^2(z)\right)\,,\qquad G(z)=C^2\vartheta_3^2\vartheta_4^2\vartheta_4^2(z)+\sigma^2\vartheta_3^2(z)\,,$$

and then squaring. After making use of (3.6) to eliminate $\vartheta_1^2(z)$, $\vartheta_2^2(z)$, $\vartheta_3(\Delta)$ and $\vartheta_4(\Delta)$

[2] Specifically, (3.8) can be derived as the ratio of the identities

$$\begin{aligned}\vartheta_3(y+z)\vartheta_4(y-z)\vartheta_3\vartheta_4&=\vartheta_3(y)\vartheta_4(y)\vartheta_3(z)\vartheta_4(z)-\vartheta_1(y)\vartheta_2(z)\vartheta_1(z)\vartheta_2(z)\\ \vartheta_4(y+z)\vartheta_4(y-z)\vartheta_4^2&=\vartheta_4^2(y)\vartheta_4^2(z)-\vartheta_1^2(y)\vartheta_1^2(z)\end{aligned}$$

found in *Chapter XXI, Miscellaneous Examples*, p.487-488 of [119].

(3.9) becomes

$$\begin{aligned}\left(\vartheta_3(z)^4-\vartheta_4(z)^4\right)\left(C\vartheta_3\vartheta_4\vartheta_1(\Delta)+\sigma\vartheta_2(\Delta)\right)^2 = \\ \frac{2\vartheta_3(z)^2\vartheta_4(z)^2}{\vartheta_3\vartheta_4}\Big[\left(\sigma\vartheta_4\vartheta_1(\Delta)-C\vartheta_3^3\vartheta_2(\Delta)\right)\left(C\vartheta_4^3\vartheta_2(\Delta)-\sigma\vartheta_3\vartheta_1(\Delta)\right) \\ \pm\sqrt{(C^2\vartheta_3^4+\sigma^2)(C^2\vartheta_4^4+\sigma^2)(\vartheta_4^2\vartheta_1(\Delta)^2+\vartheta_3^2\vartheta_2(\Delta)^2)(\vartheta_3^2\vartheta_1(\Delta)^2+\vartheta_4^2\vartheta_2(\Delta)^2)}\Big]\,.\end{aligned}$$

In order for all the coefficients of this polynomial in $\vartheta_3(z)^2$ and $\vartheta_4(z)^2$ to vanish it is required that

$$\frac{\vartheta_1(\Delta)}{\vartheta_2(\Delta)}=-\frac{\sigma}{\vartheta_3\vartheta_4 C}\,. \tag{3.10}$$

Note that since the zeros of Jacobi theta functions are given by [119, §21.12]

$$\vartheta_1(z)=0 \iff z=2\pi i n+Bm\,, \tag{3.11a}$$
$$\vartheta_2(z)=0 \iff z=2\pi i n+Bm+i\pi\,, \tag{3.11b}$$
$$\vartheta_3(z)=0 \iff z=2\pi i n+Bm+i\pi+B/2\,, \tag{3.11c}$$
$$\vartheta_4(z)=0 \iff z=2\pi i n+Bm+B/2\,, \tag{3.11d}$$

where $n,m\in\mathbb{Z}$, it is clear that the theta constants ϑ_2, ϑ_3, ϑ_4 are non-zero and that $\vartheta_1(\Delta)$ and $\vartheta_2(\Delta)$ cannot be simultaneously be zero. This observation eliminates the other possible constraints on the parameters that might cause the coefficients of $\vartheta_3(z)^2$, $\vartheta_4(z)^2$ to vanish. Assuming (3.10), the expression for Y_z obtained by solving (3.5) can then be shown to be true using the addition formula for $\vartheta_1(z+\Delta)\vartheta_2(z+\Delta)/\vartheta_4^2(z+\Delta)$ [119] [3] and the identities for the squares of theta functions (3.6).

Using (3.10) it is now apparent that the $\pm$ in (3.7) is a consequence of the fact that $\vartheta_3(\Delta)\vartheta_4(\Delta)$ is only determined by $\vartheta_1(\Delta)$ and $\vartheta_2(\Delta)$ up to a sign by the square relations (3.6). This indicates that there are two distinct (mod 4π) purely phase-shifted elliptic fields which satisfy the defect equations, just as there were in the soliton case. In fact, if Δ solves (3.10) then so does $-\Delta+B$,

$$\frac{\vartheta_1(-\Delta+B)}{\vartheta_2(-\Delta+B)}=-\frac{\vartheta_1(-\Delta)}{\vartheta_2(-\Delta)}=\frac{\vartheta_1(\Delta)}{\vartheta_2(\Delta)}\,,$$

since $\vartheta_1(z)$ is an odd function of z and $\vartheta_2(z)$, $\vartheta_3(z)$, $\vartheta_4(z)$ are even. The two possible values of Δ corresponds to two distinct solutions for the field v,

$$e^{iv/2}=\frac{\vartheta_3(z+\Delta)}{\vartheta_4(z+\Delta)}\,,\qquad e^{iv/2}=-\frac{\vartheta_3(z-\Delta)}{\vartheta_4(z-\Delta)}\,. \tag{3.12}$$

Examples of these two solutions to the defect equations are plotted in Fig. (3.2). In Fig. (3.1) examples are given of how the two possible phase shifts in the elliptic case varies

[3] An addition formula for $\vartheta_1(z+\Delta)\vartheta_2(z+\Delta)/\vartheta_4^2(z+\Delta)$ can be derived from the identities

$$\begin{aligned}\vartheta_1(y+z)\vartheta_4(y-z)\vartheta_2\vartheta_3&=\vartheta_1(y)\vartheta_4(y)\vartheta_2(z)\vartheta_3(z)+\vartheta_2(y)\vartheta_3(y)\vartheta_1(z)\vartheta_4(z)\\ \vartheta_2(y+z)\vartheta_4(y-z)\vartheta_2\vartheta_4&=\vartheta_2(y)\vartheta_4(y)\vartheta_2(z)\vartheta_4(z)-\vartheta_1(y)\vartheta_3(y)\vartheta_1(z)\vartheta_3(z)\\ \vartheta_4(y+z)\vartheta_4(y-z)\vartheta_4^2&=\vartheta_4^2(y)\vartheta_4^2(z)-\vartheta_1^2(y)\vartheta_1^2(z)\end{aligned}$$

found in *Chapter XXI, Miscellaneous Examples*, p.487-488 of [119].

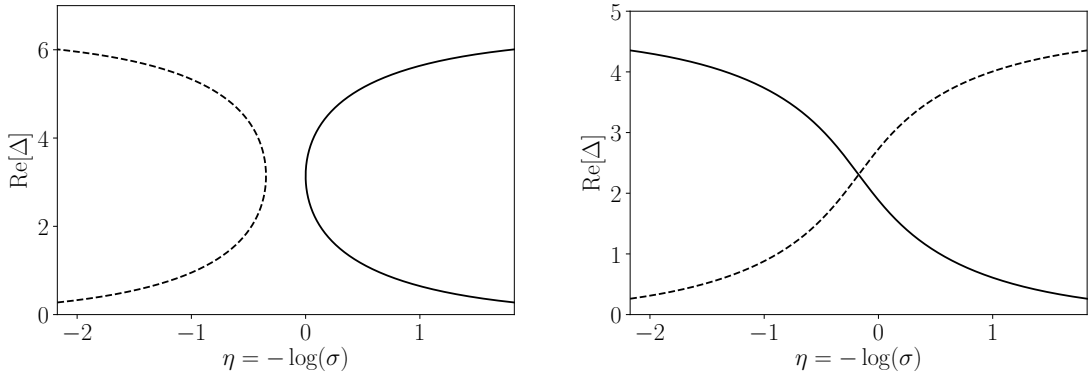

(a) $p_1 = -2$, $q_1 = -1$ (b) $p_1 = -1 - i$, $q_1 = -1 + i$

Figure 3.1: The two values of the phase shift Δ, satisfying (3.10), corresponding to a range of values for the defect parameter σ for a pair of (a) real and (b) conjugate branch points. Where the line is solid Δ is real while the dashed line indicates that $\mathrm{Im}[\Delta] = \pi$.

as a function of the defect parameter for real and conjugate values of the branch points. It is also true that $\Delta + 2i\pi n + 2Bm$ will satisfy (3.10) if Δ does for any $n, m \in \mathbb{Z}$ but this does not lead to a distinct expression for v.

One feature of (3.10), which agrees with the soliton case, is that the effect of the defect disappears in the limit where $\sigma \to 0$. In this limit (3.10) implies that $\vartheta_1(\Delta) = 0$ in which case $v = u$ or $v = u + 2\pi$. In the soliton case, if $\sigma \to 0$ then (1.9) becomes $v = u$ and (1.10) becomes $v = u + 2\pi$.

3.1 The 'reality gap'

A feature of the elliptic phase-shifted solutions, which is apparent from Fig. (3.1a), is that for a given choice of distinct real branch points there exists a range of values for the defect parameter σ such that the reality condition on Δ,

$$\mathrm{Im}[\Delta] = 0 \text{ or } \pi \pmod{2\pi}, \tag{3.13}$$

cannot be satisfied. This 'reality gap' has no analogue in the purely solitonic case where for a given soliton rapidity and defect parameter there is always a real solution to the defect equations.

An explanation for this gap comes from noting that if B is real (i.e. the branch points are real) then there exists the bounds,

$$-\frac{\vartheta_4}{\vartheta_3} \leq i\frac{\vartheta_1(\Delta)}{\vartheta_2(\Delta)} \leq \frac{\vartheta_4}{\vartheta_3} \qquad \text{for } \mathrm{Im}[\Delta] = 0 \tag{3.14a}$$

$$i\frac{\vartheta_1(\Delta)}{\vartheta_2(\Delta)} \geq \frac{\vartheta_3}{\vartheta_4} \text{ or } i\frac{\vartheta_1(\Delta)}{\vartheta_2(\Delta)} \leq -\frac{\vartheta_3}{\vartheta_4} \qquad \text{for } \mathrm{Im}[\Delta] = \pi \tag{3.14b}$$

Therefore, in the region

$$\frac{\vartheta_4}{\vartheta_3} < \frac{\sigma}{iC\vartheta_3\vartheta_4} < \frac{\vartheta_3}{\vartheta_4}, \tag{3.15}$$

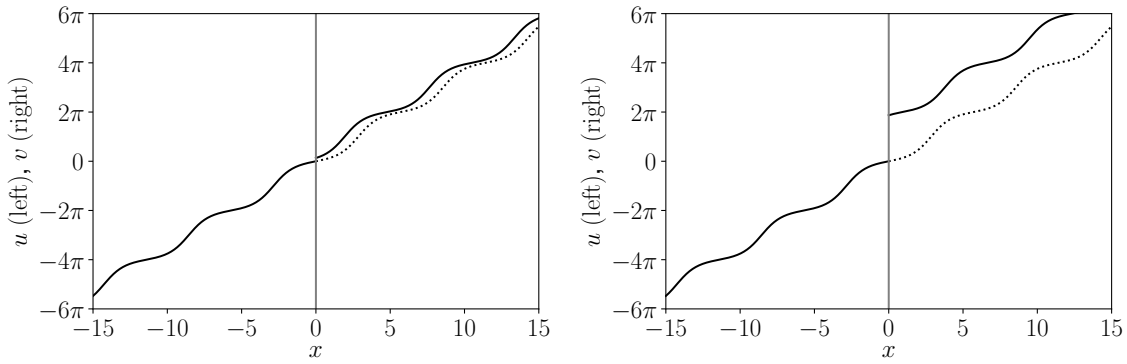

(a) $p_1 = -0.6$, $q_1 = -0.3$, $\eta = 1.2$

(b) $p_1 = -0.6$, $q_1 = -0.3$, $\eta = 1.2$

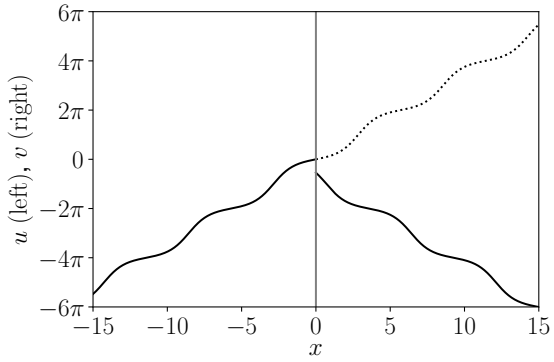

(c) $p_1 = -0.6$, $q_1 = -0.3$, $\eta = 0.2$

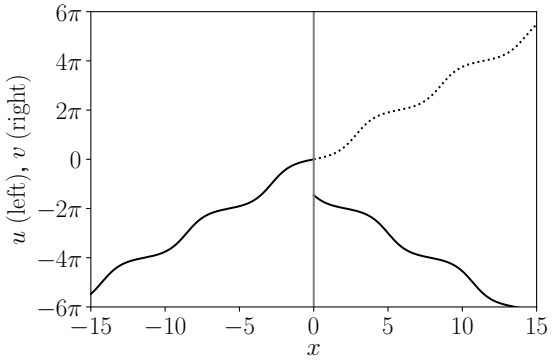

(d) $p_1 = -0.6$, $q_1 = -0.3$, $\eta = 0.2$

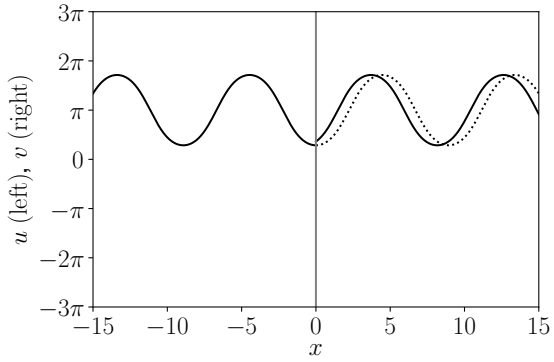

(e) $p_1 = \overline{q_1} = -0.4 - 0.5i$, $\eta = 1.2$

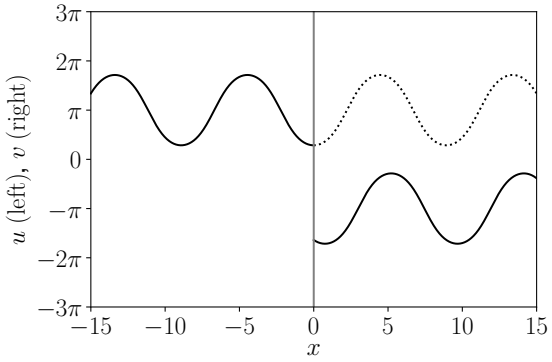

(f) $p_1 = \overline{q_1} = -0.4 - 0.5i$, $\eta = 1.2$

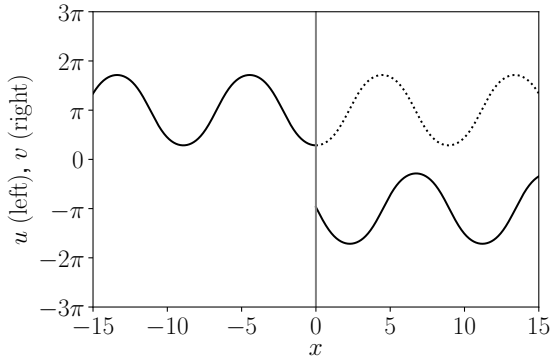

(g) $p_1 = \overline{q_1} = -0.4 - 0.5i$, $\eta = 0.2$

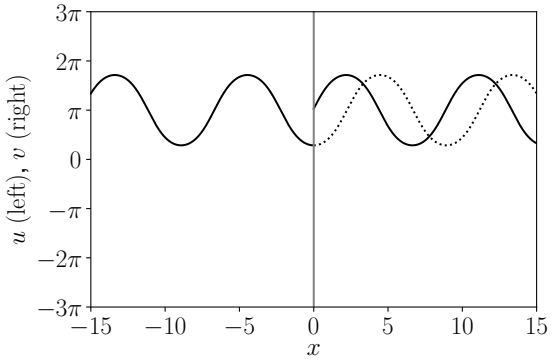

(h) $p_1 = \overline{q_1} = -0.4 - 0.5i$, $\eta = 0.2$

Figure 3.2: Examples of elliptic, purely phase-shifted solutions to the type I integrable defect equations (1.7) for sine-Gordon plotted at $t = 0$ with the defect placed at $x = 0$. Each row plots the two phase-shifted solutions for the given values of branch points p_1, q_1 and defect parameter $\sigma = \exp(-\eta)$. In every case the field to the left of the defect corresponds to the choice $x_0 = \varepsilon = 0$ so that $D = i\pi\kappa/2$. For comparison, the dotted line to the right of the defect is the continuation of the field to the left in the absence of the defect.

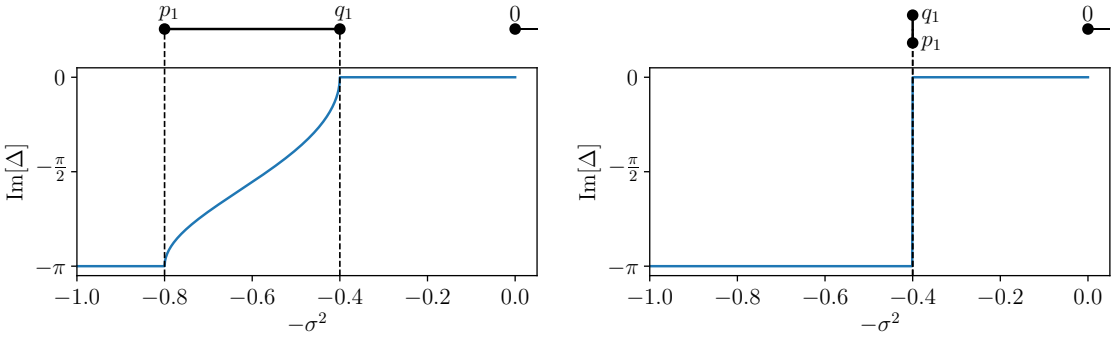

(a) $p_1 = -0.8$, $q_1 = -0.4$ (b) $p_1 = \overline{q_1} = -0.4 - 0.5i$

Figure 3.3: The imaginary part of the phase shift Δ, given by (3.20), plotted for examples of real (a) and conjugate (b) branch points.

or equivalently

$$p_1 < -\sigma^2 < q_1\,, \tag{3.16}$$

neither of the bounds for (3.14a) and (3.14b) can be satisfied and hence there can be no real solutions of the form (3.1). For complex conjugate branch points $\vartheta_1(\Delta)/\vartheta_2(\Delta)$ is not bounded so real solutions to (3.10) exist for any σ, as demonstrated in Fig. (3.1b).

An alternative way to view the reality gap can be seen by writing the phase shift explicitly as an integral of the holomorphic differential ω. The ratios of Jacobi theta functions are related to Jacobi elliptic functions,

$$\frac{\theta_1(\Delta)}{\theta_2(\Delta)} = \frac{\vartheta_4}{\vartheta_3}\,\mathrm{sc}\left(\frac{\Delta\vartheta_3^2}{2i}\right)\,. \tag{3.17}$$

The inverse of this elliptic function [119, §22.122],

$$\mathrm{sc}^{-1}(z) = \int_0^z \frac{dt}{\sqrt{1+t^2}\sqrt{1+q_1t^2/p_1}}\,, \tag{3.18}$$

can, with the substitution $\lambda = -q_1t^2$, be related to an integral of the holomorphic differential,

$$\mathrm{sc}^{-1}(z) = \frac{\sqrt{-p_1}}{2C}\int_0^{-q_1z^2}\omega\,, \quad q_1z^2 \in \mathbb{R}\,, \tag{3.19}$$

where the integral is performed on the upper sheet (the same sheet that the a-cycle is on). Then the phase shift for $\sigma > 0$ is written, up to periods of sc, as

$$\Delta = \int_0^{-\sigma^2}\omega\,. \tag{3.20}$$

So in the case of real branch points Δ is, as shown in Fig. (3.3a), real when $-\sigma^2 \geq q_1$ and has imaginary part $-\pi$ when $-\sigma^2 \leq p_1$ but for $p_1 < -\sigma^2 < q_1$ the integral is generically complex and does not satisfy the reality conditions (3.13). For conjugate branch points the imaginary part of Δ, demonstrated in Fig. (3.3b), is real for $-\sigma^2 \geq \mathrm{Re}[p_1]$ and has imaginary part $-\pi$ for $-\sigma^2 < \mathrm{Re}[p_1]$ so in this case Δ always satisfies the reality condition (3.13).

3.2 Soliton limit

The one soliton solution to the sine-Gordon equation can be recovered from the genus one or elliptic solution by taking the limit in which the branch points p_1 and q_1 coincide [22, 19]. Here it is checked that the phase-shifted soliton solutions can be recovered from the phase-shifted elliptic solutions to the defect equations in the soliton limit.

In the limit where p_1 and q_1 coalesce one finds, as recalled for convenience in §A.2, that $B \to -\infty$ and the field to the left of the defect becomes,

$$e^{iu/2} = \frac{\vartheta_3(z)}{\vartheta_4(z)} \to \frac{1+iE}{1-iE}\,, \qquad E = (-1)^{\varepsilon} \exp(\cosh(\theta)x - \sinh(\theta)t + x_0)\,, \tag{3.21}$$

where $\theta = -\ln(p_1 q_1)/4 \to -\ln(p_1)/2$ is the rapidity in the soliton limit. The two solutions for the phase-shifted field to the right of the defect (3.12) become

$$e^{iv/2} \to \frac{1+ie^{\Delta}E}{1-ie^{\Delta}E}\,, \qquad e^{iv/2} \to -\frac{1+ie^{-\Delta}E}{1-ie^{-\Delta}E}\,. \tag{3.22}$$

With $\theta = -\ln(p_1 q_1)/4$ and $\sigma = \exp(-\eta)$ the phase shift (3.10) can generally be written as

$$\frac{\vartheta_1(\Delta)}{\vartheta_2(\Delta)} = -ie^{\theta-\eta}\,. \tag{3.23}$$

Then in the soliton limit

$$-ie^{\theta-\eta} = \frac{\vartheta_1(\Delta)}{\vartheta_2(\Delta)} \to -i\tanh\left(\frac{\Delta}{2}\right)\,,$$

so that

$$e^{\Delta} = \coth\left(\frac{\eta-\theta}{2}\right)\,. \tag{3.24}$$

Therefore the two phase-shifted elliptic solutions in the soliton limit, (3.22), match the two purely phase-shifted soliton solutions, (1.9) and (1.10). Finally, in the soliton limit p_1 and q_1 are equal so the region (3.16), where no real phase-shifted solutions exist, disappears as it must.

3.3 Effectiveness of the phase shift ansatz

In the special case when $g = 1$ it was possible to substitute for the field to the right of the defect a phase-shifted version of the field to the left and to solve for the phase shift using the defect equations. However, in the hyperelliptic case, when $g > 1$, it seems very difficult to directly substitute a phase shift ansatz into the defect equations because there does not appear to be a simple formula analogous to (3.4) for the derivatives. In any case, one might anticipate the existence of solutions to the defect equations involving soliton emission on a finite-gap background, analogous to the 'one-to-two' soliton solution discussed in §1.1.3, which would not fall into the class of solutions included in the phase shift ansatz. Instead, these kinds of solutions to the defect equations will be found in the next chapter using a different approach.

4 | Defects and Darboux transformations

In §1.1.4 the idea of using Bäcklund transformations to construct certain solutions to integrable PDEs in the presence of an integrable defect was introduced. This idea exploits the fact that the type I integrable defects for sine-Gordon (1.7) and KdV (1.19) both have the form of Bäcklund transformations but applied only at a point $x = x_D$ rather than over the full line. The method is then to first take a field u which satisfies the integrable PDE everywhere and compute its Bäcklund transformation, v, so that u, v together satisfy the defect equations for all x. Then in particular the field

$$w(x,t) = \begin{cases} u(x,t) & \text{if } x \leq x_D \\ v(x,t) & \text{if } x \geq x_D \end{cases}$$

will satisfy the type I integrable defect equations at $x = x_D$ and the integrable PDE everywhere else.

If u is a constant solution such as $2\pi n, n \in \mathbb{Z}$ for sine-Gordon or 0 for KdV then v can be computed by direct integration of the Bäcklund transformation. In this case v will be a one soliton solution with its velocity determined by the Bäcklund parameter while its initial position appears as an integration constant.

If u is only a single or multi-soliton solution then v can be computed using Bianchi's permutability theorem [95], which is essentially the statement that with a suitable choice of integration constants Bäcklund transformations can be made to commute [82, 83, 84]. That is to say that if u_i is the Bäcklund transformation of u_0 with parameter σ_i and u_{ij} is the Bäcklund transformation of u_i with parameter σ_j then it can be arranged that

$$u_{12} = u_{21}\,.$$

For the sine-Gordon equation this leads to the nonlinear superposition formula [121]

$$u_{12} = u_0 + 4\arctan\left[\frac{\sigma_1+\sigma_2}{\sigma_1-\sigma_2}\tan\left[\frac{u_1-u_2}{4}\right]\right], \tag{4.1}$$

while for the KdV equation this gives the analogous relation between the potentials p_i such that $u_i = \partial_x p_i$ [80]

$$p_{12} = p_0 - 4\frac{\sigma_1-\sigma_2}{p_1-p_2}\,. \tag{4.2}$$

A two soliton solution can be derived by taking u_0 to be a constant solution, obtaining

the one soliton solutions u_1 and u_2 by direct integration of the Bäcklund transformation equations and then using the superposition formula. Further multi-soliton solutions can then be found without any additional integration by repeated use of the superposition formula, for example, the three soliton solution for sine-Gordon is related to the one and two soliton solutions by

$$u_{123} = u_2 + 4\arctan\left[\frac{\sigma_1+\sigma_3}{\sigma_1-\sigma_3}\tan\left[\frac{u_{21}-u_{23}}{4}\right]\right].$$

However, this approach requires an initial integration from u_0 to u_1 and if u_0 is an algebro-geometric solution such as (2.89) or (2.114) then this is not straightforward. This case therefore requires a different approach where the Bäcklund transformation is implemented indirectly as a transformation of the field and the Lax pair eigenfunction which is known as a Darboux transformation. In this chapter the Darboux transformations for the KdV and sine-Gordon equations are reviewed in some detail and used to rederive the soliton solutions to the defect equations discussed in §1 before explicitly determining the algebro-geometric solutions in the presence of a type I integrable defect.

4.1 KdV

The KdV equation,

$$u_t - 6uu_x + u_{xxx} = 0\,, \tag{4.3}$$

is the compatibility condition of the Lax pair,

$$\psi_{xx} = (u-\lambda)\psi\,, \tag{4.4a}$$
$$\psi_t = (2u+4\lambda)\psi_x - u_x\psi\,, \tag{4.4b}$$

with eigenfunction $\psi(x,t,\lambda)$ and spectral parameter $\lambda\in\mathbb{C}$. It is straightforward to confirm that if u_0 and ψ_0 satisfy (4.4) then so too does [88, 122]

$$u_1 = u_0 - 2\partial_x^2\ln(f_1)\,, \tag{4.5a}$$
$$\psi_1 = \partial_x\psi_0 - \psi_0\,\partial_x\ln(f_1)\,, \tag{4.5b}$$

where $f_1(x,t)=\psi_0(x,t,\lambda=\sigma_1)$ for some choice of constant σ_1. This transformation $(u_0,\psi_0)\to(u_1,\psi_1)$ is the *Darboux transformation* for KdV.

Let the potentials p and q be such that $p_x=u_0$, $q_x=u_1$ and p satisfies the potential KdV equation

$$p_t - 3p_x^2 + p_{xxx} = 0\,. \tag{4.6}$$

Then p and q together satisfy a Bäcklund transformation which has the form of the defect equations (1.19) but applied over all x and with Bäcklund parameter σ_1. To show this first replace u_0 and u_1 in (4.5a) with p_x and q_x and integrate once with respect to x to find

$$p - q = 2\partial_x\ln(f_1)\,, \tag{4.7}$$

where an arbitrary function of t has been absorbed into q since this does not change u_1.

Then taking (4.5a) and using (4.4a) and (4.7) to substitute for $(f_1)_{xx}$ and $(f_1)_x$ respectively gives the first Bäcklund transformation equation

$$p_x + q_x = 2\sigma_1 + \frac{1}{2}(p-q)^2 \,. \tag{4.8}$$

The second Bäcklund transformation equation,

$$p_t + q_t = 2(p_x^2 + p_x q_x + q_x^2) - (p-q)(p_{xx} - q_{xx}) \,, \tag{4.9}$$

can also be verified by using (4.7) and its derivatives to eliminate q from (4.9) and (4.4) to eliminate f_1, leaving the constraint (4.6) which is assumed. Equations (4.8) and (4.9) constitute a Bäcklund transformation [80] from the field $u_0 = p_x$ to $u_1 = q_x$ which is satisfied for all x, t.

For a given u_0 it is always possible to choose a p satisfying $p_x = u_0$ and (4.6) since inserting $u_0 = p_x$ into the KdV equation (4.3) and integrating with respect to x gives

$$\frac{\partial}{\partial x}\left[p_t - 3p_x^2 + p_{xxx}\right] = 0$$

and a function of t can be absorbed into p without changing u_0. In addition, if p satisfies (4.6) then so too does q since differentiating (4.8) twice to obtain an expression for $(p-q)(p_{xx} - q_{xx})$ and substituting this into (4.9) gives

$$p_t + q_t = 3p_x^2 + 3q_x^2 - p_{xxx} - q_{xxx} \,. \tag{4.10}$$

Therefore, if the Darboux transformation is repeatedly applied then each potential and its successive Darboux transformed potential will satisfy the Bäcklund transformation equations (4.8) and (4.9).

4.1.1 Multi-soliton solutions

Here, the one-to-two soliton solution discussed in §1.2.2 is reproduced via a Darboux transformation in order to demonstrate the effectiveness of Darboux transformations for generating solutions to the KdV equation in the presence of a type I integrable defect.

The fields p and u_0 given by

$$p = p_0 - a + c_0 x + 3c_0^2 t \,, \qquad u_0 = p_x = c_0 \,, \qquad a, c_0 \in \mathbb{R} \,, \tag{4.11}$$

satisfy the potential KdV equation (4.6) and KdV equation (4.3) respectively. By directly solving the Lax pair (4.4) the corresponding eigenfunction is found to be,

$$\begin{aligned} \psi_0(x,t,\lambda;b) &= E^{-1/2} + bE^{1/2} \,, \qquad b \in \mathbb{C} \,, \\ E = \exp\left[\varphi(x - (\varphi^2 - 6c_0)t)\right] \,, &\qquad \lambda = -\frac{\varphi^2}{4} + c_0 \,. \end{aligned} \tag{4.12}$$

Starting from this seed the Darboux transformation $(u_0, \psi_0) \to (u_1, \psi_1)$ with

$$f_1(x,t) = \psi_0(x,t,\lambda_1;b_1) \,, \qquad \lambda_1 = -\frac{a^2}{4} + c_0 \,, \qquad b_1 \in \mathbb{C} \tag{4.13}$$

gives

$$q_1 = p_0 - \frac{2ab_1E_1}{1+b_1E_1} + c_0x + 3c_0^2t\,, \tag{4.14a}$$

$$\psi_1(x,t,\lambda;b) = \frac{(bE-1)(b_1E_1+1)\varphi - (b_1E_1-1)(bE+1)a}{2E^{1/2}(1+b_1E_1)}\,, \tag{4.14b}$$

where

$$E_1 = \exp\left[a(x-(a^2-6c_0)t)\right]\,.$$

If $b_1 = e^{-ax_a}$ then q_1 is the one soliton potential (1.20) which is to the left of the defect in §1.2. It can also be seen that there is a discrete bound state eigenvalue at $\lambda = \lambda_1$ which corresponds to the soliton.

Applying a further Darboux transformation $(u_1, \psi_1) \to (u_2, \psi_2)$ with

$$f_2(x,t) = \psi_0(x,t,\lambda_2;b_2)\,, \qquad \lambda_2 = -\frac{\chi^2}{4} + c_0\,, \tag{4.15}$$

leads to the two soliton potential

$$q_2 = p_0 - a + \frac{(a^2-\chi^2)(1+b_1E_1+b_2E_2+b_1b_2E_1E_2)}{(a-\chi)(1-b_1b_2E_1E_2)-(a+\chi)(b_1E_1-b_2E_2)} + c_0x + 3c_0^2t\,, \tag{4.16}$$

where

$$E_2 = \exp\left[\chi(x-(\chi^2-6c_0)t)\right]\,.$$

For q_2 to be regular either $b_1 \leq 0$, $b_2 \geq 0$ and $|a| > |\chi|$ or $b_1 \geq 0$, $b_2 \leq 0$ and $|a| < |\chi|$. If $|a| = |\chi|$ then the Darboux transformation eliminates the soliton created in the first transformation. If $b_1 = e^{-ax_a}$ and $b_2 = -e^{-\chi x_\chi}$ for real x_a, x_χ then q_2 is the two soliton potential (1.25) which is the field to the right of the defect in the one-to-two soliton solution discussed in §1.2.2.

4.1.2 Algebro-geometric Darboux transformation

Now the algebro-geometric solutions for the KdV equation in the presence of a type I integrable defect can be generated in an analogous way to the soliton solutions above. The initial potential is given by (2.88),

$$p = -2\partial_x \log\theta\left(iUx + 4iWt - D\right) + 2c_1x + 8c_3t\,,$$

while the corresponding Lax pair eigenfunction is taken to be a linear combination of (2.77),

$$\psi(P) = \frac{\theta\left(\int_\infty^P \omega + iUx + 4iWt - D\right)\theta\left(D\right)}{\theta\left(\int_\infty^P \omega - D\right)\theta\left(iUx + 4iWt - D\right)} e^{i\Omega_1(P)x + 4i\Omega_3(P)t}\,,$$

evaluated on the upper and lower sheets of the Riemann surface,

$$\psi_0(x,t,\lambda;b) = \psi(x,t,P^+) + b\,\psi(x,t,P^-)\,, \quad P^\pm = (\pm\mu,\lambda)\,, \tag{4.17}$$

with some constant $b \in \mathbb{C}$ which will later be constrained by reality conditions.

So with the integrable defect (1.19) at $x = x_D$ and p in the region $x \leq x_D$ then a field q in $x \geq x_D$ which satisfies the defect equations is, using (4.7),

$$\begin{gathered} q = -2\partial_x \log\left[\theta\left(z + \int_\infty^{\sigma^+} \omega\right) + \tilde{b}E_\sigma \theta\left(z - \int_\infty^{\sigma^+} \omega\right)\right] + 2c_1 x - 2i\Omega_1(\sigma^+) + 8c_3 t\,, \\ z = iUx + 4iWt - D\,, \quad \tilde{b} = b\frac{\theta\left(\int_\infty^{\sigma^+}\omega - D\right)}{\theta\left(\int_\infty^{\sigma^+}\omega + D\right)}\,, \quad E_\sigma = e^{-2i\Omega_1(\sigma^+)x - 8i\Omega_3(\sigma^+)t}\,, \end{gathered} \tag{4.18}$$

where the fact that for any branch point λ_{BP}

$$\int_{\lambda_{BP}}^{P^-} d\Omega_{1,3} = -\int_{\lambda_{BP}}^{P^+} d\Omega_{1,3}\,, \qquad \int_{\lambda_{BP}}^{P^-} \omega = -\int_{\lambda_{BP}}^{P^+} \omega\,,$$

has been used.

4.1.3 Reality and smoothness conditions

For $v = q_x$ to be real it is sufficient to require that the argument of the logarithm and the constant c_1 in (4.18) are real. From the reality conditions for u recalled in §2.6.2, it has already been established that

$$c_1 \in \mathbb{R}\,, \quad iU,\, iW,\, D \in \mathbb{R}^g\,, \quad iC \in \mathbb{R}^{g\times g}\,, \qquad \overline{\theta(r,B)} = \theta(\bar{r},B)\,. \tag{4.19}$$

In order for the theta functions in (4.18) to be real the each element of $\int_\infty^\sigma \omega_i$ must be real or have imaginary part $i\pi$. Because

$$\int_{\lambda_{2i-1}}^{\lambda_{2i}} \omega_j = \frac{1}{2}\oint_{a_i} \omega_j = i\pi\delta_{ij}$$

and

$$\mu(\lambda) \in \mathbb{R}, \quad i\omega \in \mathbb{R}^g \quad \text{for} \quad \lambda \in R_1 = [\lambda_1,\lambda_2]\cup[\lambda_3,\lambda_4]\cup\cdots\cup[\lambda_{2g+1},\infty] \tag{4.20a}$$

$$i\mu(\lambda) \in \mathbb{R}, \quad \omega \in \mathbb{R}^g \quad \text{for} \quad \lambda \in R_2 = [-\infty,\lambda_1]\cup[\lambda_2,\lambda_3]\cup\cdots\cup[\lambda_{2g},\lambda_{2g+1}] \tag{4.20b}$$

the reality of the theta functions requires that $\sigma \in R_2$. The Abelian differentials of the second kind $d\Omega_1$, $d\Omega_3$ are also real on R_2 and their integrals along each cut

$$\int_{\lambda_{2i-1}}^{\lambda_{2i}} d\Omega_{1,3} = \frac{1}{2}\oint_{a_i} d\Omega_{1,3} = 0\,.$$

So the condition $\sigma \in R_2$ also implies that $i\Omega_1(\sigma)$ and $i\Omega_3(\sigma^+)$ are real and consequently $E_\sigma \in \mathbb{R}$. Therefore, the field v is real provided that $\sigma \in R_2$ and $\tilde{b} \in \mathbb{R}$.

However, v will still be singular at the zeros of

$$\theta\left(z + \int_\infty^{\sigma^+} \omega\right) + \tilde{b}E_\sigma\theta\left(z - \int_\infty^{\sigma^+}\omega\right)\,. \tag{4.21}$$

To ensure that (4.21) has no zeros for $x,t \in \mathbb{R}$ it is first required that $\sigma < \lambda_1$ so that

$\int_\infty^\sigma \omega$ is real. Then since z and B are real the theta functions $\theta(z \pm \int_\infty^{\sigma^+} \omega)$, as a sum of exponentials with real exponents, will be strictly positive, as will E_σ. Requiring, in addition, $\tilde{b} \geq 0$ makes (4.21) strictly positive and so ensures that v has no singularities.

If instead $\sigma \in R_2 \setminus [-\infty, \lambda_1]$ then one or more elements of $\int_\infty^\sigma \omega_i$ would have imaginary part $i\pi$ and the theta functions $\theta(z \pm \int_\infty^{\sigma^+} \omega)$ would have an infinite number of zeros, leading to an infinite number of singularities for v. This is straightforward to see in the elliptic genus $g = 1$ case where $\theta(i\pi + B/2 + Bm, B) = 0$ for $m \in \mathbb{Z}$.

If $\sigma < \lambda_1$ but $\tilde{b} < 0$ then v would have a single singularity on an otherwise smooth background corresponding to the single zero of (4.21).

To summarise, with $\sigma < \lambda_1$ and $\tilde{b} \geq 0$ the field to the right of the defect $v = q_x$ is real and regular.

4.1.4 Interpretation

It is known that the effect of the Bäcklund or equivalent Darboux transformation is to add (or in special cases remove) a soliton and this is also the case when the initial field is of algebro-geometric type [123, 124, 122, 125, 126]. Accordingly, the potential q given by (4.18) is that of a soliton on an algebro-geometric background, as seen in Fig. (4.1). The pair (2.88) and (4.18) therefore corresponds to soliton emission by the defect on an algebro-geometric background, analogous to the one-to-two soliton solutions to the defect equations discussed in §1.2.2.

An N soliton solution on a g genus algebro-geometric background can also be obtained by the partial degeneration of a $g + N$ genus curve in which N pairs of the branch points coalesce to N points [127]. In particular, it is explicitly shown in appendix B that the field (4.18) can be obtained as the limit of a $g + 1$ genus algebro-geometic solution in which the most negative pair of branch points coalesce to the point σ.

4.1.5 Soliton limit

The one-to-two soliton solution (1.25) can be recovered from the general algebro-geometric solution (4.18) in the limit $\lambda_2 \to \lambda_1$ of the elliptic ($g = 1$) case. Using the results of appendix A, the potential to the left of the defect (2.88) becomes,

$$\begin{aligned} p &= -2\partial_x \log(1 + E_a) + \lambda_3 x + 3\lambda_3^2 t \\ &= -\frac{2aE_a}{1 + E_a} + \lambda_3 x + 3\lambda_3^2 t \,. \end{aligned} \tag{4.22}$$

where

$$E_a = \exp\left[a(x - (a^2 - 6\lambda_3)t - x_a)\right] \,, \qquad a = iU = 2\sqrt{\lambda_3 - \lambda_1} \,,$$

and before taking the soliton limit D has been defined to be $D = ax_a + B/2$ for some choice of $x_a \in \mathbb{R}$. This is precisely the one soliton potential (1.20).

To obtain the field to the right of the defect let $\chi = 2\sqrt{\lambda_3 - \sigma}$ and use the expressions

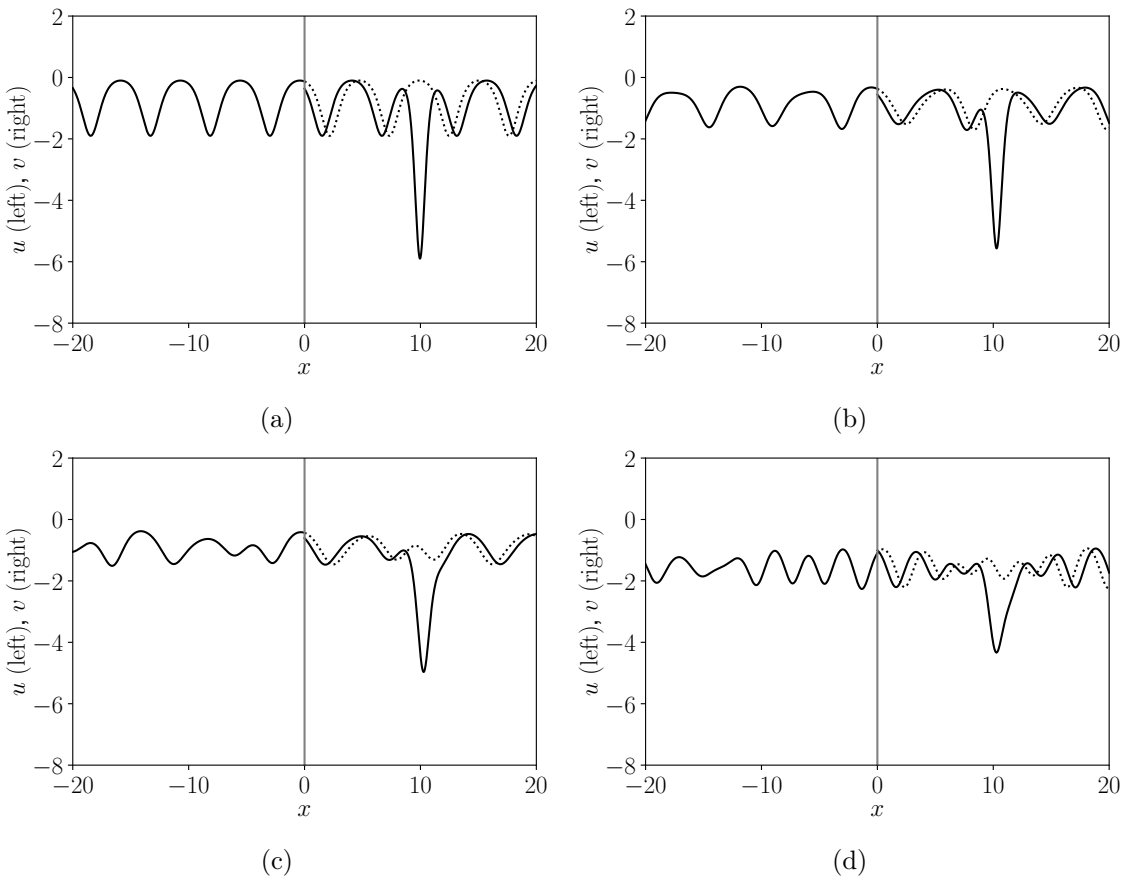

Figure 4.1: Examples of genus 1 (a), 2 (b), 3 (c) and 4 (d) algebro-geometric solutions to the KdV equation with a type I integrable defect at $x = 0$. In each of these examples the field to the right contains a soliton which is the trough at $x \approx 10$. For comparison, the dotted line shows the continuation of the field to the left in the absence of the defect.

(A.10) for $d\Omega_1$ and $d\Omega_3$ in the soliton limit to find

$$\Omega_1(\sigma^+) \to i\sqrt{\lambda_3 - \sigma} = \frac{i\chi}{2}\,, \tag{4.23a}$$

$$\Omega_3(\sigma^+) \to \frac{i}{2}\sqrt{\lambda_3 - \sigma}(2\sigma + \lambda_3) = -\frac{i\chi}{8}\left(\chi^2 - 6\lambda_3\right)\,. \tag{4.23b}$$

Using (A.2), the integral of ω in the soliton limit is given by

$$\exp\left[\int_\infty^{\sigma^+} \omega\right] \to \frac{\chi + a}{\chi - a} =: \Delta\,. \tag{4.24}$$

It will be convenient to parameterise $\widetilde{b}$ by

$$\widetilde{b} = \Delta \exp\left[-\chi x_\chi\right]\,, \qquad x_\chi \in \mathbb{R}\,, \tag{4.25}$$

so that in the soliton limit,

$$\widetilde{b}E_\sigma \to \Delta E_\chi = \Delta \exp\left[\chi\left(x - (\chi^2 - 6\lambda_3)t - x_\chi\right)\right]\,. \tag{4.26}$$

The parameterisation (4.25) is consistent with the smoothness condition $\widetilde{b} \geq 0$ since $\sigma < \lambda_1 < \lambda_3$ implies that $\chi = 2\sqrt{\lambda_3 - \sigma} > 2\sqrt{\lambda_3 - \lambda_1} = a$. Finally, using these limits and the

results of appendix A, the potential to the right of the defect (4.18) becomes in the soliton limit

$$q = -2\partial_x \log\left[1 + \Delta E_a + \Delta E_\chi \left(1 + \Delta^{-1} E_a\right)\right] + \lambda_3 x + 3\lambda_3^2 t + \chi\,. \tag{4.27}$$

The expressions for p (4.22) and q (4.27) derived here in the degenerate limit of the general elliptic solutions to the defect equations are precisely the potentials (1.20) and (1.25) that constitute the one-to-two soliton solution discussed in §1.2.2 with $p_0 = 0$ and $c_0 := \lambda_3$. This shows that the algebro-geometric solutions found here for the KdV equation in the presence of a type I integrable defect are indeed more general than the purely solitonic solutions considered up to now.

4.2 Sine-Gordon

In the light cone coordinates

$$\xi = \frac{t-x}{4}\,, \qquad \rho = \frac{t+x}{4}\,, \tag{4.28}$$

the sine-Gordon equation,

$$u_{\xi\rho} = -4\sin u\,, \tag{4.29}$$

is the compatibility condition, $U_\xi - V_\rho + [U, V] = 0$, of the Lax pair

$$\psi_\rho = U(u)\psi = \begin{pmatrix} 0 & i\lambda e^{-iu} \\ ie^{iu} & 0 \end{pmatrix}\psi\,, \qquad \psi_\xi = V(u)\psi = \begin{pmatrix} -\frac{iu_\xi}{2} & i \\ i\lambda^{-1} & \frac{iu_\xi}{2} \end{pmatrix}\psi\,, \tag{4.30}$$

which was used to derive the algebro-geometric solutions [26] in §2.7.

The Darboux transformation is encoded in a Darboux matrix $F(\rho, \xi, \lambda)$ which must satisfy the relations

$$F_\rho = U(v)\,F - F\,U(u) \tag{4.31a}$$

$$F_\xi = V(v)\,F - F\,V(u) \tag{4.31b}$$

in order for the Darboux transformed eigenfunction,

$$\widetilde{\psi}(\rho, \xi, \lambda) = F(\rho, \xi, \lambda)\psi(\rho, \xi, \lambda)\,, \tag{4.32}$$

to satisfy the Lax pair

$$\widetilde{\psi}_\rho = U(v)\widetilde{\psi}\,, \qquad \widetilde{\psi}_\xi = V(v)\widetilde{\psi}\,, \tag{4.33}$$

so that the new field v satisfies the sine-Gordon equation. The task is to find the Darboux matrix such that the relations (4.31) are equivalent to the Bäcklund transformation

$$\partial_\xi(v+u) = -\frac{4}{\sigma}\sin\left(\frac{v-u}{2}\right) \tag{4.34a}$$

$$\partial_\rho(v-u) = 4\sigma\sin\left(\frac{v+u}{2}\right) \tag{4.34b}$$

which is the integrable defect (1.7) applied to all ξ, ρ and written in light cone coordinates.

Starting with the assumption

$$F(\rho,\xi,\lambda) = F_0(\rho,\xi) + \lambda F_1(\rho,\xi)\,, \tag{4.35}$$

a suitable Darboux matrix is found to be

$$F = \begin{pmatrix} i\lambda e^{\frac{i}{2}(u-v)} & \lambda\sigma \\ \sigma & i\lambda e^{-\frac{i}{2}(u-v)} \end{pmatrix}. \tag{4.36}$$

The Darboux matrix (4.36) has an explicit dependence on the unknown field v so given only the original eigenfunction ψ and field u it cannot be directly used to generate $\widetilde{\psi}$. However, it is possible to use the Darboux matrix to find an expression for v in terms of only u and the matrix Ψ whose columns form a basis for the Lax pair eigenfunctions corresponding to u,

$$\Psi(\lambda) = \begin{pmatrix} \Psi_{11}(\lambda) & \Psi_{12}(\lambda) \\ \Psi_{21}(\lambda) & \Psi_{22}(\lambda) \end{pmatrix}. \tag{4.37}$$

This is done, following the argument of [83], by noting that the columns of the matrix $\widetilde{\Psi} = F\Psi$ are linearly dependent for $\lambda = 0$ or $-\sigma^2$ since

$$\mathrm{Det}\left[\tilde{\Psi}(\lambda)\right] = \mathrm{Det}\left[F(\lambda)\right]\mathrm{Det}\left[\Psi(\lambda)\right] = -\lambda(\lambda+\sigma^2)\mathrm{Det}\left[\Psi(\lambda)\right]. \tag{4.38}$$

Therefore,

$$\widetilde{\Psi}(0)\begin{pmatrix} \alpha_1 \\ \beta_1 \end{pmatrix} = 0\,, \qquad \widetilde{\Psi}(-\sigma^2)\begin{pmatrix} \alpha_2 \\ \beta_2 \end{pmatrix} = 0\,, \tag{4.39}$$

for some constants α_i, β_i, which are not both zero. Assuming $\alpha_2 \neq 0$, let $b = \beta_2/\alpha_2$, then $\tilde{\Psi} = F\Psi$ and (4.39) can be used to derive the relations,

$$\alpha_1\Psi_{11}(0) + \beta_1\Psi_{12}(0) = 0\,, \tag{4.40a}$$

$$\frac{\Psi_{21}(-\sigma^2) + b\,\Psi_{22}(-\sigma^2)}{\Psi_{11}(-\sigma^2) + b\,\Psi_{12}(-\sigma^2)} = \frac{1}{i\sigma}e^{\frac{i}{2}(u-v)}\,, \tag{4.40b}$$

the second of which provides the promised expression for the new field

$$v = u + 2i\log\left[i\sigma\frac{\Psi_{21}(-\sigma^2) + b\,\Psi_{22}(-\sigma^2)}{\Psi_{11}(-\sigma^2) + b\,\Psi_{12}(-\sigma^2)}\right]. \tag{4.41}$$

Analogous expressions for the Darboux transformation (4.41) but corresponding to different choices for the sine-Gordon Lax pair than the one taken here may be found in [122, 83].

4.2.1 Multi-soliton solutions

As in the KdV case, the one-to-two soliton solution for sine-Gordon with a type I integrable defect discussed in §1.1.3 can be rederived using the Darboux transformation (4.41).

Starting from a vacuum solution

$$u_0 = 0\,, \qquad \Psi_0 = \begin{pmatrix} \cos\left(\rho\sqrt{\lambda} + \frac{\xi}{\sqrt{\lambda}}\right) & i\sqrt{\lambda}\sin\left(\rho\sqrt{\lambda} + \frac{\xi}{\sqrt{\lambda}}\right) \\ \frac{i}{\sqrt{\lambda}}\sin\left(\rho\sqrt{\lambda} + \frac{\xi}{\sqrt{\lambda}}\right) & \cos\left(\rho\sqrt{\lambda} + \frac{\xi}{\sqrt{\lambda}}\right) \end{pmatrix}, \tag{4.42}$$

and applying (4.41) gives,

$$u_1 = 2i \log \left[\frac{\sinh\left(\frac{\xi}{\sigma_1} - \rho\sigma_1\right) + ib_1\sigma_1 \cosh\left(\frac{\xi}{\sigma_1} - \rho\sigma_1\right)}{\cosh\left(\frac{\xi}{\sigma_1} - \rho\sigma_1\right) + ib_1\sigma_1 \sinh\left(\frac{\xi}{\sigma_1} - \rho\sigma_1\right)} \right] ,$$

which after setting

$$b_1 = \frac{i}{\sigma_1} \frac{1 + ie^{x_{01}}}{1 - ie^{x_{01}}} , \qquad E_i = \exp\left(2\sigma_i\rho - \frac{2\xi}{\sigma_i} - x_{0i}\right) ,$$

becomes

$$u_1 = 2i \log \left[\frac{1 - iE_1}{1 + iE_1} \right] . \tag{4.43}$$

After a change of coordinates back to x, t this is recognised as the one soliton solution (1.8) with rapidity θ_1 given by $\sigma_1 = \exp(-\theta_1)$. With u_1 now known the Darboux matrix (4.36) can be applied to Ψ_0 to compute the new basis of eigenfunctions corresponding to u_1,

$$\Psi_1 = \begin{pmatrix} \frac{i\lambda(1-iE_1)(1+E_\lambda^2) - \sigma_1\sqrt{\lambda}(1+iE_1)(1-E_\lambda^2)}{2E_\lambda(1+iE_1)} & -\lambda\frac{i\sqrt{\lambda}(1-iE_1)(1-E_\lambda^2) - \sigma_1(1+iE_1)(1+E_\lambda^2)}{2E_\lambda(1+iE_1)} \\ -\frac{i\sqrt{\lambda}(1+iE_1)(1-E_\lambda^2) - \sigma_1(1-iE_1)(1+E_\lambda^2)}{2E_\lambda(1-iE_1)} & \frac{i\lambda(1+iE_1)(1+E_\lambda^2) - \sigma_1\sqrt{\lambda}(1-iE_1)(1-E_\lambda^2)}{2(1-iE_1)E_\lambda} \end{pmatrix} , \tag{4.44}$$

where

$$E_\lambda = e^{i\left(\rho\sqrt{\lambda} + \xi/\sqrt{\lambda}\right)} . \tag{4.45}$$

So now, supposing the field u_1 is to the left of the integrable defect as in §1.1.3, the field to the right of the defect, the restriction of u_2 to $x \geq x_D$, can be directly computed using (4.41). Parameterising b_2 and σ_2 as

$$b_2 = \frac{i}{\sigma_2} \frac{\varepsilon_2 + i\delta e^{x_{02}}}{\varepsilon_2 - i\delta e^{x_{02}}} , \qquad \varepsilon_2 = \mp 1 , \qquad \sigma_2 = e^{-\theta_2} , \tag{4.46}$$

$$\delta = \frac{\sigma_1 + \sigma_2}{\sigma_1 - \sigma_2} = \coth\left(\frac{\theta_2 - \theta_1}{2}\right) , \tag{4.47}$$

allows u_2 to be written as

$$u_2 = 2i \log \left[\frac{1 - i\delta E_1 + \varepsilon_2 i E_2 + \varepsilon_2 \delta^{-1} E_1 E_2}{1 + i\delta E_1 - \varepsilon_2 i E_2 + \varepsilon_2 \delta^{-1} E_1 E_2} \right] . \tag{4.48}$$

The field given by u_1 (4.43) for $x \leq x_D$ and u_2 (4.48) for $x \geq x_D$ is precisely the one-to-two soliton solution, discussed in §1.1.3, for sine-Gordon in the presence of a type I integrable defect.

4.2.2 Algebro-geometric Darboux transformation

The algebro-geometric solutions for sine-Gordon with the type I integrable defect (1.7) at $x = x_D$ can now be constructed. Suppose that the field u in $x \leq x_D$ is the algebro-geometric solution

$$e^{iu(x,t)/2} = \frac{\theta(iVx + iWt + D)}{\theta(iVx + iWt + D + i\pi\mathbb{1})} , \tag{4.49}$$

recalled in §2.7. Then applying the transformation (4.41) with

$$\Psi(\lambda) = \begin{pmatrix} \psi_1(P^+) & \psi_1(P^-) \\ \psi_2(P^+) & \psi_2(P^-) \end{pmatrix}, \qquad P^\pm = (\pm\mu, \lambda), \tag{4.50}$$

and $\psi_{1,2}(P^\pm)$ given by (2.110) provides a corresponding field v in the region $x \geq x_D$,

$$\begin{aligned} v &= 2i \log \left[\frac{\theta\left(z + i\pi\mathbb{1} + \int_0^{-\sigma^2}\omega\right) - \tilde{b}E_\sigma\theta\left(z + i\pi\mathbb{1} - \int_0^{-\sigma^2}\omega\right)}{\theta\left(z + \int_0^{-\sigma^2}\omega\right) + \tilde{b}E_\sigma\theta\left(z - \int_0^{-\sigma^2}\omega\right)} \right], \\ z &= iB_\infty\rho + iB_0\xi + D\,, \quad \tilde{b} = b\,\frac{\theta\left(D + \int_0^{-\sigma^2}\omega\right)}{\theta\left(D - \int_0^{-\sigma^2}\omega\right)}, \\ E_\sigma &= \exp\left[-2i(\Omega_\infty(-\sigma^2)\rho + \Omega_0(-\sigma^2)\xi)\right], \end{aligned} \tag{4.51}$$

where, for definiteness, $-\sigma^2$ is taken as a point on the upper sheet (the sheet the $a-$cycles are on) for the purposes of integration.

4.2.3 Reality conditions

If ϕ is the argument of the logarithm in (4.51) then the reality of v is equivalent to $\phi\bar{\phi} = 1$. From the discussion of the reality conditions for u in §2.7.2 it is already known that

$$\overline{\theta(r,B)} = \theta\left(\bar{r} + i\pi(\kappa - \mathbb{1}), B\right), \qquad \kappa_i = \begin{cases} 1, & \text{if } p_i, q_i \in \mathbb{R} \\ 0, & \text{if } p_i = \overline{q}_i \end{cases} \quad i = 1 \ldots g\,,$$
$$iB_1,\, iB_2 \in \mathbb{R}^g\,, \qquad iC \in \mathbb{R}^{g\times g}\,, \qquad \bar{D} = D - i\pi\kappa - 2i\pi\varepsilon\,.$$

The complex conjugate of ϕ is then

$$\bar{\phi} = \frac{\theta\left(z + \overline{\int_0^{-\sigma^2}\omega}\right) - \overline{\tilde{b}}\,\overline{E_\sigma}\theta\left(z - \overline{\int_0^{-\sigma^2}\omega}\right)}{\theta\left(z + i\pi\mathbb{1} + \overline{\int_0^{-\sigma^2}\omega}\right) + \overline{\tilde{b}}\,\overline{E_\sigma}\theta\left(z + i\pi\mathbb{1} - \overline{\int_0^{-\sigma^2}\omega}\right)},$$

and therefore v is real if $\overline{\tilde{b}}\,\overline{E_\sigma} = -\tilde{b}E_\sigma$ and each element of $\int_0^{-\sigma^2}\omega_i$ is either real or has imaginary part $i\pi$. Since $\int_{p_i}^{q_i}\omega_j = i\pi\delta_{ij}$ and,

$$\mu(\lambda) \in \mathbb{R}, \quad i\omega \in \mathbb{R} \quad \text{for} \quad \lambda \in R_1 = \bigcup_{p_i, q_i \in \mathbb{R}} [p_i, q_i] \cup [0, \infty] \tag{4.52a}$$

$$i\mu(\lambda) \in \mathbb{R}, \quad \omega \in \mathbb{R} \quad \text{for} \quad \lambda \in R_2 = \mathbb{R} \setminus R_1 \tag{4.52b}$$

this condition on $\int_0^{-\sigma^2}\omega_i$ is satisfied if $-\sigma^2 \in R_2$, i.e. $-\sigma^2$ does not lie on any of the real branch cuts pictured in Fig. (2.9).

Turning to E_σ, the Abelian differentials of the second kind $d\Omega_\infty$, $d\Omega_0$ are real on R_1 and imaginary on R_2 and their normalisation condition requires $\int_{p_i}^{q_i} d\Omega_1 = \int_{p_i}^{q_i} d\Omega_2 = 0$. Therefore the restriction that $-\sigma^2 \in R_2$ guarantees that $\Omega_\infty(-\sigma^2)$ and $\Omega_0(-\sigma^2)$ are purely imaginary and hence $\overline{E_\sigma} = E_\sigma$. So, finally, if $\overline{\tilde{b}} = -\tilde{b}$ and $-\sigma^2 \in R_2$ then v is real.

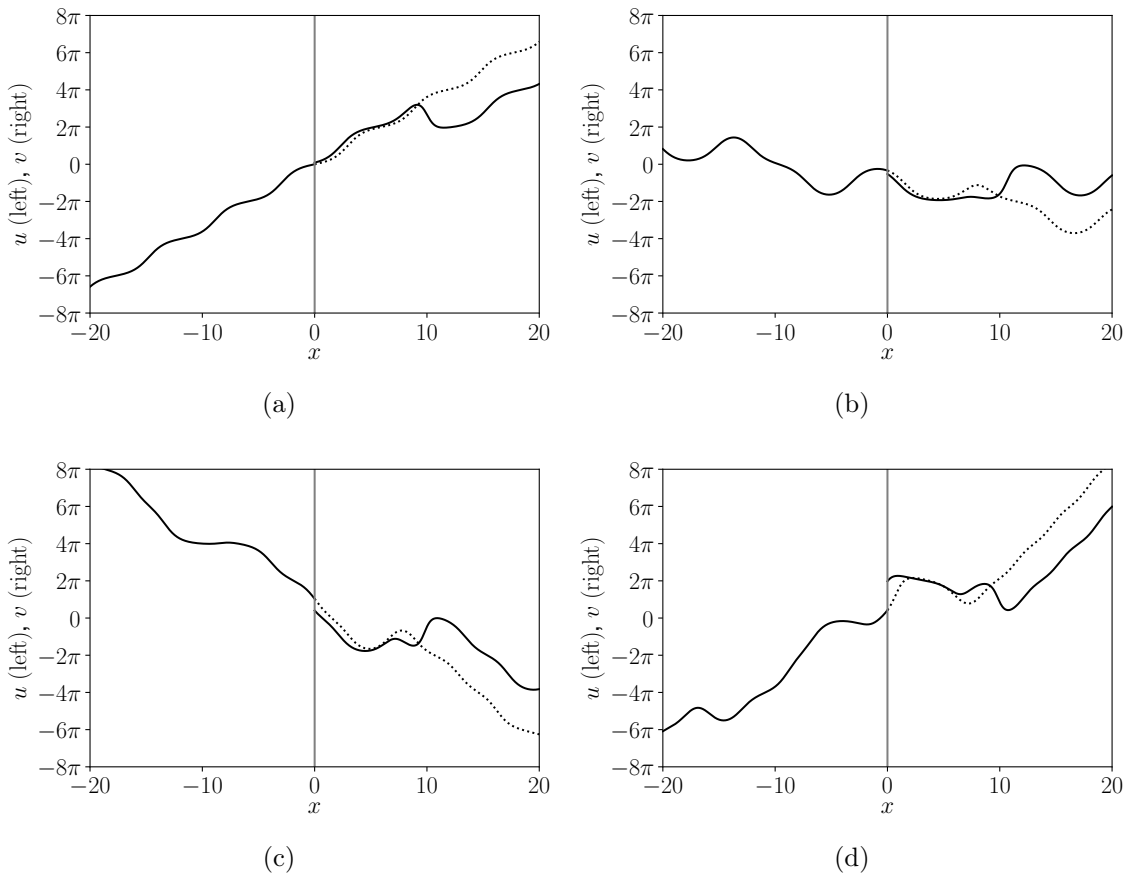

Figure 4.2: Examples of genus 1 (a), 2 (b), 3 (c), 5 (d) algebro-geometric solutions to the sine-Gordon equation with a type I integrable defect at $x = 0$. In each of these examples the field to the right of the defect contains a soliton at $x \approx 10$. For comparison, the dotted line shows the continuation of the field to the left in the absence of the defect.

4.2.4 Phase-shifted and soliton limits

Just as for KdV, the Darboux transformed v (4.51) consists of a soliton on the background of the original algebro-geometric solution u, as shown in Fig. (4.2). The field (4.51) can also be derived as the limit of a genus $g+1$ algebro-geometric solution to sine-Gordon in which one of the pairs of branch points coalesce to the point $-\sigma^2$ [128]. This is explicitly shown in appendix B.

Just as was the case for the one-to-two soliton solution (1.12), it is possible to obtain purely phase-shifted solutions to the defect from (4.51) by taking the limits in which the position of the additional soliton is taken to $\pm\infty$:

$$e^{iv/2} \to \frac{\theta\left(z + \int_0^{-\sigma^2} \omega\right)}{\theta\left(z + i\pi\mathbb{1} + \int_0^{-\sigma^2} \omega\right)}, \qquad \text{as } b \to 0\,,$$

$$e^{iv/2} \to -\frac{\theta\left(z - \int_0^{-\sigma^2} \omega\right)}{\theta\left(z + i\pi\mathbb{1} - \int_0^{-\sigma^2} \omega\right)}, \qquad \text{as } b \to \infty\,.$$

For comparison with (2.114) this can also be written as

$$e^{iv/2} \to \frac{\theta(z+\Delta)}{\theta(z+i\pi\mathbb{1}+\Delta)}, \qquad \Delta = \begin{cases} \int_0^{-\sigma^2} \omega & \text{for } b \to 0 \\ Bn - \int_0^{-\sigma^2} \omega & \text{for } b \to \infty \end{cases} \tag{4.53}$$

for some $n \in \mathbb{Z}^g$ whose sum of elements $\sum n_i$ is odd. This is the natural generalisation to higher genera of the integral expression for Δ obtained in the elliptic ($g = 1$) case in §3.

The one-to-two soliton solution discussed in §1.1.3 can also be recovered from (4.51) by taking $g = 1$ and the soliton limit in which $q_1 \to p_1 =: \lambda_1 < 0$. The details of this limit for a genus g solution to sine-Gordon are reviewed for convenience in appendix A. As in appendix A, parameterise D by

$$D = -x_\theta + i\pi/2 + i\pi\varepsilon - B/2\,, \quad x_\theta \in \mathbb{R}\,,$$

so that in the soliton limit the algebro-geometric solution for the field in $x \le x_D$, (2.114) with $g = 1$, becomes

$$\begin{gathered} e^{iu/2} \to \frac{1+iE_\theta}{1-iE_\theta}\,, \\ E_\theta = (-1)^\varepsilon \exp\left[\cosh(\theta)x - \sinh(\theta)t - x_\theta\right], \quad \theta = -\frac{1}{2}\log(-\lambda_1)\,. \end{gathered} \tag{4.54}$$

Upon setting $\varepsilon = 0$ this matches the one soliton solution (1.8).

For the field to the right of the defect, it was already found in (3.2) that in the soliton limit

$$\exp\left[\int_0^{-\sigma^2} \omega\right] \to \delta = \coth\left(\frac{\eta-\theta}{2}\right),$$

where $\sigma = \exp(-\eta)$. This can also be confirmed by directly integrating the holomorphic differential in the soliton limit (A.2) for the case where $\lambda_{2g+1} = 0$ and $g = 1$. The soliton limit of the Abelian integrals of the second kind can be similarly found, using (A.17) and assuming $\sigma > 0$, to be

$$\Omega_\infty(-\sigma^2) \to \int_0^{-\sigma^2} \frac{1}{2\sqrt{\lambda}} = i\sigma\,, \qquad \Omega_0(-\sigma^2) \to \int_\infty^{-\sigma^2} -\frac{1}{2\lambda\sqrt{\lambda}} = \frac{1}{i\sigma}\,,$$

where the path of integration for Ω_0 avoids the singularity at 0. Finally, reparameterize $\widetilde{b} = \pm i\exp(-x_\eta)$ for $x_\eta \in \mathbb{R}$ so that in the soliton limit

$$\widetilde{b}E_\sigma \to \pm iE_\eta = \pm i\exp\left[\cosh\eta\, x - \sinh\eta\, t - x_\eta\right],$$

then in the original x, t coordinates (4.51) becomes

$$e^{iv/2} \to \frac{(1+i\delta E_\theta) \pm iE_\eta(1+i\delta^{-1}E_\theta)}{(1-i\delta E_\theta) \mp iE_\eta(1-i\delta^{-1}E_\theta)}\,, \tag{4.55}$$

which is precisely the two soliton field (1.12) to the right of the defect in the one-to-two soliton solution, discussed in §1.1.3, which involves soliton emission by the defect.

The N phase-shifted or N-to-N+1 soliton solution could be derived in the same way using the multi-soliton limit (A.20) of the genus $g = N$ algebro-geometric solution to the

defect equations. This approach can be used to prove that each soliton is individually phase-shifted by the defect since, in the soliton limit, the phase shift experienced by the i^{th} soliton due to the defect,

$$\exp\left[\int_0^{-\sigma^2} \omega_i\right] \to \coth\left[\frac{\eta - \theta_i}{2}\right], \tag{4.56}$$

depends only on the i^{th} soliton's rapidity, θ_i and the defect parameter $\sigma = \exp(-\eta)$.

The field consisting of the general algebro-geometric solution to sine-Gordon, (4.49), for $x \leq x_D$ and the Darboux transformed field, (4.51), for $x \geq x_D$ is therefore an algebro-geometric generalisation of all the soliton solutions to the sine-Gordon equation with a type I integrable defect at $x = x_D$.

5 | Defects in 2+1 dimensions

The integrable defects for nonlinear integrable PDEs considered in the literature up to now all have the form of a set of sewing conditions at a point relating the fields of a 1+1 dimensional field theory on each side to one another. However, there are nonlinear integrable PDEs in higher dimensions so one might wonder if similar integrable defects but on a curve or surface could also be constructed for these systems. This chapter is an initial exploration of defects on a line for the integrable 2+1 dimensional Kadomtsev-Petviashvili (KP) equation [28],

$$3\varepsilon^2 u_{yy} = \frac{\partial}{\partial x}\left[4u_t - 6uu_x - u_{xxx}\right] , \tag{5.1}$$

where $\varepsilon^2 = \pm 1$. When $\varepsilon^2 = -1$ $(+1)$ the above equation is known as the KP1 (KP2) equation. If the field $u(x, y, t)$ is independent of y then the KP equation reduces to the KdV equation (2.59) after rescaling $t \to -4t$ and $u \to -u$.

Given the relationship between the type I integrable defect and the Bäcklund transformation for the KdV equation, it might be expected that a Bäcklund transformation for the KP equation applied along a curve in the x, y plane, rather than for all x, y, would constitute an integrable defect. This conjecture will not be proved here but it will be shown that defects applied along the lines $y = 0$ or $x = 0$ with sewing conditions equivalent to a Bäcklund transformation on the line do allow for the energy and momentum of the system to be conserved. However, only in the $y = 0$ case is a Lagrangian description for this defect found. Conservation of energy and momentum in the presence of a defect appears to be an indicator of integrability, at least in 1+1 dimensions where the conditions imposed on the defect by requiring conservation of energy and momentum were sufficient to derive the integrable defect [73, 75].

As with the KdV equation it is convenient to work in terms of the potential field p where $u = p_x$ and

$$3\varepsilon^2 p_{yy} = \partial_x\left(4p_t - 3p_x^2 - p_{xxx}\right) , \tag{5.2}$$

which becomes (5.1) after differentiating once with respect to x. A Bäcklund transformation for the potential KP equation (5.2) is

$$\varepsilon\partial_y\partial_x^{-1}(q-p) = q_x + p_x + \frac{1}{2}(q-p)^2 + 2\sigma(q-p) , \tag{5.3a}$$

$$\begin{aligned} 2\partial_t\partial_x^{-1}(q-p) = {} & \frac{1}{2}(q_{xx} - p_{xx}) + \frac{3}{2}(2\sigma + q - p)(q_x + p_x) + \frac{1}{2}(q-p)^3 + 3\sigma(q-p)^2 \\ & + 6\sigma^2(q-p) + \frac{3\varepsilon}{2}(p_y + q_y) , \end{aligned} \tag{5.3b}$$

where σ is a constant. The antiderivative operator ∂_x^{-1} might be expressed as an integral

but this may be difficult in the defect model since p and q will not be defined everywhere. Instead ∂_x^{-1} will be defined here such that $\partial_x^{-1}p = \log(f)$ where $u = \log(f)_{xx}$ and

$$(3\varepsilon^2 D_y^2 + D_x^4 - 4D_xD_t)f \cdot f = 0\,, \tag{5.4}$$

where the D is the Hirota derivative,

$$D_t^m D_x^n a \cdot b = \left[(\partial_t - \partial_{t'})^m (\partial_x - \partial_{x'})^n a(t,x)b(t',x')\right]\big|_{t'=t,x'=x}\,.$$

Similarly, $\partial_x^{-1}q = \log(g)$ where g also satisfies (5.4). With these definitions (5.3) agrees with the Bäcklund transformation given in [129] in terms of f, g. When (5.4) is divided by f^2 and then differentiated twice with respect to x it becomes the KP equation (5.1). As expected, $\partial_x\partial_x^{-1} = 1$.

Another oddity of the Bäcklund transformation (5.3) is that $\varepsilon \to -\varepsilon$ alters the Bäcklund transformation but not the KP equation. Despite this, (5.3) remains a Bäcklund transformation after taking $\varepsilon \to -\varepsilon$.

5.1 Conserved quantities

Without any defect the energy on the full x, y plane [130],

$$E = \int_{-\infty}^{\infty}\int_{-\infty}^{\infty} \mathcal{E}\,dxdy\,, \qquad \mathcal{E} = p_{xx}^2 - 2p_x^3 - 3\varepsilon^2 p_y^2\,, \tag{5.5}$$

is conserved since, using (5.2),

$$\partial_t\mathcal{E} = \partial_x\left(4p_t^2 + 2p_{xx}p_{xt} - 2p_{xxx}p_t - 6p_x^2p_t\right) - \partial_y\left(6\varepsilon^2 p_y p_t\right)\,,$$

and it is assumed that the derivatives of p vanish at $\pm\infty$. Similarly, the quantities

$$P_X = \int_{-\infty}^{\infty}\int_{-\infty}^{\infty} 2p_x^2\,dxdy \tag{5.6a}$$

$$P_Y = \int_{-\infty}^{\infty}\int_{-\infty}^{\infty} 2p_xp_y\,dxdy \tag{5.6b}$$

are also conserved since,

$$\partial_t\left(2p_x^2\right) = \partial_y\left(3\varepsilon^2 p_x p_y\right) + \partial_x\left(2p_x^3 + p_xp_{xxx} - \frac{3\varepsilon^2}{2}p_y^2 - \frac{1}{2}p_{xx}^2\right)\,,$$

$$\begin{aligned}\partial_t\left(2p_xp_y\right) = \partial_y&\left(2p_x^3 - 2p_{xt}p + 6pp_xp_{xx} + pp_{xxxx} + \frac{3\varepsilon^2}{2}p_y^2 - \frac{1}{2}p_{xx}^2\right)\\ &+\partial_x\left(2p_{yt}p - 6pp_{xy}p_x - p_{xxxy}p + p_{xxy}p_x\right)\,.\end{aligned}$$

P_X and P_Y are the x and y components respectively of the conserved momentum [130].

5.2 Defect along $y = 0$

Now suppose a defect is placed on the line $y = 0$ so that the total action is

$$S = \iint \left[\int_{-\infty}^{0} \mathcal{L}(p) dy + B + \int_{0}^{\infty} \mathcal{L}(q) dy \right] dt\, dx\,,$$

where the Lagrangian density for the potential KP equation is

$$\mathcal{L} = -\frac{3\varepsilon^2}{2} p_y^2 + 2 p_t p_x + \frac{1}{2} p_{xx}^2 - p_x^3\,.$$

If it is assumed that the defect term is of the form

$$B = B(p, \partial_t \partial_x^{-1} p, p_x, q, \partial_t \partial_x^{-1} q, q_x)$$

then the variation of the action is

$$\begin{aligned}
\delta S = \int_{-\infty}^{\infty} \int_{-\infty}^{\infty} dt dx \Bigg(& \int_{-\infty}^{0} (-3\varepsilon^2 \delta p_y p_y + 2\delta p_t p_x + 2 p_t \delta p_x + \delta p_{xx} p_{xx} - 3\delta p_x p_x^2) dy \\
& + \left[\delta p \frac{\partial B}{\partial p} + \delta(\partial_t \partial_x^{-1} p) \frac{\partial B}{\partial(\partial_t \partial_x^{-1} p)} + \delta p_x \frac{\partial B}{\partial p_x} + \delta q \frac{\partial B}{\partial q} + \delta(\partial_t \partial_x^{-1} q) \frac{\partial B}{\partial(\partial_t \partial_x^{-1} q)} + \delta q_x \frac{\partial B}{\partial q_x} \right] \Bigg|_{y=0} \\
& + \int_{0}^{\infty} (-3\varepsilon^2 \delta q_y q_y + 2\delta q_t q_x + 2 q_t \delta q_x + \delta q_{xx} q_{xx} - 3\delta q_x q_x^2) dy \Bigg)\,.
\end{aligned}$$

After using integration by parts and (5.2) there remains only the boundary terms at $y = 0$,

$$\begin{aligned}
\delta S = \iint dt dx \Bigg[& \delta p \left(-3\varepsilon^2 p_y + \frac{\partial B}{\partial p} + \partial_t \partial_x^{-1} \frac{\partial B}{\partial(\partial_t \partial_x^{-1} p)} - \frac{\partial}{\partial x} \frac{\partial B}{\partial p_x} \right) \\
& + \delta q \left(3\varepsilon^2 q_y + \frac{\partial B}{\partial q} + \partial_t \partial_x^{-1} \frac{\partial B}{\partial(\partial_t \partial_x^{-1} q)} - \frac{\partial}{\partial x} \frac{\partial B}{\partial q_x} \right) \Bigg] \Bigg|_{y=0}\,,
\end{aligned} \tag{5.7}$$

which give the defect equations at $y = 0$,

$$3\varepsilon^2 p_y = \frac{\partial B}{\partial p} + \partial_t \partial_x^{-1} \frac{\partial B}{\partial(\partial_t \partial_x^{-1} p)} - \frac{\partial}{\partial x} \frac{\partial B}{\partial p_x}\,, \tag{5.8a}$$

$$-3\varepsilon^2 q_y = \frac{\partial B}{\partial q} + \partial_t \partial_x^{-1} \frac{\partial B}{\partial(\partial_t \partial_x^{-1} q)} - \frac{\partial}{\partial x} \frac{\partial B}{\partial q_x}\,. \tag{5.8b}$$

Note that for the terms involving ∂_x^{-1} it is possible to perform integration by parts because $\partial_x \partial_x^{-1} = 1$. For example,

$$(\partial_x^{-1} F) G = (\partial_x^{-1} F) \partial_x \partial_x^{-1} G = \partial_x \left[(\partial_x^{-1} F)(\partial_x^{-1} G) \right] - F \partial_x^{-1} G\,.$$

It is also clear from (5.7) that if a $\partial_y^n p$ or $\partial_y^n q$ term had been included in B then

$$\frac{\partial B}{\partial(\partial_y^n p)} = 0\,, \qquad \frac{\partial B}{\partial(\partial_y^n q)} = 0\,,$$

since there is no $\delta p_{y\ldots}$ term coming from the bulk in (5.7). The dependence of B on higher order derivatives of x and t is not ruled out but it will been seen that the present

assumption is sufficient.

The form of the defect equations (5.8) already ensures that, with the addition of a suitable defect term, the x component of the momentum is conserved since

$$\begin{aligned}(P_X)_t &= \int_{-\infty}^{\infty} 3\varepsilon^2 \left[p_x p_y - q_x q_y\right]\Big|_{y=0} dx \\ &= \int_{-\infty}^{\infty} \left[p_x \frac{\partial B}{\partial p} + p_t \frac{\partial B}{\partial(\partial_t \partial_x^{-1} p)} - \frac{\partial}{\partial t}\left(p \frac{\partial B}{\partial(\partial_t \partial_x^{-1} p)}\right) + p_{xx} \frac{\partial B}{\partial p_x}\right. \\ &\qquad \left. + q_x \frac{\partial B}{\partial q} + q_t \frac{\partial B}{\partial(\partial_t \partial_x^{-1} q)} - \frac{\partial}{\partial t}\left(q \frac{\partial B}{\partial(\partial_t \partial_x^{-1} q)}\right) + q_{xx} \frac{\partial B}{\partial q_x}\right]\Big|_{y=0} dx \\ &= \int_{-\infty}^{\infty} \left[-\frac{\partial}{\partial t}\left(p \frac{\partial B}{\partial(\partial_t \partial_x^{-1} p)} + q \frac{\partial B}{\partial(\partial_t \partial_x^{-1} q)}\right) + \frac{dB}{dx}\right]\Big|_{y=0} dx \\ &= \int_{-\infty}^{\infty} \left[-\frac{\partial}{\partial t}\left(p \frac{\partial B}{\partial(\partial_t \partial_x^{-1} p)} + q \frac{\partial B}{\partial(\partial_t \partial_x^{-1} q)}\right)\right]\Big|_{y=0} dx\,.\end{aligned}$$

The energy can be similarly modified to give a conserved quantity because

$$E_t = 2\int_{-\infty}^{\infty} \left[\frac{\partial}{\partial t}\left((\partial_t \partial_x^{-1} p) \frac{\partial B}{\partial(\partial_t \partial_x^{-1} p)} + (\partial_t \partial_x^{-1} q) \frac{\partial B}{\partial(\partial_t \partial_x^{-1} q)}\right) - \frac{dB}{dt}\right]\Big|_{y=0} dx\,.$$

Ensuring the conservation of the y component of the momentum is not so straightforward but this can be arranged if the defect conditions (5.8) have the same form as the Bäcklund transformation (5.3). Accordingly, let the defect conditions have the form

$$3\varepsilon p_y = 2\partial_t \partial_x^{-1}(q-p) + 6\sigma^2(p-q) + \frac{1}{2}(p-q)^3 - 3\sigma(p-q)^2 - 3(2\sigma+q-p)q_x - p_{xx} - 2q_{xx} \quad (5.9a)$$

$$-3\varepsilon q_y = 2\partial_t \partial_x^{-1}(p-q) - 6\sigma^2(p-q) - \frac{1}{2}(p-q)^3 + 3\sigma(p-q)^2 + 3(2\sigma+q-p)p_x - 2p_{xx} - q_{xx} \quad (5.9b)$$

so that subtracting and adding these two equations gives (5.3b) and the x derivative of (5.3a). These conditions follow from (5.8) if B is chosen to be

$$\begin{aligned}B = \varepsilon \Big[&(p-q)\partial_t \partial_x^{-1}(q-p) + 3\sigma^2(p-q)^2 - \sigma(p-q)^3 + \frac{1}{8}(p-q)^4 \\ &+ \frac{3}{2}(p^2 q_x + q^2 p_x) + p_x q_x + \frac{1}{2}(p_x + q_x)^2 + 3\sigma(q p_x - p q_x)\Big]\,.\end{aligned} \quad (5.10)$$

With the particular defect equations (5.9) the y component of the momentum is then conserved,

$$(P_Y)_t = \int_{-\infty}^{\infty} \partial_t \left[q p_x - p q_x - \frac{1}{3}(p-q)^3 + 2\sigma(q-p)^2\right]\Big|_{y=0} dx\,.$$

5.3 Comments on defects along $x = 0$

It is encouraging that an energy and momentum conserving defect along $y = 0$ can be constructed but this appears to be much more challenging to do for a general defect geometry, at least using the above Lagrangian based method. In the case where the defect lies along

$x = 0$ the variation of the action gives

$$\delta S = \iint dtdy \left[\delta p(2p_t - p_{xxx} - 3p_x^2) + \delta p_x p_{xx} - \delta q(2q_t - q_{xxx} - 3q_x^2) - \delta q_x q_{xx} + \delta B\right]\Big|_{x=0} \tag{5.11}$$

leading to the defect equations

$$2p_t - p_{xxx} - 3p_x^2 = -\frac{\delta B}{\delta p}\,, \quad 2q_t - q_{xxx} - 3q_x^2 = \frac{\delta B}{\delta q}\,, \quad p_{xx} = -\frac{\delta B}{\delta p_x}\,, \quad q_{xx} = \frac{\delta B}{\delta q_x}\,. \tag{5.12}$$

As with the $y = 0$ defect it is fairly straightforward to show that the energy and the component of the momentum parallel to the $x = 0$ defect, in this case P_Y, can be conserved without any strong assumptions on the specific form of B. If it is further assumed that the defect equations (5.12) are

$$p_{xx} + q_{xx} = \varepsilon(q_y - p_y) - (q_x - p_x)(2\sigma + q - p) \tag{5.13a}$$

$$p_{xxx} - q_{xxx} = 4(p_t - q_t) + 3(q_x^2 - p_x^2) + 3\varepsilon(p_{xy} + q_{xy}) + 3\varepsilon(2\sigma + q - p)(q_y - p_y) \tag{5.13b}$$

$$\begin{aligned} p_{xx} - q_{xx} = {} & -\frac{4}{\varepsilon}\partial_y^{-1}\left[q_{tx} + p_{tx} + (2\sigma + q - p)(q_t - p_t)\right] + 3(2\sigma + q - p)(p_x + q_x) \\ & + (q - p)^3 + 6\sigma(q - p)^2 + 12\sigma^2(q - p) + 3\varepsilon(p_y + q_y) \end{aligned} \tag{5.13c}$$

$$p_{xxx} + q_{xxx} = \varepsilon(q_{yx} - p_{yx}) - (q_x - p_x)^2 - (2\sigma + q - p)(q_{xx} - p_{xx}) \tag{5.13d}$$

then P_X with an additional defect term is also conserved,

$$(P_X)_t = \int \partial_t \left[\frac{2}{3}(p - q)^3 - 2\sigma(p - q)^2 + 2(p_x + q_x)(p - q)\right]\Big|_{x=0} dy\,.$$

However, it does not appear to be possible to construct a B such that (5.13) follows from (5.12). Equations (5.13a) (the x derivative of (5.3a)) and (5.13b) (the x derivative of (5.3b) after using (5.13a) to eliminate $p_{xx} + q_{xx}$) can be obtained readily enough with a suitable choice of B. Equation (5.13c) is the combination of (5.3b) and the equation obtained from applying $\partial_t\partial_y^{-1}\partial_x$ to (5.3a) and can also be obtained by adding terms involving $\partial_y^{-1}p$ and $\partial_y^{-1}q$ to B. It appears to be necessary to write (5.13c) in this way, using ∂_y^{-1}, because the expression for $p_{xx} - q_{xx}$ given directly by (5.3b) involves ∂_x^{-1} terms which cannot be introduced from the defect equations (5.12) since there is no $\delta\partial_x^{-1}p$ or $\delta\partial_x^{-1}q$ term appearing from the bulk in the variation of the action (5.11). However, this then leads to an unwanted $(2k + q - p)\partial_y^{-1}\left[(2\sigma + q - p)(q_t - p_t)\right]$ term in the expression for $p_{xxx} + q_{xxx}$ derived from (5.12) which it seems cannot be removed to give (5.13d) (the x derivative of (5.13a)).

One possible resolution of this issue might be to work with the field ϕ where $u = \phi_{xx}$ instead of p since this would eliminate the ∂_x^{-1} operators from (5.3). The equation obtained from substituting $u = \phi_{xx}$ into the KP equation (5.1) does have a corresponding Lagrangian [131] and it is likely that B would not need to depend on inverse derivatives in order to lead to defect equations equivalent to the Bäcklund transformation in terms of ϕ. Finding a Lagrangian description for a defect which conserves the energy and momentum equivalents for this system in terms of ϕ may therefore be a more tractable problem, although one which will be left to the future.

6 | Integrable boundaries and algebro-geometric solutions

Returning to 1+1 dimensions, another way to modify an integrable field theory, apart from introducing internal boundary conditions such as defects, is to restrict the field theory to the half-line $x \leq 0$ and introduce boundary conditions at $x = 0$.

A simple integrable boundary condition for the sine-Gordon equation

$$u_{tt} - u_{xx} + \sin(u) = 0\,,$$

is the Dirichlet boundary condition $u(0,t) = u_0 \in \mathbb{R}$. In the soliton case the sine-Gordon equation with a Dirichlet boundary condition can be solved using a method of images by treating $u(0,t) = u_0$ as an internal boundary condition on the full line. In the specific case $u(0,t) = 0$ two kinks or two antikinks positioned symmetrically with respect to the point $x = 0$ and with opposite velocities will satisfy $u(0,t) = 0$ [132]. For general u_0 it is necessary to place a stationary third soliton in the vicinity of $x = 0$ in order to satisfy $u(0,t) = u_0$ [68]. Solutions involving higher numbers of solitons colliding with the boundary can be accommodated by adding the corresponding 'image' solitons. The solution on the half-line is then the restriction of these soliton or multi-soliton solutions on the full line to $x \leq 0$.

One interesting way to derive more complex integrable boundary conditions is by the application of a Bäcklund transformation [133, 65, 70, 68, 134]

$$u_x = v_t - \sigma \sin\left(\frac{u+v}{2}\right) - \frac{1}{\sigma}\sin\left(\frac{u-v}{2}\right)\,, \tag{6.1a}$$

$$v_x = u_t + \sigma \sin\left(\frac{u+v}{2}\right) - \frac{1}{\sigma}\sin\left(\frac{u-v}{2}\right)\,. \tag{6.1b}$$

Specifically, if $u(0,t) = 0 \pmod{2\pi}$ then (6.1b) implies that at $x = 0$ the Bäcklund transformed field v satisfies

$$v_x = \pm 2\cosh\eta \,\sin\left(\frac{v}{2}\right)\,, \tag{6.2}$$

where $\sigma = \exp(-\eta)$ and the $+$ corresponds to $u(0,t) = 0 \pmod{4\pi}$ while the $-$ to $u(0,t) = 2\pi \pmod{4\pi}$. If instead $u(0,t) = \pi \pmod{2\pi}$ then at $x = 0$

$$v_x = \pm 2\sinh\eta \,\cos\left(\frac{u}{2}\right)\,, \tag{6.3}$$

where $\pm$ corresponds to $u(0,t) = \mp\pi \pmod{4\pi}$. More generally, if $u(0,t) = u_0$, $u_0 \in \mathbb{R}$

then at $x = 0$,

$$v_x = 2\cosh(\eta)\cos\left(\frac{u_0}{2}\right)\sin\left(\frac{v}{2}\right) - 2\sinh(\eta)\sin\left(\frac{u_0}{2}\right)\cos\left(\frac{v}{2}\right) . \tag{6.4}$$

After using the reparametrization suggested in [68],

$$M\cos\left(\frac{\phi}{2}\right) \equiv 2\cosh(\eta)\cos\left(\frac{u_0}{2}\right), \qquad M\sin\left(\frac{\phi}{2}\right) \equiv 2\sinh(\eta)\sin\left(\frac{u_0}{2}\right) \tag{6.5}$$

where $0 \leq \eta < \infty$ and $-\pi < u_0/2 \leq \pi$, (6.4) becomes the integrable boundary condition

$$v_x = M\sin\left(\frac{v-\phi}{2}\right) . \tag{6.6}$$

The boundary (6.2) was first obtained by Sklyanin [64] while the more general boundary condition (6.6) was later found by Ghoshal and Zamolodchikov (GZ) [66] using an approach which will be summarised later in §7.2.

As has already been discussed the type I integrable defects for sine-Gordon have the same form as the Bäcklund transformation equations (6.1) but are applied at a point, say $x = x_D$, rather than over the full line. Therefore, an equivalent way to view the dressing of boundaries by Bäcklund transformations is to instead consider an integrable defect placed next to an integrable boundary. Suppose the field $v(x,t)$ exists on a segment $x_D \leq x \leq 0$ between a type I integrable defect at x_D and a Dirichlet boundary $v(0,t) = v_0$, $v_0 \in \mathbb{R}$. In the limit $x_D \to 0$, v only exists at the point $x = 0$ and the first of the defect equations (6.1a) implies that

$$u_x = 2\sinh(\eta)\sin\left(\frac{v_0}{2}\right)\cos\left(\frac{u}{2}\right) - 2\cosh(\eta)\cos\left(\frac{v_0}{2}\right)\sin\left(\frac{u}{2}\right) ,$$

which after using

$$M\cos\left(\frac{\phi}{2}\right) \equiv -2\cosh(\eta)\cos\left(\frac{v_0}{2}\right) , \qquad M\sin\left(\frac{\phi}{2}\right) \equiv -2\sinh(\eta)\sin\left(\frac{v_0}{2}\right) ,$$

becomes

$$u_x = M\sin\left(\frac{u-\phi}{2}\right) .$$

In addition, the dressing of integrable boundaries by integrable defects in the setting of quantum field theory was recently examined in [135] for sine-Gordon as well as the $a_2^{(1)}$ and $a_2^{(2)}$ affine Toda field theories.

A single soliton solution to the GZ boundary (6.6) can, similarly to the Dirichlet case, be constructed as the restriction to the half-line of a three soliton solution on the full line consisting of a static soliton near the boundary and an 'image' soliton with opposite rapidity to the 'real' soliton [68]. The initial position and topological charge of the 'image' and static boundary solitons depend on the values of the boundary parameters M, ϕ. Therefore, on the half-line a soliton encountering such a boundary is seen to be reflected without loss of energy but may reverse its topological charge depending on M, ϕ. An N soliton solution to the GZ boundary can similarly be constructed using a $2N+1$ solution on the full line [69]. Boundary breather solutions can also be constructed by taking the

rapidities of pairs of 'real' and 'image' solitons to be complex conjugate as well as equal and opposite (i.e. purely imaginary) [68, 69].

Algebro-geometric solutions to the sine-Gordon equation on the half-line have been found for the integrable boundaries $u = u_0 \pmod{2\pi}$ [70] and $u_x = M\sin(u/2)$ [71] by imposing a constraint on the Lax pair eigenfunction such that the Lax pair equations imply the boundary condition. This chapter will discuss the construction of algebro-geometric solutions to the more general GZ boundary (6.6) via a Bäcklund transformation of a slightly modified version of the Dirichlet boundary solution found in [70] (satisfying $u = u_0 \bmod 4\pi$ instead of mod 2π) or, alternatively, by solving a corresponding boundary condition on the Lax pair eigenfunctions.

6.1 The Dirichlet boundary problem

This section summarises the algebro-geometric solutions to the sine-Gordon equation with the Dirichlet boundary problem,

$$u(0,t) = u_0 \mod 2\pi\,, \tag{6.7}$$

as in [70] but with some alternate conventions. This chapter will use the Lax pair

$$\begin{gathered} \psi_x = U(x,t,\lambda)\psi\,, \qquad \psi_t = V(x,t,\lambda)\psi\,, \\ U(u) = \frac{i}{4}\begin{pmatrix} u_t - u_x & \lambda e^{-iu} - 1 \\ e^{iu} - \frac{1}{\lambda} & u_x - u_t \end{pmatrix}, \qquad V(u) = \frac{i}{4}\begin{pmatrix} u_x - u_t & \lambda e^{-iu} + 1 \\ e^{iu} + \frac{1}{\lambda} & u_t - u_x \end{pmatrix}, \end{gathered} \tag{6.8}$$

which is the Lax pair (2.102) for sine-Gordon expressed in lab coordinates x, t. The Lax pair eigenfunctions (2.110) corresponding to algebro-geometric solutions for the sine-Gordon equation can be written in lab coordinates as

$$\psi_1(x,t,P^\pm) = \frac{\theta(D)\,\theta(iVx + iWt + D + \int_0^{P^\pm}\omega)}{\theta(D + \int_0^{P^\pm}\omega)\,\theta(iVx + iWt + D)}\,E(x,t,P^\pm) \tag{6.9a}$$

$$\psi_2(x,t,P^\pm) = \pm\frac{1}{\sqrt{\lambda}}\frac{\theta(D)\,\theta(iVx + iWt + i\pi\mathbb{1} + D + \int_0^{P^\pm}\omega)}{\theta(D + \int_0^{P^\pm}\omega)\,\theta(iVx + iWt + i\pi\mathbb{1} + D)}\,E(x,t,P^\pm) \tag{6.9b}$$

$$E(x,t,P) = \exp\left[\frac{it}{4}\left(\Omega_\infty(P) + \Omega_0(P)\right) + \frac{ix}{4}\left(\Omega_\infty(P) - \Omega_0(P)\right)\right] \tag{6.9c}$$

where $P^\pm = (\pm\mu, \lambda)$ refers to the points on the upper $(+)$ and lower $(-)$ sheets of the Riemann surface which have the same value of λ.

Now suppose that at the boundary at $x = 0$,

$$\theta\left(iWt + D + i\pi\mathbb{1} + \int_0^{P_0}\omega\right) = 0\,, \quad \forall\, t\,, \tag{6.10}$$

where P_0 can be either point on the Riemann surface for which

$$\lambda = \lambda_0 \equiv -e^{-iu_0}\,. \tag{6.11}$$

Then $\psi_2(0,t,P_0)=0$ and the 't-part' of the Lax pair equations, $\psi_t = V\psi$, implies

$$\exp\left[iu_0 - iu(0,t)\right] = 1\,, \tag{6.12}$$

which is equivalent to the Dirichlet boundary condition (6.7).

The condition (6.10) can be arranged by imposing some restrictions on the constant vector D and the branch points λ_i of the Riemann surface [70]

$$\mu^2 = \lambda\prod_{i=1}^{2g}(\lambda-\lambda_i)\,. \tag{6.13}$$

In particular, let the Riemann surface be of odd genus $g=2k+1$, $k\in\mathbb{Z}$, $k\geq 0$ and let the set of branch points $\{\lambda_i\}_{i=1}^{2g}$ be invariant under the transformation $\nu:\lambda\to 1/\lambda$ which permutes the sheets of the Riemann surface. This leads to the symmetries [70]

$$\mathcal{A}=\mathbb{P}\mathcal{A}\mathbb{P}\,,\quad B=\mathbb{P}B\mathbb{P}\,,\quad V=\mathbb{P}V\,,\quad W=-\mathbb{P}W\,, \tag{6.14}$$

where $\mathbb{P}$ is the $g\times g$ exchange matrix $\mathbb{P}_{ij}=\delta_{j,g+1-i}$. In addition,

$$\Omega_\infty(\nu P)=\Omega_0\left(P\right)\,,\quad \Omega_0(\nu P)=\Omega_\infty(P)\,. \tag{6.15}$$

The relation $B=\mathbb{P}B\mathbb{P}$ implies that

$$\theta(\mathbb{P}z)=\theta(z)\,. \tag{6.16}$$

In addition to the restriction on the branch points the constant vector D (2.127) should also be chosen to satisfy [70], [1]

$$\mathbb{P}D+D+\mathbb{P}U(P_0)+U(P_0)+BN=2i\pi\mathbb{1}\,,\qquad U(P)=\int_\infty^P\omega\,, \tag{6.17}$$

where the vector $N\in\mathbb{Z}^g/(2\mathbb{Z}^g)$ is chosen such that

$$N_{(g+1)/2}=1\,,\qquad \mathbb{P}N=N\,. \tag{6.18}$$

Effectively, this fixes the central element $D_{(g+1)/2}$ and choosing the, say, first k elements of D fixes the last k elements. The constraints on the Riemann surface and on D are sufficient to ensure that the field u given by

$$e^{iu/2}=\frac{\theta(iVx+iWt+D)}{\theta(iVx+iWt+D+i\pi\mathbb{1})} \tag{6.19}$$

satisfies $u(0,t)=u_0 \bmod 2\pi$ [70].

For u to be real the boundary conditions (6.17) on D must be compatible with the

[1] Because of the different choice of Lax pair the condition actually implemented in [70] is $\theta(U(P_0)-iWt-D)=0$ instead of (6.10) so the formulas which implement that condition there are related by $U(P_0)\to -U(P_0)$ to those used here.

established reality conditions,

$$\mathrm{Im}[D] = \frac{\pi}{2}\kappa + \pi\varepsilon\,, \quad \varepsilon, \kappa \in \mathbb{Z}^g\,, \quad \kappa_i = \begin{cases} 1, & \text{if } p_i, q_i \in \mathbb{R} \\ 0, & \text{if } p_i = \bar{q}_i \end{cases} \qquad i = 1, \ldots, g\,. \tag{6.20}$$

It should be emphasised that, while each element of ε can be any integer for u to be real, only the value of ε_i modulo 2 is significant due to the symmetries of the Riemann theta function. Requiring the compatibility of the constraints on D leads to

$$\pi\varepsilon_{(g+1)/2} = \frac{\pi}{2} - \mathrm{Im}[U(P_0)_{(g+1)/2}]\,, \tag{6.21a}$$

$$\pi[\kappa + \mathbb{P}\varepsilon + \varepsilon]_i = 2\pi - \pi(1-\kappa_i)N_i - \mathrm{Im}[\mathbb{P}U(P_0) + U(P_0)]_i\,, \quad i = 1, \ldots, \frac{g-1}{2}\,. \tag{6.21b}$$

In order for it to be possible to satisfy (6.21) for some integer values of ε it is necessary to have $U(P_0)$ be such that

$$\mathrm{Im}[U(P_0)_{(g+1)/2}] = \frac{\pi}{2} + n\pi\,, \quad \mathrm{Im}[\mathbb{P}U(P_0) + U(P_0)]_i = m_i\pi\,, \quad i = 1, \ldots, \frac{g-1}{2}\,, \tag{6.22}$$

for some arbitrary $m_i, n \in \mathbb{Z}$.

It is shown in [70] that if all the branch points are real then, for a particular choice of sheet for P_0, $\mathrm{Im}[\mathbb{P}U(P_0) + U(P_0)] = -\pi\mathbb{1}$ which satisfies (6.22). In the general case it is necessary to specify that if the central pair of branch points are complex conjugate (in which case they must lie on the unit circle) then the point $\lambda_0 = -e^{-iu_0}$ must not lie on the arc of the unit circle joining the central pair of branch points and passing through the point $\lambda = -1$. If λ_0 does lie on this arc then $U(P_0) + \mathbb{P}U(P_0)$ becomes generically complex instead of satisfying (6.22) and the reality condition on D will be incompatible with the boundary condition.

This 'reality gap' is essentially the same phenomenon as was found for the algebro-geometric solutions to the type I integrable defects discussed in §3.1. Here, this gap can be viewed as a consequence of the fact that the range of the genus 1 field corresponding to complex branch points is contained within but not equal to $[0, 2\pi]$, as shown in Fig. (6.1b). There will therefore be certain values of $u_0 \in [0, 2\pi]$ (mod 2π) which lie outside of the range of the field and for these cases it will be impossible to satisfy $u(0,t) = u_0$ for the given choice of branch points.

In the genus 1 case, shown in Fig. (6.1a) and Fig. (6.1b), the antisymmetry of W implies that $W = 0$ and therefore the field is static. For higher genera $g = 2k+1$, shown in Fig. (6.1), the field may be thought of as a nonlinear superposition of g components corresponding to the g pairs of branch points joined by finite-length branch cuts. In this view the field consists of a static component corresponding to the central pair of branch points while half of the remaining $2k$ components have opposite velocity and, if the corresponding pairs of branch points are real, equal ε to the other half. This mimics the method of images in the soliton case where, for example, a three soliton solution to the non-homogeneous Dirichlet problem consists of a static kink or anitkink placed near the boundary to satisfy the boundary condition and two solitons of opposite velocity and equal topological charge.

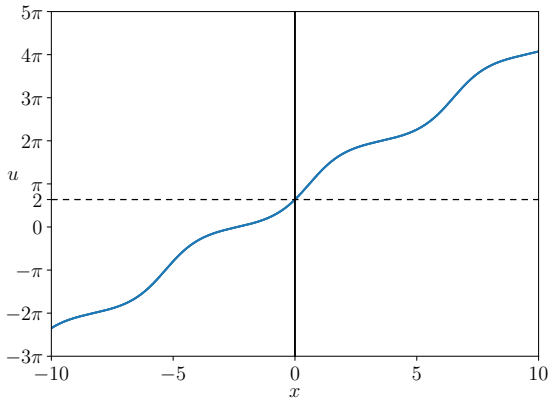

(a) A genus 1 solution.

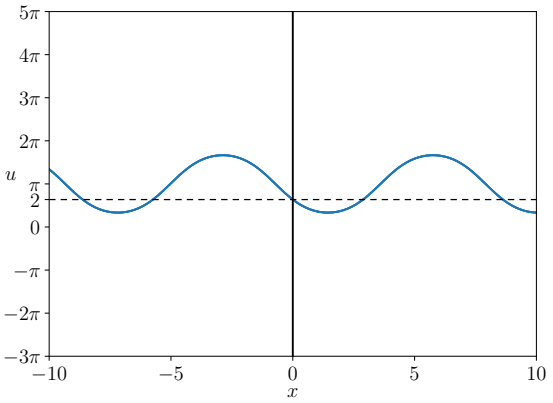

(b) A genus 1 solution.

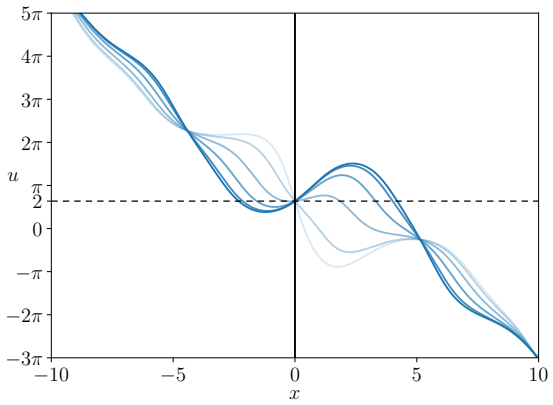

(c) A genus 3 solution with $\varepsilon_1 = 1$, $N_1 = 1$.

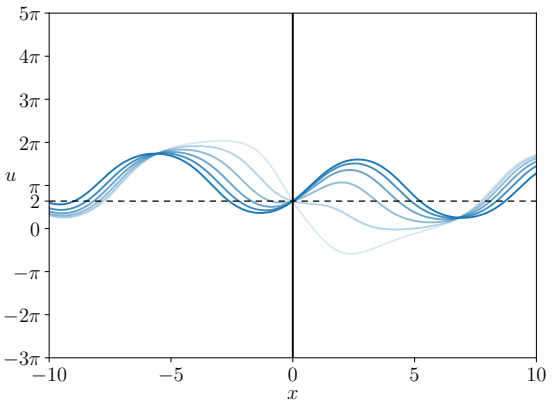

(d) A genus 3 solution with $\varepsilon_1 = 0$, $N_1 = 0$.

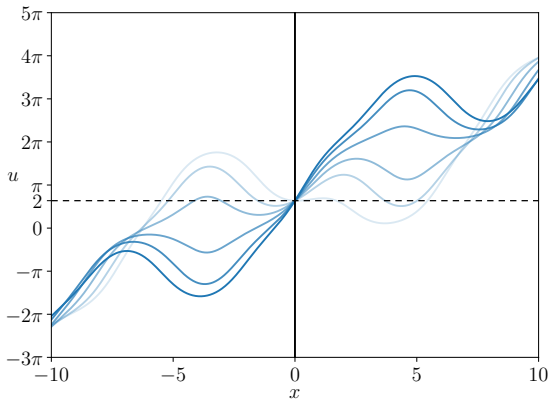

(e) A genus 5 solution with $\varepsilon_1 = 0$, $\varepsilon_2 = 0$, $N_1 = 0$, $N_2 = 0$.

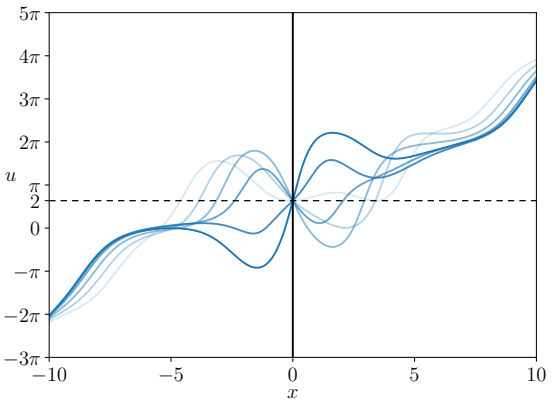

(f) A genus 5 solution with $\varepsilon_1 = 0$, $\varepsilon_2 = 1$, $N_1 = 1$, $N_2 = 0$.

Figure 6.1: Some examples of algebro-geometric solutions satisfying the boundary condition $u(0,t) = 2$. The blue lines are the fields plotted at $t = 0, 1, 2, 3, 4, 5$ with the opacity increasing with time. The chosen branch points $\{(p_1, q_1), \ldots, (p_g, q_g)\}$ in each case are:
a) $\{(-3/2, -2/3)\}$
b) $\{(\exp(-2i\pi/3), \exp(2i\pi/3))\}$
c) $\{(-4, -3), (\exp(-3i\pi/4), \exp(3i\pi/4)), (-1/3, -0.25)\}$
d) $\{(-1-i, -1+i), (\exp(-3i\pi/4), \exp(3i\pi/4)), (-0.5-0.5i, -0.5+0.5i)\}$
e) & f) $\{(-4, -3), (-2-i, -2+i), (-3/2, -2/3), (-0.4-0.2i, -0.4+0.2i), (-1/3, -0.25)\}$

6.1.1 An adjustment

Having described the algebro-geometric solution to the Dirichlet boundary problem the aim is now to apply a Bäcklund transformation to obtain an alegbro-geometric solution to the two parameter Ghoshal-Zamolodchikov boundary.

However, the solution just described solves the Dirichlet boundary $u(0,t) = u_0 \bmod 2\pi$ while the boundary condition (6.4) is not invariant under shifts of $u_0 \to u_0 + 2\pi n$, $n \in \mathbb{Z}$, instead the right hand side gains a factor of $(-1)^n$. In order to define the GZ boundary condition it is therefore necessary to know the value of $u_0 \bmod 4\pi$ and so the solution above needs to be adjusted so that $u(0,t) = u_0 \bmod 4\pi$.

To see how the modulo 2π manifests itself consider for simplicity the elliptic or $g = 1$ case. D and B are now simply numbers and the restriction (6.17) becomes

$$D = i\pi - U(P_0) - B/2\,.$$

Because of the path-dependent nature of integrals on the Riemann surface $U(P_0)$ is only defined mod $2\pi i$ and mod B. Due to the quasi-periodic properties of theta functions (2.48) the mod $2\pi i$ is inconsequential but the mod B is the source of the 2π ambiguity for u since,

$$\frac{\theta(iVx + iWt + D + B)}{\theta(iVx + iWt + D + i\pi + B)} = e^{i\pi}\frac{\theta(iVx + iWt + D)}{\theta(iVx + iWt + D + i\pi)} = -e^{iu/2}\,.$$

A statement of the problem in the genus 1 case is then how to choose the $\pm$ in

$$D = i\pi - U(P_0) \pm B/2\,, \tag{6.23}$$

in order to fix the ambiguity of $U(P_0)$ such that $u(0,t) = u_0 \bmod 4\pi$.

For higher genera a shift $D \to D + BL$ for any $L \in \mathbb{Z}^g$ for which $\sum L_i$ is odd will correspond to the shift of $u \to u + 2\pi \bmod 4\pi$. In particular let $L_i = -\delta_{i,(g+1)/2}$ then the shift $D \to D + BL$ or $U(P_0) \to U(P_0) + BL$ is equivalent to changing $N_{(g+1)/2}$ from 1 to -1. Therefore, one statement of the solution to $u(0,t) = u_0 \bmod 4\pi$ is to simply modify (6.18) so that N is instead given by

$$N_{(g+1)/2} = \pm 1\,, \qquad \mathbb{P}N = N\,, \tag{6.24}$$

where the $\pm$ must be chosen so that $u(0,t) = u_0 \bmod 4\pi$.

Numerically, the right choice of sign for $N_{(g+1)/2}$ can be made by simply testing both cases and choosing the sign that gives $u(0,0) = u_0 \bmod 4\pi$. Analytically, it is not yet clear how to fix this ambiguity *a priori*.

6.2 The Ghoshal-Zamolodchikov boundary problem

Given a field u which satisfies $u(0,t) = u_0 \bmod 4\pi$, a solution to sine-Gordon equation satisfying the two parameter boundary condition (6.4) is given by v, the Bäcklund transformation of u with parameter $\sigma = \exp(-\eta)$. This Bäcklund transformation can implemented

via a Darboux transformation, as in §4.2.2, to find

$$v = 2i \log \left[\frac{\theta\left(z + i\pi\mathbb{1} + \int_0^{-\sigma^2} \omega\right) - \tilde{b} E_\sigma \theta\left(z + i\pi\mathbb{1} - \int_0^{-\sigma^2} \omega\right)}{\theta\left(z + \int_0^{-\sigma^2} \omega\right) + \tilde{b} E_\sigma \theta\left(z - \int_0^{-\sigma^2} \omega\right)} \right],$$
$$E_\sigma = \exp\left[-\frac{it}{2} \left(\Omega_\infty(P) + \Omega_0(P)\right) - \frac{ix}{2} \left(\Omega_\infty(P) - \Omega_0(P)\right) \right], \tag{6.25}$$
$$z = iVx + iWt + D\,, \quad \tilde{b} = b\, \frac{\theta\left(D + \int_0^{-\sigma^2} \omega\right)}{\theta\left(D - \int_0^{-\sigma^2} \omega\right)}\,.$$

If D satisfies its reality conditions, (6.20), then for v to be real it will be required, as in §4.2.3, that $\overline{\tilde{b}} = -\tilde{b}$ and $-\sigma^2 \in R_2$, that is $-\sigma^2$ does not lie on any of the intervals between pairs of real branch points joined by branch cuts. Some examples of algebro-geometric solutions for the sine-Gordon equation satisfying the Ghoshal-Zamolodchikov boundary condition are shown in Fig. (6.2). As before, the E_σ corresponds to a soliton, which can be seen in figures (6.2c) and (6.2d). Taking $\tilde{b} \to 0$ or ∞ recovers the pure algebro-geometric solutions without a soliton.

6.2.1 An alternate approach

Rather than performing a Bäcklund transformation on a solution satisfying the Dirichlet boundary condition, the two parameter boundary (6.4) can also be obtained directly from a condition on the Lax pair eigenfunctions, similarly to how $\psi_2(0,t,P_0) = 0$ was equivalent to the Dirichlet boundary condition.

Suppose there is a field $v(x,t)$ satisfying the sine-Gordon equation with a corresponding Lax pair eigenfunction $\psi = (\psi_1, \psi_2)^T$ satisfying (6.8) such that

$$\psi_1(0,t,P_0) = \frac{1}{i\sigma} \exp\left[-\frac{i}{2}(u_0 + v(0,t)) \right] \psi_2(0,t,P_0)\,, \tag{6.26}$$

where, as before, P_0 is a point on the Riemann surface for which $\lambda = -e^{-iu_0}$. This expression for ψ_1 can be substituted into $\psi_t = V\psi$, given by (6.8), and then using the second row of $\psi_t = V\psi$ to eliminate ψ_{2t} from the first one finds

$$-\frac{1}{2} e^{-\frac{i}{2}(u_0 + v(0,t))} \psi_2(0,t,Q) \left[\frac{1}{\sigma^2} \sin\left(\frac{u_0 - v(0,t)}{2} \right) - \sin\left(\frac{u_0 + v(0,t)}{2} \right) + \frac{1}{\sigma} v_x(0,t) \right] = 0\,. \tag{6.27}$$

The term in square brackets is precisely the two parameter integrable boundary condition (6.4) with $\sigma = \exp(-\eta)$.

Using the explicit form of ψ given by (6.9),

$$\frac{\psi_1(0,t,P_0)}{\psi_2(0,t,P_0)} = \pm\sqrt{-e^{-iu_0}} \frac{\theta(iWt + D + \int_0^{P_0} \omega)\theta(iWt + i\pi\mathbb{1} + D)}{\theta(iWt + D)\theta(iWt + i\pi\mathbb{1} + D + \int_0^{P_0} \omega)}$$
$$= \pm i e^{-iu_0/2} e^{-iv(0,t)/2} \frac{\theta(iWt + D + \int_0^{P_0} \omega)}{\theta(iWt + i\pi\mathbb{1} + D + \int_0^{P_0} \omega)}$$

where the $\pm$ originates from the choice of P_0 lying the upper or lower sheet of the Riemann

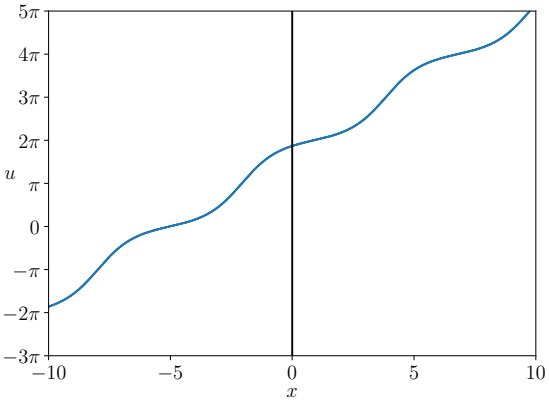

(a) A genus 1 solution with $\tilde{b} = 0$.

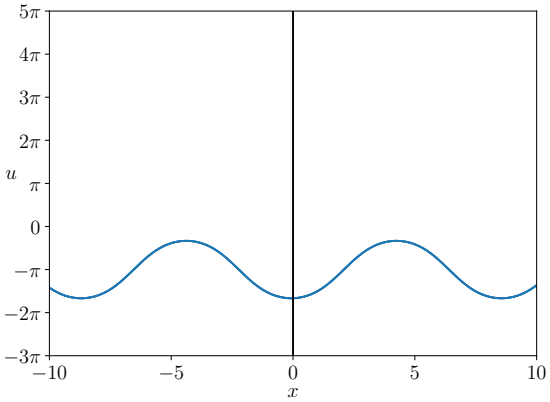

(b) A genus 1 solution with $\tilde{b} = 0$.

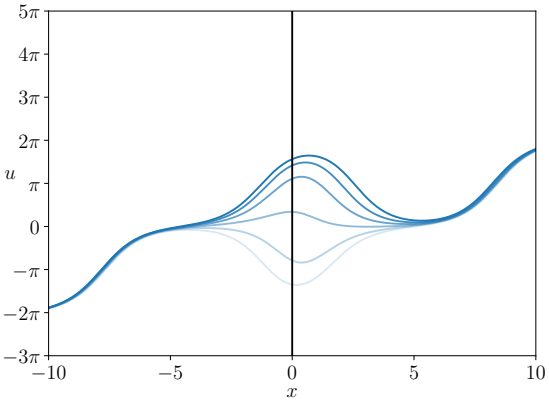

(c) A genus 1 solution with a soliton.

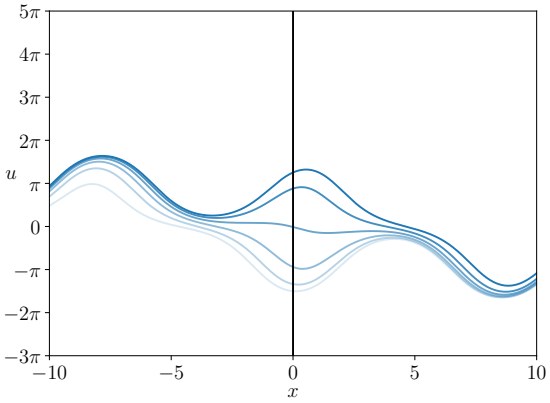

(d) A genus 1 solution with a soliton.

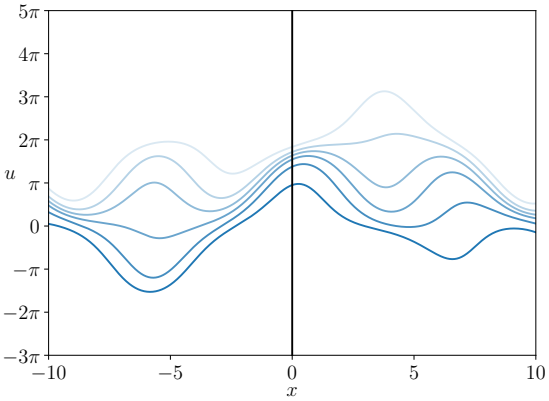

(e) A genus 3 solution with $\tilde{b} = 0$, $\varepsilon_1 = 1$, $N_1 = 0$.

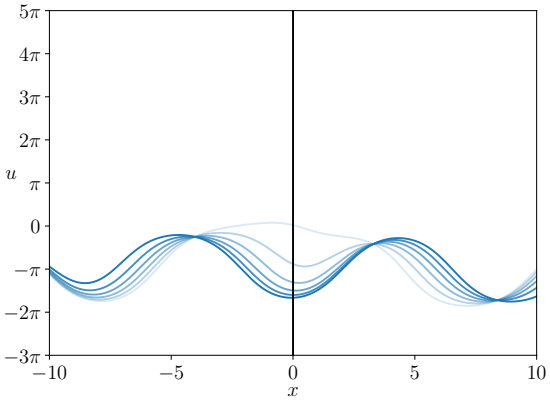

(f) A genus 3 solution with $\tilde{b} = 0$, $\varepsilon_1 = 0$, $N_1 = 0$.

Figure 6.2: Some examples of algebro-geometric solutions satisfying the Ghoshal-Zamolodchikov type boundary condition $u_x(0,t) = 0.8\sin((u(0,t) - 1.2)/2)$. The blue lines are the fields plotted at $t = 0, 1, 2, 3, 4, 5$ with the opacity increasing with time. The chosen branch points $\{(p_1, q_1), \ldots, (p_g, q_g)\}$ in each case are:
a) & c) $\{(-3/2, -2/3)\}$
b) & d) $\{(\exp(-2i\pi/3), \exp(2i\pi/3))\}$
e) $\{(-4, -3), (\exp(-3i\pi/4), \exp(3i\pi/4)), (-1/3, -0.25)\}$
f) $\{(-1 - i, -1 + i), (\exp(-3i\pi/4), \exp(3i\pi/4)), (-0.5 - 0.5i, -0.5 + 0.5i)\}$

surface. Therefore to satisfy (6.26) D must be chosen so that

$$\frac{\theta(iWt + D + \int_0^{P_0}\omega)}{\theta(iWt + i\pi\mathbb{1} + D + \int_0^{P_0}\omega)} = \mp\sigma^{-1}\,. \tag{6.28}$$

It is recognised that $-2i\log$ of the left hand side of this equation is itself a solution to the sine-Gordon equation at $x = 0$ which has been shifted from the usual expression, (2.114), by the integral $\int_0^{P_0}\omega$. Therefore (6.28) has the appearance of another Dirichlet boundary problem, albeit it one where the 'field' has to take a imaginary value, $-2i\eta$, (or $2\pi - 2i\eta$ if the negative sign in (6.28) is chosen) at the boundary.

Based on the recollection in §6.1, the new Dirichlet problem (6.28), at least up to the $\mp$ sign, should be solved by requiring

$$\theta\left(iWt + D + \int_0^{P_0}\omega + i\pi\mathbb{1} + \int_0^{S}\omega\right) = 0\,, \quad \forall\, t\,, \tag{6.29}$$

where S is a point on the Riemann surface where $\lambda = -e^{-2\eta} = -\sigma^2$. The corresponding restriction on D is therefore,

$$\mathbb{P}\left[D + \int_0^{S}\omega\right] + D + \int_0^{S}\omega + \mathbb{P}U(P_0) + U(P_0) + BN = 2i\pi\mathbb{1}\,, \tag{6.30}$$

and, as before, the branch points are required to be symmetric under $\lambda \to 1/\lambda$.

This restriction is the same as (6.17) except that D has been shifted by the integral $\int_0^S\omega$. But this shift is the same as that introduced by the Bäcklund (Darboux) transformation with parameter σ of the solution to the Dirichlet problem $u = u_0$. Therefore, the field obtained here from implementing the constraint (6.30) can be recovered from (6.25) in the phase-shifted limit where $\tilde{b} \to 0$ or $\tilde{b} \to \infty$ and in this sense the two approaches agree.

Since implementing the constraint (6.26) also involves solving a Dirichlet boundary problem it does not circumvent the issue discussed in §6.1.1, which can be expressed as the sign ambiguity (6.24). Clearly, fixing this ambiguity so that it could be guaranteed that $u(0,t) = u_0 \mod 4\pi$ would be the primary goal of future work in this direction. It should also be possible to recover the odd genus algebro-geometric solutions to the Sklyanin boundary, $u_x - M\sin(u/2) = 0$, constructed in [71], as a limit of the solutions to the GZ boundary found here, although this has not yet been shown explicitly.

It does at least appear that the algebro-geometric solutions to the Sklyanin boundary possess the same ambiguity as the one discussed in §6.1.1, although it is not explicitly addressed in [71]. Specifically, [71] implements the boundary condition

$$u_x \mp i\left(\sqrt{\lambda_0} - \frac{1}{\sqrt{\lambda_0}}\right)\sin\frac{u}{2} = 0\,, \tag{6.31}$$

by requiring that

$$\theta\left(\int_\infty^{P_0}\omega - iWt - D\right) = \mp\theta\left(\int_\infty^{P_0}\omega - iWt - D - i\pi\mathbb{1}\right)\,,$$

where the sign choice is correlated with (6.31). However, the conditions prescribed by [71]

only arrange for

$$\left(\frac{\theta\left(\int_\infty^{P_0} \omega - iWt - D\right)}{\theta\left(\int_\infty^{P_0} \omega - iWt - D - i\pi\mathbb{1}\right)} \right)^2 = 1\,,$$

and therefore it does not seem clear whether, for a given λ_0, one is solving (6.31) with the positive or negative sign. As was the case here, the value of u would need to be determined mod 4π to fix the sign in (6.31).

7 | Sine-Gordon with Robin boundary conditions

Non-integrable boundary conditions are of course much more common than the integrable boundaries discussed in the previous chapter. However, one interesting non-integrable boundary is the homogeneous Robin boundary condition

$$u_x + 2ku = 0\,, \qquad k \in \mathbb{R}\,. \tag{7.1}$$

This can be derived as the linearisation in u of the integrable boundary

$$u_x + 4K \sin\left(\frac{u}{2}\right) = 0\,, \tag{7.2}$$

or equivalently the dressing of the integrable boundary $v(0,t) = 0$ by placing the non-integrable linearisation of the defect equations,

$$u_x = v_t + v\sinh\eta - u\cosh\eta\,, \tag{7.3a}$$
$$v_x = u_t + v\cosh\eta - u\sinh\eta\,, \tag{7.3b}$$

where $\sigma = \exp(-\eta)$ next to the boundary. The boundary (7.1) is interesting because, while it is non-integrable in general, it has two integrable limits: as $k \to 0$ the boundary becomes free (Neumann), $u_x(0,t) = 0$ while as $k \to \infty$ the boundary becomes fixed (Dirichlet), $u(0,t) = 0$. Therefore when $k \to \infty$ an antikink colliding with the boundary will be perfectly reflected while when $k = 0$ it will be reflected but will also flip its topological charge, becoming a kink. The central goal of this chapter is to address how the outcome of the antikink/boundary collision interpolates between these two integrable extremes. In doing so some remarkable structures, such as resonance windows, will be found.

7.1 Linearised model

As a simple example of how the Robin boundary interpolates between the Neumann and Dirichlet cases consider the linearisation of the sine-Gordon equation,

$$\phi_{tt} - \phi_{xx} + \phi = 0\,, \tag{7.4}$$

which is known as the Klein-Gordon equation. The travelling wave solution

$$\phi = (e^{i\kappa x} + Re^{-i\kappa x})e^{-i\omega t}\,, \qquad \omega^2 = \kappa^2 + 1\,, \tag{7.5}$$

solves the Klein-Gordon equation in the bulk and the boundary condition $\phi_x + 2k\phi = 0$ determines the reflection coefficient to be

$$R = \frac{\kappa - 2ik}{\kappa + 2ik}\,. \tag{7.6}$$

If $k = 0$ the boundary becomes Neumann and $R = 1$ while in the limit $k \to \infty$ the boundary becomes Dirichlet and $R = -1$.

The Klein-Gordon equation with Robin boundary conditions has been used as a toy model in the context of quantum field theory. For example, Appendix A of [136] checks that the calculation of the reflection factor using a perturbative expansion around the Neumann boundary agrees with the analytical result (7.6).

7.2 Conservation laws

The sine-Gordon equation on the full line possesses an infinite number of independent constants of motion in involution. Here, it will be shown how the Robin boundary modifies some of these low-lying charges in order to investigate the extent of its non-integrability. One way to generate the constants of motion is to consider an infinitesimal Bäcklund transformation, as in [137, 138].

In the light cone coordinates

$$x_\pm = \frac{t \pm x}{4} \tag{7.7}$$

the sine-Gordon equation becomes

$$u_{+-} = -4 \sin u\,. \tag{7.8}$$

If u solves the sine-Gordon equation, (7.8), and u and v satisfy the Bäcklund transformation equations

$$\partial_-(v+u) = -\frac{4}{\sigma}\sin\left(\frac{v-u}{2}\right)\,, \tag{7.9a}$$

$$\partial_+(v-u) = 4\sigma \sin\left(\frac{v+u}{2}\right)\,, \tag{7.9b}$$

then it is easily verified by cross differentiation that v also satisfies (7.8).

In order to generate conservation laws first take the Bäcklund parameter σ to be small and then, following [137, 138], expand v in orders σ,

$$v(x_+, x_-, \sigma) = \sum_{j=0}^{\infty} v_j(x_+, x_-)\sigma^j\,. \tag{7.10}$$

Inserting (7.10) into the first Bäcklund equation (7.9a) and equating coefficients for powers

of σ gives

$$\begin{aligned} v_0 &= u \\ v_1 &= -\partial_- u \\ v_2 &= \frac{1}{2}\partial_-^2 u \\ v_3 &= -\frac{1}{24}\left(u_-^3 + 6u_{---}\right) \\ v_4 &= \frac{1}{8}\left(u_-^2 u_{--} + \partial_-^4 u\right) \\ &\vdots \end{aligned} \tag{7.11}$$

The second Bäcklund equation (7.9b) can be written in the conservation form [138]

$$\partial_+ \left[\frac{u_-}{2}\tan\left(\frac{u-v}{4}\right)\right] = \sigma\partial_- \left[\cos u - 1 + \sin u \tan\left(\frac{u-v}{4}\right)\right] . \tag{7.12}$$

This can be used to generate an infinite number of conservation laws of the forms

$$\partial_+ T_{-s-1} = \partial_- \Theta_{-s+1} , \tag{7.13a}$$

$$\partial_- T_{s+1} = \partial_+ \Theta_{s-1} , \tag{7.13b}$$

where the integer $s > 1$ refers to the Lorentz spin of the conserved charge Q_s,

$$Q_{\pm s} = \int_{-\infty}^{\infty} \left(T_{\pm(s+1)} - \Theta_{\pm(s-1)}\right) dx , \tag{7.14}$$

which to say that it transforms under the Lorentz boost $L_\phi : x_\pm \to x'_\pm = e^{\mp\phi} x_\pm$ with rapidity ϕ as $Q_s \to Q'_s = e^{s\phi} Q_s$. The charges (7.14) are conserved on the full line since

$$\begin{aligned} \partial_t \left(T_{s+1} - \Theta_{s-1}\right) &= \frac{1}{4}\left(\partial_+ T_{s+1} - \partial_- \Theta_{s-1}\right) = \partial_x \left(T_{s+1} + \Theta_{s-1}\right) , \\ \partial_t \left(T_{-s-1} - \Theta_{-s+1}\right) &= \frac{1}{4}\left(\partial_- T_{-s-1} - \partial_+ \Theta_{-s+1}\right) = -\partial_x \left(T_{-s-1} + \Theta_{-s+1}\right) . \end{aligned}$$

The first set of conservation laws (7.13a) can be generated by inserting (7.10), with the expansion coefficients v_j given by (7.11), into (7.12) and again expanding and equating coefficients at each order of σ. The first few orders in σ give:

$$\begin{aligned} O(\sigma): &\quad T_{-2} = \frac{1}{8}u_-^2 && \Theta_0 = \cos u - 1 \\ O(\sigma^2): &\quad T_{-3} = -\frac{1}{4}\partial_- T_2 && \Theta_{-1} = -\frac{1}{4}\partial_- \Theta_0 \\ O(\sigma^3): &\quad T_{-4} = \frac{1}{128}\left(u_-^4 + 4u_- u_{---}\right) && \Theta_{-2} = -\frac{1}{8}\sin u\, u_{--} \\ &\quad \vdots && \vdots \end{aligned}$$

The conservation law $\partial_+ T_{-3} = \partial_- \Theta_{-1}$ is trivial in the sense that it is already implied by $\partial_+ T_{-2} = \partial_- \Theta_0$. Since the sine-Gordon equation (7.8) is invariant under the interchange of $+$ and $-$ the second set of conservation laws (7.13b) can be obtained by transposing $+$

and − derivatives so

$$\begin{aligned} T_2 &= \frac{1}{8}u_+^2 & \Theta_0 &= \cos u - 1 \\ T_4 &= \frac{1}{128}\left(u_+^4 + 4u_+u_{+++}\right) & \Theta_2 &= -\frac{1}{8}\sin u\, u_{++} \\ &\vdots & &\vdots \end{aligned}$$

An infinity of conserved charges can then be defined as

$$E_s = \int_{-\infty}^{\infty} \frac{1}{2}\left[T_{-s-1} - \Theta_{-s+1} + T_{s+1} - \Theta_{s-1}\right] dx\,, \tag{7.15a}$$

$$P_s = \int_{-\infty}^{\infty} \frac{1}{2}\left[T_{-s-1} - \Theta_{-s+1} - T_{s+1} + \Theta_{s-1}\right] dx\,, \tag{7.15b}$$

where the lowest conserved charges are the energy,

$$E \equiv E_1 = \int_{-\infty}^{\infty} \frac{1}{2}\left[\frac{1}{8}u_+^2 + \frac{1}{8}u_-^2 + 2(1-\cos u)\right] dx\,, \tag{7.16}$$

and momentum,

$$P \equiv P_1 = \int_{-\infty}^{\infty} \frac{1}{16}\left[u_-^2 - u_+^2\right] dx\,. \tag{7.17}$$

Turning to the sine-Gordon equation on the half-line, the momentum-like charges will not be conserved but the energy-like charges,

$$E_s = \int_{-\infty}^{0} \frac{1}{2}\left[T_{-s-1} - \Theta_{-s+1} + T_{s+1} - \Theta_{s-1}\right] dx + \mathcal{B}_s\,, \tag{7.18}$$

can be conserved with a suitable boundary contribution $\mathcal{B}_s$, engineered such that

$$\frac{dE_s}{dt} = \frac{1}{2}\left[-T_{-s-1} - \Theta_{-s+1} + T_{s+1} + \Theta_{s-1}\right]\big|_{x=0} + \frac{d\mathcal{B}_s}{dt} = 0\,. \tag{7.19}$$

So, using the Robin boundary condition, $u_x(0,t) = -2ku(0,t)$, the boundary contribution to the energy $\mathcal{B} \equiv \mathcal{B}_1$ must obey

$$\frac{d\mathcal{B}}{dt} = \frac{1}{2}\left[T_{-2} - T_2\right]\big|_{x=0} = \left[-u_t u_x\right]\big|_{x=0} = \left[2kuu_t\right]\big|_{x=0}\,, \tag{7.20}$$

and therefore with $\mathcal{B} = ku^2$ the energy of the system is conserved. In the Neumann or Dirichlet limits the energy is automatically conserved since $u_x(0,t) = 0$ or $u_t(0,t) = 0$ respectively.

However, the $s = 3$ energy-like charge is not conserved since

$$\begin{aligned} \frac{d\mathcal{B}_3}{dt} &= \frac{1}{2}\left[T_{-4} - T_4 + \Theta_{-2} - \Theta_2\right]\big|_{x=0} \\ &= 2k\left[\partial_t\left[4\cos u + k^2u^4 - 2u_t^2 + 4u(\sin u + \partial_t^2 u)\right] + uu_t^3\right]\big|_{x=0} \end{aligned} \tag{7.21}$$

and $2kuu_t^3 = -u_x u_t^3$ cannot be written as a total time derivative. Although, in the integrable limits, $k \to 0$ or $k \to \infty$, the derivatives at the boundary become $u_x \to 0$ or $u_t \to 0$ respectively and the remaining $2kuu_t^3$ term would vanish, as expected.

This is a specific instance of a result in [66] where it was noted that for a boundary condition of the form

$$\partial_x u(0,t) + V'(u(0,t)) = 0$$

to satisfy the E_3 charge the boundary potential $V(u(0,t))$ should satisfy

$$4V''(u) + V(u) = 0\,. \tag{7.22}$$

Indeed, the integrable boundary condition

$$\left[u_x + 4K\sin\left(\frac{u-\widehat{u}}{2}\right)\right]\Bigg|_{x=0} = 0\,, \qquad K, \widehat{u} \in \mathbb{R}\,, \tag{7.23}$$

was originally constructed to satisfy this condition in [66] and was later shown in [67] to allow for an infinite number independent of constants of motion in involution. For the Robin boundary $V = -8k + ku^2$ and (7.22) becomes

$$ku^2 = 0 \tag{7.24}$$

which is not true for general k.

It should be noted that the failure to conserve E_3 does not strictly prove the non-integrability of the boundary. There are, after all, an infinity of conserved charges that could still be checked. But the violation of the E_3 charge together with the annihilation and creation of solitons that will later be observed in §7.7 is enough to state with some confidence that the sine-Gordon equation on the half-line with the Robin boundary condition (7.1) is not integrable.

7.3 Vacuua

The sine-Gordon equation on the full line has infinitely many degenerate vacua at $u(x) = 2\pi n$, $n \in \mathbb{Z}$. The integrable Neumann boundary $u_x(0) = 0$ preserves these vacua while the integrable homogeneous Dirichlet boundary $u(0) = 0$ is only compatible with one vacuum, $u(x) = 0$. The way that the boundary interpolates between these two integrable limits is the subject of this section. Here, and elsewhere in this chapter, it will be assumed that the boundary parameter $k \geq 0$ so that the contribution of the boundary to the energy $ku^2 \geq 0$. Some remarks on the $k < 0$ case will be made later in §7.9.

Away from the boundary as $x \to -\infty$ the field must tend to one of the bulk vacua $u(x) \to 2\pi n$. The lowest energy state will be static and in $-\infty < x < 0$ will saturate the Bogomolnyi bound on the energy,

$$\begin{aligned} E &= \int_{-\infty}^{0} \left[\frac{1}{2}u_t^2 + \frac{1}{2}u_x^2 + 1 - \cos u\right] dx + ku_0^2 \\ &\geq \int_{-\infty}^{0} \left[\frac{1}{2}u_x^2 + 1 - \cos u\right] dx + ku_0^2 \\ &= \int_{-\infty}^{0} \frac{1}{2}\left(u_x - 2\varepsilon\sin\left(\frac{u}{2}\right)\right)^2 dx - 4\varepsilon\cos\left(\frac{u_0}{2}\right) + 4 + ku_0^2\,, \end{aligned}$$

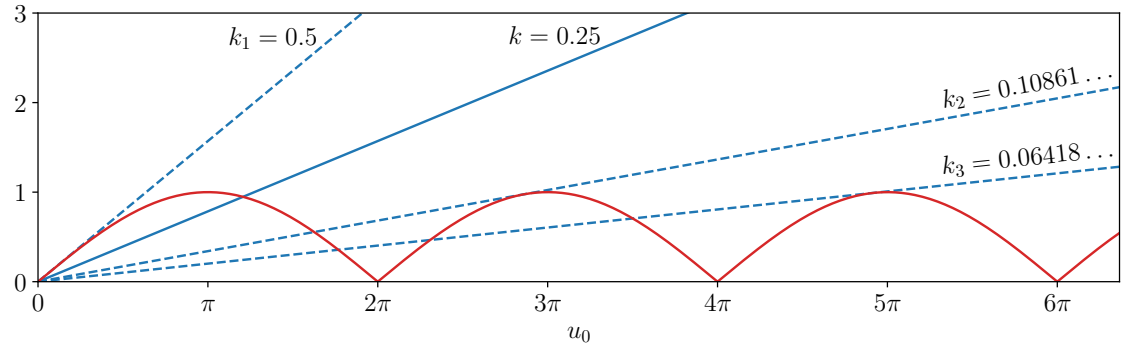

Figure 7.1: The graphical solution of (7.27) with $|\sin(u_0/2)|$ plotted in red and ku_0 in blue for $k = 0.25$ (solid line), and for the first three critical values of k (dashed lines).

where $\varepsilon = (-1)^n$ and $u_0 = u(x = 0)$, by satisfying the Bogomolnyi equation

$$u_x = 2\varepsilon \sin\left(\frac{u}{2}\right) . \tag{7.25}$$

Combining (7.25) in the limit $x \to 0$ with the Robin boundary condition gives

$$ku_0 = -\varepsilon \sin(u_0/2) . \tag{7.26}$$

Supposing for the moment that n is positive then the field at the boundary must curve downwards since $(u_0)_x = -2ku_0 < 0$. Therefore, $2\pi(n-1) < u_0 < 2\pi n$ and $\text{sign}[\sin(u_0/2)] = -\varepsilon$. The boundary condition satisfied by the lowest energy static solution with $u(x) \to 2\pi n > 0$ as $x \to -\infty$ is then

$$ku_0 = \left|\sin\left(\frac{u_0}{2}\right)\right| . \tag{7.27}$$

The graphical solution of this equation is illustrated in Fig. (7.1). As k decreases from $+\infty$ (Dirichlet) towards 0 (Neumann), the number of non-negative static solutions to the boundary problem jumps from 1 to 2 at $k = 0.5$. Further transitions in the number of solutions occur at the critical values $k = k_j$ where

$$k_j = \left|\frac{1}{2}\cos\left(\frac{u_0^{(j)}}{2}\right)\right| , \quad u_0^{(j)} = 2\tan\left(\frac{u_0^{(j)}}{2}\right) \geq 0 . \tag{7.28}$$

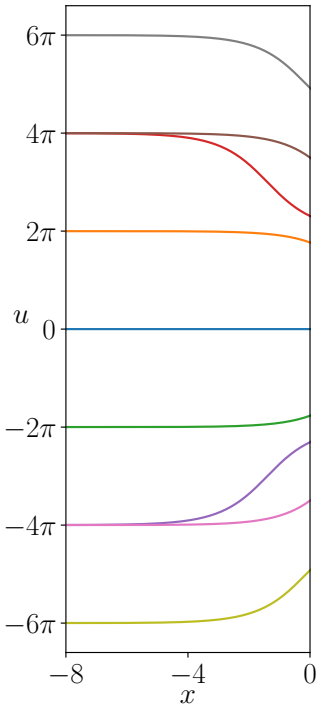

Figure 7.2: The lowest energy static fields corresponding to the solutions of (7.26) for the critical value of $k = k_3 \approx 0.064187$.

The first three critical values of k are shown in Fig. (7.1).

For each nontrivial positive solution (the trivial solution being $u_0 = 0$) there is a corresponding negative solution to (7.26) where $n < 0$ and $\text{sign}[\sin(u_0/2)] = \varepsilon$. Therefore, the *total* number of static solutions is 1 for $k_1 \leq k$, 3 for $k_2 < k < k_1$ then 5 at precisely $k = k_2$, 7 for $k_3 < k < k_2$ and so on as k decreases. For example, all of the 9 static solutions for $k = k_3$, the third critical value of k, are shown in Fig. (7.2).

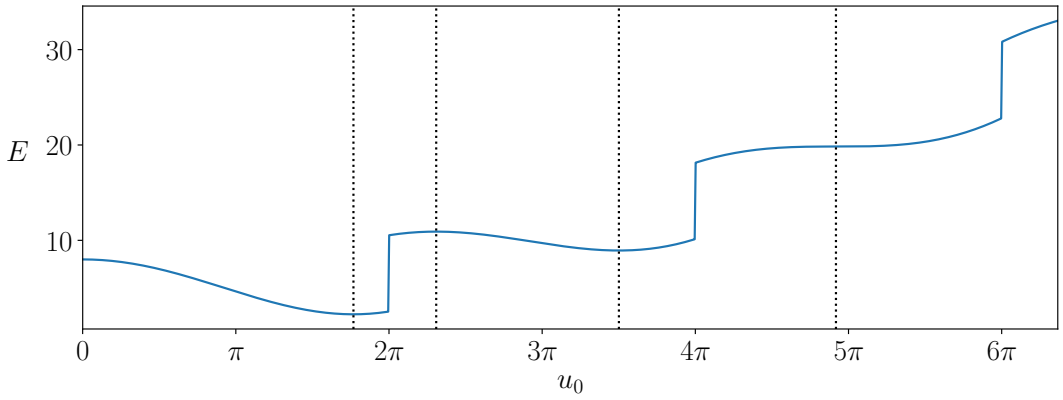

Figure 7.3: The energy, E, of a static antikink $u(x)$ with $u(0) = u_0$ as given by (7.29) with $k = k_3 \approx 0.064187$, the third critical value of k shown in Fig. (7.1). The vertical dotted lines indicate the solutions of (7.27), which are also the stationary points of $E(u_0)$.

The energy of these static solutions,

$$E = 4 - 4\varepsilon \cos\left(\frac{u_0}{2}\right) + ku_0^2\,, \tag{7.29}$$

is illustrated as a function of u_0 in Fig. (7.3) and as demonstrated there $E(u_0)$ has discontinuities at $u_0 = 2\pi m$, $m \in \mathbb{Z}$, where ε changes sign. Approaching one of these discontinuities from above, $u_0 > 2\pi m$, the static antikink satisfying $u(0) = u_0$ is $u(x) = 4\arctan\left(\exp(x_0 - x)\right) + 2\pi m$ and the position $x_0 \to -\infty$ as $u_0 \to 2\pi m$. Approaching from below $u_0 < 2\pi m$ the antikink is $u(x) = 4\arctan\left(\exp(x_0 - x)\right) + 2\pi(m-1)$ whose position $x_0 \to +\infty$ as $u_0 \to 2\pi m$ so that on the half-line $x \leq 0$ all that can be seen is the field relaxing to $u(x) \to 2\pi m$. In order to illustrate this difference antikinks approaching $u_0 \to 2\pi$ from above and below are shown in Fig. (7.4). The bulk energy contribution of $u(x) = 2\pi m$ is zero while a static antikink on the full line has energy 8 and therefore $E(u_0)$ has a discontinuity of magnitude 8 every $u_0 = 2\pi m$.

Note that

$$\frac{dE}{du_0} = 2\varepsilon \sin\left(\frac{u_0}{2}\right) + 2ku_0 = -2\left|\sin\left(\frac{u_0}{2}\right)\right| + 2ku_0 \tag{7.30}$$

so $E(u_0)$ is stationary exactly when (7.27) holds, as expected. In addition, for $n > 1$, $\frac{dE}{du_0}$ is negative between the two stationary points in each interval $2\pi(n-1) < u_0 < 2\pi n$ and positive elsewhere in the interval, as demonstrated in Fig. (7.3). The larger (right-most) of the two stationary points in each interval $2\pi(n-1) < u_0 < 2\pi n$ is therefore a local minimum of the energy, a metastable vacuum, while the smaller (left-most) is an unstable local maximum. The unstable local maximum can be interpreted as a static antikink perched so that the force exerted on it by the boundary is zero but it is unstable to decay by either moving its position further to the right so as to reach the metastable vacuum in $2\pi(n-1) < u_0 < 2\pi n$ or by escaping to $-\infty$ which would allow for the lower metastable state in $2\pi(n-2) < u_0 < 2\pi(n-1)$.

Similar metastable and saddle-point static solutions also exist for the ϕ^4 theory on the half-line with a suitably-signed boundary magnetic field [139].

In the integrable limit $k \to 0$ the static antikinks corresponding to the unstable local maxima of the energy all escape with $x_0 \to -\infty$ while the antikinks corresponding to the

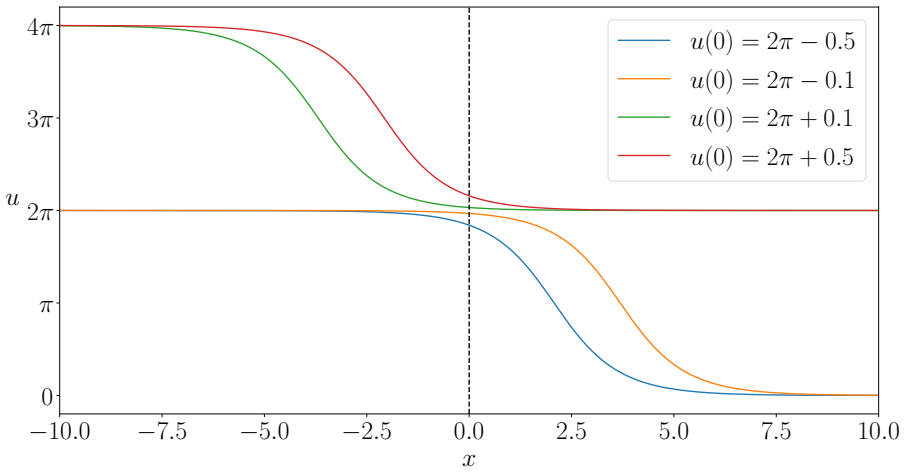

Figure 7.4: Antikinks satisfying $u(0) = u_0$ for u_0 close to 2π. This illustrates the difference in approaching $u_0 \to 2\pi$ from above and below. For $u_0 < 2\pi$, $u(x) = 4\arctan(\exp(x_0 - x))$ with a suitably chosen x_0 while for $u_0 > 2\pi$, $u(x) = 4\arctan(\exp(x_0 - x)) + 2\pi$.

metastable vacua all move past the boundary $x_0 \to \infty$ so that the field relaxes to the degenerate vacua $u(x) = 2\pi n$ of the Neumann boundary.

7.4 Numerical method

This section details the numerical method used to catalogue the soliton content produced from an antikink scattering with the Robin boundary. Consider an antikink solution to the sine-Gordon equation at initial time $t = 0$,

$$u(x,0) = 4\arctan\left(e^{-\gamma(v_0)(x-x_0)}\right), \qquad \gamma(v_0) = (1 - v_0^2)^{-1/2}, \tag{7.31}$$

with initial velocity $v_0 > 0$ and position $x_0 \ll 0$ far enough away from the boundary at $x = 0$ that the Robin boundary condition,

$$u_x(0,t) + 2ku(0,t) = 0,$$

is satisfied to a good approximation at $t = 0$. Note that both the sine-Gordon equation and the Robin boundary have the discrete symmetry $u \to -u$ so investigating instead the collision of kinks with the Robin boundary would not provide any additional information.

This system was then evolved in time numerically for particular values of v_0 and k using a simple Euler finite difference scheme in the bulk $x < 0$:

$$u_{tt}(x,t) = \frac{u(x+dx,t) - 2u(x,t) + u(x-dx,t)}{dx^2} - \sin u(x,t), \tag{7.32a}$$

$$u_t(x,t+dt) = u_t(x,t) + dt\, u_{tt}(x,t), \tag{7.32b}$$

$$u(x,t+dt) = u(x,t) + dt\, u_t(x,t), \tag{7.32c}$$

and then at the $x = 0$ boundary:

$$u(0,t+dt) = \frac{u(-dx,t+dt)}{1+2kdx}. \tag{7.33}$$

At the left hand boundary $u = 2\pi$ but the position of the boundary was dynamically extended during the time evolution so that any excitation in the field caused by the collision with the Robin boundary never reached the left hand boundary. This effectively implemented the boundary condition $u \to 2\pi$ as $x \to -\infty$. The typical space and time steps used were $dx = 0.025$ and $dt = 0.02$ but a finer grid of $dx = 0.0025$ and $dt = 0.002$ was used in situations with a greater sensitivity to errors such as in figures 7.7, 7.8, 7.9, 7.13, 7.15b, 7.19, 7.18 and 7.17.

The time evolution is then continued until the antikink has collided with the boundary and any solitons produced have moved sufficiently far away from the boundary. If the topological charge of the field (loosely defined as the number of kinks minus the number of antikinks) changes as a result of the collision then there will be a deformation near the boundary corresponding to a metastable vacuum described in §7.3.

Therefore the field at the boundary may never be close to the bulk vacua $u = 2\pi n$ so instead of waiting for that to happen, a point $x_R < 0$ is chosen and the time evolution will stop if the field and its derivatives at $x = x_R$ are sufficiently close to zero and the total 'available energy' in the region $[x_R, 0]$ is less than 1, well below the mass of a single kink or antikink. The available energy is defined by

$$\int_{x_R}^{0} \left[\frac{1}{2}u_t^2 + \frac{1}{2}u_x^2 + 1 - \cos u + \delta(x) k u^2 \right] dx - E_{\text{Min}} \tag{7.34}$$

where E_{Min} is the energy, (7.29), of the static metastable solution whose value of the field at the boundary, u_0, is closest to the current value of the field at the boundary at this point in the time evolution.

The time evolution is also halted if a time of $1000 + |x_0|/v_0$ has elapsed. This can happen, for example, when a breather created by the antikink/boundary collision becomes trapped at the boundary and only very slowly emits radiation while it oscillates. These criteria ensure that any excitations with significant energy have had enough time to have been emitted from the boundary.

The collision of the antikink with the boundary typically produces one or more solitons together with some radiation depending on the initial choice of velocity v_0 and boundary parameter k. If the soliton content of the field is quite simple, containing only a kink or antikink, then the velocity of the soliton can be approximated numerically by taking the position of the soliton to be the place where the field reaches π for an antikink and 3π for a kink, as was done in [93] for certain values of the initial parameters. A map of the types of solitons present in the reflected field for different values of the initial parameters was also produced in [93] by, it appears, running the time evolution and judging by eye the soliton content of the field produced in the collision.

However, for more complicated final states, such as that shown in Fig. (7.5), it is often difficult to accurately measure the velocity of a kink/antikink on a background of radiation and other solitons and still more difficult to measure the velocity and frequency of a breather since high frequency (low mass) breathers can be hard to distinguish from radiation. Instead, to accurately determine the soliton content of the field use will be made of the fact that the solitons are encoded in the bound state eigenvalues $\{\lambda_i\}$ of the direct scattering problem associated with the Lax pair.

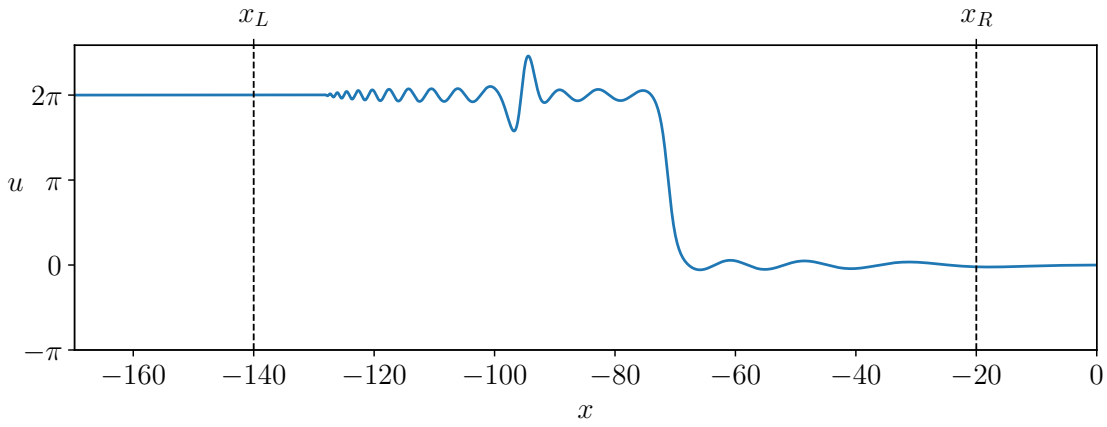

Figure 7.5: The field at $t = 150$ after an antikink (7.31), placed at $x_0 = -20$ and with initial velocity $v_0 = 0.95$, collided with the Robin boundary with parameter $k = 0.145$.

It will be convenient in this chapter to take the Lax pair to be, as in [24],

$$\psi_x = U(u, u_x, u_t; \lambda)\psi = \begin{pmatrix} -\frac{i}{4}(u_x + u_t) & \lambda - \frac{e^{-iu}}{16\lambda} \\ \frac{e^{iu}}{16\lambda} - \lambda & \frac{i}{4}(u_x + u_t) \end{pmatrix} \psi \,, \tag{7.35a}$$

$$\psi_t = V(u, u_x, u_t; \lambda)\psi = \begin{pmatrix} -\frac{i}{4}(u_x + u_t) & \lambda + \frac{e^{-iu}}{16\lambda} \\ -\frac{e^{iu}}{16\lambda} - \lambda & \frac{i}{4}(u_x + u_t) \end{pmatrix} \psi \,. \tag{7.35b}$$

On the full line, assuming that the field and its derivatives tend to a vacuum $u \to 2\pi n$, $n \in \mathbb{Z}$ as $|x| \to \infty$ then for $\mathrm{Im}[\lambda] > 0$ two solutions ψ_+ and ψ_- to (7.35a) can be defined at any fixed time by the asymptotics:

$$\psi_-(x) \sim \begin{pmatrix} 1 \\ -i \end{pmatrix} \exp\left(-i\left(\lambda - \frac{1}{16\lambda}\right)x\right) \qquad \text{as } x \to -\infty \,, \tag{7.36a}$$

$$\psi_+(x) \sim \begin{pmatrix} 1 \\ i \end{pmatrix} \exp\left(i\left(\lambda - \frac{1}{16\lambda}\right)x\right) \qquad \text{as } x \to +\infty \,. \tag{7.36b}$$

Note that $\psi_-(x)$ decays as $x \to -\infty$, and $\psi_+(x)$ decays as $x \to +\infty$.

Of course, the Robin boundary system is not on the full line but due to the dynamic extension of the $u = 2\pi$ left-hand boundary during time evolution there will be a point $x = x_L$ to the left of anything generated by the collision and where $u(x_L) = 2\pi$ and $u_t(x_L) = u_x(x_L) = 0$, as demonstrated in Fig. (7.5). Similarly, the stopping criteria for the time evolution allows for the assumption that there is a point $x = x_R$ to the right of any solitons generated by the collision and where the field and its derivatives are sufficiently close to the vacuum, as in Fig. (7.5). Therefore, for the purposes of computation the points x_L and x_R are effectively identified with the points $-\infty$ and $+\infty$ as they relate to the direct scattering problem on the full line.

For a given value of λ (7.35a) can be solved as an initial value problem for $\psi_-(x)$ from $x = x_L$ to $x = x_R$ with the initial condition $\psi_-(x_L)$ defined by the asymptotic form (7.36a). If λ is a bound state eigenvalue, $\lambda \in \{\lambda_i\}$, then $\psi_-(x) \propto \psi_+(x)$ and these points

will be the zeros of the Wronskian

$$W(\lambda) = \mathrm{Det}\left[\psi_-(x = x_R), \psi_+(x = x_R)\right] , \tag{7.37}$$

where the value of $\psi_-(x_R)$ is the result of solving (7.35a) over the interval $x_L < x < x_R$ while $\psi_+(x_R)$ is given by the asymptotic form (7.36b).

The problem of finding the bound state eigenvalues is then reduced to the problem of finding the zeros of $W(\lambda)$, which is a complex analytic function in the region $\mathrm{Im}[\lambda] > 0$ [24]. For the results presented here this problem was addressed using the QZ-40 algorithm proposed in [140]. QZ-40 first computes the number of zeros, N, within a given initial contour C using the argument principle,

$$N = \frac{1}{2\pi i} \oint_C \frac{W'(\lambda)}{W(\lambda)} d\lambda \, . \tag{7.38}$$

If $N \neq 1$ then C is subdivided repeatedly until a set of sub-contours $\{\gamma_i\}_{i=1}^N$, is obtained which all contain only a single root (this assumes that all roots are simple, which is the case here). Then for each γ_i the Newton-Raphson method is repeatedly used with random start points inside γ_i until the root within in each contour, λ_i, is found. This algorithm was implemented in the Python programming language with the numerical integration performed using the Romberg algorithm as implemented in `SciPy` [115].

The QZ-40 algorithm has the advantage of being quite reliable and straightforward to implement but it was found that it can sometimes take quite a long time to complete. Roots which are quite close together may take many contour divisions and integrations to separate them into the interiors of different contours. Even once a root is isolated within a contour it may take many attempts of the Newton-Raphson method for the random start point to be suitable for convergence to the root.

To overcome these problems in future work the present author developed the open-source Python module `cxroots` [89] which implements the method of [141, 90]. Contour integration is used to approximate the roots and their multiplicities within a contour, removing the need to isolate roots and giving the Newton-Raphson method a good approximation for the root to iterate on. This approach and the implementation and use of `cxroots` is discussed in greater detail in Appendix C.

Once all the bound state eigenvalues $\{\lambda_i\}$ have been found the velocity, v, of each soliton and the velocity and frequency, ω, of each breather can be simply calculated,

$$v = \frac{1 - 16\left|\lambda_i\right|^2}{1 + 16\left|\lambda_i\right|^2} , \qquad \omega = \frac{\mathrm{Re}[\lambda_i]}{|\lambda_i|} . \tag{7.39}$$

A kink and antikink corresponds to a single bound state eigenvalue, λ_i such that $\mathrm{Re}[\lambda_i] = 0$ while a breather corresponds to two bound state eigenvalues, λ_i and λ_j satisfying $\lambda_i = -\overline{\lambda_j}$. Note that, due to the choice of Lax pair here, this chapter differs in this respect from the rest of this thesis where kinks and antikinks corresponded to real, negative bound state eigenvalues and breathers to complex conjugate bound state eigenvalues.

As part of the input for the rootfinding algorithm it is necessary to choose an initial contour C in the complex plane of λ whose interior contains all the bound state eigenvalues

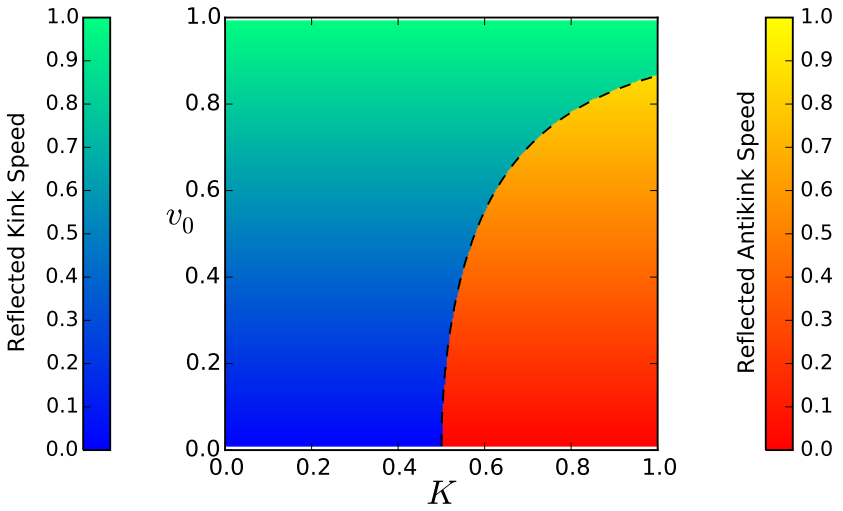

Figure 7.6: Numerical results for the speed of the kink/antikink reflected from the scattering of an antikink of initial velocity v_0 and the integrable boundary (7.41) with parameter K. The dashed line, $2K\sqrt{1-v_0^2} = 1$, is the theoretical boundary between where a kink and antikink is returned from the boundary collision [68]. Precisely on this line an incoming antikink should be infinitely phase-shifted.

of interest. This was done here by noting that any excitation in the field after scattering must have $v < 0$ so, by (7.39), $|\lambda_i| > 0.25$. The energy of a kink or antikink with velocity v is $8\gamma(v)$ and so conservation of energy implies that $-v \leq v_0$ where v_0 is the initial antikink velocity and equality only holds in the integrable limits $k = 0$ or $k \to \infty$. This implies, using (7.39), that for λ_i corresponding to kinks or antikinks,

$$|\lambda_i| \leq \frac{1}{4}\sqrt{\frac{1+v_0}{1-v_0}}\,. \tag{7.40}$$

However, the energy of a breather is $16\gamma(v)/\gamma(\omega)$ and therefore high frequency (low mass) breathers are able to exceed the speed of the original antikink. Since the breather speed cannot be bounded using energetic arguments, the upper bound on $|\lambda_i|$ was taken to be the higher of 1.25 and (7.40), meaning that breathers with speeds below 0.923 were always detected. Some high frequency breathers would be able to exceed this speed and therefore go undetected but they will be of very low energies and are therefore supposed to be largely insignificant to the overall scattering process.

7.5 Integrable boundary

As a test of the numerical method in §7.4 consider the collision of an antikink of initial velocity v_0 with the integrable boundary,

$$u_x + 4K\sin\left(\frac{u}{2}\right) = 0\,, \qquad K \in \mathbb{R}\,. \tag{7.41}$$

The velocity of the reflected kink or anitkink measured after the collision is shown in Fig. (7.6). Over the range of v_0 and K shown in the figure the maximum difference between the theoretical and measured final speed was 0.0014. Fig. (7.6) also shows a very good agreement between the observed and theoretical boundary [68] between the regions where the antikink is reflected into a kink or an antikink.

7.6 Forces

Before discussing the antikink - Robin boundary collisions it will be helpful to first consider the force of the Robin boundary on a static antikink placed to the left of the boundary in its ground state, with $u_0 \approx 0$ initially. As in [139] the asymptotic force on a static antikink placed at $x_1 < 0$ with $|x_1| \gg 1$ can be calculated by placing an 'image' kink (or, for larger values of k, an antikink) at $x_2 > 0$ such that the combined configuration satisfies the Robin boundary condition at $x = 0$. Then the force can be calculated using the well known result that on the full line a sine-Gordon antikink and kink a distance $R \gg 1$ apart experience an attractive force $F = 32\, e^{-R}$ [27, 142].

The antikink-kink combination can be approximated as

$$u(x) = 4 \arctan\left(e^{-(x-x_1)}\right) + 4 \arctan\left(e^{x-x_2}\right) , \tag{7.42}$$

so for $|x_1|$ and $|x_2|$ both large the Robin boundary condition $[u_x + 2ku]\,|_{x=0} = 0$ becomes

$$4(-e^{x_1} + e^{-x_2}) + 8k(e^{x_1} + e^{-x_2}) = 0 . \tag{7.43}$$

Solving for e^{-x_2} and computing the force yields

$$F = 32\, e^{-(x_2 - x_1)} = 32\, \frac{1-2k}{1+2k}\, e^{2x_1} . \tag{7.44}$$

For $k > 1/2$ an image antikink should be used instead but the final formula is unchanged, with the force now repulsive instead of attractive. Recalling that the mass of an antikink is 8, the trajectory $x_1(t)$ of the antikink according to the force law (7.44) is

$$e^{x_1(t)-x_0} = \operatorname{sech}\left(2e^{x_0} t \sqrt{\frac{2k-1}{2k+1}}\right) , \qquad x_1(0) = x_0 , \qquad x_1'(0) = 0 . \tag{7.45}$$

In the integrable Neuamnn ($k = 0$) and Dirichlet ($k \to \infty$) limits the force law (7.44) matches the as asymptotic behaviour of the corresponding exact solutions. Outside of these limits (7.44) still provides an excellent approximation, as shown in Fig. (7.7) which plots the numerical and theoretical (described by (7.45)) trajectories of an antikink placed near the boundary for a range of k, including the 'critical' value $k_c = 1/2$ where the force is predicted to vanish.

For a breather placed near the Robin boundary the general situation is more subtle but in the integrable limits the boundary force can be modelled on the full line by placing an 'image' breather exactly in phase with the 'real' breather for the Neumann boundary and exactly out of phase for the Dirichlet boundary. It can be shown that two in phase breathers feel an attractive force while two out of phase breathers experience a repulsive force [143] and this can be verified by constructing the relevant exact two-breather solutions, as in [144]. Therefore a stationary breather is attracted by the $k = 0$ boundary and repelled when $k = \infty$. As of yet there is no analytical result for the general Robin boundary analogous to (7.44), however, the numerical results in Fig. (7.8) show that the breather trajectories interpolate between the two integrable limits in a similar way to the antikink trajectories in Fig. (7.7).

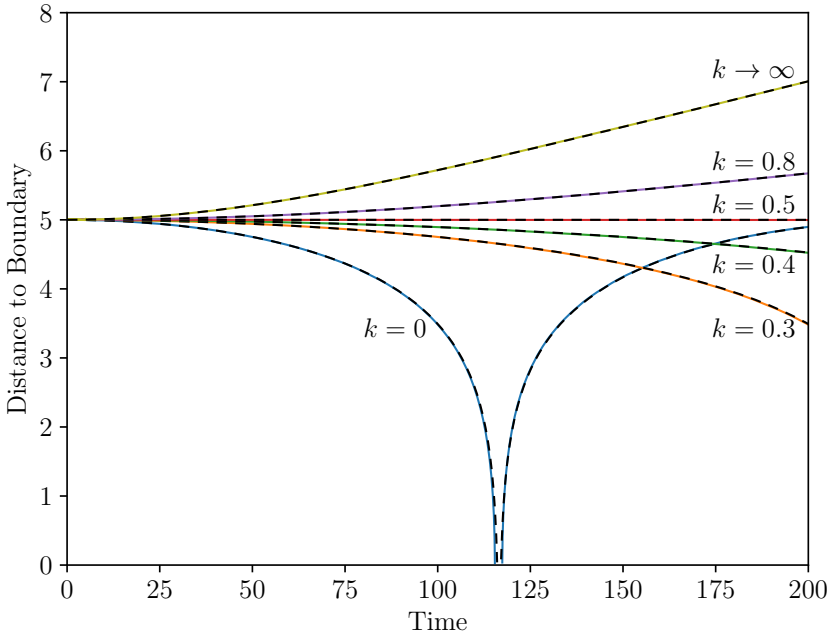

Figure 7.7: The numerically determined trajectories of an antikink with zero initial velocity placed at $x = -5$ with a (ground state) Robin boundary at $x = 0$ for various values of the boundary parameter k. For the $k = 0$ trajectory the position of the antikink is plotted up to the point of collision and then the trajectory of the reflected kink is tracked instead. The dashed lines show the distance given by the theoretical trajectory (7.45).

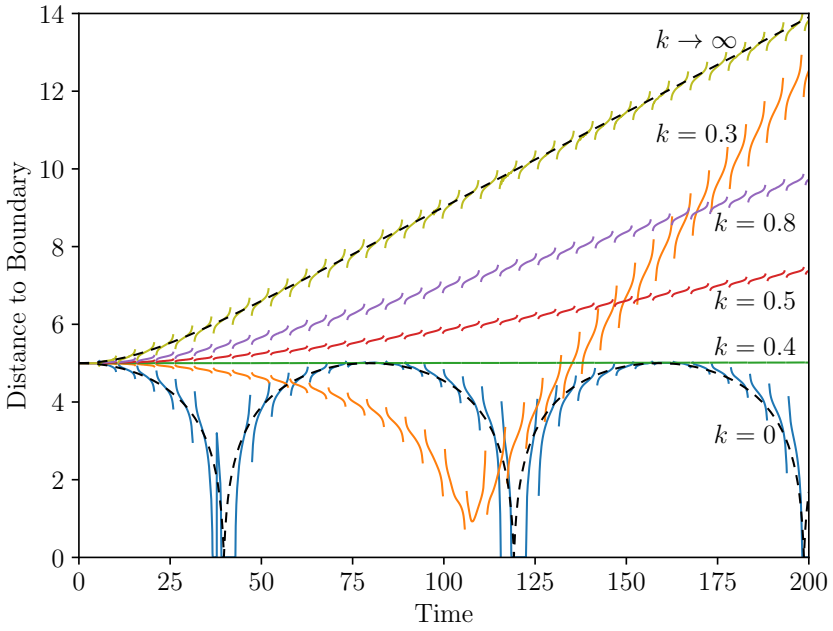

Figure 7.8: The numerically determined trajectories of a breather with zero initial velocity and frequency $\omega = 0.6$ placed at $x = -5$ with a Robin boundary at $x = 0$ and initially $u(0) \approx 0$, for various values of the boundary parameter k. For numerical purposes the position of the breather is defined as the point where the absolute value of the field reaches its maximum. Points on the spacetime diagram where the maximum of the field is less than 1 are omitted for clarity. The dashed lines are the theoretical trajectories for Dirichlet (top) and Neumann (bottom) boundaries calculated as half the breather separation for two exactly out of phase and in phase breathers respectively as computed in [143] using a collective coordinates method.

The conclusion is then that the Neumann boundary is repulsive and the Dirichlet attractive for kinks, antikinks and breathers and that the homogeneous Robin boundary based on the $u = 0$ ground state transitions smoothly from attractive to repulsive as k increases from 0 to infinity. For kinks and antikinks the Robin boundary transitions from attractive to repulsive at $k = 1/2$, where the force is zero, while for breathers numerical experiments show that this critical point is frequency dependent and only tends (from below) to $1/2$ as the frequency tends to zero.

The situation is complicated further when one considers the force exerted on kinks, antikinks and breathers built on one of the metastable vacua discussed in §7.3. The metastable vacua for positive n, where $u(x) \to 2\pi n$ as $x \to -\infty$, can be modelled on the full line by an antikink placed at $x = x_2 > 0$. If a kink or antikink is subsequently added at some point $x_1 < 0$ (so that now $2\pi(n\pm1)$ as $x \to -\infty$) then so long as x_1 is sufficiently negative the combined full-line kink-antikink or antikink-antikink configuration will continue to satisfy the Robin boundary condition with only a small change in x_2. Therefore, a distant antikink will be repelled by a metastable boundary with $n > 0$, and a kink will be attracted.

However, when an antikink gets closer to the boundary the situation changes. The position of the boundary antikink (which models the metastable boundary) increases, eventually diverging to infinity at the moment when the incident antikink on its own satisfies the boundary condition and hence experiences no force. At this point the situation replicates the unstable solution corresponding to a local maximum of the energy that tends to $2(n+1)\pi$ as $x \to -\infty$. If the antikink moves further forward then it will experience an attractive force from the boundary. The trajectories of antikinks incident on the $n = 1$ metastable boundary for a range of initial velocities is shown in Fig. (7.9), in particular the transition from attractive to repulsive is demonstrated. The point at which the $n = 1$ metastable boundary exhibits no force is given by the position, $x_1 = \ln(\tan(u_0/4-\pi/2))$, of the unstable static antikink which solves the boundary conditions, which is to say that u_0 is the solution to (7.27) in the interval $[2n\pi, (2n+1)\pi]$. For $k = 0.01$ the distance where no force is exerted by the boundary is $-x_1 = 3.439\ldots$, which agrees well with the numerical results pictured in Fig. (7.9).

For a breather incident on a metastable boundary the situation is even more complicated. However, numerical simulations for the $n = 1$ metastable vacuum indicate that while $k \lesssim 0.3$ and for breather frequencies $\omega \approx 0.6$ (which appears typical for the intermediate breathers discussed in §7.8) the force is always attractive, confirming the behaviour, shown in Fig. (7.18)a–g and Fig. (7.17)c below, of intermediate breathers incident on Robin boundaries close to the $n = 1$ metastable boundary.

7.7 Robin boundary overview for $k > 0$

With the numerical method and analytical facts established, the original problem of an antikink with velocity $v_0 > 0$ colliding with the Robin boundary, $u_x + 2ku = 0$, with parameter $k > 0$ can be addressed. An overview of the outcome of such a collision is given by Fig. (7.10) which shows a 'snapshot' of the value of the field at the boundary for a range of initial parameters v_0 and k. The more detailed plots in Fig. (7.11) use the numerical

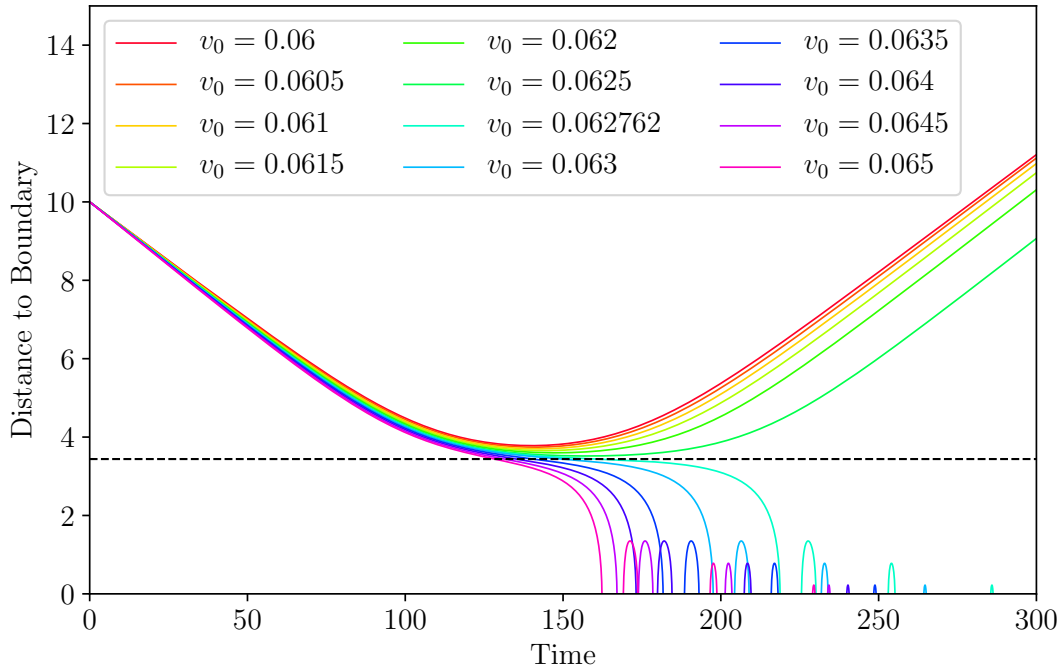

Figure 7.9: The numerically determined trajectories of an antikink with various initial velocities incident on the $n = 1$ metastable Robin boundary at $x = 0$, with boundary parameter $k = 0.01$. The horizontal dashed line shows the distance from the boundary, $-x_1 = 3.439\ldots$, at which the force is predicted to vanish. Based on a comparison of the energy of a distant antikink with velocity v_0 with that of a static antikink placed so as to construct the $n = 1$ metastable Robin boundary, the transition from reflection to capture should occur at $v_0 = 0.062762$, in good agreement with the numerical results pictured here.

method of §7.4 to classify different regions of this initial parameter space based on the soliton content of the reflected field. It should be noted that a map of scattering outcomes similar to Fig. (7.11a), although lacking certain details, was produced in [93] by judging by eye the soliton content of the reflected field. Away from the integrable limits the reflected field also contains some radiation and in some areas, like region VI of Fig. (7.11a) very low energy breathers were also detected. These breathers are hard to distinguish from radiation since their corresponding bound state eigenvalues are very close to the real axis and understanding the structure of their dependence on v_0 and k is beyond the present study. Examples of reflected fields and corresponding bound state eigenvalues for each of the regions in Fig. (7.11) are given in Fig. (7.12). Finally, Fig. (7.13) shows the time evolution of the boundary scattering process for certain illustrative examples of the initial parameters.

For $k = 0$ the Robin boundary (7.1) becomes the integrable Neumann boundary and in this case an incoming antikink is perfectly reflected into a kink, as shown in Fig. (7.13)a.

When k is increased slightly from zero the incoming antikink is still reflected into a kink but some energy is lost to radiation and to the $n = 2$ metastable state discussed in §7.3. An example of this process is shown in Fig. (7.13)b. The region of the initial parameter space where the only solitons produced are kinks is shown in region I on Fig. (7.11a).

As k is increased further the outcome of the collision varies drastically depending on the value of v_0. For sufficiently small initial velocities ($v_0 \lesssim 0.877$) the system has insufficient energy for the reflected kink to escape and instead the kink recollides with the boundary

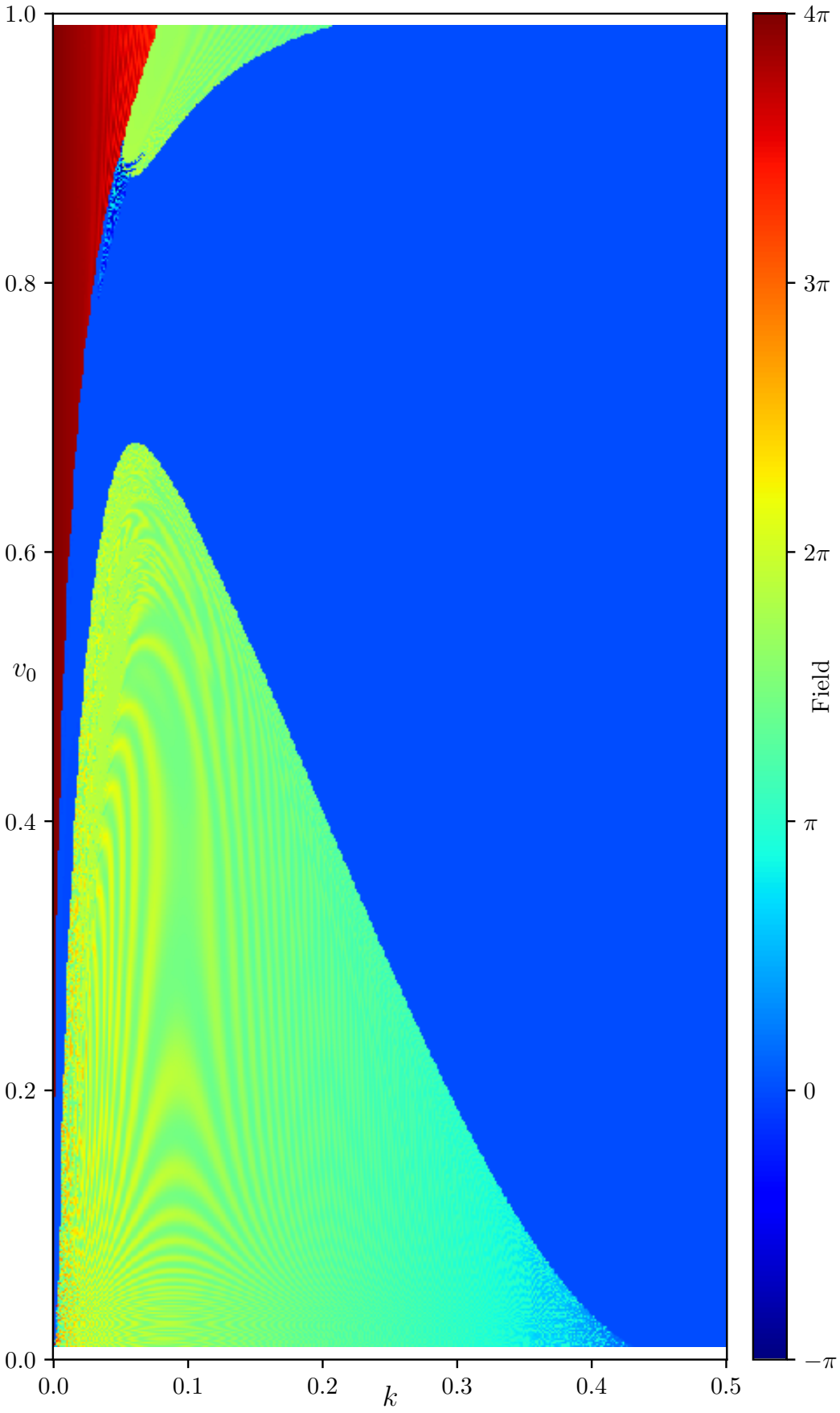

Figure 7.10: The value of the field at $x = 0$, $t = |x_0|/v_0 + 1000$ created by the scattering of an antikink with initial velocity v_0 and initial position x_0 at $t = 0$ with a Robin boundary at $x = 0$ with boundary parameter k. Fig. (7.16) shows a zoomed-in view of the complicated structure near to $k = 0.06$, $v_0 = 0.89$.

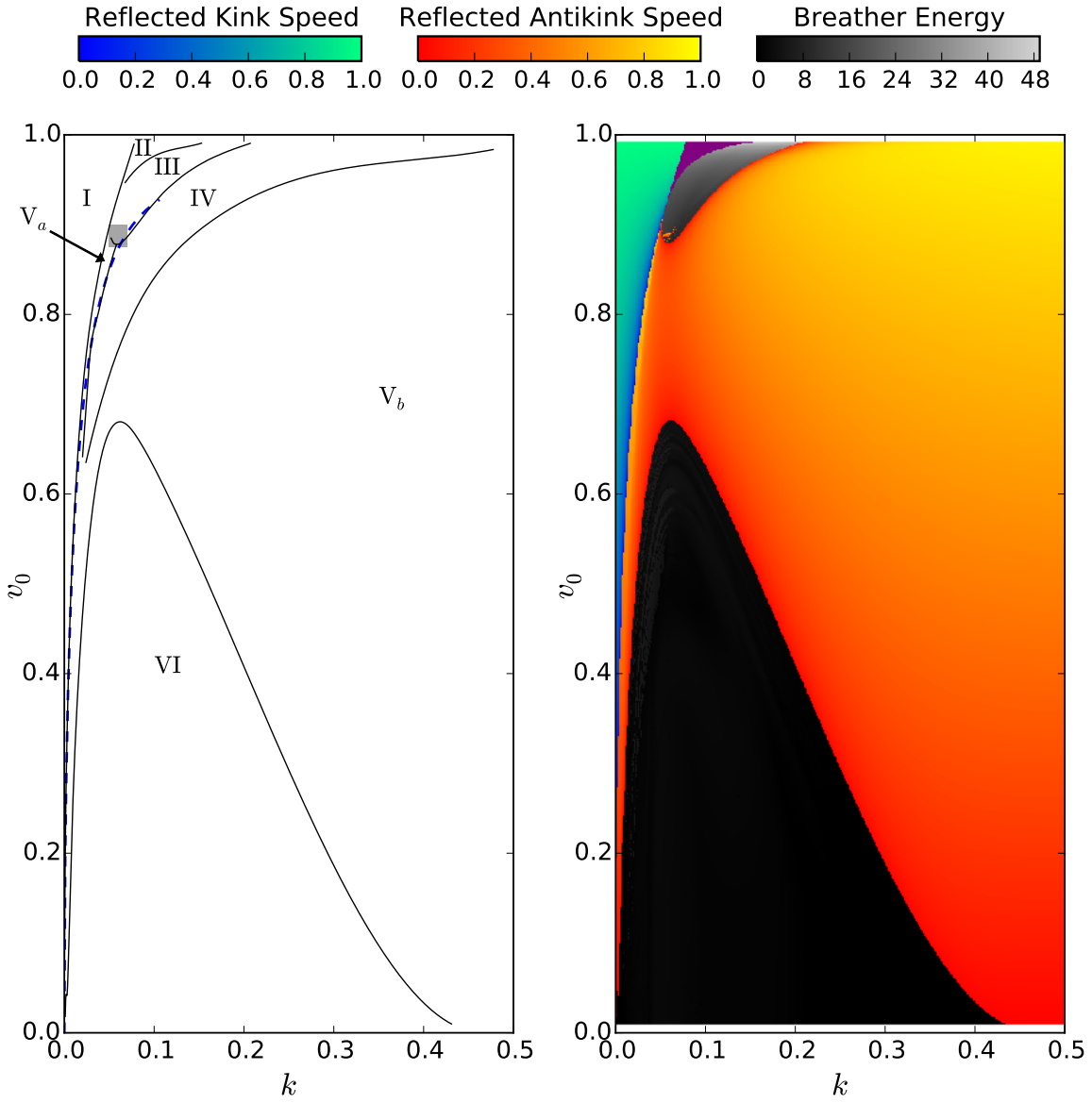

(a) Final states classified by kink, antikink and high energy breather content:
I: Kink
II: Kink and antikink
III: High-energy breather
IV: High-energy breather and antikink
V$_a$ & V$_b$: Antikink
VI: None of the above.

(b) Final state kinematics: If the reflected field contains a single kink or antikink, its speed is plotted; if neither, then the total energy of all breathers detected in the final state is shown instead. In the solid purple region the final state contains both a kink and an antikink. Note that low-energy breathers are hard to distinguish from radiation, so the patterns in region VI should be treated with caution.

Figure 7.11: Maps characterising the soliton content of the field reflected from the collision of an antikink with initial speed v_0 with a Robin boundary with parameter k. The small shaded region in Fig. (7.11a) is shown in greater detail in Fig. (7.16) and discussed further in §7.8. The dashed line in Fig. (7.11a) shows an approximation for the outer limit for region I, (7.46).

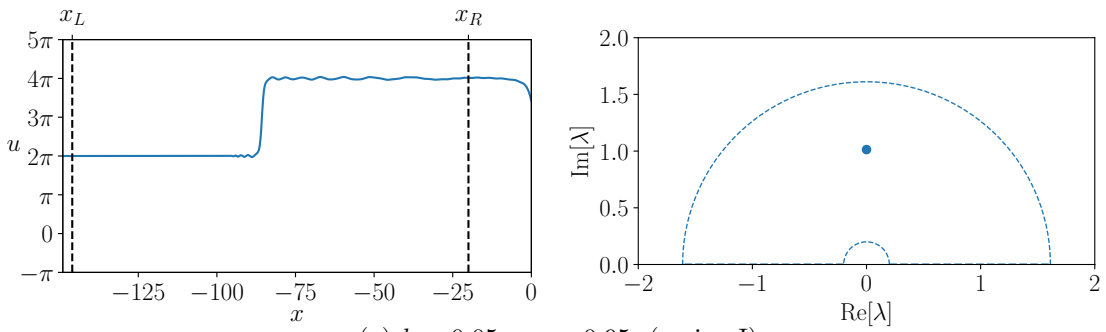

(a) $k = 0.05$, $v_0 = 0.95$ (region I)

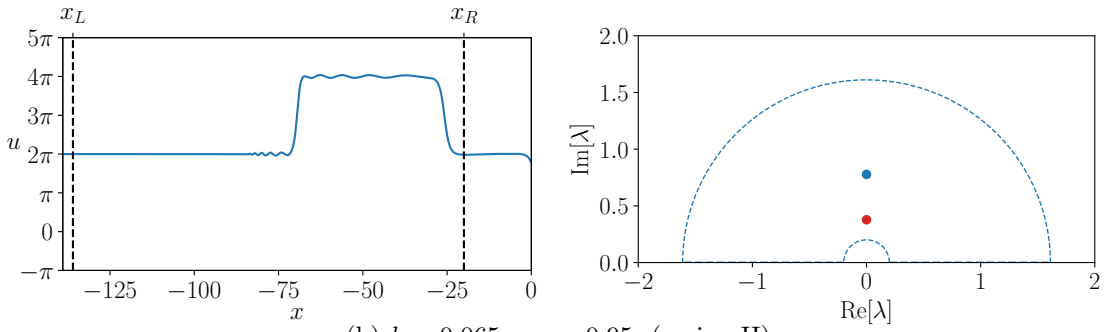

(b) $k = 0.065$, $v_0 = 0.95$ (region II)

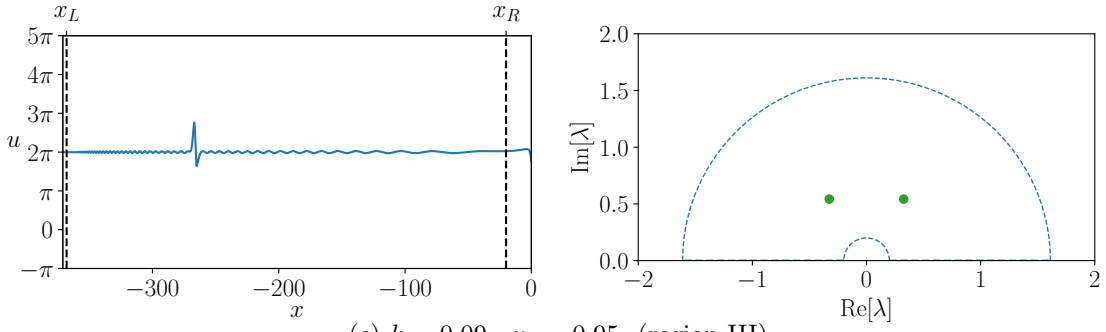

(c) $k = 0.09$, $v_0 = 0.95$ (region III)

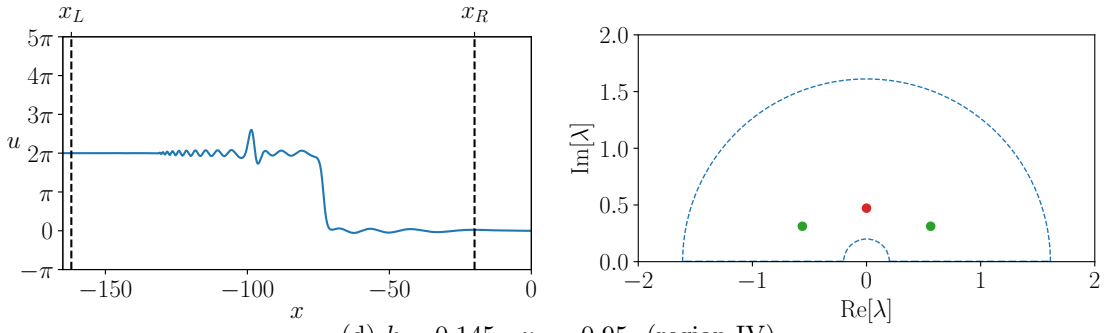

(d) $k = 0.145$, $v_0 = 0.95$ (region IV)

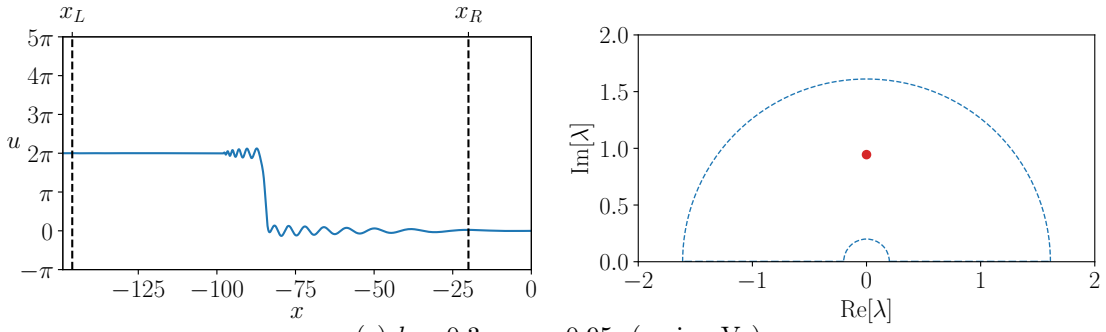

(e) $k = 0.3$, $v_0 = 0.95$ (region V$_b$)

Figure 7.12: The scattered field (left) and bound state eigenvalues (right) for $v_0 = 0.95$ and a sequence of values for k, illustrating how the eigenvalues evolve with changing k. The eigenvalues coloured green correspond to breathers, red to antikinks and blue to kinks.

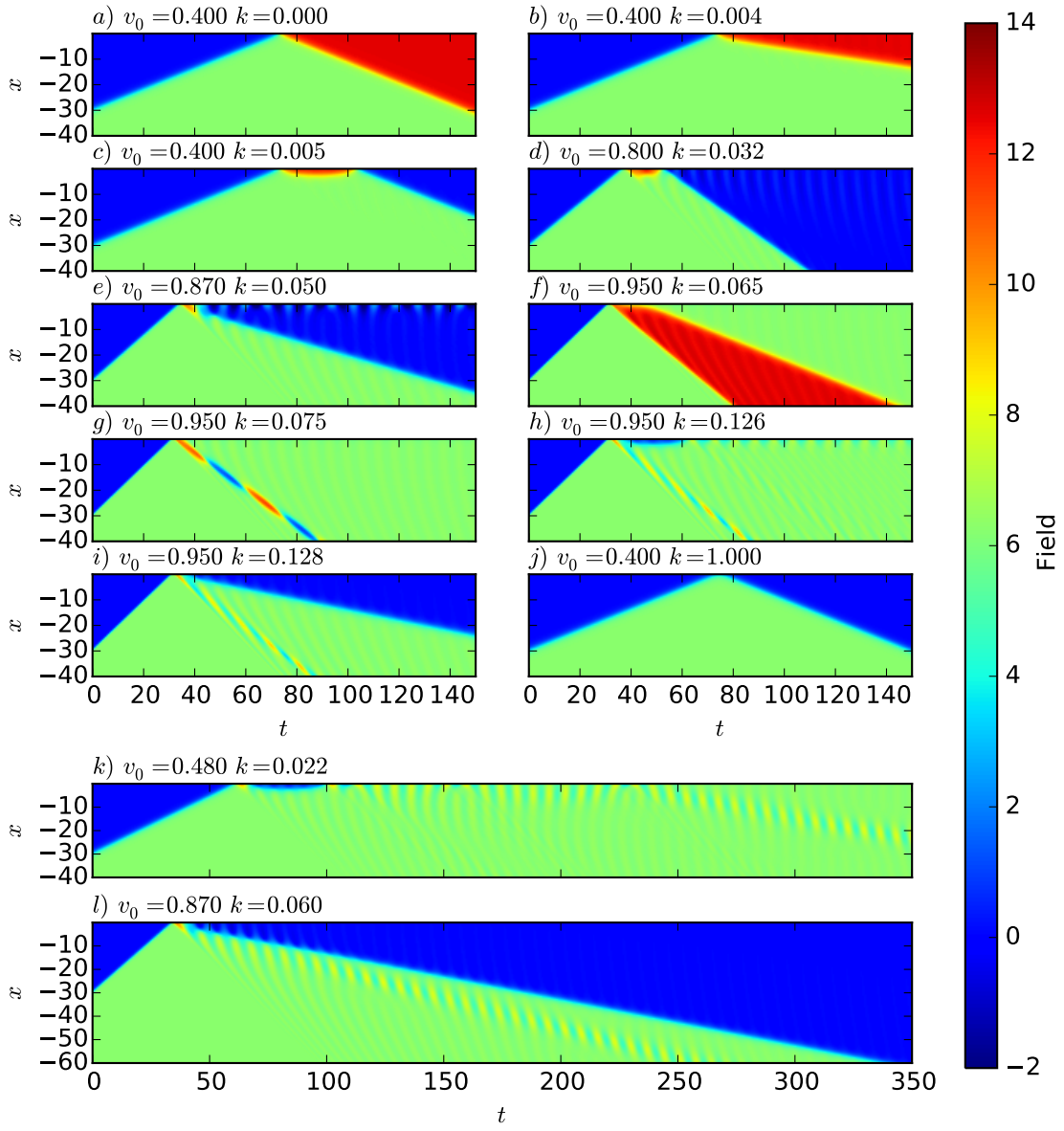

Figure 7.13: Spacetime plots showing the collision of an antikink with initial velocity v_0 with the Robin boundary (7.1) with boundary parameter k. The types, velocities v and frequencies ω of the excitations produced by the collisions, excluding breathers with $\omega > 0.999$, are:

a) a kink with $v = -0.400$
b) a kink with $v = -0.149$
c) an antikink with $v = -0.391$
d) an antikink with $v = -0.69$ and breather with $v = -0.107$, $\omega = 0.996$
e) an antikink with $v = -0.29$
f) an antikink with $v = -0.40$ and a kink with $v = -0.81$
g) a breather with $v = -0.710$, $\omega = 0.30$
h) a breather with $v = -0.72$, $\omega = 0.78$
i) an antikink with $v = -0.2$ and breather with $v = -0.722$ and $\omega = 0.80$
j) an antikink with $v = -0.400$
k) a breather with $v \approx -0.1$, $\omega \approx 0.93$
l) an antikink with $v = -0.195$ and breather with $v = -0.26$, $\omega = 0.93$

The numbers of digits quoted gives a rough estimate of the accuracy of the results for each plot, based on the extent to which the values had stabilised by the time the finest grid of $dx = 0.0025$, $dt = 0.002$ was reached.

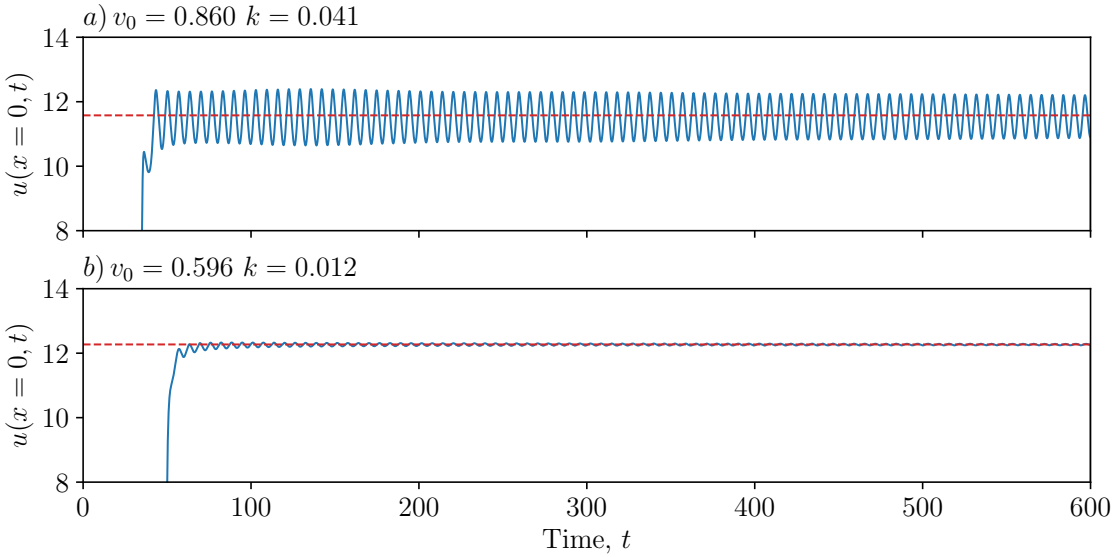

Figure 7.14: The solid blue line shows the oscillations in the value of the field at the boundary, $u(x = 0, t)$, during and after an antikink with initial velocity v_0 collides with the Robin boundary (7.1) with boundary parameter k. The dashed red line is the value of $u(x = 0)$ for the $n = 2$ metastable vacuum given by the solution of (7.27) in the interval $[3\pi, 4\pi]$.

and is reflected back as an antikink. This process is demonstrated in Fig. (7.13)c and occurs in region V_a of Fig. (7.11a).

An approximation for the curve in parameter space describing the transition from kink to antikink can be obtained by noting that the energy of the reflected field, aside from radiation, must contain the energy of the kink, which is at least 8, and the energy of the $n = 2$ metastable vacuum. Therefore, region I must lie within the region

$$8\gamma(v_0) \geq 8 + E^{(2)}(k)\,, \tag{7.46}$$

where $E^{(2)}(k)$ is the energy of the $n = 2$ metastable vacuum,

$$E^{(2)}(k) = 4 - 4\cos\left(\frac{u_0}{2}\right) + k^2 u_0\,, \quad ku_0 = \left|\sin\left(\frac{u_0}{2}\right)\right|\,, \quad 3\pi < u_0 < 4\pi\,,$$

discussed in §7.3. As region $\mathrm{V}_{a/b}$ is approached from region I the velocity of the reflected kink approaches zero and so the boundary between these regions is approximated by the saturation of the bound (7.46), which is plotted as the dashed blue line on Fig. (7.11a). It can be seen in Fig. (7.11a) that while this provides a good approximation for the boundary between region I and regions $\mathrm{V}_a/\mathrm{V}_b$ at low energies (low v_0) it becomes worse as v_0 increases. This is due to the amount of energy in the form radiation, which (7.46) ignores. This radiation is caused by boundary oscillations which are excited by the initial collision and, as demonstrated in Fig. (7.14), become more significant at higher v_0.

Increasing k further moves from region V_a to region IV of Fig. (7.11a) where a relatively high-energy (low frequency or loosely coupled) breather is produced from the boundary scattering. This can be seen in Fig. (7.13)d, where the breather is slower than the anitkink, or Fig. (7.13)l, where the breather is faster. At the transition from region IV to V_a the breather speed goes to zero, as shown in Fig. (7.15a), so that in V_a the breather becomes

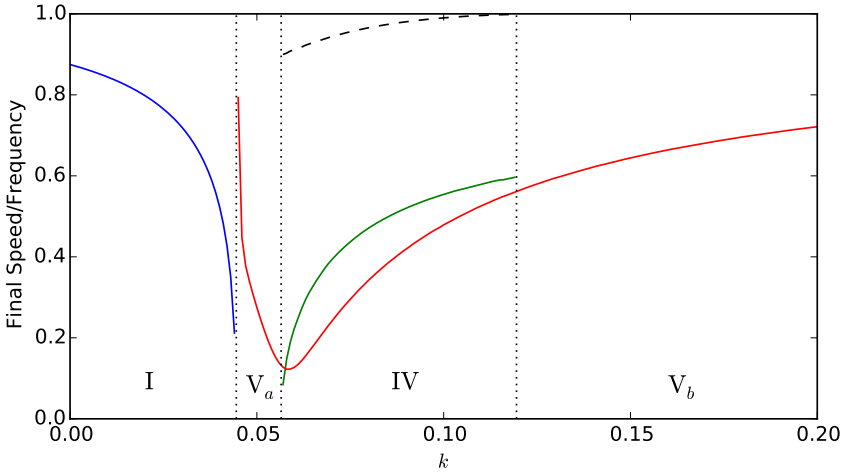

(a) $v_0 = 0.875$

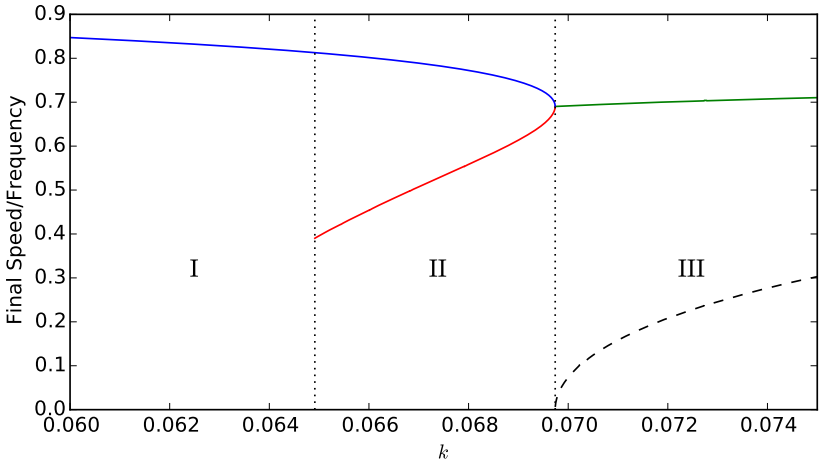

(b) $v_0 = 0.95$

Figure 7.15: The speed of the kinks (blue), antikinks (red) and breathers (green) and the frequency of breathers (black, dashed) found in the final state after the collision of an antikink with initial velocity (a) $v_0 = 0.875$ and (b) $v_0 = 0.95$ with the Robin boundary parameterised by k. In each case only the speed and frequency of the highest energy breather, with $\omega < 0.999$, is shown.

trapped at the boundary. This process is demonstrated in Fig. (7.13)e. This can also be clearly seen in Fig. (7.16) where on the left side of the plot (in V_a) the field value varies a great deal, corresponding to the trapped breather, while in the other areas of the plot where the antikink escapes from the boundary (blue) the field at the boundary is much more uniform since the breather has escaped.

When moving from region IV to region V_b the breather frequency goes to one and consequently the breather energy goes to zero, as shown in Fig. (7.15a). Therefore, the reflected field in region V_b contains only antikinks and radiation. As k increases further the amount of energy lost to radiation decreases while the antikink becomes almost perfectly reflected, as shown in Fig. (7.13)j. As $k \to \infty$ the antikink must be perfectly reflected with no loss of energy to radiation since the boundary becomes the integrable Dirichlet boundary.

As k is increased from a low value in region I but at higher initial antikink velocities

close to 1 the kink is still produced in the initial collision but there is enough energy left at the boundary for the $n = 2$ metastable boundary to produce an antikink and decay to the $n = 1$ metastable boundary. The final state therefore contains a kink and an antikink and this occurs in region II of Fig. (7.11a) and is illustrated in Fig. (7.13)f. As k increases within region II the speeds of the antikink and kink approach the same value, and the time between the release of the kink and antikink becomes smaller. At the threshold between regions II and III the kink and antikink 'fuse' into a loosely bound (low frequency, high mass) breather, as demonstrated in Fig. (7.13)g. As k is increased further within region III the breather frequency increases. The transition from regions I to II to III is shown in Fig. (7.15b) for $v_0 = 0.95$. Note that the boundary between regions I and II will not be approximated by the saturation of the energy bound (7.46) since the kink velocity does not approach zero at the transition from region I to II, as clearly shown in Fig. (7.15b).

At the lower tip of region III (within the shaded region of Fig. (7.11a)), the high energy breather produced in the initial antikink/boundary collision does not have enough energy to escape the boundary and instead collides with the boundary producing an intricate pattern of results which will be discussed in greater detail in §7.8.

In region III the boundary is in an $n = 1$ metastable state after the initial antikink/boundary collision. As k is increased from region III to IV this boundary is able to decay into an antikink, leaving the ground state ($u_0 = 0$) vacuum at the boundary. The final state in region IV therefore contains a breather and antikink. The space-time plot Fig. (7.13)h is in region III and shows the antikink emerging but it is unable to escape from the boundary while Fig. (7.13)i shows an example from region IV where the antikink is able to escape from the boundary.

Breathers can also be found at lower energies in region VI of Fig. (7.11a). Here, after the initial antikink/boundary collision the antikink fails to escape the boundary and instead collides again, forming a breather. This breather appears to collide multiple times with the boundary and may eventually escape the boundary, as in Fig. (7.13)k, or fail to do so over the time we evolve the sine-Gordon equation. The result seems quite unpredictable due to the strong dependence of the outcome on the phase the breather is in when it hits the boundary. This point will be discussed further at the end of §7.8. The numerical method §7.4 also often detected several very low energy breathers with $\omega > 0.999$ although a pattern in their appearance could not be discerned.

7.8 Resonance structure

Perhaps the most striking feature of the phase diagram Fig. (7.11) is the 'chaotic' band structure shown in Fig. (7.16). A window-like pattern of final velocities for the antikinks and breathers can be seen in Fig. (7.19) for a cross section of this region for $k = 0.058$. This is reminiscent of the well-known patterns of resonance windows found in the non-integrable ϕ^4 theory [145, 146, 147]. In the ϕ^4 theory the resonance windows present in the final velocities for kink-antikink scattering are caused by the presence of an internal shape mode for the kinks and antikinks which can temporarily store energy [145]. Here, sine-Gordon kinks and antikinks have no internal mode but in region III of Fig. (7.11a) the initial antikink/Robin boundary collision creates a breather which does have an internal oscillation

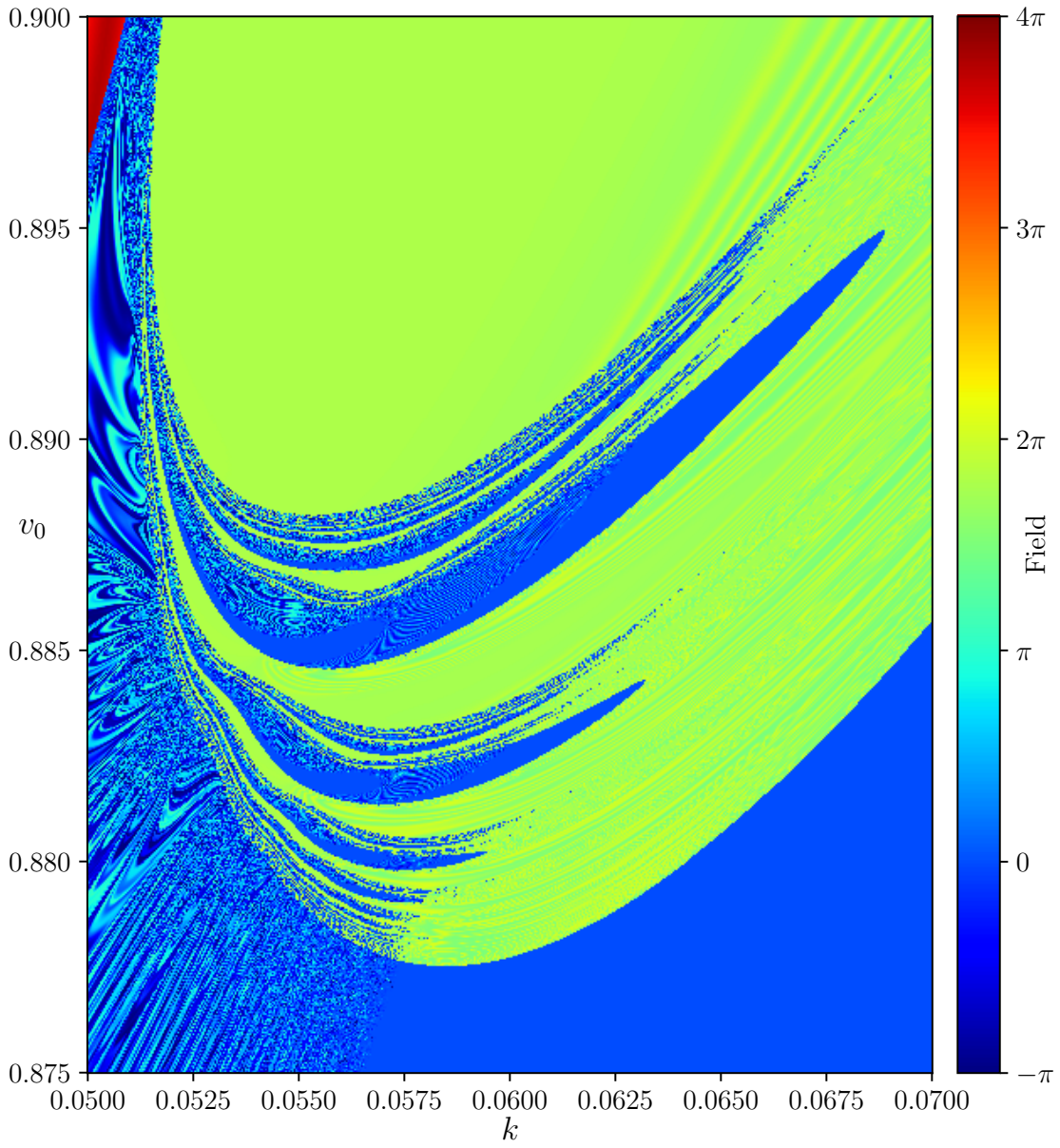

Figure 7.16: A zoomed-in plot of the shaded area in Fig. (7.11a), showing the value of the field at $x = 0$, $t = t_f = |x_0|/v_0 + 1000$ after the collision of an antikink with initial velocity v_0 and initial position x_0, with the Robin boundary (7.1) parameterised by k. In the green areas, where $u(0, t_f)$ is near 2π, only breathers are emitted while in the blue areas, where $u(0, t_f)$ is near zero, an antikink is emitted. Between the blue bands in the centre of the figure and the light green areas there are indeterminate regions where a very slight change in the initial parameters can cause an antikink to be produced or not. The oscillations in the boundary value of the left of the plot are caused by a breather becoming trapped at the boundary which decays very slowly, while in the bottom right of the figure this breather is able to escape and so the field relaxes to zero much more quickly. The line separating these two regions, running from approximately $(k, v_0) = (0.0565, 0.875)$ to $(k, v_0) = (0.0574, 0.8776)$, is the top portion of the boundary between regions V_a and IV in Fig. (7.11a).

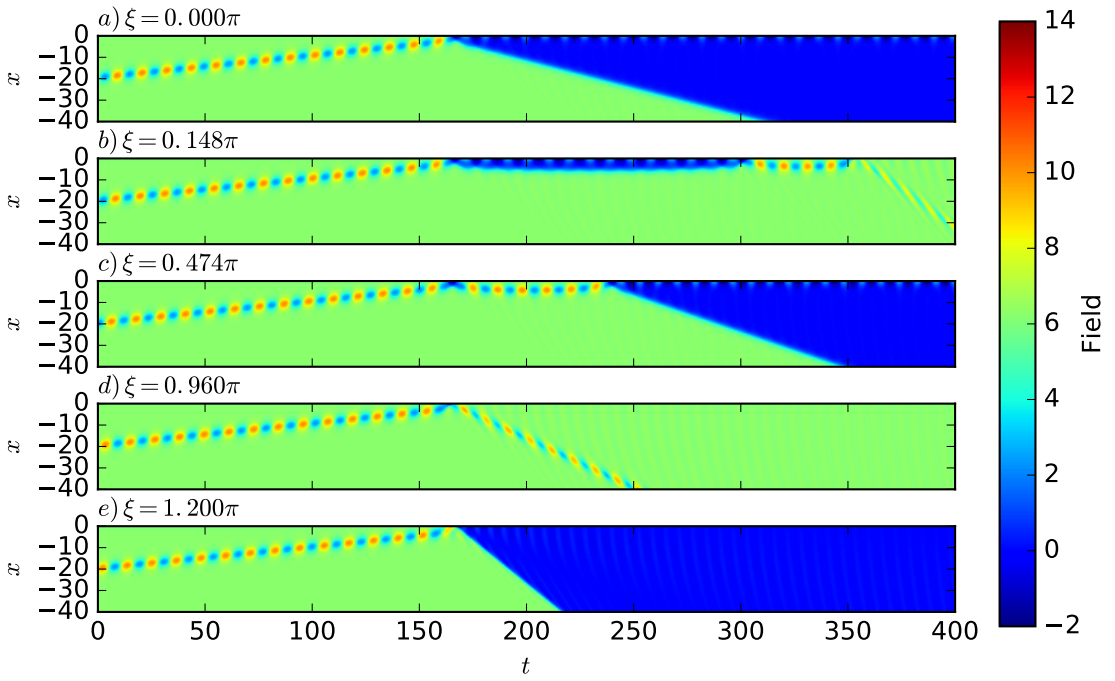

Figure 7.17: Spacetime plots showing a breather with initial velocity $v_0 = 0.1$, frequency $\omega = 0.55$ and a variety of initial phases $\xi \in [0, 2\pi)$ colliding with an $n = 1$ metastable Robin boundary with boundary parameter $k = 0.058$. The metastable boundary was created by placing a static antikink at $x = 1.79$ to satisfy the boundary condition. This models the environment in which an intermediate breather created by an antikink collision recollides with the boundary. In each case the antikinks and/or breathers escaping from the boundary are: a) an antikink; b) a breather; c) an antikink; d) a breather; e) an antikink and a breather.

mode. In the lower part of region III, shown in Fig. (7.16), the breather is attracted back towards the boundary to collide with it again. The collision of this intermediate breather with the boundary can produce dramatically different final states, as shown in Fig. (7.18).

The reason for the variety of outcomes in Fig. (7.18) is that the result of a breather colliding with the $n = 1$ metastable Robin boundary is highly dependent on the point in the breather's oscillatory cycle it is in when it hits the boundary. This is demonstrated in Fig. (7.17) where breathers with the same velocity and frequency but different initial phases produce completely different final states after colliding with the Robin boundary. In Fig. (7.17)a the breather fissions into an antikink and a breather trapped at the boundary, while Fig. (7.17)c has a similar outcome but only after an intermediate breather is created and recollides with the boundary. Fig. (7.17)d demonstrates the ability of the breather to reconfigure into a breather of lower mass and higher speed, and Fig. (7.17)b shows a similar outcome but after the creation of an intermediate antikink followed by an intermediate breather.

This strong phase dependence suggests that the breather and antikink resonance windows demonstrated in Fig. (7.19) occur when the frequency, velocity and initial phase of the intermediate breather are such that it recollides with the boundary at exactly the 'right' phase to produce an antikink and/or breather which escapes the boundary. Of course for the model under consideration here it is the initial antikink speed, v_0, and the boundary parameter, k, which indirectly controls all the characteristics of the intermediate breather.

Consider moving between these resonance windows in more detail for the specific case

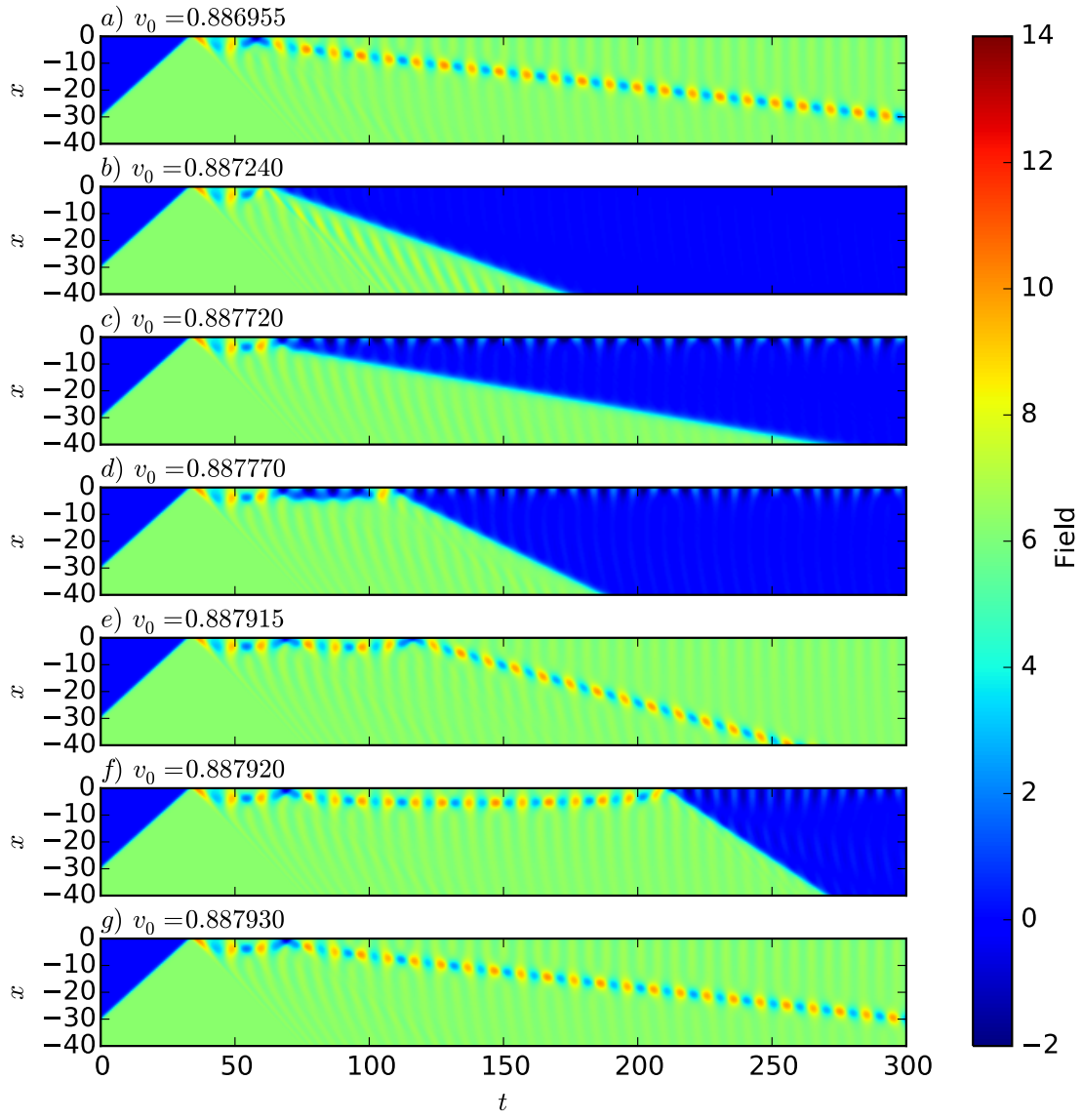

Figure 7.18: Spacetime plots of an antikink with initial velocity v_0 colliding with the Robin boundary with boundary parameter $k = 0.058$. For each plot the soliton and breather content of the final state, excluding breathers for which $\omega > 0.999$, is: a) a breather; b) an antikink and a breather; c) an antikink; d) an antikink; e) a breather; f) an antikink; g) a breather. Note that the multiple recollisions of breathers and kinks with the boundary causes the final state to depend very sensitively both on the initial conditions and on any numerical errors in the time evolution.

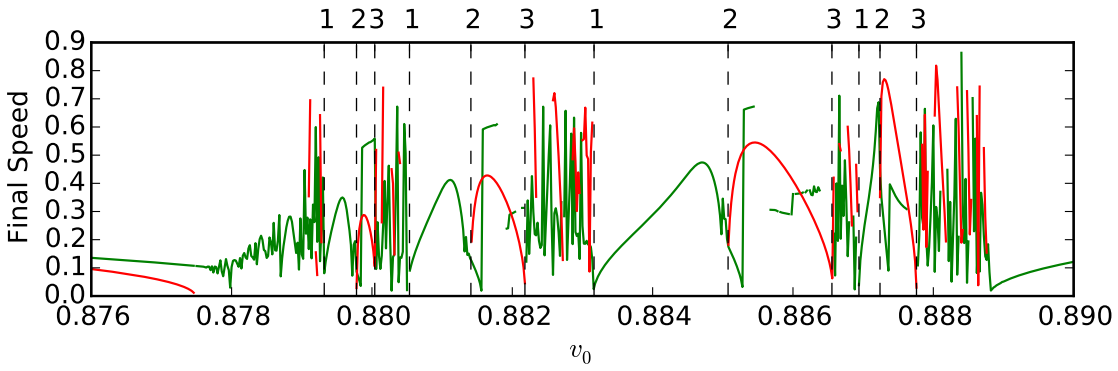

Figure 7.19: The speed for the highest energy breathers (green) and antikinks (red) produced by an antikink with initial velocity v_0 colliding with the Robin boundary with boundary parameter $k = 0.058$. The bands shown in Fig. (7.16) correspond to the regions between the 1, 2, 3 labels. Between 1 and 2 there is a resonance window for the production of breathers, while between 2 and 3 there is an antikink dominated resonance window and between 3 and 1 an indeterminate region where a slight change in the initial parameters gives drastically different results.

where $k = 0.058$, as shown in Fig. (7.19). Starting at a label 1 in Fig. (7.19) the intermediate breather collides with the boundary and produces a breather which then escapes the boundary, as in Fig. (7.18)a. If v_0 is increased then at label 2 in Fig. (7.19) an antikink is produced in addition to the breather, as shown in Fig. (7.18)b. Then as the breather speed decreases it becomes trapped at the boundary, as in Fig. (7.18)c. Increasing v_0 further will eventually cause the antikink speed to plateau and then decrease until it fails to escape the boundary at the point denoted by label 3 in Fig. (7.19). This label 3 to 1 region is the chaotic intermediate region which, as shown in Fig. (7.18)d, e and f is caused by multiple intermediate antikinks and breathers scattering off the boundary. Of course each successive intermediate breather produced will have its own resonance windows that may allow a breather or antikink to escape so the chaotic appearance of the intermediate 3-1 region in Fig. (7.19) is a product of one or more of these nested resonance windows. As v_0 continues to increase there will eventually come a point at label 1 in Fig. (7.19) where the phase of the intermediate breather cycles back to its original value where a breather is produced. This can be seen in Fig. (7.18)g where the breather has undergone an additional full cycle in its oscillation compared to Fig. (7.18)a and the final states are quite similar.

Beyond this cyclic region, if v_0 is sufficiently high (the precise value being dependent upon k) then the breather formed after the initial collision has enough energy to escape the boundary in the first instance and this is the process that occurs in the rest of region III shown in Fig. (7.11a).

If v_0 is instead sufficiently low (again, depending on k) then an antikink with (in region IV) or without (in region V_a) a breather is produced. Comparing Fig. (7.13)l and Fig. (7.13)e to Fig. (7.18)b and Fig. (7.18)c suggests that this transition to regions IV and V_a can be interpreted as the intermediate breather becoming very short lived and colliding with the boundary before oscillating a full cycle. Because the breather is so short-lived it appears very much like a short-lived kink. This coincides with the interpretation discussed in §7.7 that as k is increased from region I into $V_{a/b}$ there is an intermediate kink which exists for a progressively shorter time. For example, compare the progression

from Fig. (7.13)c to d to e.

Finally, a basic explanation for the behaviour observed in region VI and demonstrated in Fig. (7.13)k, where the recollision of an intermediate antikink creates a breather which may collide with the boundary multiple times before escaping, is now apparent. The breather only escapes when its velocity, frequency and, crucially, its phase as it hits the boundary is such that after the collision it has a mass and speed that allows it to escape the boundary. This is schematically similar to the case shown in Fig. (7.17)d. It is therefore expected that region VI should exhibit a similarly chaotic pattern of breather escape windows as was seen in the lower portion of region III. However, in region VI the total energy available to the breather is less than the escape energy of an antikink, since the breather itself was formed by an antikink which recollided with the boundary after failing to escape. For this reason any chaotic patterns will only be visible in the breather spectrum, making them much harder to see than in region III. Further study using higher-precision numerics will be required before the full picture in this region is clear.

7.9 Comments on Robin boundary with $k < 0$

This chapter has focused on the Robin boundary with parameter $k \geq 0$ but it is worth making some brief remarks on the case $k < 0$.

The integrable boundary

$$u_x + 4K \sin\left(\frac{u}{2}\right) = 0\,, \qquad K \in \mathbb{R}\,,$$

is known to be unstable for $K \leq -1/2$ since the boundary potential, $8K(1-\cos(u/2))$, allows for zero energy and negative energy solutions [148]. In particular, if $K = -1/2$ then the family of time-independent kink solutions, $u = 4\arctan(\exp(x - x_0))$, parameterised by the position x_0, have zero energy [148].

The Robin boundary appears to exhibit a similar instability. Close to $k = 0$ the incoming antikink is converted into a kink with greater amounts of radiation as k decreases. The detailed observations for $k > 0$ have not yet been repeated for $k < 0$ but for sufficiently negative k (approximately $k \lesssim -0.05$) an infinite number of additional kinks are produced so that the field at the boundary blows up to $+\infty$. There is some dependence on v_0 but this does not appear to be particularly strong with this transition occurring at $k \approx -0.05252$ for $v_0 = 0.1$ and $k \approx -0.05139$ for $v_0 = 0.95$.

Essentially, this occurs because the boundary contribution to the energy, ku_0^2, is now negative so for sufficiently negative k or large u_0 the boundary can decay by emitting a kink. Note that for $u(x = 0) = u_0 > 0$, $(u_0)_x = -2ku_0 > 0$ so the static solutions satisfying $u(x) \to 2\pi n$ as $x \to -\infty$ are kinks for which $2\pi n \leq u_0 < 2\pi(n+1)$ and $\varepsilon = (-1)^n = \text{sign}[\sin(u_0/2)]$.

The initial antikink/boundary collision produces a kink but leaves some energy at the boundary which, if k is sufficiently close to zero, will simply cause oscillations around the $n = 2$ metastable state. For more negative k there is eventually sufficient energy left at the boundary to overcome the $n = 2$ local maximum for the energy of a static kink (i.e. the local maximum of $E(u_0)$, given by (7.29), in $u_0 \in [5\pi, 6\pi]$). In this case the boundary can decay to the $n = 3$ metastable state, producing an additional kink. However, for

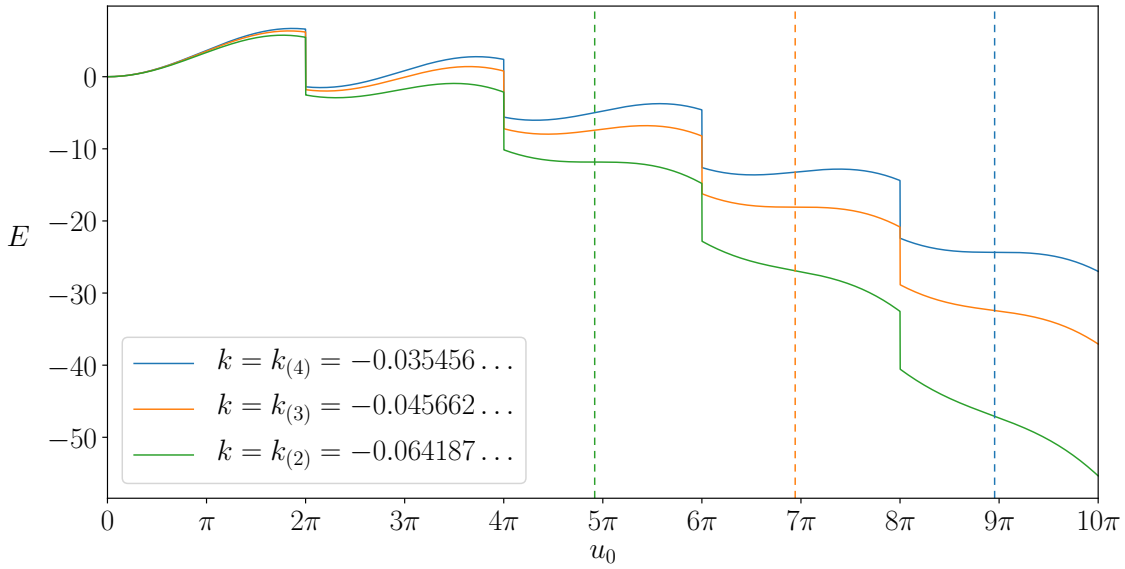

Figure 7.20: The energies, E, of a static kink $u(x)$ with $u(0) = u_0$ as given by (7.29) for $k = k_{(n)}$ being the negative critical values of k given by (7.47). The dashed lines are, from left to right, $u_0^{(2)}$, $u_0^{(3)}$ and $u_0^{(4)}$ which are the saddle points, given by (7.47), for the energy functions corresponding to $k = k_{(2)}, k_{(3)}, k_{(4)}$ respectively.

$k = k_{(3)} = -0.04566\ldots$, where (in analogy with (7.28)),

$$k_{(n)} = -\frac{1}{2}\left|\cos\left(\frac{u_0^{(n)}}{2}\right)\right|, \quad u_0^{(n)} = 2\tan\left(\frac{u_0^{(n)}}{2}\right), \quad 2\pi n < u_0 < 2\pi n + \pi\,, \tag{7.47}$$

the $n = 3$ static kink satisfying the Robin boundary condition corresponds to a saddle point, $u_0^{(3)}$, for the energy of a static kink, as shown in Fig. (7.20). Therefore, if $k < k_{(3)}$ then the $n = 3$ metastable state does not exist and $\frac{dE}{du_0} < 0$ for u_0 greater than the position of the $n = 2$ local maximum, as shown in Fig. (7.20). So if $k < k_{(3)}$ and the value of u_0 moves past the $n = 2$ local maximum then the boundary will decay to $u_0 \to \infty$ and in doing so produce an infinite number of kinks.

A more precise treatment of the transition from the production of a single kink to infinite kinks in the $k < 0$ region would appear to require a model for how much energy is left at the boundary after the production of the initial kink.

8 | Discussion

This thesis has examined several different topics under the umbrella of integrable nonlinear partial differential equations in the presence of integrable defects and integrable and non-integerable boundaries.

The first of these topics concerned the sine-Gordon and KdV equations with a type I integrable defect where the goal was to determine the effect of the defect on algebro-geometric type fields. The simplest algebro-geometric solutions can be expressed in terms of Jacobi theta functions and this made it possible to find solutions to the defect sewing conditions for sine-Gordon via the direct substitution of a phase-shifted ansatz. For higher genera this approach was not feasible and instead the field to the right of the defect for sine-Gordon and KdV was constructed as the Darboux transformation of the given algebro-geometric field to the left. This method relied on the fact that the type I integrable defect equations have the form of a Bäcklund transformation at the defect point so any field satisfying the integrable PDE on the full line together with its Darboux (or equivalently Bäcklund) transformation will satisfy the defect equations at any point.

Indeed, all the solutions to the type I integrable defect equations for sine-Gordon and KdV considered here actually satisfy the defect equations everywhere, not just at the defect point. However, it is not necessarily true that all solutions to the defect equations at the defect point must also satisfy them everywhere. For example, the type I integrable defect equations for the nonlinear Schrödinger equation allow a bound state solution which satisfies the defect equations only in the region $x \leq x_0$ or $x \geq x_0$, depending on the sign of the square root in the defect equations, where x_0 is a parameter of the solution [75]. But, to the best of the author's knowledge, there is no example of a pair of fields which satisfy the defect equations at *only* the defect point. Such an example would be very interesting to have since it would emphasise the integrable defect as something more than the manifestation of a Bäcklund transformation at a point, which is what it is effectively treated as here.

The reality and regularity conditions of the algebro-geometric solutions for the type I integrable defects were examined and in both the sine-Gordon and KdV cases a 'reality gap' was discovered. That is to say that given a real field to the left of the defect that there may be a range of values for the defect parameter (depending on the choice of underlying algebraic curve) for which the reality conditions for the field to the right of the defect cannot be satisfied. This is a new feature of these solutions which does not appear in the purely solitonic case where it is always possible to maintain the reality of the field across the defect.

The algebro-geometric solutions to the type I integrable defects constructed here are

a generalisation of the multi-soliton solutions to the defect equations involving soliton emission by the defect. In particular, it was explicitly shown that these soliton solutions can be recovered using previously known limits where the underlying algebraic curve becomes degenerate. It was also shown that the purely phase-shifted soliton and elliptic solutions appear as limits in which the initial position of a soliton emitted by the defect is sent to $\pm\infty$. In this way the algebro-geometric solutions constructed here generalise all the known soliton solutions for the sine-Gordon and KdV equations in the presence of a type I integrable defect.

One avenue for future work would be to apply a similar method, using Darboux transformations, to other integrable models possessing type I integrable defects, such as the nonlinear Schrödinger and modified KdV (mKdV) equations [75] or the $a_n^{(1)}$ affine Toda field theories [74]. It is also expected that a solution to an integrable system with n type I integrable defects could be found through n Darboux transformations. A more distinct problem would be to find algebro-geometric solutions in the presence of type II integrable defects, which are distinguished from type I in that they have a time-dependent parameter defined on the defect [76, 149, 150, 151, 152, 153]. For example, the sine-Gordon and Tzitzéica equations [154] (also known as the Bullough-Dodd or Zhiber-Mikhailov-Shabat equation or the $a_2^{(2)}$ affine Toda field theory) both permit type II integrable defects [76]. For both these models a defect matrix relating the Lax eigenfunctions on one side of the type II integrable defect to the other was found in [155] and algebro-geometric solutions to the Tzitzéica equation on the full line are known [156]. In addition, multi-soliton solutions on an algebro-geometric background were constructed on the full line for the Tzitzéica equation using the method of Darboux transformations [157] while a more explicit description of a soliton on an elliptic background was provided in [158]. It therefore seems quite plausible that the methods used here could also be employed to construct algebro-geometric solutions to type II integrable defects and the Tzitzéica equation, in particular, would be an interesting test case since it does not permit a type I integrable defect [76, 74].

The topic of integrable defects in 2+1 dimensions was tentatively introduced here although a great deal of work on this subject remains to be done. It was shown for the KP equation that the defect whose sewing conditions, (5.9), have the form of a Bäcklund transformation along the line $y = 0$ allows the total energy and momentum of the system, with suitable defect contributions, to be conserved and a Lagrangian description for this defect was found, (5.10). Conservation of energy and momentum is not a proof of integrability but in 1+1 dimensions conservation of momentum is typically a sufficiently constraining requirement to derive integrable defects (as in, for example, [73, 75]) so this should at least be an indicator of integrability in higher dimensions. An attempt was made to do the same for a defect along $x = 0$ but a Lagrangian description for the defect could not be found. As explained in §5.3, requiring conservation of energy and momentum for the system defined by a Lagrangian in terms of ϕ rather than p (where the original field is $u = p_x = \phi_{xx}$) might be a better strategy since it would eliminate the ∂_x^{-1} terms from the defect equations. It would also be interesting to understand the behaviour of the various solutions to the KP equation, such as line solitons [159] for KP2 and lump solitons [37] for KP1 as well as algebro-geometric solutions [19] in the presence of these defects.

Ultimately, one would like to be able to treat defects in 2+1 dimensions which lie along

a general curve in the x, y plane since this is the main novelty which might be allowed by integrable defects in higher dimensional models. However, this seems quite challenging to do with the Lagrangian method used here, in part because of the KP equation's lack of symmetry in the x, y coordinates. A spectral approach, perhaps in the style of [72], might prove more appropriate. It may also be helpful to instead work with an equation which exhibits more symmetry, such as the integrable Novikov-Veselov equation [160],

$$u_t = (\partial_z^3 + \partial_{\bar{z}}^3)u + 3\partial_z(uv) + 3\partial_{\bar{z}}(u\bar{v})\,, \quad \partial_{\bar{z}}v = \partial_z u\,, \quad z, v(z) \in \mathbb{C}\,, \quad u(z) \in \mathbb{R}\,,$$

in order to construct defects with more complex geometries than the ones considered here.

Another topic of this thesis was the construction of algebro-geometric solutions to the sine-Gordon equation on the half-line with an integrable Ghoshal-Zamolodchikov boundary. This was done in two ways: via a Bäcklund transformation of the known Dirichlet solution and via a restriction on the Lax pair eigenfunctions equivalent to the boundary conditions. It was shown that the results of these two methods agree. However, as explained in §6.1.1, the obtained solution has an ambiguity due to the integral of the holomorphic differentials only being well defined modulo the lattice Λ generated by the periods of the holomorphic differential. This is also expressed by the fact that the known solutions to the Dirichlet boundary only satisfy $u(0,t) = u_0 \mod 2\pi$. This ambiguity was shown to be equivalent to the choice of sign in (6.24) and so can be fixed numerically on a case by case basis by testing both signs and choosing whichever results in the boundary condition being satisfied. It is not yet clear how to resolve this ambiguity analytically so that the Ghoshal-Zamolodchikov boundary condition is guaranteed to be satisfied, however, this would certainly be a worthwhile task for the future.

The final chapter of this thesis concerned the collision of an antikink in the sine-Gordon model with a typically non-integrable Robin boundary which revealed a rich structure of outcomes and processes despite integrability only being broken at one point. An important tool in this analysis was a numerical implementation of the direct scattering transform to find the bound state eigenvalues that encode the solitons present in the reflected field. This enabled the creation of a detailed picture of how the scattering outcomes depend on the initial antikink velocity, v_0, and boundary parameter, k, shown in Fig. (7.10) and Fig. (7.11b). The space of initial parameters was categorised into different regions depending on the outcome of the antikink/boundary collision, as shown in Fig. (7.11). Close to the integrable Neumann limit at $k = 0$ the incoming antikink reflects into a kink (region I), while for large k the antikink remains an antikink after the collision (region V_b) and the amount of radiation produced vanishes in the integrable Dirichlet limit $k \to \infty$. Further away from these integrable limits the boundary can produce a kink and antikink (region II), high energy breathers (region III), an antikink accompanied by a breather (region IV), or the annihilation of the initial antikink into either radiation or low energy breathers (region VI).

The most exotic feature observed was the resonance structure, shown in Fig. (7.16) and Fig. (7.19), which was found to be due to the creation of an intermediate breather whose subsequent recollision with the boundary is highly dependent on the breather phase. In the future a better analytical understanding of this process would require some model of how the characteristics of the intermediate breather depend on the initial antikink velocity and

boundary parameter and subsequently how those characteristics determine the outcome of breather/boundary collisions. A likely next step would therefore be an examination of how a breather with a given initial phase, frequency and velocity collides with the Robin boundary in order to more directly observe this resonance phenomena. This study would be greatly aided by the use of a higher precision time evolution method than the simple Euler finite difference scheme used here since it was observed that the outcome of this resonance phenomena appeared to be much more sensitive to numerical errors than the outcomes in other regions of the initial parameter space.

While an approximation to the boundary between region I and $\mathrm{V}_{a/b}$ was given it became worse at high energies due to the presence of radiation which was not accounted for in the energy analysis. Improving this approximation, as well as deriving the boundaries of other transitions, would first require some model of how much energy is lost in the initial collision of an antikink with the boundary for a given v_0 and k. This would allow for a more accurate estimation of whether the initial state has sufficient energy to produce a particular final state.

A more ambitious task would be to see whether the integrability of the model away from the boundary can be exploited more directly using the Fokas (or unified transform) method. With respect to integrable PDEs on the half-line this method can be viewed as a generalisation of the inverse scattering transform [161, 162, 163]. For sine-Gordon specifically, the Fokas method requires the initial data $u(x,0)$ and $u_t(x,0)$ as well as the, most likely unknown, boundary data $u(0,t)$ and $u_x(0,t)$. A key component of this method is therefore the 'global relation' which is an equation relating spectral functions defined by the initial and boundary data. If $u(0,t)$ is a specified function of time then it is possible to derive a 'Dirichlet to Neumann map' and obtain a perturbative expansion for the unknown $u_x(0,t)$ [164, 165]. An analogous procedure can be carried out when $u_x(0,t)$ is known and $u(0,t)$ unknown. Alternatively, for some boundary conditions, called 'linearizable', there exists an additional symmetry of the Lax pair eigenfunctions which makes it possible to solve the global relation algebraically, bypassing the need for a perturbative expression for $u_x(0,t)$. For sine-Gordon the known linearizable boundary conditions are simply the integrable Dirichlet $u(0,t) = u_0$ and Ghoshal-Zamolodchikov (6.6) boundary conditions [166]. However, the Robin boundary is not linearizable and neither $u(0,t)$ or $u_x(0,t)$ are known *a priori* for $t > 0$. Instead, the Robin boundary $u_x(0,t) + 2ku(0,t) = 0$ belongs to a different class of boundaries which provide only a relationship between $u(0,t)$ and $u_x(0,t)$. This class of boundaries does not appear to have been treated with the Fokas method before and the complexity of the behaviour observed makes the Robin boundary an interesting test case for the wider applicability of the method.

While the content of this thesis has been entirely classical in nature it is worth remarking that breaking integrability at only the boundary may be a fruitful approach in the context of quantum field theories. Non-integrable bulk quantum field theories have been considered as deformations of integrable field theories before, for example in [167]. However, applying similar methods to a system with an integrable bulk but a non-integrable boundary would have the advantage that the space of asymptotic incoming and outgoing states should be exactly the same as in the fully integrable theory. For the quantum sine-Gordon theory in particular, the exact reflection matrices corresponding to the integrable

Neumann and Dirichlet boundaries are known [66] and it may be interesting to see how a non-integrable Robin boundary interpolates between these two limits and whether there is any correspondence with the classical behaviour observed here.

Returning to classical matters, the method of breaking integrability at a point and using a numerical implementation of the direct scattering method to categorise the results could be applied to any integrable model with a non-integrable boundary or defect. An analogous method could even be applied to a network with integrable field theories existing on the edges with non-integrable defect-like sewing conditions relating the fields at the vertices. This system could also benefit from the framework of the Fokas method which has been adapted by Caudrelier to star graphs, N semi-infinite edges connected at a single vertex [168].

In fact, the topic of fully integrable networks would itself be an interesting direction for future work. Integrable vertices have been found which connect differently scaled versions of the sine-Gordon equation, $\partial_t^2 u_k - a_k^2 \partial_x^2 u_k + \sin u = 0$, where u_k is the field on the k^{th} edge and the corresponding scaling parameters a_k satisfy a sum rule for the vertex to be integrable [169]. Similar results have also been obtained for the nonlinear Schrödinger equation [170]. A sine-Gordon soliton incident on such an integrable vertex is purely transmitted to the other connecting vertices but its energy is split according to the ratio of the scaling parameters corresponding to the incoming and outgoing edges [169]. Algebro-geometric solutions for this kind of network do not appear to have been studied and this would make an interesting problem for the future. It is also worth remarking that when the number of edges equals two these integrable vertices reduce to the trivial 'transparent' case where the resulting defect has no effect. One might therefore wonder if integrable vertices exist which are instead generalisations of the integrable defects of the type considered in this thesis. It is hoped that this problem, and the others posed in this discussion, will be the subject of future research.

A | Full soliton limit

It is well known that the multi-soliton solutions for sine-Gordon and KdV can be recovered from the algebro-geometric solutions by taking what is called the soliton or degenerate limit in which pairs of finite branch points coalesce [20, 21, 22, 19]. The argument for obtaining multi-soliton solutions from algebro-geometric solutions is detailed here for convenience in order to help show that the results for algebro-geometric solutions in the presence of an integrable defect do indeed generalise the known soliton solutions. The presentation here mirrors that of [19, §4.4] which carries out a similar degeneration, obtaining the N soliton solutions for the nonlinear Schrödinger equation from the $g = N$ genus algebro-geometric solutions.

Consider a hyperelliptic Riemann surface where ∞ is a branch point and where each pair of branch points joined by finite length branch cuts coalesces to a point so that the only branch cut remaining is (λ_{2g+1}, ∞). In either the KdV or sine-Gordon cases the algebraic curve for the now degenerate Riemann surface has the form

$$\mu^2 = (\lambda - \lambda_{2g+1}) \prod_{k=1}^{g} (\lambda - \lambda_k)^2 \,. \tag{A.1}$$

For KdV $\lambda_k \in \mathbb{R}$ just as was the case for the original curve (2.74). For sine-Gordon $\lambda_{2g+1} = 0$ and $\lambda_k \in \mathbb{R}$ since the branch cuts were chosen to be either on the real axis or connect conjugate branch points, as in Fig. (2.9). This choice for sine-Gordon means that in the degenerate limit all the solitons will be kinks or antikinks. Although it will not be addressed here, bringing together branch points joined by a different choice of cuts, such as in Fig. (A.1), would lead to pairs of complex conjugate λ_k corresponding to breathers, bound states of kinks and antikinks.

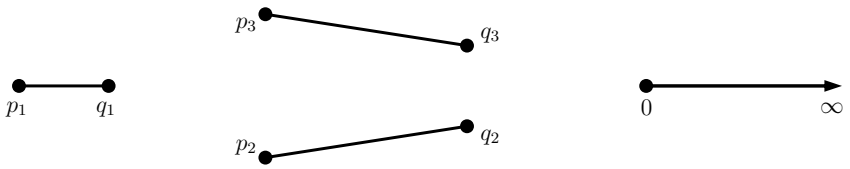

Figure A.1: An alternate choice of branch cuts for sine-Gordon which in a degenerate limit where $q_i \to p_i$ would lead to a single kink or antikink and a breather. The case where breathers appear in the degenerate limit will not be considered here.

In the soliton limit of (A.1) the normalised holomorphic differential becomes [19]

$$\omega_k = -\frac{\sqrt{\lambda_k - \lambda_{2g+1}}\prod_{\substack{l=1\\l\neq k}}(\lambda-\lambda_l)}{\sqrt{\lambda-\lambda_{2g+1}}\prod_{j=1}^{g}(\lambda-\lambda_j)}d\lambda = -\frac{\sqrt{\lambda_k-\lambda_{2g+1}}}{\sqrt{\lambda-\lambda_{2g+1}}(\lambda-\lambda_k)}d\lambda\,. \tag{A.2}$$

The Riemann matrix can then be written as

$$B_{jk} = \oint_{b_j}\omega_k = 2\int_{\lambda_j}^{\lambda_{2g+1}}\omega_k = -2\sqrt{\lambda_k-\lambda_{2g+1}}\int_{\lambda_j}^{\lambda_{2g+1}}\frac{d\lambda}{\sqrt{\lambda-\lambda_{2g+1}}(\lambda-\lambda_k)}\,, \tag{A.3}$$

which, making the substitution $\sqrt{\lambda-\lambda_{2g+1}} = \sqrt{\lambda_k-\lambda_{2g+1}}\tanh(s)$, is evaluated as [19],

$$B_{jk} = -4\,\mathrm{arctanh}\left(\frac{\sqrt{\lambda_j-\lambda_{2g+1}}}{\sqrt{\lambda_k-\lambda_{2g+1}}}\right)\,, \qquad j>k \tag{A.4a}$$

$$B_{jk} = B_{kj} = -4\,\mathrm{arctanh}\left(\frac{\sqrt{\lambda_k-\lambda_{2g+1}}}{\sqrt{\lambda_j-\lambda_{2g+1}}}\right)\,, \qquad j<k \tag{A.4b}$$

$$B_{jk} \to -\infty\,, \qquad j=k \tag{A.4c}$$

When $B_{ii}\to-\infty$ the Riemann theta function decomposes to [22],

$$\begin{aligned}
\theta\left(z-\frac{B_{ii}}{2},B\right) &= \sum_{n\in\mathbb{Z}^g} e^{\frac{1}{2}nBn+\sum_i^g n_i(z_i-B_{ii}/2)} \\
&= \sum_{n\in\mathbb{Z}^g}\left[\prod_{i=1}^{g} e^{\frac{1}{2}n_i(n_i-1)B_{ii}+n_iz_i}\prod_{\substack{j=1\\j>i}}^{g} e^{n_in_jB_{ij}}\right] \\
&\xrightarrow[B_{ii}\to-\infty]{} \sum_{\substack{n=(n_1,\ldots,n_g)\\ n_i=0\,\mathrm{or}\,1}}\prod_{i=1}^{g} e^{n_iz_i}\prod_{\substack{j=1\\j>i}}^{g} e^{n_in_jB_{ij}} \\
&= 1+\sum_{i=1}^{g} e^{z_i}+\sum_{\substack{j=1\\j>i}}^{g} e^{z_i+z_j}e^{B_{ij}}+\sum_{\substack{k=1\\k>j>i}}^{g} e^{z_i+z_j+z_k}e^{B_{ij}+B_{ik}+B_{jk}}+\cdots
\end{aligned} \tag{A.5}$$

A.1 KdV

Following these general remarks, the specific case of the soliton or degenerate limit for KdV will now be detailed [22]. Comparing (A.2) with

$$\omega_j = C_{jk}\frac{\lambda^{k-1}}{\mu}d\lambda\,,$$

shows that in the soliton limit

$$C_{ig} = -\sqrt{\lambda_i-\lambda_{2g+1}}\,, \qquad C_{i(g-1)} = \sqrt{\lambda_i-\lambda_{2g+1}}\sum_{\substack{l=1\\l\neq i}}^{g}\lambda_l\,, \tag{A.6}$$

so that, using the result of the Riemann bilinear relations (2.93), the b periods for the differentials of the second kind become

$$U_i = -2\sqrt{\lambda_i - \lambda_{2g+1}}\,, \tag{A.7a}$$

$$W_i = -\left(2\lambda_i + \lambda_{2g+1}\right)\sqrt{\lambda_i - \lambda_{2g+1}}\,. \tag{A.7b}$$

The normalisation constants α_i and β_i for the differentials of the second kind Ω_1 and Ω_2 are defined by $\oint_{a_i} d\Omega_1 = \oint_{a_i} d\Omega_3 = 0$ and in the soliton limit become

$$\alpha_i = \frac{\lambda_i^g}{2\sqrt{\lambda_i - \lambda_{2g+1}}\prod_{\substack{k=1\\k\neq i}}^{g}(\lambda_i - \lambda_k)}\,, \tag{A.8}$$

$$\beta_i = \frac{3}{4}\left(\frac{2\lambda_i^{g+1} - \widehat{E}\lambda_i^g}{\sqrt{\lambda_i - \lambda_{2g+1}}\prod_{\substack{k=1\\k\neq i}}^{g}(\lambda_i - \lambda_k)}\right). \tag{A.9}$$

which simplifies the explicit form for the differentials of the second kind (2.91) to

$$d\Omega_1 = \frac{d\lambda}{2\sqrt{\lambda - \lambda_{2g+1}}}\,, \qquad d\Omega_3 = \frac{3(2\lambda - \lambda_{2g+1})d\lambda}{4\sqrt{\lambda - \lambda_{2g+1}}}\,. \tag{A.10}$$

These expressions also confirm the formulas (A.7) for the b periods in the soliton limits. The coefficients c_1 and c_3 in the asymptotic expansions (2.76) are found, either by directly expanding the integrals Ω_1, Ω_3 of (A.10) or using the formulas (2.92), to be

$$c_1 = \frac{1}{2}\lambda_{2g+1}\,, \qquad c_3 = \frac{3}{8}\lambda_{2g+1}^2\,. \tag{A.11}$$

Putting this all together the potential p, given by (2.88), such that the field $u = p_x$ solves the KdV equation becomes in the soliton limit

$$p(x,t) = -2\partial_x \log\left[\sum_{\substack{n=(n_1,\ldots,n_g)\\ n_i=0\text{ or }1}}\prod_{i=1}^{g} e^{n_i z_i(x,t)}\prod_{\substack{j=1\\j>i}}^{g} e^{n_i n_j B_{ij}}\right] + \lambda_{2g+1}x + 3\lambda_{2g+1}^2 t\,, \tag{A.12}$$

$$\begin{aligned} z_i(x,t) &= iU(x + t(U^2 + 6\lambda_{2g+1}) - x_0) \\ &= 2\sqrt{\lambda_{2g+1} - \lambda_i}\,(x + 2(\lambda_{2g+1} + 2\lambda_i)t - (x_0)_i)\,, \end{aligned} \tag{A.13}$$

where the limit of the theta function (A.5) has been used with $D_i = iU_i(x_0)_i + B_{ii}/2$ for some choice of $x_0 \in \mathbb{R}^g$. Note that in the soliton limit

$$\exp(B_{ij}) = \left(\frac{\sqrt{\lambda_i - \lambda_{2g+1}} - \sqrt{\lambda_j - \lambda_{2g+1}}}{\sqrt{\lambda_i - \lambda_{2g+1}} + \sqrt{\lambda_j - \lambda_{2g+1}}}\right)^2,$$

and therefore, when $\lambda_{2g+1} = 0$, p can be recognised as the potential of the g-soliton solution to the KdV equation given by Hirota in [171]. Each z_i determines the velocity of the i^{th} soliton and each B_{ij} corresponds to the interaction of the i^{th} and j^{th} solitons.

A.2 Sine-Gordon

In the sine-Gordon case $\lambda_{2g+1} = 0$ and therefore $\lambda_k < 0$ for $k = 1, \dots, g$. The relevant normalisation constants are then, comparing (A.2) with $\omega_j = C_{jk}\lambda^{k-1}d\lambda/\mu$,

$$C_{ig} = -\sqrt{\lambda_i}\,, \qquad C_{i1} = -\sqrt{\lambda_i}\prod_{\substack{k=1\\k\neq i}}^{g}(-\lambda_k)\,, \tag{A.14}$$

and so from (2.117),

$$(B_\infty)_i = -2\sqrt{\lambda_i}\,, \qquad (B_0)_i = -\frac{2}{\sqrt{\lambda_i}}\,. \tag{A.15}$$

The normalisation constants for the normalised Abelian differentials of the second kind $d\Omega_\infty$, $d\Omega_0$ (2.116) in the soliton limit become, respectively,

$$\alpha_i = \frac{\lambda_i^g}{2\sqrt{\lambda_i}\prod_{\substack{j=1\\j\neq i}}^{g}(\lambda_i - \lambda_j)}\,, \tag{A.16a}$$

$$\beta_i = (-1)^{g+1}\frac{\prod_{k=1}^{g}\lambda_k}{2\lambda_i\sqrt{\lambda_i}\prod_{\substack{j=1\\j\neq i}}^{g}(\lambda_i - \lambda_j)}\,, \tag{A.16b}$$

which simplifies the differentials to,

$$d\Omega_\infty = \frac{d\lambda}{2\sqrt{\lambda}}\,, \qquad d\Omega_2 = -\frac{d\lambda}{2\lambda\sqrt{\lambda}}\,. \tag{A.17}$$

Turning now to the limit of the genus g solution to the sine-Gordon equation (2.114), first define,

$$\theta_i := -\frac{1}{2}\log(-\lambda_i)\,, \tag{A.18}$$

and let,

$$D_i = -(x_0)_i + \frac{i\pi}{2} + i\pi\varepsilon_i - \frac{B_{ii}}{2}\,, \quad i = 1, \dots, g\,, \tag{A.19}$$

for some choice of $x_0 \in \mathbb{R}^g$ and $\varepsilon_i = 0$ or 1 for each $i = 1, \dots, g$. Then, using the limit of the theta function (A.5), the field u which solves the sine-Gordon equation is given by

$$\exp\left(\frac{i}{2}u(x,t)\right) = \frac{\tau_0}{\tau_1}\,, \quad \tau_\alpha = \sum_{\substack{n=(n_1,\dots,n_g)\\n_i=0\text{ or }1}}\prod_{i=1}^{g}\left[i(-1)^{\varepsilon_i+\alpha}e^{z_i(x,t)}\right]^{n_i}\prod_{\substack{j=1\\j>i}}^{g}e^{n_i n_j B_{ij}}\,, \tag{A.20}$$

$$z_i(x,t) = \cosh\theta_i\, x - \sinh\theta_i\, t - (x_0)_i\,. \tag{A.21}$$

This can be recognised as the g-soliton solution for sine-Gordon written in the Hirota form [172].

B | Partial soliton limit

Here it is shown that the Darboux transformed fields (4.18) and (4.51) of a genus g solution to the KdV and sine-Gordon equations respectively can also be found as the limit of a $g+1$ genus solution where one of the pairs of branch points coalesce to the point α. This limit corresponds to a single soliton on a genus g algebro-geometric background [128, 127, 19].

The Riemann surface R defined by the algebraic curve

$$\mu^2(\lambda) = (\lambda - p_{g+1}) \prod_{i=1}^{g} (\lambda - p_i)(\lambda - q_i)\,, \tag{B.1}$$

will be compared with the partially degenerate Riemann surface $\widetilde{R}$ defined by the curve

$$\widetilde{\mu}^2(\lambda) = (\lambda - \alpha)^2 \mu^2(\lambda)\,. \tag{B.2}$$

Associated with α are the cycles a_0 and b_0 which are defined analogously to the other cycles and shown in Fig. (B.1).

The holomorphic differentials ω, associated with the surface R, have the usual form,

$$\omega_i = \frac{\varphi_i(\lambda)}{\mu(\lambda)} d\lambda\,, \qquad \varphi_i(\lambda) = \sum_{j=1}^{g} C_{ij} \lambda^{j-1}\,, \qquad i = 1, \ldots, g \tag{B.3}$$

while the differentials on the surface $\widetilde{R}$ are $\widetilde{\omega}$, given by

$$\widetilde{\omega}_\mu = \frac{\widetilde{\varphi}_\mu(\lambda)}{\mu(\lambda)(\lambda - \alpha)} d\lambda\,, \qquad \widetilde{\varphi}_\mu(\lambda) = \sum_{\nu=0}^{g} \widetilde{C}_{\mu\nu} \lambda^\nu\,, \qquad \mu = 0, \ldots, g\,. \tag{B.4}$$

The normalisation condition

$$\oint_{a_0} \widetilde{\omega}_\mu = -2\pi i \frac{\widetilde{\varphi}_\mu(\alpha)}{\mu(\alpha)} = 2\pi i \delta_{0\mu}\,, \qquad \mu = 0, \ldots, g\,,$$

implies that

$$\tilde{\varphi}_0(\lambda) = -\mu(\lambda) + \sum_{j=1}^{g} \widetilde{C}_{0j} (\lambda^j - \alpha^j)\,, \tag{B.5}$$

$$\widetilde{\varphi}_i(\lambda) = \sum_{j=1}^{g} \widetilde{C}_{ij} (\lambda^j - \alpha^j)\,, \qquad i = 1, \ldots, g \tag{B.6}$$

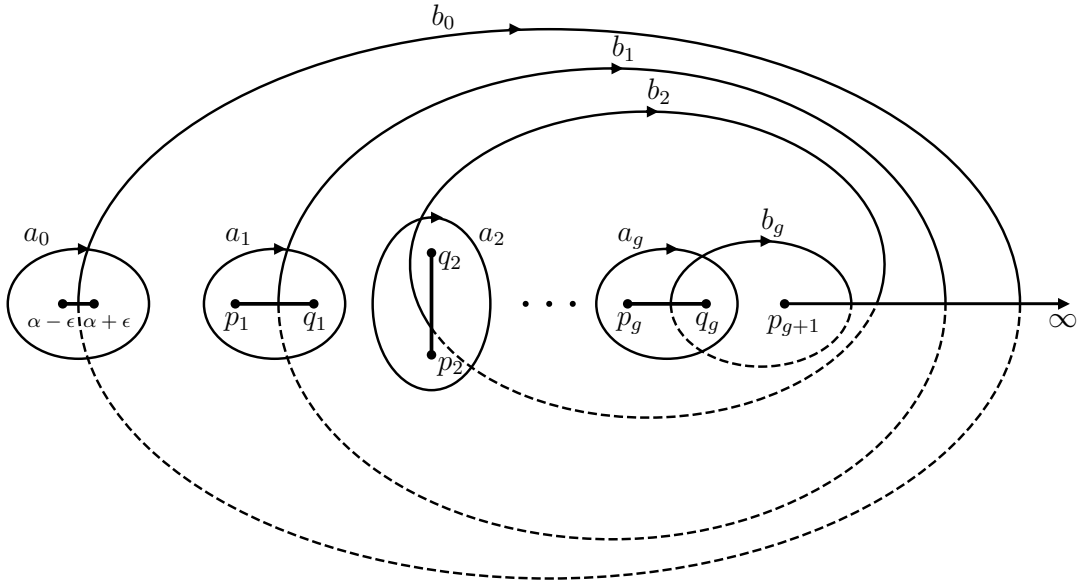

Figure B.1: The chosen basis of cycles for a genus $g+1$ Riemann surface which in the limit $\epsilon \to 0$ becomes the partially degenerate surface $\widetilde{R}$.

and since

$$\sum_{j=1}^{g} \widetilde{C}_{ij}(\lambda^j - \alpha^j) = (\lambda-\alpha)\sum_{j=1}^{g}\widetilde{C}_{ij}\sum_{k=1}^{j}\alpha^{j-k}\lambda^{k-1} = (\lambda-\alpha)\sum_{k=1}^{g}\lambda^{k-1}\sum_{j=k}^{g}\widetilde{C}_{ij}\alpha^{j-k}$$

the differential for the partially degenerate surface can be written as

$$\widetilde{\omega}_\mu = \frac{d\lambda}{\mu(\lambda)}\left(-\delta_{0\mu}\frac{\mu(\alpha)}{\lambda-\alpha} + \sum_{k=1}^{g}\sum_{j=k}^{g}\widetilde{C}_{ij}\alpha^{j-k}\lambda^{k-1}\right), \qquad \mu = 0,\ldots,g\,. \tag{B.7}$$

For $i = 1,\ldots,g$, $\widetilde{\omega}_{i>0}$ and ω_i and have the same normalisation condition for the same cycles $a_{i>0}$ and therefore

$$\omega_i = \widetilde{\omega}_i\,, \qquad C_{ik} = \sum_{j=k}^{g}\widetilde{C}_{ij}\alpha^{j-k}\,, \quad i,k = 1,\ldots,g\,. \tag{B.8}$$

This shows that $\widetilde{B}_{ij} = B_{ij}$ for $i,j = 1,\ldots,g$ while, as in (A.4c), $B_{00} \to -\infty$, and

$$\widetilde{B}_{0i} = \oint_{b_0}\widetilde{\omega}_i = 2\left[\int_\alpha^{p_1} + \sum_{k=1}^{g}\int_{q_k}^{p_{k+1}}\right]\widetilde{\omega}_i = -2\int_\infty^\alpha \widetilde{\omega}_i = -2\int_\infty^{\alpha^+}\omega_i\,, \quad i = 1,\ldots,g\,, \tag{B.9}$$

where the third equality uses

$$-\int_\infty^{\lambda_0}\widetilde{\omega}_j + \sum_{k=1}^{g}\int_{p_k}^{q_k}\widetilde{\omega}_j = 0\,, \qquad j = 1,\ldots,g\,. \tag{B.10}$$

In the partially degenerate limit when $\widetilde{B}_{00} \to -\infty$ the theta function associated with

$\widetilde{R}$ becomes

$$\begin{gathered}\theta\left(\widetilde{Z}\,,\widetilde{B}\right)\to\theta(z,B)+\theta\left(z-2\int_{\infty}^{\alpha^+}\omega,B\right)\exp(\tilde{z}_0)\,,\\ \widetilde{Z},\tilde{z}\in\mathbb{C}^{g+1}\,,\quad \widetilde{Z}_\mu=\tilde{z}_\mu-\delta_{\mu0}\frac{\widetilde{B}_{00}}{2}\,,\qquad \mu=0,\dots,g\,,\\ z\in\mathbb{C}^g\,,\quad z_i=\tilde{z}_i\,,\qquad i=1,\dots,g\,.\end{gathered}\tag{B.11}$$

B.1 Sine-Gordon

Turning now to the parameters specifically associated with sine-Gordon, the differential of the second kind $d\widetilde{\Omega}_\infty$ for the partially degenerate surface $\widetilde{R}$ is

$$d\widetilde{\Omega}_\infty=\frac{\lambda^{g+1}}{2\mu(\lambda)(\lambda-\alpha)}d\lambda+\sum_{\mu=0}^{g}\widetilde{\alpha}_\mu\widetilde{\omega}_\mu\,,\tag{B.12}$$

where the normalisation $\oint_{a_0}d\widetilde{\Omega}_\infty=0$ implies that

$$\widetilde{\alpha}_0=\frac{\alpha^{g+1}}{2\mu(\alpha)}\,.\tag{B.13}$$

To compare $d\widetilde{\Omega}_\infty$ with $d\Omega_\infty$ one can use (B.7) to compute

$$\begin{aligned}d\widetilde{\Omega}_\infty&=\frac{\lambda^{g+1}-\alpha^{g+1}}{2\mu(\lambda)(\lambda-\alpha)}d\lambda+\sum_{k=1}^{g}\left[\widetilde{\alpha}_0\sum_{j=k}^{g}\widetilde{C}_{0j}\alpha^{j-k}+\sum_{i=1}^{g}\widetilde{\alpha}_iC_{ik}\right]\frac{\lambda^{k-1}}{\mu(\lambda)}d\lambda\\&=\frac{\lambda^g}{2\mu(\lambda)}d\lambda+\sum_{k=1}^{g}\left[\frac{\alpha^{g+1-k}}{2}+\widetilde{\alpha}_0\sum_{j=k}^{g}\widetilde{C}_{0j}\alpha^{j-k}+\sum_{i=1}^{g}\widetilde{\alpha}_iC_{ik}\right]\frac{\lambda^{k-1}}{\mu(\lambda)}d\lambda\,.\end{aligned}$$

Then, since $d\widetilde{\Omega}_\infty$ and the corresponding differential on the original surface R,

$$d\Omega_\infty=\frac{\lambda^g}{2\mu(\lambda)}d\lambda+\sum_{i=1}^{g}\sum_{k=1}^{g}\alpha_iC_{ik}\frac{\lambda^{k-1}}{\mu(\lambda)}d\lambda\,,$$

have the same form and normalisation $\oint_{a_i}d\widetilde{\Omega}_\infty=\oint_{a_i}d\Omega_\infty=0$ for $i=1,\dots,g$ it follows that

$$d\widetilde{\Omega}_\infty=d\Omega_\infty\,,\qquad\sum_{i=1}^{g}\alpha_iC_{ik}=\frac{\alpha^{g+1-k}}{2}+\widetilde{\alpha}_0\sum_{j=k}^{g}\widetilde{C}_{0j}\alpha^{j-k}+\sum_{i=1}^{g}\widetilde{\alpha}_iC_{ik}\,.\tag{B.14}$$

Therefore $(\widetilde{B}_\infty)_i=(B_\infty)_i$ for $i=1,\dots,g$ while, recalling that for sine-Gordon $p_{g+1}=0$,

$$(\widetilde{B}_\infty)_0=\oint_{b_0}d\widetilde{\Omega}_\infty=2\left[\int_\alpha^{p_1}+\sum_{k=1}^{g}\int_{q_k}^{p_{k+1}}\right]d\widetilde{\Omega}_\infty=-2\int_0^\alpha d\widetilde{\Omega}_\infty=-2\int_0^{\alpha^+}d\Omega_\infty\,,\tag{B.15}$$

where in the third equality the normalisation conditions have been used to add

$$\int_{p_i}^{q_i}d\widetilde{\Omega}_\infty=\frac{1}{2}\oint_{a_i}d\widetilde{\Omega}_\infty=0\,.$$

The other differential of the second kind,

$$d\widetilde{\Omega}_0 = -\frac{\sqrt{\Lambda\alpha^2}}{2\lambda\mu(\lambda)(\lambda-\alpha)}d\lambda + \sum_{\mu=0}^{g}\widetilde{\beta}_\mu\tilde{\omega}_\mu\,, \qquad \Lambda = \prod_{i=1}^{g} p_i q_i\,, \tag{B.16}$$

can be treated similarly. The normalisation condition for the a_0 cycle, $\oint_{a_0} d\widetilde{\Omega}_0 = 0$, gives

$$\widetilde{\beta}_0 = -\frac{\sqrt{\Lambda\alpha^2}}{2\alpha\mu(\alpha)}\,. \tag{B.17}$$

Then computing $d\widetilde{\Omega}_0$ explicitly, with $\alpha < 0$, gives

$$d\widetilde{\Omega}_0 = -\frac{\sqrt{\Lambda}}{2\lambda\mu(\lambda)}d\lambda + \sum_{k=1}^{g}\left[\widetilde{\beta}_0\sum_{j=k}^{g}\widetilde{C}_{0j}\alpha^{j-k} + \sum_{i=1}^{g}\widetilde{\beta}_i C_{ik}\right]\frac{\lambda^{k-1}}{\mu(\lambda)}d\lambda\,,$$

which is of the same form as $d\Omega_0$ and satisfying the same a-period normalisation. Therefore,

$$d\widetilde{\Omega}_0 = d\Omega_0, \qquad \sum_{i=1}^{g}\beta_i C_{ik} = \widetilde{\beta}_0\sum_{j=k}^{g}\widetilde{C}_{0j}\alpha^{j-k} + \sum_{i=1}^{g}\widetilde{\beta}_i C_{ik}\,. \tag{B.18}$$

So $(\widetilde{B}_0)_i = (B_0)_i$ for $i = 1,\ldots,g$ and, as in (B.15),

$$(\widetilde{B}_0)_0 = \oint_{b_0} d\widetilde{\Omega}_0 = 2\left[\int_\alpha^{p_1} + \sum_{k=1}^{g-1}\int_{q_k}^{p_{k+1}} + \int_{q_g}^{\infty}\right] d\widetilde{\Omega}_0 = -2\int_\infty^\alpha d\widetilde{\Omega}_0 = -2\int_\infty^{\alpha^+} d\Omega_0\,. \tag{B.19}$$

Using (B.11) and the results of this section, the algebro-geometric solution to the sine-Gordon equation corresponding to the partially degenerate surface $\widetilde{R}$ is, in terms of quantities defined on R,

$$\begin{aligned} e^{iv/2} &= \frac{\theta(z,B) + \theta\left(z - 2\int_\infty^{\alpha^+}\omega, B\right)\exp(\tilde{z}_0)}{\theta(z + i\pi\mathbb{1}, B) - \theta\left(z + i\pi\mathbb{1} - 2\int_\infty^{\alpha^+}\omega, B\right)\exp(\tilde{z}_0)}\,, \\ z &= iB_\infty\rho + iB_0\xi + D\,, \qquad \tilde{z}_0 = -2i\left(\rho\int_0^{\alpha^+} d\Omega_\infty + \xi\int_\infty^{\alpha^+} d\Omega_0\right) + \widetilde{D}_0\,, \end{aligned} \tag{B.20}$$

where $\widetilde{B}_{00}/2$ has been absorbed into the constant $\widetilde{D}_0 \in \mathbb{C}$. The field v given by (B.20) corresponds to the degeneration of a single pair of branch points and therefore consists of a single soliton on a genus g algebro-geometric background [128, 19].

To compare this with the expression (4.51) obtained by Darboux transformation first note that $\int_\infty^{\alpha^+}\omega$ in (B.20) can be replaced with $\int_0^{\alpha^+}\omega$ since

$$\int_\infty^{\alpha^+}\omega = \int_\infty^0\omega + \int_0^{\alpha^+}\omega = i\pi + \int_0^{\alpha^+}\omega\,,$$

and the Riemann theta function is periodic in $2\pi i$. Then after setting $\alpha = -\sigma^2$, $\exp(\widetilde{D}_0) = \tilde{b}$ and shifting $D \to D + \int_0^{-\sigma^2}\omega$ it can be seen that the one soliton solution on a genus g background (B.20) has the same form as the field (4.51) obtained via a Darboux transformation of a genus g algebro-geometric field (2.114).

B.2 KdV

For KdV the procedure is similar. In this section the branch points will be labeled as in §2.6,

$$\mu^2(\lambda) = \prod_{i=1}^{2g+1} (\lambda - \lambda_i)\,.$$

The differentials of the second kind for the partially degenerate surface $\widetilde{R}$ are

$$d\widetilde{\Omega}_1 = \frac{\lambda^{g+1}}{2\mu(\lambda)(\lambda-\alpha)}d\lambda + \sum_{\mu=0}^{g} \widetilde{\alpha}_\mu \widetilde{\omega}_\mu\,, \tag{B.21a}$$

$$d\widetilde{\Omega}_3 = \frac{3}{4}\left(\frac{2\lambda^{g+2} - (2\alpha+\widehat{E})\lambda^{g+1}}{\mu(\lambda)(\lambda-\alpha)}\right)d\lambda + \sum_{\mu=0}^{g} \widetilde{\beta}_i \widetilde{\omega}_i\,, \quad \widehat{E} = \sum_{i=1}^{2g+1}\lambda_i\,. \tag{B.21b}$$

The normalisation conditions $\oint_{a_0} d\widetilde{\Omega}_1 = \oint_{a_0} d\widetilde{\Omega}_3 = 0$ imply that

$$\widetilde{\alpha}_0 = \frac{\alpha^{g+1}}{2\mu(\alpha)}\,, \qquad \widetilde{\beta}_0 = -\frac{3\widehat{E}\alpha^{g+1}}{4\mu(\alpha)}\,. \tag{B.22}$$

As in §B.1, the explicit form of $\widetilde{\omega}_0$ (B.7) can be used to relate the differentials on $\widetilde{R}$ and their normalisation constants to their counterparts on R,

$$d\widetilde{\Omega}_1 = d\Omega_1\,, \qquad \sum_{i=1}^{g}\alpha_i C_{ik} = \frac{1}{2}\alpha^{g+1-k} + \widetilde{\alpha}_0\sum_{j=k}^{g}\widetilde{C}_{0j}\alpha^{j-k} + \sum_{i=1}^{g}\widetilde{\alpha}_i C_{ik}\,, \tag{B.23a}$$

$$d\widetilde{\Omega}_3 = d\Omega_3\,, \qquad \sum_{i=1}^{g}\beta_i C_{ik} = -\frac{3\widehat{E}}{4}\alpha^{g+1-k} + \widetilde{\beta}_0\sum_{j=k}^{g}\widetilde{C}_{0j}\alpha^{j-k} + \sum_{i=1}^{g}\widetilde{\beta}_i C_{ik}\,. \tag{B.23b}$$

It therefore follows immediately that

$$\widetilde{c}_1 = c_1\,, \quad \widetilde{c}_3 = c_3\,, \qquad \widetilde{U}_i = U_i\,, \quad \widetilde{W}_i = W_i\,, \qquad i = 1\ldots g\,. \tag{B.24}$$

As for the period around b_0,

$$\widetilde{U}_0 = \oint_{b_0} d\widetilde{\Omega}_1 = 2\left[\int_\alpha^{\lambda_1} + \sum_{k=1}^{g}\int_{\lambda_{2k}}^{\lambda_{2k+1}}\right] d\widetilde{\Omega}_1 = -2\int_{\lambda_{2g+1}}^{\alpha} d\widetilde{\Omega}_1 = -2\int_{\lambda_{2g+1}}^{\alpha^+} d\Omega_1\,, \tag{B.25a}$$

$$\widetilde{W}_0 = \oint_{b_0} d\widetilde{\Omega}_3 = 2\left[\int_\alpha^{\lambda_1} + \sum_{k=1}^{g}\int_{\lambda_{2k}}^{\lambda_{2k+1}}\right] d\widetilde{\Omega}_3 = -2\int_{\lambda_{2g+1}}^{\alpha} d\widetilde{\Omega}_3 = -2\int_{\lambda_{2g+1}}^{\alpha^+} d\Omega_3\,, \tag{B.25b}$$

where the third equality on each line uses

$$\int_{\lambda_{2i-1}}^{\lambda_{2i}} d\widetilde{\Omega}_{1,3} = \frac{1}{2}\oint_{a_i} d\widetilde{\Omega}_{1,3} = 0\,.$$

Using (B.11) the $g+1$ genus KdV solution (2.89) in the partially degenerate limit

$B_{00} \to -\infty$ becomes, in terms of quantities defined on R,

$$\begin{gathered} v = -2\partial_{xx} \log \left[\theta(z, B) + \theta \left(z - 2 \int_{\infty}^{\alpha^+} \omega, B \right) \exp(\tilde{z}_0) \right] + 2c_1 \,, \\ z = iUx + 4iWt - D \,, \quad \tilde{z}_0 = -2ix \int_{\lambda_{2g+1}}^{\alpha^+} d\Omega_1 - 8it \int_{\lambda_{2g+1}}^{\alpha^+} d\Omega_3 - \widetilde{D}_0 \,, \end{gathered} \tag{B.26}$$

where again $\widetilde{B}_{00}/2$ has been absorbed into $\widetilde{D}_0$. The field (B.26), corresponding to the degeneration of one pair of branch points, consists of a single soliton on a g genus algebro-geometric background [127, 22, 19].

After setting $\alpha = \sigma$, $\exp(-\widetilde{D}_0) = \tilde{b}$ and shifting $D \to D - \int_{\infty}^{\sigma^+} \omega$ (the reality conditions §2.6.2 already require $\int_{\infty}^{\sigma^+} \omega_i \in \mathbb{R}$) then the partially degenerate solution (B.26) matches the field $v = q_x$ where q, given by (4.18), was obtained by the Darboux transformation of the genus g potential p, (2.88).

C | Finding the roots of complex analytic functions: cxroots

In §7 the problem of finding all the roots of a complex analytic function within a given contour arose from the need to extract information about the soliton content of a field using the bound state eigenvalues of an associated linear scattering problem. There, the QZ-40 algorithm of [140] was used to find these roots but, as discussed in §7.4, this approach does have some limitations.

The purpose of this appendix is to introduce the `cxroots` [89] module written by the present author in the Python programming language. The goal of `cxroots` is to find all the roots of any given analytic function within a given contour which can be a rectangle, circle, annulus or sector of an annulus in the complex plane. The mathematical approach of `cxroots` to this problem follows the method presented in [141, 90] which will now be briefly described.

C.1 Theory

Let C be a positively oriented contour in the complex plane and let $f(z)$ be a function which is complex analytic in the interior of C and without any poles or zeros on C itself. The aim is to find the set $\{z_i\}_{i=1}^n$ of roots of $f(z)$ within C and the multiplicity, m_i, of each root. It will be assumed that both the function itself $f(z)$ and its derivative $f'(z)$ are available. If the derivative cannot be analytically computed then `cxroots` will approximate it with a finite difference method.

Let $\mathcal{P}$ be the linear space of polynomials with complex coefficients and $\langle \cdot, \cdot \rangle : \mathcal{P} \times \mathcal{P} \to \mathbb{C}$ the symmetric bilinear form given by

$$\langle \phi, \psi \rangle := \frac{1}{2\pi i} \oint_C \phi(z)\psi(z)\frac{f'(z)}{f(z)}dz = \sum_{i=1}^{n} m_i \phi(z_i)\psi(z_i)\,. \tag{C.1}$$

Given the functions $\psi(z)$ and $\phi(z)$ the integration is performed numerically by calling the `quad` routine provided by `SciPy` [115] which uses a Clenshaw-Curtis method with Chebyshev moments. The total number of roots, N, of $f(z)$ in C, counting multiplicities, is given by

$$N := \sum_{i=1}^{n} m_i = \langle 1, 1 \rangle\,. \tag{C.2}$$

One way to compute the roots and multiplicities involves the $k \times k$ Hankel matrix,

$$H_k := \left[\langle 1, z^{p+q}\rangle\right]_{p,q=0}^{k-1} = \begin{bmatrix} \langle 1,1\rangle & \langle 1,z\rangle & \cdots & \langle 1,z^{k-1}\rangle \\ \langle 1,z\rangle & \ddots & & \vdots \\ \vdots & & \ddots & \vdots \\ \langle 1,z^{k-1}\rangle & \cdots & \cdots & \langle 1,z^{2k-2}\rangle \end{bmatrix} .$$

It can be proved [141, 90] that the number of distinct roots $n = \mathrm{rank}(H_{n+p})$ for every non-negative integer p and that in particular $n = \mathrm{rank}(H_N)$. H_n is therefore nonsingular while H_k for $k > n$ is singular. The distinct roots themselves are the eigenvalues of the generalised eigenvalue problem [90],

$$H_n^{(1)}\chi = \lambda H_n \chi\,, \qquad H_k^{(1)} := \left[\langle 1, z^{p+q+1}\rangle\right]_{p,q=0}^{k-1}\,, \tag{C.3}$$

for some eigenfunction $\chi \in \mathbb{C}^n$. This can be proved by noting that H_n and $H_n^{(1)}$ can be factorised as

$$H_n = V_n D_n V_n^T\,, \qquad H_n^{(1)} = V_n D_n^{(1)} V_n^T \tag{C.4}$$

where $D_n := \mathrm{diag}(m_1, \ldots, m_n)$, $D_n^{(1)} := \mathrm{diag}(m_1 z_1, \ldots, m_n z_n)$ and V_n is the Vandermonde matrix

$$V_n := \begin{bmatrix} 1 & \cdots & 1 \\ z_1 & \cdots & z_n \\ \vdots & & \vdots \\ z_1^{n-1} & \cdots & z_n^{n-1} \end{bmatrix} . \tag{C.5}$$

Once the roots are known the multiplicities $\{m_i\}_{i=1}^n$ can be computed by solving [141, 90],

$$V_n \left[m_i\right]_{i=1}^n = \left[\langle 1, z^p\rangle\right]_{p=0}^{n-1} . \tag{C.6}$$

Unfortunately, it appears that computing the roots using (C.3) is often quite inaccurate, particularly if some of the roots are fairly close together [173]. More accurate results are obtained if instead of working in the monomial basis,

$$H_k := \left[\langle 1, z^{p+q}\rangle\right]_{p,q=0}^{k-1}\,, \qquad H_k^{(1)} := \left[\langle 1, z^{p+q+1}\rangle\right]_{p,q=0}^{k-1}\,,$$

a basis of formal orthogonal polynomials $\psi_k(z)$,

$$G_k := \left[\langle \psi_p, \psi_q\rangle\right]_{p,q=0}^{k-1}\,, \qquad G_k^{(1)} := \left[\langle \psi_p, \psi_1\psi_q\rangle\right]_{p,q=0}^{k-1}\,, \tag{C.7}$$

is used instead [141, 90].

A *formal orthogonal polynomial* (FOP) of degree $k \geq 0$ is a monic polynomial

$$\psi_k(z) = z^k + a_{k-1}^{(k)} z^{k-1} + a_{k-2}^{(k)} z^{k-2} + \cdots + a_1^{(k)} z + a_0^{(k)} \tag{C.8}$$

which for $k \geq 1$ satisfies the orthogonality relations

$$\langle z^p, \psi_k(z)\rangle = 0\,, \qquad p = 0, 1, \ldots, k-1\,. \tag{C.9}$$

The word 'formal' refers to the fact that the $\langle\cdot,\cdot\rangle$ form does not generally define a true inner product. For $k = 0$ the FOP is simply $\psi_0(z) = 1$. The conditions (C.9) can be written out as

$$H_k \left[a_i^{(k)}\right]_{i=0}^{k-1} + [s_{k+i}]_{i=0}^{k-1} = 0\,, \tag{C.10}$$

where

$$s_p := \langle 1, z^p\rangle = \sum_{i=1}^{n} m_i z_i^p\,.$$

Therefore the coefficients $a_i^{(k)}$ (and hence the FOP ψ_k) are uniquely determined for $k \geq 1$ if and only if H_k is nonsingular. If it is the case that ψ_k is unique then it is called a *regular* FOP and k is a *regular index*. If ψ_k is regular then (C.10) can be solved to find

$$\psi_k(z) = \frac{1}{\det H_k}\begin{vmatrix} s_0 & s_1 & \cdots & s_{k-1} & 1 \\ s_1 & \ddots & & \vdots & z \\ \vdots & & \ddots & \vdots & \vdots \\ s_{k-1} & \cdots & \cdots & s_{2k-2} & z^{k-1} \\ s_k & \cdots & \cdots & s_{2k-1} & z^k \end{vmatrix}\,. \tag{C.11}$$

In particular ψ_n, which is regular since H_n is nonsingular, has the roots of $f(z)$ within C as its simple zeros [141, 90],

$$\psi_n(z) = (z - z_1)(z - z_2)\ldots(z - z_n)\,, \tag{C.12}$$

which can be verified directly using (C.11).

For a regular FOP ψ_k the eigenvalues λ_i of the generalised eigenvalue problem,

$$G_k^{(1)}\chi = \lambda G_k \chi\,, \tag{C.13}$$

are given by $\lambda_i = \psi_1(z_i^{(k)})$ where $z_i^{(k)}$ are the zeros of ψ_k [141, 90]. Note that the G_k and $G_k^{(1)}$ matrices depend only on formal orthogonal polynomials of degree $< k$.

The core strategy of [141, 90] and of `cxroots` is therefore to start with the two lowest degree regular formal orthogonal polynomials

$$\psi_0(z) = 1\,, \qquad \psi_1(z) = z - \frac{s_1}{s_0}\,,$$

and use (C.13) with $k = 2$ to compute ψ_2 and so on until ψ_n (and hence the distinct roots, z_i, of $f(z)$) has been computed.

However, it may be that ψ_k is not regular, which is to say that H_k (and therefore G_k) is singular or, practically speaking, numerically close to singular. This means that some of the eigenvalues of (C.13) (and hence the roots of ψ_k) may be infinite or assume arbitrary values [141]. To avoid this breakdown the algorithm checks if any of the computed roots of ψ_k lie outside the integration contour. If so then ψ_k is replaced by an 'inner polynomial': $\psi_k = \psi_{k-r}\psi_r$ where r is the degree of the highest degree regular FOP currently known. These inner polynomials are defined such that if the whole series of polynomials are split

into vectors

$$\begin{aligned}\Psi^{(0)} &= [\psi_0] \\ \Psi^{(1)} &= [\psi_1, \psi_2, \ldots, \psi_{k_2-1}] \\ \Psi^{(2)} &= [\psi_{k_2}, \psi_{k_2+1}, \ldots, \psi_{k_3-1}] \\ &\vdots\end{aligned}$$

with the first element of each vector being a regular FOP and the rest being inner polynomials then polynomials belonging to different vectors are orthogonal [90]. This skips over the singular breakdown while maintaining the necessary structure for G_k and $G_k^{(1)}$ [90].

To decide when ψ_n has been computed the algorithm, after a regular FOP, ψ_r, has been generated, examines the sequence, as in [141, 90],

$$\{|\langle \psi_1(z)^j \psi_r(z), \psi_r(z)\rangle|\}_{j=0}^{N-1-r}. \tag{C.14}$$

If $r \geq n$ then, because of (C.1) and (C.12), $\langle z^p, \psi_r\rangle = 0$ for all $p \geq 0$, $p \in \mathbb{Z}$ [90]. So if each element of (C.14) plus the associated integration error is less than a user supplied value `errStop` (by default 10^{-8}) then the algorithm decides that $n = r$ and stops. The roots of $f(z)$ within C, approximated by the roots of ψ_n, are further refined using the iterative Newton-Raphson method if $f'(z)$ is provided or Muller's method (implemented by `mpmath` [174]) if only $f(z)$ is supplied by the user. The multiplicities of the roots are computed by solving (C.6).

The error in the approximations to the roots of $f(z)$ tend to grow as the number of roots increases and therefore `cxroots` subdivides the original contour C into contours which contain at most `M` roots (counting multiplicities). `M` is a user supplied value which is 5 by default but should be as large as the highest multiplicity present. If the integration around a sub-contour fails to converge or the computed number of roots within the sub-contour is not within the user specified `integerTol` (0.1 by default) of an integer then this is usually an indication that the contour is very close to a root so the sub-contour is rejected and a new subdivision of its parent contour is attempted instead. If the multiplicities obtained by solving (C.6) are not within `integerTol` of an integer then it is likely that some roots are clustered together and the contour is further subdivided since isolating the cluster within a smaller contour should produce more accurate results.

Before giving some examples of `cxroots` in use it should be mentioned that some of authors of the root finding algorithm described here also developed the software called `ZEAL`, written in Fortran 90, which uses their method [175]. Presently, the main advantages of `cxroots` over `ZEAL` are the ability to choose the initial contour C to be a rectangle, circle, annulus or sector of an annulus (for `ZEAL` C must be a rectangle) and a more flexible user interface. Of course usability is to some extent in the eye of the user, however `ZEAL` requires the user to edit variables in up to three different files in order to specify the problem before compiling and running the program while, as demonstrated below, `cxroots` can be installed, imported, run and the output displayed in a few lines within any Python script or in the Python terminal on the command line. This makes `cxroots` much easier to use as part of a larger program and indeed it was written with this goal in mind.

C.2 Using `cxroots`

`cxroots` is open source (BSD licensed) and freely available, as are all its dependencies, including the Python programming language itself. It is most easily downloaded and installed by invoking the Python Package Index (`pip`), which comes installed with Python, on the command line:

```
pip install cxroots
```

The code and documentation are also available at [89].

As an example, suppose the roots of the function

$$f(z) = z^2(z+2)^2\left(e^{2z}\cos(z) - 1 - \sin(z) + z^5\right)$$

within in the interior of the circle $|z| = 3$ are sought. In Python this function is written as

```
from numpy import exp, cos, sin
f = lambda z: (z*(z+2))**2 * (exp(2*z)*cos(z)-1-sin(z)+z**5)
```

and `cxroots` is invoked with

```
from cxroots import Circle
C = Circle(0,3)
roots = C.roots(f)
```

This defines a circle of centre 0 and radius 3 and finds the roots of $f(z)$ within it. A full list of the arguments that the `C.roots(...)` method takes can be found in the documentation [89]. The roots can be printed in a table

```
print(roots)
```

```
 Multiplicity |               Root
-----------------------------------------------
      2       | -2.000000000000 -0.000000000000i
      1       | -0.651114070264 -0.390425719088i
      1       | -0.651114070264 +0.390425719088i
      3       |  0.000000000000 +0.000000000000i
      1       |  0.648578080954 -1.356622683988i
      1       |  0.648578080954 +1.356622683988i
      1       |  2.237557782467 +0.000000000000i
```

or viewed using `matplotlib`:

```
roots.show()
```

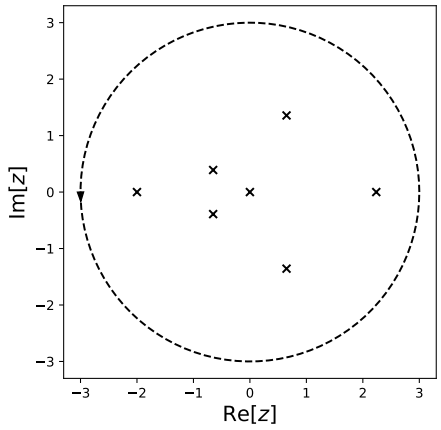

The roots and multiplicities can also be accessed as Python lists with the attributes `roots.roots` and `roots.multiplicities` and used as part of a larger program.

All the contours that can be used as the initial contour C are shown in Fig. (C.1).

It is also possible to exploit the particular symmetries of $f(z)$ if known. For example, if z_i is a root of

$$f(z) = z^{26} - 2z^{10} + \frac{1}{2}z^6 - 1$$

then so is $\overline{z_i}$ and $-z_i$. It is possible to inform `cxroots` of this symmetry:

```
f  = lambda z: z**26-2*z**10+0.5*z**6-1
df = lambda z: 26*z**25-20*z**9+3*z**5

from cxroots import Rectangle
C = Rectangle([-1.5,1.5], [-1.5,1.5])
rootSymmetry = lambda z: [z.conjugate(), -z]
roots = C.roots(f, df, guessRootSymmetry = rootSymmetry)
roots.show()
```

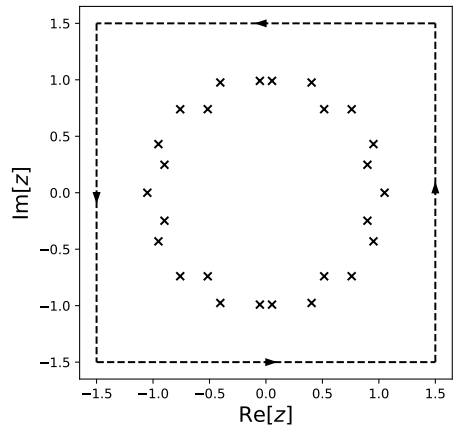

and doing this can save some time:

```
from time import time
t0 = time()
C.roots(f, df)
t1 = time()
C.roots(f, df, guessRootSymmetry = rootSymmetry)
t2 = time()

print('Time without symmetry:', t1-t0)
print('Time with symmetry:', t2-t1)
```

```
Time without symmetry: 7.860443115234375
Time with symmetry: 2.6706297397613525
```

Known roots can also be passed to `cxroots` using the `guessRoots` argument which should be a list of roots or, if the multiplicity is known, a list of (root, multiplicity) tuples:

```
from numpy import exp, sin, cos
from cxroots import Circle
C = Circle(0, 3)
f = lambda z: (z-2.5)**2 * (z+1.2) * (exp(-z)*sin(z/2)-1.2*cos(z))

roots = C.roots(f, guessRoots=[(2.5,2), (-1.2,1)])
print(roots)
```

```
 Multiplicity |               Root
-------------------------------------------------
      1       | -1.200000000000 +0.000000000000i
      1       | -0.974651035111 +1.381047768247i
      1       | -0.974651035111 -1.381047768247i
      1       |  1.440251130167 +0.000000000000i
      2       |  2.500000000000 +0.000000000000i
```

One key area of future improvement for `cxroots` would be to implement a reliable derivative free algorithm, such as in [176], which does not require $f'(z)$. Another is to properly detect and treat clusters of roots which are distinct but quite close together [141]. Currently, m clustered but distinct simple roots may be registered by `cxroots` as a single root at the centre of the cluster of multiplicity m. This can be avoided, for example, if the user chooses C to be a small contour which closely bounds the cluster or if it is known that all the roots must be simple then setting `M` $= 1$ will force the algorithm to subdivide C until all the roots are isolated. However, these approaches are problem specific and require some prior knowledge of $f(z)$ that will not always be available.

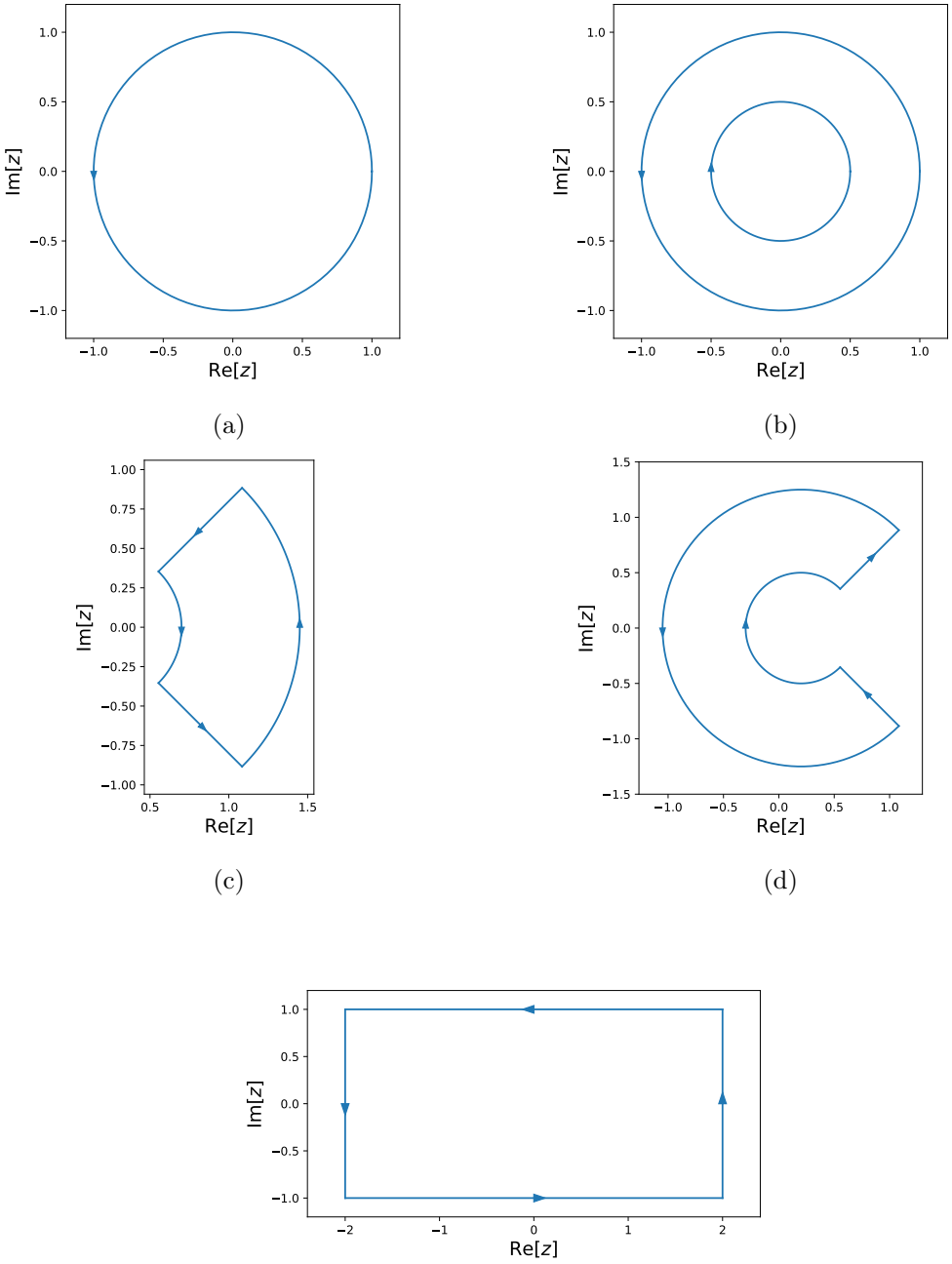

Figure C.1: Contours that can be used as the original contour C that `cxroots` will find the roots within. The commands used to create them are:

a) `Circle(center=0, radius=1)`
b) `Annulus(center=0, radii=[0.5,1])`
c) `AnnulusSector(center=0.2, rRange=[0.5, 1.25], phiRange=[-pi/4, pi/4])`
d) `AnnulusSector(center=0.2, rRange=[0.5, 1.25], phiRange=[pi/4, -pi/4])`
e) `Rectangle(xRange=[-2, 2], yRange=[-1, 1])`

Bibliography

[1] O. Babelon, D. Bernard, and M. Talon. *Introduction to classical integrable systems*. Cambridge University Press, 2003.

[2] V. I. Arnold. *Mathematical methods of classical mechanics*. 2nd ed. Springer, New York, 1989.

[3] D. J. Korteweg and G. de Vries. "On the Change of Form of Long Waves advancing in a Rectangular Canal, and on a New Type of Long Stationary Waves". *Philosophical Magazine* **5**.39 (1895), pp. 422–443.

[4] J. Scott Russell. "Report on Waves". In: *Report of the Fourteenth Meeting of the British Association for the Advancement of Science*. York, 1844, pp. 311–390.

[5] N. J. Zabusky and M. D. Kruskal. "Interaction of "solitons" in a collisionless plasma and the recurrence of initial states". *Physical Review Letters* **15**.6 (1965), pp. 240–243.

[6] C. S. Gardner, J. M. Greene, M. D. Kruskal, and R. M. Miura. "Method for solving the Korteweg-deVries equation". *Physical Review Letters* **19**.19 (1967), pp. 1095–1097.

[7] W. Magnus and S. Winkler. *Hill's Equation*. Dover, New York, 1979.

[8] S. P. Novikov. "The periodic problem for the Korteweg-de vries equation". *Functional Analysis and Its Applications* **8**.3 (1974), pp. 236–246.

[9] B. A. Dubrovin. "Inverse problem for periodic finite-zoned potentials in the theory of scattering". *Functional Analysis and Its Applications* **9**.1 (1975), pp. 61–62.

[10] A. R. Its and V. B. Matveev. "Hill's operator with finitely many gaps". *Functional Analysis and Its Applications* **9**.1 (1975), pp. 65–66.

[11] A. R. Its and V. B. Matveev. "Schrödinger operators with finite-gap spectrum and N-soliton solutions of the Korteweg-de Vries equation". *Theoretical and Mathematical Physics* **23**.1 (1975), pp. 343–355.

[12] H. P. McKean and P. van Moerbeke. "The spectrum of Hill's equation". *Inventiones Mathematicae* **30**.3 (1975), pp. 217–274.

[13] P. D. Lax. "Periodic Solutions of the KdV Equation". *Communications on Pure and Applied Mathematics* **28**.1 (1975), pp. 141–188.

[14] V. B. Matveev. "30 years of finite-gap integration theory". *Philosophical Transactions of the Royal Society A: Mathematical, Physical and Engineering Sciences* **366**.1867 (2008), pp. 837–875.

[15] F. Gesztesy and H. Holden. *Soliton Equations and Their Algebro-Geometric Solutions*. Cambridge University Press, 2003.

[16] H. F. Baker. "Note on the foregoing paper "Commutative Ordinary Differential Operators" by J. L. Burchnall and J. W. Chaundy." *Proceedings of the Royal Society A* **118** (1928), pp. 584–593.

[17] N. I. Akhiezer. "Continuous analogues of orthogonal polynomials on a system of intervals". *Doklady Akademii Nauk SSSR* **141**.2 (1961), pp. 263–266.

[18] B. A. Dubrovin and S. P. Novikov. "Periodic and conditionally periodic analogs of the many-soliton solutions of the Korteweg-de Vries equation". *Soviet Physics JETP* **40**.6 (1974), pp. 1058–1063.

[19] E. D. Belokolos, A. I. Bobenko, V. Z. Enol'skii, A. R. Its, and V. B. Matveev. *Algebro-geometric Approach to Nonlinear Integrable Equations*. Springer, Berlin, Heidelberg, 1994.

[20] V. B. Matveev. "Abelian functions and solitons". *University of Wroclaw, Preprint 373* (1976).

[21] H. P. McKean. "Theta functions, solitons, and singular curves". In: *Partial Differential Equations and Geometry*. Ed. by C. I. Byrnes. Marcel Dekker, New York, 1979, pp. 237–254.

[22] D. Mumford. *Tata Lectures on Theta II*. Birkhäuser, Boston, 1984.

[23] P. D. Lax. "Integrals of nonlinear equations of evolution and solitary waves". *Communications on Pure and Applied Mathematics* **21**.5 (1968), pp. 467–490.

[24] L. A. Takhtadzhyan and L. D. Faddeev. "Essentially Nonlinear One-dimensional model of classical field theory". *Theoretical and Mathematical Physics* **21**.2 (1974), pp. 1046–1057.

[25] V. A. Kozel and V. P. Kotlyarov. "Almost periodic solutions of the equation $u_{tt} - u_{xx} + \sin(u) = 0$". *Doklady Akademii Nauk Ukrainskoj SSR Serija A* **10** (1976), pp. 878–881. English reprint in: arXiv: `1401.4410`.

[26] I. M. Krichever. "Nonlinear equations and elliptic curves". *Journal of Soviet Mathematics* **28**.1 (1985), pp. 51–90.

[27] J. K. Perring and T. H. R. Skyrme. "A model unified field equation". *Nuclear Physics* **31** (1962), pp. 550–555.

[28] B. B. Kadomtsev and V. I. Petviashvili. "On the stability of solitary waves in weakly dispersing media". *Soviet Physics - Doklady* **15**.6 (1970), pp. 539–541.

[29] V. S. Dryuma. "Analytic solution of the two-dimensional Korteweg-de Vries (KdV) equation". *Journal of Experimental and Theoretical Physics Letters* **19**.12 (1974), pp. 387–388.

[30] V. E. Zakharov and A. B. Shabat. "A scheme for integrating the nonlinear equations of mathematical physics by the method of the inverse scattering problem. I". *Functional Analysis and Its Applications* **8**.3 (1974), pp. 226–235.

[31] M. J. Ablowitz and P. A. Clarkson. *Solitons, Nonlinear Evolution Equations and Inverse Scattering*. Cambridge University Press, 1991.

[32] J. Satsuma. "N-Soliton Solution of the Two-Dimensional Korteweg-de Vries Equation". *Journal of the Physical Society of Japan* **40** (1976), pp. 286–290.

[33] J. Villarroel and M. J. Ablowitz. "The Cauchy Problem for the Kadomtsev-Petviashili II Equation with Nondecaying Data along a Line". *Studies in Applied Mathematics* **109**.3 (2002), pp. 151–162.

[34] G. Biondini and Y. Kodama. "On a family of solutions of the Kadomtsev-Petviashvili equation which also satisfy the Toda lattice hierarchy". *Journal of Physics A: Mathematical and General* **36**.42 (2003), pp. 10519–10536. arXiv: `0306003 [nlin]`.

[35] H. Yeh and W. Li. "Laboratory realization of KP-solitons". *Journal of Physics: Conference Series* **482** (2014).

[36] S. V. Manakov, V. E. Zakharov, L. A. Bordag, A. R. Its, and V. B. Matveev. "Two-dimensional solitons of the Kadomtsev-Petviashvili equation and their interaction". *Physics Letters A* **63**.3 (1977), pp. 205–206.

[37] J. Satsuma and M. J. Ablowitz. "Two-dimensional lumps in nonlinear dispersive systems". *Journal of Mathematical Physics* **20**.7 (1979), pp. 1496–1503.

[38] A. A. Minzoni and N. F. Smyth. "Evolution of lump solutions for the KP equation". *Wave Motion* **24**.3 (1996), pp. 291–305.

[39] J. Villarroel and M. J. Ablowitz. "On the Discrete Spectrum of the Nonstationary Schrödinger Equation and Multipole Lumps of the Kadomtsev-Petviashvili I Equation". *Communications in Mathematical Physics* **207**.1 (1999), pp. 1–42.

[40] W. Hu, W. Huang, Z. Lu, and Y. Stepanyants. "Interaction of multi-lumps within the Kadomtsev-Petviashvili equation". *Wave Motion* **77** (2018), pp. 243–256.

[41] I. M. Krichever. "Integration of nonlinear equations by the methods of algebraic geometry". *Functional Analysis and Its Applications* **11**.1 (1977), pp. 12–26.

[42] B. A. Dubrovin and S. M. Natanzon. "Real Theta-Function Solutions of the Kadomtsev-Petviashvili Equation". *Mathematics of the USSR-Izvestiya* **32**.2 (1989), pp. 269–288.

[43] J. Hammack, N. Scheffner, and H. Segur. "Two-dimensional periodic waves in shallow water". *Journal of Fluid Mechanics* **209** (1989), pp. 567–589.

[44] J. Hammack, D. McCallister, N. Scheffner, and H. Segur. "Two-dimensional periodic waves in shallow water. Part 2. Asymmetric waves". *Journal of Fluid Mechanics* **285** (1995), pp. 95–122.

[45] J. L. Hammack and H. Segur. "The Korteweg-de Vries equation and water waves. Part 2. Comparison with experiments". *Journal of Fluid Mechanics* **65**.2 (1974), pp. 289–314.

[46] D. G. Crighton. "Applications of KdV". *Acta Applicandae Mathematicae* **39** (1995), pp. 39–67.

[47] T. Dauxois and M. Peyrard. *Physics of Solitons*. Cambridge University Press, 2006.

[48] S. Yomosa. "Solitary waves in large blood vessels". *Journal of the Physical society of Japan* **56**.2 (1987), pp. 506–520.

[49] Y. Hashizume. "Nonlinear pressure wave propagation in arteries". *Journal of the Physical Society of Japan* **57**.12 (1988), pp. 4160–4168.

[50] W. S. Duan, B. R. Wang, and R. J. Wei. "Reflection and transmission of nonlinear blood waves due to arterial branching". *Physical Review E* **55**.2 (1997), pp. 1773–1778.

[51] C. S. Gardner and G. K. Morikawa. "The effect of temperature on the width of a small-amplitude, solitary wave in a collision-free plasma". *Communications on Pure and Applied Mathematics* **18** (1965), pp. 35–49.

[52] H. Washimi and T. Taniuti. "Propagation of ion-acoustic solitary waves of small amplitude". *Physical Review Letters* **17**.19 (1966), pp. 996–998.

[53] A. Jeffrey. "The Role of Korteweg-de Vries Equation in Plasma Physics". *Quarterly Journal of the Royal Astronomical Society* **14** (1973), pp. 183–189.

[54] A. R. Osborne and T. L. Burch. "Internal Solitons in the Andaman Sea". *Science* **208**.4443 (1980), pp. 451–460.

[55] A. C. Scott. "A Nonlinear Klein-Gordon Equation". *American Journal of Physics* **37**.1 (1969), pp. 52–61.

[56] A. Barone, F. Esposito, C. J. Magee, and A. C. Scott. "Theory and Applications of the Sine-gordon Equation". *La Rivista del Nuovo Cimento* **1**.2 (1971), pp. 227–267.

[57] V. G. Ivancevic and T. T. Ivancevic. "Sine-Gordon Solitons, Kinks and Breathers as Physical Models of Nonlinear Excitations in Living Cellular Structures". *Journal of Geometry and Symmetry in Physics* **31** (2013), pp. 1–56. arXiv: 1305.0613.

[58] S. W. Englander, N. R. Kallenbach, A. J. Heeger, J. A. Krumhansl, and S. Litwin. "Nature of the open state in long polynucleotide double helices: Possibility of soliton excitations". *Proceedings of the National Academy of Sciences USA* **77**.12 (1980), pp. 7222–7226.

[59] S. Yomosa. "Soliton excitations in deoxyribonucleic acid (DNA) double helices". *Physical Review A* **27**.4 (1983), pp. 2120–2125.

[60] C. T. Zhang. "Soliton excitations in deoxyribonucleic acid (DNA) double helices". *Physical Review A* **35**.2 (1987), pp. 886–891.

[61] M. Manghi and N. Destainville. "Physics of base-pairing dynamics in DNA". *Physics Reports* **631** (2016), pp. 1–41. arXiv: 1510.05574.

[62] D. W. McLaughlin and A. C. Scott. "Perturbation analysis of fluxon dynamics". *Physical Review A* **18**.4 (1978), pp. 1652–1680.

[63] O. H. Olsen and M. R. Samuelsen. "Fluxon propagation in long Josephson junctions with external magnetic field". *Journal of Applied Physics* **52**.10 (1981), pp. 6247–6251.

[64] E. K. Sklyanin. "Boundary Conditions for Integrable Equations". *Functional Analysis and Its Applications* **21**.2 (1987), pp. 164–166.

[65] V. O. Tarasov. "The integrable initial-boundary value problem on a semiline: nonlinear Schrodinger and sine-Gordon equations". *Inverse Problems* **7**.3 (1991), pp. 435–449.

[66] S. Ghoshal and A. Zamolodchikov. "Boundary S-Matrix and Boundary State in Two-Dimensional Integrable Quantum Field Theory". *International Journal of Modern Physics A* **9**.21 (1994), pp. 3841–3886. arXiv: 9306002 [hep-th].

[67] A. MacIntyre. "Integrable boundary conditions for classical sine-Gordon theory". *Journal of Physics A: Mathematical and General* **28**.4 (1995), pp. 1089–1100. arXiv: 9410026 [hep-th].

[68] H. Saleur, S. Skorik, and N. P. Warner. "The boundary sine-Gordon theory: classical and semi-classical analysis". *Nuclear Physics B* **441**.3 (1995), pp. 421–436. arXiv: 9408004 [hep-th].

[69] P. A. Mattsson. "Integrable quantum field theories, in the bulk and with a boundary". PhD thesis. Durham University, 2000. arXiv: 0111261 [hep-th].

[70] R. F. Bikbaev and V. O. Tarasov. "A Nonhomogeneous Boundary Value Problem on a Semiaxis and on an Interval for the sine-Gordon equation". *St. Petersburg Mathematical Journal* **3**.4 (1992), pp. 775–789.

[71] R. F. Bikbaev and A. R. Its. "Algebrogeometric solutions of the nonlinear boundary problem on a segment for the sine-Gordon equation". *Mathematical Notes* **52**.4 (1992), pp. 1005–1011.

[72] V. Caudrelier. "On a systematic approach to defects in classical integrable field theories". *International Journal of Geometric Methods in Modern Physics* **5**.7 (2008), pp. 1085–1108. arXiv: 0704.2326.

[73] P. Bowcock, E. Corrigan, and C. Zambon. "Classically integrable field theories with defects". *International Journal of Modern Physics A* **19** (2004), p. 82. arXiv: 0305022 [hep-th].

[74] P. Bowcock, E. Corrigan, and C. Zambon. "Affine Toda field theories with defects". *Journal of High Energy Physics* 1 (2004). arXiv: 0401020 [hep-th].

[75] E. Corrigan and C. Zambon. "Jump-defects in the nonlinear Schrödinger model and other non-relativistic field theories". *Nonlinearity* **19**.6 (2006), pp. 1447–1469. arXiv: 0512038 [nlin].

[76] E. Corrigan and C. Zambon. "A new class of integrable defects". *Journal of Physics A: Mathematical and Theoretical* **42**.47 (2009). arXiv: 0908.3126.

[77] P. Bowcock and J. M. Umpleby. "Defects and Dressed Boundaries in Complex Sine-Gordon Theory". *Journal of High Energy Physics* 1 (2009). arXiv: 0805.3668.

[78] P. Bowcock, E. Corrigan, and C. Zambon. "Some aspects of jump-defects in the quantum sine-Gordon model". *Journal of High Energy Physics* 8 (2005). arXiv: 0506169 [hep-th].

[79] G. L. Lamb. "Analytical Description of Ultrashort Optical Pulse Propagation in a Resonant Medium". *Reviews of Modern Physics* **43**.2 (1971), pp. 99–124.

[80] H. D. Wahlquist and F. D. Estabrook. "Bäcklund Transformation for Solutions of the Korteweg-de Vries Equation". *Physical Review Letters* **31**.23 (1973), pp. 1386–1390.

[81] A. C. Bryan, J. F. Miller, and A. E. G. Stuart. "Superposition formulae for sine-Gordon multisolitons". *Il Nuovo Cimento B* **101**.6 (1988), pp. 637–652.

[82] P. G. Drazin and R. S. Johnson. *Solitons: an Introduction*. Cambridge University Press, 1989.

[83] C. Gu. "Bäcklund Transformations and Darboux Transformations". In: *Soliton Theory and Its Applications*. Ed. by C. Gu. Springer, Berlin, Heidelberg, 1995.

[84] C. Rogers and W. K. Schief. *Bäcklund and Darboux transformations: Geometry and Modern Applications in Soliton Theory*. Cambridge University Press, 2002.

[85] A. V. Bäcklund. "Om ytor med konstant negativ krökning". *Lunds Universitets Årsskrift* **19** (1883), pp. 1–48.

[86] I. Habibullin and A. Kundu. "Quantum and classical integrable sine-Gordon model with defect". *Nuclear Physics B* **795**.3 (2008), pp. 549–568. arXiv: 0709.4611.

[87] A. Doikou. "Classical integrable defects as quasi Bäcklund transformations". *Nuclear Physics B* **911** (2016), pp. 212–230. arXiv: 1603.04688.

[88] G. Darboux. "On a proposition relative to linear equations". *Comptes rendus de l'Académie des Sciences* **94** (1882), 1456–1459. Translated reprint: arXiv: 9908003 [physics].

[89] R. Parini. *cxroots: A Python module to find all the roots of a complex analytic function within a given contour (version 1.0.8)*. 2018. https://github.com/RParini/cxroots.

[90] P. Kravanja and M. Van Barel. *Computing the Zeros of Analytic Functions*. Springer, Berlin, Heidelberg, 2000.

[91] E. Corrigan and R. Parini. "Type I integrable defects and finite-gap solutions for KdV and sine-Gordon models". *Journal of Physics A: Mathematical and Theoretical* **50**.28 (2017). arXiv: 1612.06904.

[92] R. Arthur, P. Dorey, and R. Parini. "Breaking integrability at the boundary: The sine-Gordon model with Robin boundary conditions". *Journal of Physics A: Mathematical and Theoretical* **49**.16 (2016). arXiv: 1509.08448.

[93] R. Arthur. "Reflection of Sine-Gordon Kinks for Integrable and Non-Integrable Boundary Collisions". Undergraduate dissertation (unpublished). Durham University, 2010.

[94] P. E. Dorey and R. Parini. "Integrability breaking on the boundary" (2018).

[95] L. Bianchi. "Sulla Trasformazione di Bäcklund per le Superficie Pseudosferiche". *Rendiconti Lincei* **5** (1892), pp. 3–12.

[96] R. Konik and A. LeClair. "Purely transmitting defect field theories". *Nuclear Physics B* **538**.3 (1999), pp. 587–611. arXiv: 9703085v2 [hep-th].

[97] R. R. Silva. "The trace formulas yield the inverse metric formula". *Journal of Mathematical Physics* **39**.11 (1998), pp. 6206–6213. arXiv: 9805006 [math-ph].

[98] H. H. Zhang, W. B. Yan, and X. S. Li. "Trace Formulae of Characteristic Polynomial and Cayley-Hamilton's Theorem, and Applications to Chiral Perturbation Theory and General Relativity". *Communications in Theoretical Physics* **49**.4 (2007), pp. 801–808. arXiv: `0701116 [hep-th]`.

[99] A. I. Bobenko. "Introduction to Compact Riemann Surfaces". In: *Computational Approach to Riemann Surfaces. Lecture Notes in Mathematics, vol. 2013.* Ed. by A. I. Bobenko and C. Klein. Springer, Berlin, Heidelberg, 2011, pp. 3–64.

[100] R. Miranda. *Algebraic curves and Riemann surfaces.* American Mathematical Society, 1995.

[101] I. R. Shafarevich. *Basic Algebraic Geometry.* Springer, Berlin, Heidelberg, 1977.

[102] A. I. Bobenko and S. B. Kuksin. "Small-Amplitude Solutions of the Sine-Gordon Equation on an Interval under Dirichlet or Neumann Boundary Conditions". *Journal of Nonlinear Science* **5** (1995), pp. 207–232.

[103] S. Novikov, S. V. Manakov, L. P. Pitaevskii, and V. E. Zakharov. *Theory of Solitons.* Springer US, 1984.

[104] H. F. Baker. *Abel's Theorem and the Allied Theory, Including the Theory of the Theta Functions.* Cambridge University Press, 1897.

[105] B. A. Dubrovin. "Theta functions and non-linear equations". *Russian Mathematical Surveys* **36**.2 (1981), pp. 11–92.

[106] C. Klein and O. Richter. *Ernst Equation and Riemann Surfaces: Analytical and Numerical Methods.* Springer, Berlin, Heidelberg, 2005.

[107] P. Griffiths and J. Harris. *Principles of Algebraic Geometry.* Wiley Interscience, New York, 1978.

[108] I. M. Krichever. "Methods of Algebraic Geometry in the Theory of Non-Linear Equations". *Russian Mathematical Surveys* **32**.6 (1977), pp. 185–213.

[109] F. Lund and T. Regge. "Unified approach to strings and vortices with soliton solutions". *Physical Review D* **14**.6 (1976), pp. 1524–1535.

[110] K. Pohlmeyer. "Integrable Hamiltonian Systems and Interactions through Quadratic Constraints". *Communications in Mathematical Physics* **46**.3 (1976), pp. 207–221.

[111] P. Bowcock and G. Tzamtzis. "The complex sine-Gordon model on a half line". *Journal of High Energy Physics* 3 (2007). arXiv: `0203139 [hep-th]`.

[112] P. Bowcock and G. Tzamtzis. "Quantum complex sine-Gordon model on a half line". *Journal of High Energy Physics* 11 (2007). arXiv: `0612120 [hep-th]`.

[113] J. Frauendiener and C. Klein. "Computational Approach to Hyperelliptic Riemann Surfaces". *Letters in Mathematical Physics* **105**.3 (2015), pp. 379–400. arXiv: `1408.2201`.

[114] T. E. Oliphant. *A guide to NumPy.* Trelgol Publishing, 2006.

[115] E. Jones, T. Oliphant, P. Peterson, et al. *SciPy: Open Source Scientific Tools for Python.* `http://www.scipy.org/`.

[116] C. Swierczewski et al. *Abelfunctions: A library for computing with Abelian functions, Riemann surfaces, and algebraic curves*. 2017. `http://github.com/abelfunctions/abelfunctions`.

[117] C. Swierczewski and B. Deconinck. "Computing Riemann theta functions in Sage with applications". *Mathematics and Computers in Simulation* **127** (2016), pp. 263–272.

[118] J. D. Hunter. "Matplotlib: A 2D graphics environment". *Computing in Science and Engineering* **9**.3 (2007), pp. 99–104.

[119] E. T. Whittaker and G. N. Watson. *A Course of Modern Analysis*. 4th ed. Cambridge University Press, 1962.

[120] H. Bateman and A. Erdélyi. *Higher Transcendental Functions II*. California Institute of Technology Bateman Manuscript Project, McGraw-Hill, New York, 1953.

[121] D. W. McLaughlin and A. C. Scott. "A restricted Bäcklund transformation". *Journal of Mathematical Physics* **14**.12 (1973), pp. 1817–1828.

[122] V. B. Matveev and M. A. Salle. *Darboux Transformations and Solitons*. Springer, Berlin, Heidelberg, 1991.

[123] H. Flaschka and D. W. McLaughlin. "Some comments on Bäcklund transformations, canonical transformations, and the inverse scattering method." In: *Bäcklund Transformations, the Inverse Scattering Method, Solitons, and Their Applications*. Ed. by R. M. Miura. Springer, Berlin, Heidelberg, 1976, pp. 253–295.

[124] F. Ehlers and H. Knörrer. "An algebro-geometric interpretation of the Bäcklund transformation for the Korteweg-de Vries Equation". *Commentarii Mathematici Helvetici* **57** (1982), pp. 1–10.

[125] F. Gesztesy and H. Holden. "Darboux-type transformations and hyperelliptic curves". *Journal für die reine und angewandte Mathematik* **527** (2000), pp. 151–183. arXiv: `9901008 [solv-int]`.

[126] A. Arancibia and M. S. Plyushchay. "Chiral asymmetry in propagation of soliton defects in crystalline backgrounds". *Physical Review D* **92**.10 (2015), p. 105009. arXiv: `1507.07060`.

[127] B. M. Levitan. "Degeneration of Finite Zone Potentials". *Journal of Soviet Mathematics* **45**.5 (1989), pp. 1455–1459.

[128] J. Zagrodziński and M. Jaworski. "Mixed solutions of the sine-Gordon equation". *Zeitschrift für Physik B Condensed Matter* **49**.1 (1982), pp. 75–77.

[129] S. F. Deng. "Bäcklund transformation and soliton solutions for KP equation". *Chaos, Solitons and Fractals* **25**.2 (2005), pp. 475–480.

[130] V. Rosenhaus. "On conserved densities and asymptotic behaviour for the potential Kadomtsev-Petviashvili equation". *Journal of Physics A: Mathematical and General* **39**.24 (2006), pp. 7693–7703.

[131] T. T. Liu and M. Z. Qin. "Multisymplectic geometry and multisymplectic Preissman scheme for the KP equation". *Journal of Mathematical Physics* **43**.8 (2002), pp. 4060–4077. arXiv: `0201010 [math-ph]`.

[132] R. M. DeLeonardis, S. E. Trullinger, and R. F. Wallis. "Theory of boundary effects on sine-Gordon solitons". *Journal of Applied Physics* **51**.2 (1980), pp. 1211–1226.

[133] I. T. Khabibullin. "The Bäcklund transformation and integrable initial boundary value problems". *Mathematical Notes* **49**.4 (1991), pp. 418–423.

[134] I. T. Khabibullin. "Sine-Gordon equation on the semi-axis". *Theoretical and Mathematical Physics* **114**.1 (1998), pp. 90–98.

[135] D. Hills. "Generating Boundary Conditions for Integrable Field Theories using Defects". PhD thesis. University of York, 2016.

[136] Z. Bajnok, G. Böhm, and G. Takács. "On perturbative quantum field theory with boundary". *Nuclear Physics B* **682**.3 (2004), pp. 585–617. arXiv: 0309119 [hep-th].

[137] A. C. Scott, F. Y. F. Chu, and D. W. McLaughlin. "The Soliton: A New Concept in Applied Science". *Proceedings of the IEEE* **61**.10 (1973), pp. 1443–1483.

[138] M. Wadati, H. Sanuki, and K. Konno. "Relationships among Inverse Method, Backlund Transformation and an Infinite Number of Conservation Laws". *Progress of Theoretical Physics* **53**.2 (1975), pp. 419–436.

[139] P. Dorey, A. Halavanau, J. Mercer, T. Romanczukiewicz, and Y. Shnir. "Boundary scattering in the ϕ^4 model". *Journal of High Energy Physics* 5 (2017). arXiv: 1508.02329.

[140] M. Dellnitz, O. Schütze, and Q. Zheng. "Locating all the Zeros of an Analytic Function in one Complex Variable". *Journal of Computational and Applied Mathematics* **138**.2 (2002).

[141] P. Kravanja, T. Sakurai, and M. Van Barel. "On locating clusters of zeros of analytic functions". *BIT Numerical Mathematics* **39**.4 (1999), pp. 646–682.

[142] N. Manton and P. Sutcliffe. *Topological Solitons*. Cambridge University Press, 2004.

[143] M. Nishida, Y. Furukawa, T. Fujii, and N. Hatakenaka. "Breather-breather interactions in sine-Gordon systems using collective coordinate approach". *Physical Review E* **80**.3 (2009).

[144] S. V. Dmitriev, Y. S. Kivshar, and T. Shigenari. "Fractal structures and multiparticle effects in soliton scattering". *Physical Review E* **64**.5 (2001).

[145] D. K. Campbell, J. F. Schonfeld, and C. A. Wingate. "Resonance structure in kink-antikink interactions in ϕ^4 theory". *Physica D: Nonlinear Phenomena* **9** (1983).

[146] P. Anninos, S. Oliveira, and R. A. Matzner. "Fractal structure in the scalar $\lambda(\phi^2-1)^2$ theory". *Physical Review D* **44**.4 (1991), pp. 1147–1160.

[147] R. H. Goodman and R. Haberman. "Chaotic scattering and the n-bounce resonance in solitary-wave interactions". *Physical Review Letters* **98**.10 (2007). arXiv: 0702048 [nlin].

[148] A. Fujii and R. Sasaki. "Boundary Effects in Integrable Field Theory on a Half Line". *Progress of Theoretical Physics* **93**.6 (1995), pp. 1123–1133. arXiv: 9503083 [hep-th].

[149] A. R. Aguirre. "Inverse scattering approach for massive Thirring models with integrable type-II defects". *Journal of Physics A: Mathematical and Theoretical* **45**.20 (2012). arXiv: arXiv:1111.5249v2.

[150] C. Robertson. "Defect fusing rules in affine Toda field theory". *Journal of Physics A: Mathematical and Theoretical* **47**.48 (2014). arXiv: 1408.1960.

[151] R. Bristow and P. Bowcock. "Momentum conserving defects in affine Toda field theories". *Journal of High Energy Physics* 5 (2017). arXiv: 1612.03002.

[152] R. Bristow. "Integrability of generalised type II defects in affine Toda field theory". *Journal of High Energy Physics* 11 (2017). arXiv: 1709.03927.

[153] R. Bristow. "Momentum conserving defects in affine Toda field theory". PhD thesis. Durham University, 2018.

[154] G. Tzitzéica. "Sur une nouvelle classe de surfaces". *Comptes Rendus de l'Académie des Sciences* **144** (1907), pp. 1257–1259.

[155] A. R. Aguirre, T. R. Araujo, J. F. Gomes, and A. H. Zimerman. "Type-II Bäcklund Transformations via Gauge Transformations". *Journal of High Energy Physics* 12 (2011). arXiv: 1110.1589.

[156] I. Yu. Cherdantsev and R. A. Sharipov. "Finite-gap solutions of the Bullough-Dodd-Zhiber-Shabat equation". *Theoretical and Mathematical Physics* **82**.1 (1990), pp. 108–111.

[157] I. Yu. Cherdantzev and R. A. Sharipov. "Solitons on a finite-gap background in Bullough-Dodd-Jiber-Shabat model". *International Journal of Modern Physics A* **5**.15 (1990), pp. 3021–3027. arXiv: 0112045 [math-ph].

[158] Y. V. Brezhnev. "Darboux transformation and some multi-phase solutions of the Dodd-Bullough-Tzitzeica equation". *Physics Letters A* **211**.2 (1996), pp. 94–100.

[159] G. Biondini and S. Chakravarty. "Soliton solutions of the Kadomtsev-Petviashvili II equation". *Journal of Mathematical Physics* **47**.3 (2006).

[160] A. P. Veselov and S. P. Novikov. "Finite-zone, two-dimensional, potential Schrödinger operators. Explicit formulas and evolution equations". *Soviet Mathematics - Doklady* **30** (1984).

[161] A. S. Fokas. *A Unified Approach to Boundary Value Problems*. SIAM, 2008.

[162] B. Pelloni. "Advances in the study of boundary value problems for nonlinear integrable PDEs". *Nonlinearity* **28**.2 (2015), R1–R38.

[163] V. Caudrelier. "Interplay between the Inverse Scattering Method and Fokas's Unified Transform with an Application". *Studies in Applied Mathematics* **140**.1 (2018), pp. 3–26.

[164] A. S. Fokas. "The generalized Dirichlet to Neumann map for certain nonlinear evolution PDEs". *Communications on Pure and Applied Mathematics* **58**.5 (2005), pp. 639–670.

[165] G. Hwang. "The Fokas Method: The Dirichlet to Neumann Map for the Sine-Gordon Equation". *Studies in Applied Mathematics* **132**.4 (2014), pp. 381–406.

[166] A. S. Fokas. "Linearizable initial boundary value problems for the sine-Gordon equation on the half-line". *Nonlinearity* **17**.4 (2004), pp. 1521–1534.

[167] G. Delfino, G. Mussardo, and P. Simonetti. "Non-integrable quantum field theories as perturbations of certain integrable models". *Nuclear Physics B* **473**.3 (1996), pp. 469–508. arXiv: `9603011 [hep-th]`.

[168] V. Caudrelier. "On the Inverse Scattering Method for Integrable PDEs on a Star Graph". *Communications in Mathematical Physics* **338**.2 (2015), pp. 893–917. arXiv: `1409.5277`.

[169] Z. Sobirov, D. Babajanov, D. Matrasulov, K. Nakamura, and H. Uecker. "Sine-Gordon solitons in networks: Scattering and transmission at vertices". *EPL (Europhysics Letters)* **115**.5 (2016), p. 50002. arXiv: `1511.02314`.

[170] Z. Sobirov, D. Matrasulov, K. Sabirov, S. Sawada, and K. Nakamura. "Integrable nonlinear Schrödinger equation on simple networks: Connection formula at vertices". *Physical Review E* **81**.6 (2010).

[171] R. Hirota. "Exact Solution of the Korteweg-de Vries Equation for Multiple Collisions of Solitons". *Physical Review Letters* **27**.18 (1971), pp. 1192–1194. arXiv: `1011.1669`.

[172] R. Hirota. "Exact Solution of the Sine-Gordon Equation for Multiple Collisions of Solitons". *Journal of the Physical Society of Japan* **33**.5 (1972), pp. 1459–1463.

[173] P. Kravanja, M. Van Barel, and A. Haegemans. "Computing zeros of analytic functions via modified moments based on formal orthogonal polynomials". *Technical Report: TW 246, Katholieke Universiteit Leuven* November (1996).

[174] F. Johansson et al. *mpmath: a Python library for arbitrary-precision floating-point arithmetic (version 1.0.0)*. 2017. `http://mpmath.org/`.

[175] P. Kravanja, M. Van Barel, O. Ragos, M. N. Vrahatis, and F. A. Zafiropoulos. "ZEAL: A mathematical software package for computing zeros of analytic functions". *Computer Physics Communications* **124**.2-3 (2000), pp. 212–232.

[176] P. Kravanja and M. Van Barel. "A Derivative-Free Algorithm for Computing Zeros of Analytic Functions". *Computing* **63**.1 (1999), pp. 69–91.